COLLEGE OF MEDICINE, BIOLOGICAL SCIENCES AND PSYCHOLOGY

SCHOOL OF MEDICINE

DEPARTMENT OF INFECTION, IMMUNITY AND INFLAMMATION

THE ROLE OF FILTERED IGA IN THE PROGRESSION OF IGA NEPHROPATHY

Chee Kay Cheung

Thesis submitted for the degree of Doctor of Philosophy

2016

Abstract

IgA nephropathy (IgAN) is the commonest primary glomerulonephritis worldwide, with 20-40% of patients developing progressive kidney disease. The most accurate predictors of prognosis are the presence of proteinuria and tubulointerstitial fibrosis, while the degree of mesangial IgA deposition is not a prognostic factor. These findings imply that tubular-specific factors play a key role in progressive IgAN. The aim of this thesis was to explore whether filtered IgA has a direct effect on proximal tubular epithelial cell (PTEC) activation and generation of pro-inflammatory and pro-fibrotic cytokines.

The interaction between IgA and PTEC was initially investigated *in vivo* in Munich Wistar Frömter rats by multiphoton microscopy. These studies demonstrated that IgA, that crossed the glomerular filtration barrier, interacted with PTEC and underwent endocytosis via their apical surface. This process was greatly upregulated in a model of podocyte injury, resulting in increased amounts of filtered IgA. *In vitro*, human IgA1, and especially galactose-deficient polymeric IgA1, stimulated release of pro-inflammatory and pro-fibrotic cytokines from cultured human HK-2 PTEC. A mouse model of IgAN was optimised that developed both glomerular and tubulointerstitial inflammatory cell infiltration. Although glomerular deposition of complement component C3 was increased in the model, mice genetically deficient in key initiators of the lectin pathway, Collectin-11 (CL-11) or Mannose-binding lectin-associated serine protease-2 (MASP-2), were not protected from interstitial macrophage infiltration, while reductions in glomerular cell number and T cell infiltration were observed.

These studies provide evidence for the first time that filtered IgA is able to interact with the proximal tubule and undergo endocytosis. IgA1, and especially galactose-deficient polymeric IgA1, stimulated a pro-inflammatory and pro-fibrotic response from PTEC that may contribute towards progressive IgAN. Understanding this interaction further may reveal novel targets for therapy in this condition. Deficiencies in CL-11 and MASP-2 did not protect against tubulointerstitial inflammation in a mouse model of IgAN, and further studies should concentrate on whether the alternative pathway is activated in this model.

Acknowledgements

I am extremely grateful to my supervisors for their guidance and support. My thanks to Dr Jonathan Barratt, who has been an invaluable source of advice, and has inspired and encouraged me throughout my time in academic medicine. I am indebted to Dr Karen Molyneux, for her guidance, encouragement and expert supervision during all aspects of this research. I would like to thank Professor Nigel Brunskill, for his support and encouragement over the past few years. I would also like to thank Professor John Feehally for his advice during the funding process and beyond. I would like to thank Dr Alan Bevington and Dr Peter Topham, whose constructive comments on this work have been much appreciated. My thanks also to Professor Wilhelm Schwaeble for the very helpful discussions regarding this work.

My time during this project has been much enhanced by the friendship and assistance from all in the Leicester Renal Research Group, in particular Tricia Higgins, Iza Pawluczyk, Jez Brown, Alice Smith, Emma Watson, Nima Abbassian, David Wimbury, Dina Nilasari, Saarah Bashir, See Cheng Yeo, Joanna Boyd, Owen Vennard, Safia Blbas, Ravi Chana, Hani Kenawy and Samy Alsari.

I would like to thank Professor Bruce Molitoris, Ruben Sandoval, Sarah Wean, Silvia Campos-Bilderback, and Sudanshu Kumar at Indiana University, for their enthusiasm for this project, their kindness and generosity.

There are countless others who have generously given up their own time to assist with this project over the past few years. In particular, I would like to thank Natalie Allcock, Stefan Hyman, Dr Kees Straatman, Tracey DeHaro, Dr John Dormer, Dr Andrew Bottrill, members of the CRF, Dave Roberts, the renal research team at LGH, Angie Gillies, Linda Potter, and the many others that I do not have space to mention individually.

I am extremely grateful to the patients who donated samples for this project, often going out of their way to do so, and without whom, much of this work would not have been possible.

I am very grateful to the Medical Research Council for funding this clinical research training fellowship, the Renal Association for funding travel to Indiana, and to the Peel Medical trust and the Leicester Kidney Care appeal.

Finally I would like to thank my parents for all their love. To John and Toni for the many times that they have looked after Ellie at short notice. To my wife Lucy and my daughter Ellie, for all their love and support, especially during the final stages of this thesis.

Contributions

The intravital multiphoton microscopy studies in Chapter 3 took place at the O'Brien Center for Advanced Renal Microscopy and Analysis, Indiana University, USA. Surgical and imaging procedures were performed with the assistance of members of staff within the facility.

In vitro experiments studying the differential effects of monomeric and polymeric IgA1 on proximal tubular epithelial cells (Sections 4.2.3, 4.2.4 and 4.2.5) were undertaken alongside Ms Saarah Bashir, an intercalated BSc student under my supervision. The analysis of cytokines within cell culture supernatants by multiplex array (Section 4.2.6) was performed by Mr David Wimbury. All statistical analyses were performed by the author.

I confirm that unless otherwise stated, all of the work presented in this thesis is the candidate's own.

Publications

Papers

1. **Cheung CK**, Barratt J. Gluten and IgA nephropathy: you are what you eat? Kidney Int 2015; 88(2): 215-8.
2. **Cheung CK**, Bashir S, Barratt J. IgA Nephropathy. Br J Hosp Med 2014; 75 Suppl 11: C173-6.
3. **Cheung CK**, Boyd JK, Feehally J. Evaluation and management of IgA nephropathy. Clinical Medicine 2012;12(6):s27–s31.
4. Boyd JK, **Cheung CK**, Molyneux K, Feehally J, Barratt J. An update on the pathogenesis of IgA nephropathy and therapy. Kidney Int. 2012;81:833-843.

Book chapters

1. **Cheung CK**, Barratt J. Is IgA nephropathy a single disease? In: Tomino Y (Ed). Pathogenesis and Treatment in IgA Nephropathy. Springer, Tokyo. 2015. p3-18.
2. **Cheung CK**, Boyd JK, Barratt J. IgA nephropathy and Henoch-Schönlein purpura. In: Harber M (Ed). Practical Nephrology: A users guide to kidney disease. Springer, London. 2014. p203-13.
3. Boyd JK, **Cheung CK**, Barratt J. IgA Nephropathy. In: MacKay IR, Rose NR (Eds). Encyclopedia of Medical Immunology. Springer, New York. 2014. p467-75.

Conference presentations

1. **Cheung CK**, Sandoval R, Wean S, Campos-Bilderback S, Kumar S, Molyneux K, Brunskill NJ, Molitoris B, Barratt J. The effects of filtered IgA on the proximal tubule: a multiphoton microscopy study. British Renal Society/Renal Association conference, Birmingham, UK, June 2016 (oral).
2. **Cheung CK**, Bashir S, Molyneux K, Brunskill NJ, Barratt J. TGF-β1 release from PTEC is stimulated by galactose-deficient polymeric IgA1. American Society of Nephrology Kidney Week 2014, Philadelphia, USA. Nov 2014 (poster).

3. **Cheung CK**, Molyneux K, Boyd J, Baines RJ, Brunskill NJ, Barratt J. The role of IgA in proximal tubular cell activation and tubulointerstitial scarring in IgA nephropathy. Spring Meeting for Clinician Scientists in Training, Academy of Medical Sciences, Royal College of Physicians, London. February 2014 (poster).
4. **Cheung CK**, Jordan A, Boyd J, Brunskill NJ, Feehally J, Molyneux K, Barratt J. IgA, and not IgG, is a potent trigger of proximal tubular cell activation in IgA nephropathy. 13th International Symposium on IgA nephropathy (WCN Satellite Symposum), Nanjing, China, June 2013 (poster).
5. **Cheung CK**, Molyneux K, Chana RS, Boyd J, Smith AC, Baines RJ, Brunskill NJ, Barratt J. IgA is a more potent trigger of proximal tubular cell activation and tubulointerstitial scarring than albumin in IgA nephropathy. British Renal Society/Renal Association conference, Birmingham, UK, June 2011 (oral).
6. **Cheung CK**, Molyneux K, Chana RS, Boyd J, Smith AC, Baines RJ, Brunskill NJ, Barratt J. IgA is a more potent trigger of proximal tubular cell activation and tubulointerstitial scarring than albumin in IgA nephropathy. World Congress of Nephrology, Vancouver, Canada, April 2011 (poster).

Table of contents

Table of figures

Table of abbreviations

AKI	Acute kidney injury
APRIL	A proliferation-inducing ligand
ANOVA	Analysis of variance
ASGPR	Asialoglycoprotein receptor
ATN	Acute tubular necrosis
AU	Arbitrary unit
BGG	Bovine gamma globulin
BMP-2	Bone morphogenetic protein 2
BSA	Bovine serum albumin
C1GalT1	Core 1 β1,3 galactosyltransferase
CCL	Chemokine ligand
CD	Cluster of differentiation
C_L	Light chain constant region
CL-11	Collectin-11
CFH	Complement Factor H
CT	Cholera toxin
CTB	Cholera toxin subunit B
Cosmc	Core 1 β1,3 galactosyltransferase molecular chaperone
DAB	Diaminobenzamidine
DAF	Decay accelerating factor
dIgA	Dimeric IgA
DMEM	Dulbecco's modified eagle medium
DMF	Dimethylformamide
DNA	Deoxyribonucleic acid
DNP	Dinitrophenol
ECM	Extracellular matrix
E Coli	Escherichia coli
EDTA	Ethylenediaminetetraacetic acid
EGF	Epidermal growth factor
ELISA	Enzyme-linked immunosorbent assay
ESRD	End stage renal disease
EU	Endotoxin units
Fab	Fragment, antigen binding
Fc	Fragment, crystallisable
FcRγ	Fc receptor γ subunit
FFPE	Formalin fixed paraffin embedded
FITC	Fluorescein isothiocyanate
Fn	Fibronectin
FPLC	Fast protein liquid chromatography
Gal	Galactose
GalNac	N-acetyl galactosamine
gcs	Glomerular cross section
GDF-15	Growth differentiation factor 15
GdpIgA1	Galactose deficient polymeric IgA1
GFR	Glomerular filtration rate
GM-CSF	Granulocyte-macrophage colony-stimulating factor
GWAS	Genome wide association study
HAA	Helix Aspersa agglutinin
HCl	Hydrochloric acid
hDTR	Human diphtheria toxin receptor

HK-2	Human kidney-2
HLA	Human leukocyte antigen
HMC	Human mesangial cell
HMC-CM	Human mesangial cell conditioned medium
HPV	Human papilloma virus
HRP	Horseradish peroxidase
HS	Healthy subject
HSP	Henoch-Schönlein purpura
ICAM	Intercellular adhesion molecule
Ig	Immunoglobulin
IgAN	Immunoglobulin A nephropathy
IL	Interleukin
IP-10	Interferon gamma-induced protein 10
ITAM	Immunoreceptor tyrosine-based activation motif
J chain	Immunoglobulin joining chain
kDa	Kilodaltons
KIM-1	Kidney injury molecule-1
LAL	Limulus amoebocyte lysate
LPS	Lipopolysaccharide
MAC	Membrane attack complex
MALT	Mucosal associated lymphoid tissue
MASP	Mannose-binding lectin-associated serine protease
MBL	Mannose-binding lectin
MCP	Monocyte chemoattractant protein
MHC	Major histocompatibility complex
MIF	Macrophage migration inhibitory factor
mIgA	Monomeric IgA
MMP	Matrix metallopeptidase
mRNA	Messenger RNA
MWCO	Molecular weight cut off
MWF	Munich Wistar Frömter
NeuNAc	N-acetylneuraminic acid
PAI-1	Plasminogen activator inhibitor type **1**
PAS	Periodic acid-Schiff
PBS	Phosphate buffered saline
PCR	Polymerase chain reaction
PCR	Protein:creatinine ratio
PDGF	Platelet-derived growth factor
pIgA	Polymeric IgA
pIg	Polymeric immunoglobulin
pIgR	Polymeric immunoglobulin receptor
PLP	Paraformaldehyde lysine periodate
PMP	Per million population
PPAR	Peroxisome proliferator-activated receptor
PPRE	Peroxisome proliferator-activated receptor-response element
PTEC	Proximal tubular epithelial cells
RANTES	Regulated on activation, normal T cell expressed and secreted
RAP	Receptor associated protein
RNA	Ribonucleic acid
RRT	Renal replacement therapy
SC	Secretory component
sCD89	Soluble CD89

SDS	Sodium dodecyl sulphate
SDS-PAGE	Sodium dodecyl sulphate-polyacrylamide gel electrophoresis
SEM	Standard error of the mean
siRNA	Small interfering RNA
SNP	Single nucleotide polymorphism
TAE	Tris-acetic acid-EDTA
TBS	Tris-buffered saline
TfR1	Transferrin receptor
TGF-β	Transforming growth factor beta
Th	T helper
Thr	Threonine
TNF	Tumor necrosis factor
TR	Texas red
V_H	Heavy chain variable region
V_L	Light chain variable region
wt	Wild type

Chapter 1: Introduction

IgA nephropathy (IgAN) is the commonest form of primary glomerulonephritis worldwide and a leading cause of chronic kidney disease (CKD) (D'Amico, 1987). Approximately 20-40% of patients develop end stage renal disease (ESRD) within 20 years of diagnosis, while others have stable kidney function over this time, and it remains unknown why this disparity exists (D'Amico, 2004). IgAN is defined by the predominant deposition of IgA in the glomerular mesangium. The severity of mesangial IgA deposition does not correlate with prognosis. In common with other glomerulonephritides, the best predictor is the degree of tubulointerstitial disease, suggesting that tubular-specific processes play an important role in this condition (Cattran et al., 2009).

The aim of this thesis is to examine the hypothesis: "A major factor determining the development of progressive kidney disease in IgAN is the presence in the serum of IgA1 with PTEC-specific pro-inflammatory and pro-fibrotic activity. As non-selective proteinuria develops this IgA1 enters the proximal tubule and augments PTEC activation, accelerating renal scarring".

This thesis explores the following areas:

1. The interaction between filtered IgA and the proximal tubule *in vivo*, utilising multiphoton intravital microscopy.
2. The effects of IgA1 on proximal tubular cells *in vitro*.
3. The development of a mouse model of IgAN.
4. The effects of the lectin pathway of complement activation on the development of glomerular and tubulointerstitial inflammation in the mouse model of IgAN.

1.1 Immunoglobulin A

IgA is the most abundant immunoglobulin (Ig) isotype in humans, and its production, approximately 65 mg per kg body weight per day, exceeds that of all other Ig classes combined (Kerr, 1990; Pabst, 2012). IgA is the main Ig isotype found at mucosal surfaces, and is contained in secretions including tears, saliva, colostrum, milk, nasal fluid, intestinal fluid and bile. It is also abundant, alongside IgG, in secretions from the respiratory and urinary tracts (Woof and Mestecky, 2005). IgA therefore plays an important role in the immune system at these sites. In serum, IgA is the second most prevalent antibody class after IgG.

1.1.1 Structure of IgA

Human IgA exists in a variety of isoforms. All IgA molecules consist of two heavy chains (α1 or α2, each approximately 55 kDa) and two light chains (κ or λ, ~25 kDa), arranged to form the fragment, antigen-binding (Fab) region and fragment, crystallisable (Fc) region, in common with other Ig classes (Figure 1).

Human IgA is unique amongst Ig subclasses in that it exists in both monomeric (approximately 160kDa) and polymeric (mainly dimeric or tetrameric) forms, as opposed to IgD, IgE and IgG, which exist solely as monomers, and IgM which exists as a polymer. IgA is produced in two compartments: systemic and mucosal. Systemic IgA, produced in the bone marrow and thus the major form in serum, is >90% monomeric. Mucosal IgA, mainly produced by lymphocytes and plasma cells in lymphoid tissue at mucosal surfaces, for example in ileal Peyer's patches, is mostly polymeric.

In polymeric forms, IgA subunits are linked by a small polypeptide termed joining (J) chain (Figure 1) (Woof and Mestecky, 2005). In general, J chain exists only within pIgA and IgM. It consists of around 137 amino acid residues and has a molecular mass of 15-16kDa. According to stoichiometric studies, each molecule of pIgA, irrespective of the number of IgA subunits, contains only one J chain (Zikan et al., 1986).

The majority of pIgA in the mucosal compartment is dimeric IgA (dIgA) associated with secretory component (SC; Figure 1). This is the extracellular component of the polymeric Ig receptor (pIgR). When pIgR transporting dIgA reaches the apical

surface of the epithelial cell, cleavage of the extracellular domain occurs releasing the extracellular portion of the pIgR together with the dIgA. Together, this is termed secretory IgA (Almogren et al., 2007). SC is believed to confer resistance to proteolytic degradation. SC is bound to the Fc portion of the IgA molecules by covalent (disulphide) and non-covalent (hydrogen bond) interactions, and comprises of five Ig-like domains, with a molecular mass of 70-80 kDa (Woof and Mestecky, 2005).

The molecular composition of pIgA in the serum is highly variable and not fully understood. Previous reports indicate that components of pIgA may include dIgA, secretory IgA, and IgA complexed to other proteins, including soluble CD89, fibronectin and C3 (Oortwijn et al., 2006; Tam et al., 2009; van der Boog et al., 2005).

1.1.2 IgA1 and IgA2

Human IgA exists in two subclasses, IgA1 and IgA2 (Figure 1). These differ in composition of the α heavy chain, named α1 or α2 respectively, which are encoded by separate α genes on chromosome 14 (Flanagan and Rabbitts, 1982). Each α heavy chain consists of one N-terminal variable (V_H) and three constant region domains (Cα1, Cα2, and Cα3). A hinge region exists between the Cα2 and Cα3 domains, allowing flexibility to the structure of IgA and thus increased capacity for antigen binding (Chintalacharuvu et al., 1994). The hinge region differs between the two IgA isoforms, consisting of 26 amino acids in IgA1 and 13 amino acids in IgA2. IgA1, with its extended hinge region, is only found in humans and higher primates, with most other animals only possessing one isoform of IgA, which more closely resembles IgA2.

The proportion of IgA1 and IgA2 in humans varies according to anatomical site. Serum contains approximately 90% IgA1 and 10% IgA2. IgA1 predominates in the small airways. In the small intestine, both are found in equal abundance, while in the large intestine, IgA2 is more prevalent (van der Boog et al., 2005).

IgA2 exists in two forms: IgA2m(1), which lacks the disulphide bond between heavy and light chains, and IgA2m(2) which contains the disulphide bond.

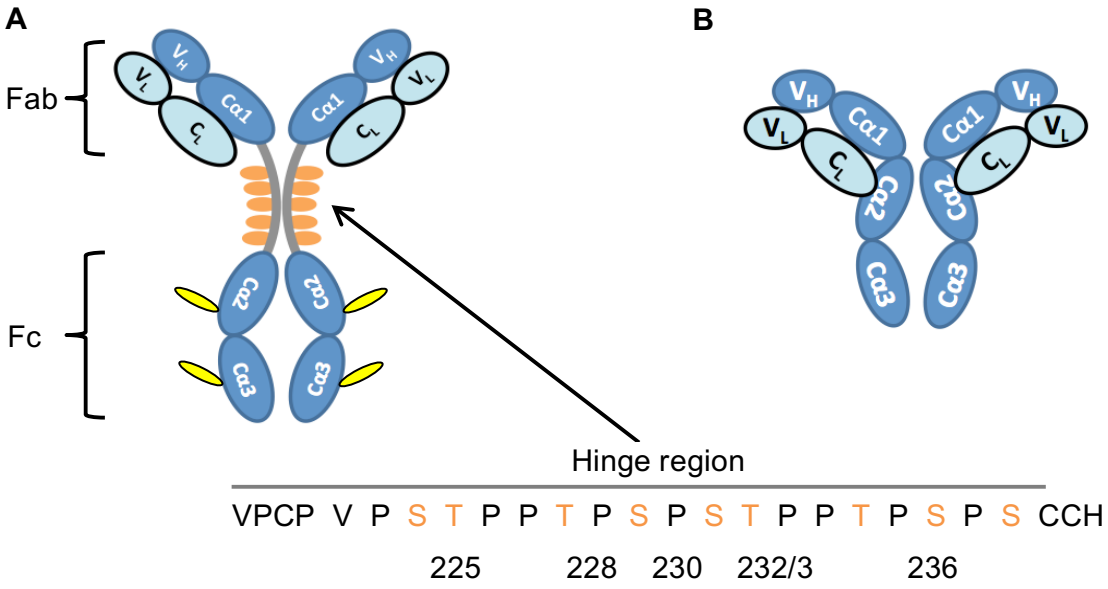
A
Fab
Fc
B
Hinge region
VPCP V P S T P P T P S P S T P P T P S P S CCH
225 228 230 232/3 236

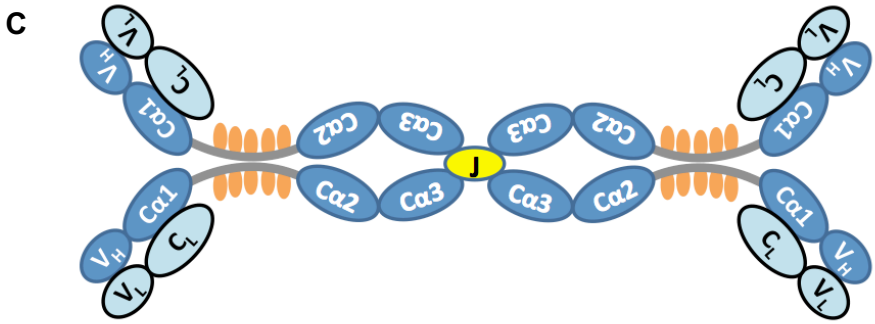
C
J

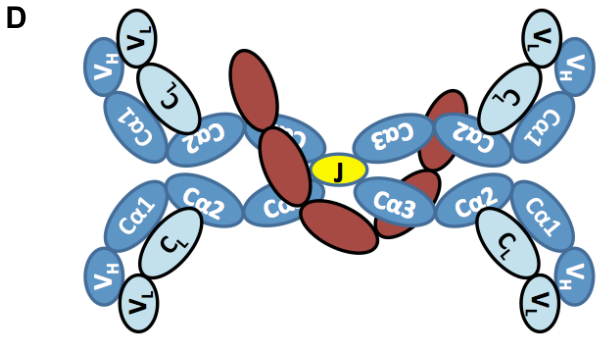
D
J

Figure 1: Structure of human IgA. (A) Monomeric IgA1 (B) Monomeric IgA2 (C) Dimeric IgA1 (D) Secretory IgA2. (A) Monomeric IgA1 consists of 2 heavy chains (dark blue) and 2 light chains (light blue). The heavy chains consist of a variable region (V_H) and 3 constant regions (Cα1-3). Each heavy chain has a hinge region between Cα1 and Cα2 and 2 N-glycans (yellow). The amino acid sequence of the hinge region is depicted and is rich in serine, threonine and proline residues. Within each IgA1 hinge region, 3-6 glycan (carbohydrate) side chains may attach to the serine or threonine residues, with the most common sites of attachment being numbered. Patients with IgAN have more circulating IgA1 molecules with hinge regions that have less than 3 galactose residues attached (undergalactosylated). Light chains consist of one variable region (V_L) and one constant region (C_L). (B) IgA2 has a shorter hinge region which is not O-glycosylated. (C) Dimeric IgA1 is linked covalently by J chain (yellow). (D) Secretory IgA differs from dimeric IgA by the addition of secretory component (brown). Part of Figures 1(A) and (C) are adapted from Wyatt and Julian, 2013.

1.1.3 Glycosylation of the IgA1 hinge region

The majority of serum proteins exist as glycoproteins. Carbohydrate moieties attach to proteins as N-linked oligosaccharide side chains (glycans), linked to aspargine residues, or O-linked glycans, linked to serine or threonine residues. N-linked glycans are by far more common, and usually consist of complex side chains (Arnold et al., 2007). O-linked glycans are most commonly found on membrane-bound proteins. Human IgA1 is one of the few circulating serum glycoproteins which contain O-linked glycans, with others including C1 inhibitor and IgD (Allen, 1999; Barratt et al., 2007).

The IgA1 hinge region contains multiple serine, threonine and proline residues. The serine and threonine residues undergo co- or post-translational glycosylation. There are nine sites where glycan side chains may be added in an O-linked manner, and of these, only 3 to 6 are usually glycosylated (Takahashi et al., 2012; Tarelli et al., 2004). Synthesis of O-glycans occurs in a stepwise manner, and is initiated by attachment of N-acetyl galactosamine (GalNac) (Figure 2). Galactose may then be β1,3-linked to GalNac by the activity of core 1 β1,3 galactosyltransferase (C1GalT1), which requires the chaperone Cosmc (core 1 β1,3 galactosyltransferase molecular chaperone) to ensure correct folding and stability (Boyd et al., 2012). Sialic acid may be added to galactose, GalNac or both (Berthoux et al., 2012). IgA2 possesses a hinge region that lacks serine and threonine residues, and is therefore not *O*-glycosylated (Kiryluk and Novak, 2014).

1.1.4 Functions of IgA

Secretory IgA is believed to aggregate and immobilise bacteria, inhibiting their adherence to mucosal surfaces. IgA is also capable of activating the alternative complement pathway. In the gut, secretory IgA acts as a barrier to limit the access of intestinal antigens to the blood circulation, by processes collectively known as ‘immune exclusion’ (Pabst, 2012). These include entrapping antigens in the mucus preventing their binding to cell surface receptors, reducing bacterial motility limiting their invasiveness, and assisting uptake of antigens across the intestinal epithelium to lymphoid compartments (Kadaoui and Corthésy, 2007). IgA may also neutralise antigens within epithelial cell endosomes and promote their excretion into the intestinal lumen (Robinson et al., 2001).

The role of serum IgA in the immune system is less well understood, but involves removal of circulating antigens (Weisbart et al., 1988). Patients who have IgA deficiency do not appear to be majorly immunocompromised, although interestingly, they do appear to be more susceptible to autoimmune and allergic disorders, suggesting that IgA also plays a regulatory role in the immune response (Schaffer et al., 1991).

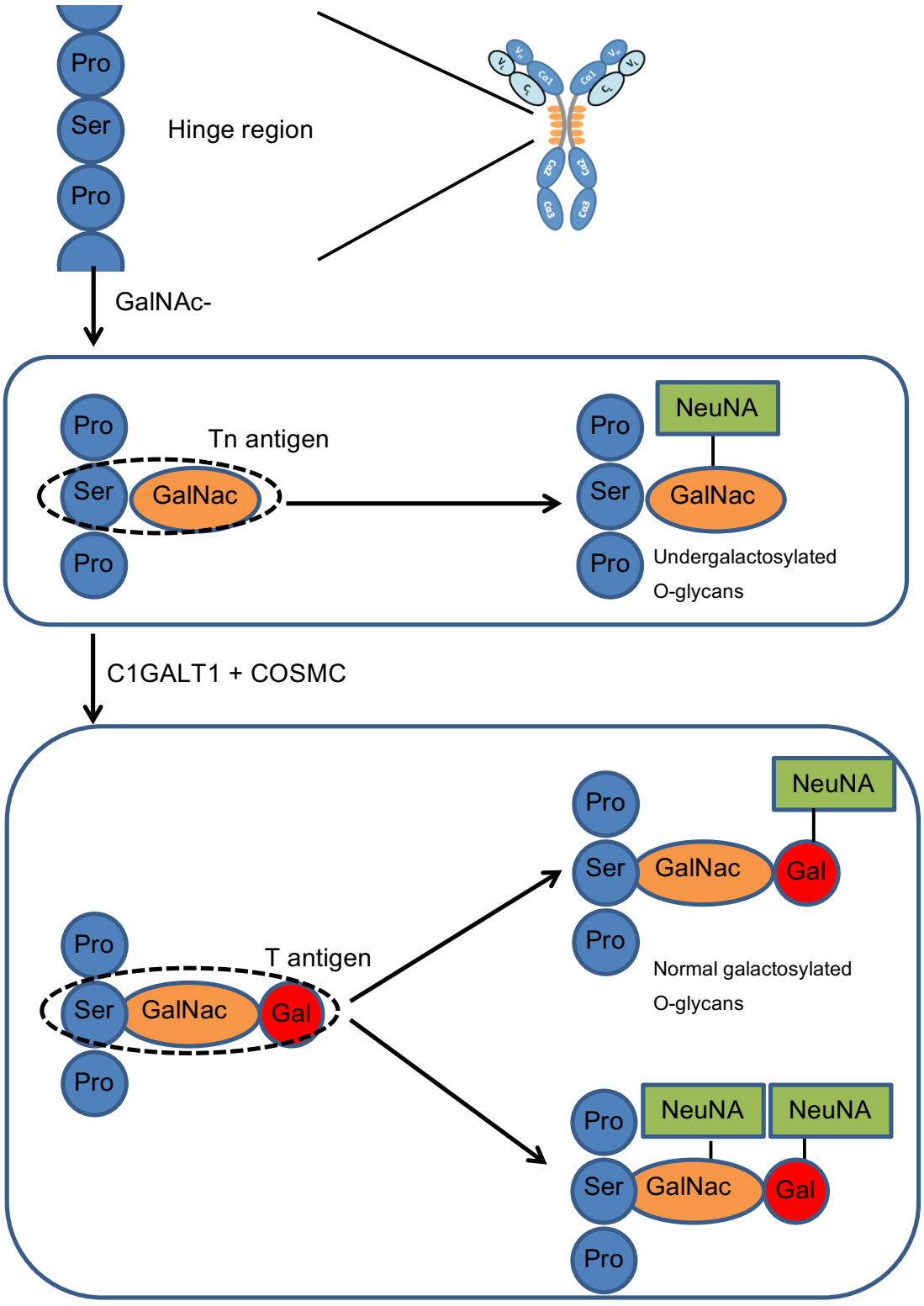
Pro
Ser
Pro
Hinge region
GalNAc-
Pro
Ser
GalNac
Pro
Tn antigen
Pro
NeuNA
Ser
GalNac
Pro
Undergalactosylated
O-glycans
C1GALT1 + COSMC
Pro
Ser
GalNac
Gal
Pro
T antigen
Pro
NeuNA
Ser
GalNac
Gal
Pro
Normal galactosylated
O-glycans
Pro
NeuNA
NeuNA
Ser
GalNac
Gal
Pro

Figure 2: O-glycan variants of IgA1. Synthesis of O-linked glycans occurs in a stepwise manner, beginning with attachment of N-acetylgalactosamine (GalNac) to serine or threonine residues by GalNac-transferase. Galactose may be β1,3 linked to GalNac, by the activity of core 1 β1,3 galactosyltransferase (C1GALT1) and its molecular chaperone Cosmc. Sialic acid (NeuNac) may be added to GalNac, Gal or both. If sialic acid is added to GalNac before attachment of Gal, subsequent addition of Gal is prevented. In patients with IgAN, there is a higher proportion of IgA1 molecules with a hinge region that have less than 3 galactose residues attached (undergalactosylated IgA1). Adapted from Schmitt, 2012.

1.1.5 Cell surface receptors for IgA

Known human IgA cell surface receptors include those from the Ig superfamily (FcαR1 (or CD89), Fcα/μR, polymeric Ig receptor (pIgR)), the lectin family (asialoglycoprotein receptor (ASGP-R)), and the transferrin receptor (TfR1 or CD71). Of these, only CD89 binds IgA exclusively, while the others bind to additional ligands (IgM for Fcα/μR and pIgR, and non-Ig ligands for ASGP-R and TfR1) (Floege et al., 2014). In mesangial cells, of these receptors, only expression of TfR1 and Fcα/μR have been demonstrated. Mesangial cells may express a further novel Fcα receptor that is yet to be fully characterised (Barratt et al., 2000).

Human FcαR1 (CD89), is a 50-100 kDa glycoprotein that is constitutively expressed by cells of myeloid lineage, including monocytes, neutrophils, macrophages, dendritic cells, eosinophils, and hepatic Kupffer cells (Woof and Mestecky, 2005). CD89 binds to both IgA1 and to IgA2 with high affinity. It preferentially binds to pIgA compared to mIgA, and does not bind to secretory IgA (Herr et al., 2003; Monteiro and Van De Winkel, 2003). Signalling responses are mediated by association of a charged arginine residue within its transmembrane domain with the common Fc receptor γ subunit (FcRγ), an immunoreceptor tyrosine-based activation motif (ITAM) containing protein. CD89 induces phagocytosis of IgA-complexed antigens, initiates antibody-dependent cellular cytotoxicity, and is important for clearance of IgA from the circulation (Fanger et al., 1980; Gorter et al., 1987; Morton et al., 1995).

On activation, a soluble form of CD89 (sCD89) is released from the surface of monocytic cells, and circulates in a covalently linked complex with IgA (van der Boog et al., 2002; van Zandbergen et al., 1999). If IgA binds to CD89 without antigen, then antibody recycling and an anti-inflammatory response occurs, via induction of an inhibitory configuration of the FcRγ (Pasquier et al., 2005). At least three isoforms of sCD89 have been described from *in vitro* experiments, although only two of these have been isolated from *in vivo* studies (Boyd and Barratt, 2010; Launay et al., 2000). The larger 50-70kDa isoform has only been found in the serum of IgAN patients. Patients with progressive IgAN, defined as doubling of serum creatinine or reaching stage 5 CKD, possessed reduced levels of sCD89-IgA1 immune complexes (Vuong et al., 2010), with some postulating that this is due to mesangial trapping of these complexes (Berthelot et al., 2012).

Fcα/μR is a type 1 transmembrane protein that binds both IgA and IgM. It is expressed in kidney, liver, spleen, thymus, small and large intestine, placenta and testis (Sakamoto et al., 2001; Shibuya et al., 2000). Fcα/μR has been reported to mediate endocytosis of IgM-Staphylococcus aureus immune complexes in B lymphocytes (Shibuya et al., 2000).

The pIgR is an integral membrane secretory component, which is expressed on most human secretory epithelial cells and transports IgA to mucosal surfaces (see Section 1.1.1). pIgR may also bind IgA-antigen immune complexes, resulting in antigen clearance.

ASGPR is an integral transmembrane glycoprotein that is present on hepatocytes and plays a role in the clearance of IgA, by recognising terminal galactose (Gal) or N-acetylgalactosamine residues. Human ASGPR consists of two units, H1 and H2.

Transferrin receptor (TfR1 or CD71) is a multi-ligand receptor that binds to transferrin, arenavirus, haemochromatosis protein and IgA1, but not IgA2 (Coulon et al., 2011). CD71 preferentially binds to pIgA1. It is expressed ubiquitously by proliferating cell types, including by renal mesangial cells.

1.2 IgA Nephropathy

IgAN was first described in 1968 by Berger and Hinglais as *les dépôts intercapillaires d'IgA-IgG* (intercapillary deposits of IgA-IgG) and is now recognised as the commonest form of primary glomerulonephritis worldwide (Berger and Hinglais, 1968; D'Amico, 1987). Diagnosis is made histologically, where there is deposition of IgA in the renal mesangium.

1.2.1 Epidemiology

Annual incidence has been estimated to be 1 case per 100 000 persons in the United States, and as high as 10 cases per 100 000 children in Japan (Utsunomiya et al., 2003; Wyatt and Julian, 2013; Wyatt et al., 1998). However the true prevalence of IgAN is unknown due to the requirement of a renal biopsy for diagnosis. In a Japanese study, glomerular IgA deposition was found in 16% of donor kidneys at zero-hour biopsy, and 1.6% displayed mesangioproliferative changes with co-deposition of C3, suggesting that the prevalence of clinically silent undiagnosed IgAN may be high (Suzuki et al., 2003). Peak incidence is between the 2nd and 3rd decade, although IgAN may affect patients of any age (Barratt et al., 2008).

The reported incidence of IgAN varies greatly amongst countries, accounting for around 40% of native renal biopsies in Asia, 20% in Europe, 5-10% in North America, and less than 5% in central Africa (Mestecky et al., 2013) (Figure 3). Some of this variability may be attributable to differences in clinical practice and thresholds for renal biopsy. For example, in countries where screening programmes for urinary abnormalities exist, more patients will be identified, who may then proceed to having a renal biopsy. A correlation between the number of renal biopsies performed per country, and the incidence of primary glomerulonephritis and IgAN has been observed (Figure 4). In keeping with this, the same study showed that between two centres in Scotland located only 100 kilometres apart, there was a 70% difference in the incidence of IgAN, which was associated with a markedly higher number of renal biopsies performed per year by one of the centres (13). This implies that increasing the number of people subjected to renal biopsy, presumable for minor urinary abnormalities, will increase the identification of IgAN.

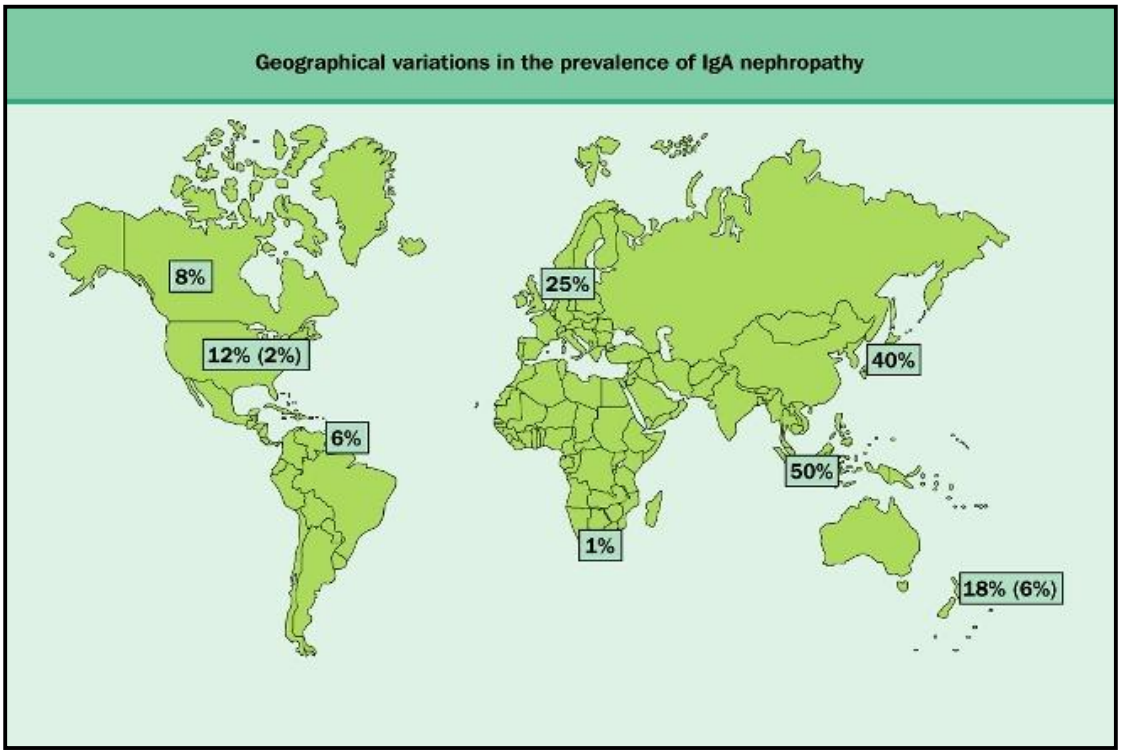

Figure 3: Geographical variations in the prevalence of IgAN. Percentages represent the proportion of cases of IgAN compared to all native kidney biopsies performed. The numbers in brackets represent minority racial groups, African Americans in the United States of America, and Polynesians in New Zealand. From Feehally and Floege, 2010.

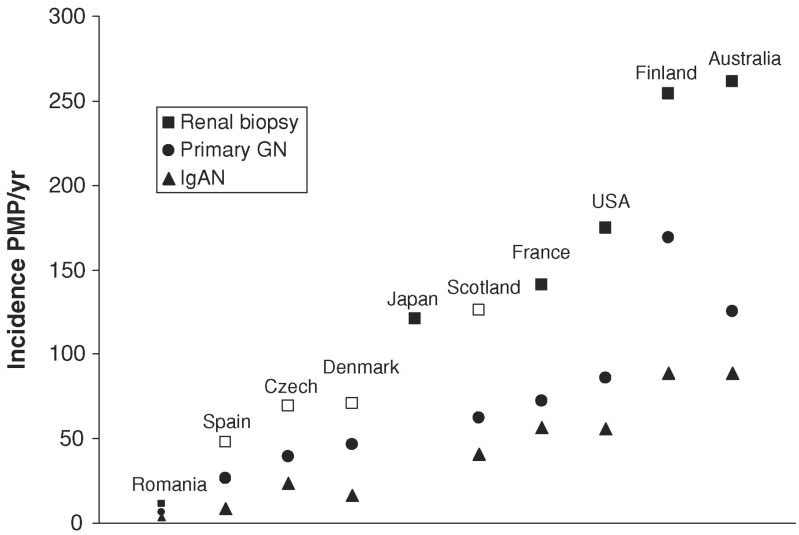

Figure 4: Reported rates of biopsy incidence per million population (PMP) in published studies from national (closed squares) and regional (open squares) native renal biopsy registries. Renal biopsy incidence appears to correlate with the incidence of primary glomerulonephritis and IgAN. From McQuarrie et al., 2009.

However, data from migrant populations suggest that true variation in susceptibility exists between people of different ethnicities. In Australia, East and South-East Asian-born patients had higher rates of IgAN accounting for ESRD compared to those born in the Middle East, Southern Europe or Australia (Stewart et al., 2004). In the USA, patients of an Asian or Pacific Island ethnicity had higher rates of IgAN than other glomerular diseases (Hall et al., 2004), whereas IgAN is much less common in African-Americans than in other ethnic groups (Feehally and Floege, 2010).

The distribution of IgAN between genders also varies according to geographical region. In North American and Western European cohorts, a male preponderance is reported, with the male-female ratio of patients with IgAN being approximately 2:1, whereas in Asia, the ratio is around 1:1 (Barratt and Feehally, 2013; Wyatt and Julian, 2013).

In certain cases, environmental factors may also play a role, although conflicting data exist. It has been hypothesised that an inverse relationship between IgAN and membranoproliferative disease exists, the former being more prevalent in countries with a higher gross domestic product and vice versa (Johnson et al., 2003). In contrast, an observational study from Scotland found that there was a higher number of renal biopsies performed on patients from areas of socio-economic deprivation, and that a higher proportion of these patients were diagnosed with IgAN (McQuarrie et al., 2014). Although most studies have found a low prevalence of IgAN amongst African-American populations (Feehally and Floege, 2010; Korbet et al., 1996), two studies conducted in specific regions of the USA have found equivalent prevalence, leading to suggestions that environmental factors may have played a role (Sehic et al., 1997; Wyatt et al., 1998).

1.2.2 Genetic factors

Genetic factors are likely to play a contributory role in IgAN, as firstly, marked differences in the incidence of IgAN exist between different ethnic groups which persist in migrant populations, and secondly, familial aggregation of IgAN is well recognised.

Familial clustering of IgAN has been reported from Europe, North America and Asia, although in some of these cases, affected relatives were identified on the basis of urinary abnormalities alone (Johnston et al., 1992; Levy, 1989; Rambausek et al., 1987; Schena et al., 1993; Scolari et al., 1999; Tam et al., 2009). Members of the Northern Italian village of Valtrompia were found to have a 3.5 fold higher risk of developing ESRD from IgAN or other primary glomerular diseases compared to the national average (C Izzi et al., 2006). Patients with IgAN were subsequently identified as having common ancestors from the 16^{th}-17^{th} centuries.

In most reported families, inheritance occurs in an autosomal dominant pattern with incomplete penetrance (Kiryluk and Novak, 2014). Clinical features of familial and sporadic IgAN are similar at presentation, with no discernable differences in the nature of immunoglobulin or C3 deposition on renal histology (Lai, 2012). Prognosis has been reported to be worse in certain cases of familial IgAN compared to sporadic IgAN (Schena et al., 2002), but not in others (Claudia Izzi et al., 2006; Julian et al., 1988). Familial IgAN has important clinical implications, for example for the selection of appropriate living related kidney donors for transplantation. Familial forms are thought to account for approximately 5% of all cases of IgAN (Mestecky et al., 2013). However, as the diagnosis of IgAN is made on renal histology, the true prevalence of familial IgAN is unknown, as a biopsy may not be performed in relatives of an index case who have isolated urinary abnormalities. Furthermore, as urinary abnormalities may occur intermittently, cases of IgAN may remain undetected. Additionally, other causes of non-visible haematuria have been reported in relatives of patients with IgAN, including thin basement membrane nephropathy, IgM nephropathy and Henoch-Schönlein purpura (Frasca et al., 2004; Lai, 2012; Levy, 1989).

A number of candidate gene loci that segregate in a Mendelian fashion have been reported in familial cases, including 2q36, 6q22-q23, 3p24-23, 4q26-q31 and 17q12-q22; however no causative genes from these loci have been identified (Maxwell and Wang, 2009). In addition, a number of candidate genes studies have been performed for sporadic IgAN, focusing on genes involved in adaptive immunity (HLA, IgA Fc receptors), cytokine signalling (TGF-β1, TNF) and

glycosylation pathways (C1GALT1, ST6GALNAC2, Cosmc) (Kiryluk et al., 2010). However, findings from these studies have in general been inconsistent.

Galactose-deficient IgA1 has been identified to be an inheritable trait (see Section 1.3.1), and was identified in 47% and 25% of first degree relatives with familial and sporadic IgAN respectively (Gharavi et al., 2008). Elevated levels have also been found in relatives of paediatric patients and those with HSP (Kiryluk et al., 2011). Elevated serum levels of macromolecular undergalactosyated IgA1 have been identified in relatives of patients with familial IgAN (Tam et al., 2009). However as most relatives with raised levels of galactose-deficient IgA1 do not develop any manifestations of renal disease, additional factors are believed to be involved in the pathogenesis of IgAN.

1.2.2.1 Genome wide association studies

With the advance of high-density genotyping technology, there has been great interest in the use of genome wide association studies (GWAS) in IgAN. A GWAS examines a large number of common genetic variants, typically single nucleotide polymorphisms (SNPs), across the entire genome to ascertain whether there are any variants that are associated with a disease. Although by design, examining common susceptibility variants means that those identified may only have a small effect, a GWAS provides an unbiased examination of disease associations in the absence of an *a priori* hypothesis.

The first genome-wide association study (GWAS) in IgAN involved 533 patients with IgAN with white European ancestry from the UK MRC/Kidney Research UK National DNA bank for Glomerulonephritis, and examined approximately 300000 SNPs. An association was found within the HLA-DQ loci, with a weaker signal from the HLA-B loci (Feehally et al., 2010). Subsequently, a GWAS involving a discovery cohort of 2096 cases and controls of Chinese ethnicity, and follow-up in Chinese and European cohorts involving 1950 cases and 1920 controls identified 5 susceptibility loci: three on chromosome 6p21 in the major histocompatibility complex (MHC), one in the complement factor H (CFH) gene cluster on chromosome 1q32, and one on chromosome 22q12 (Gharavi et al., 2011). The 6p21 loci include genes that encode components of class I and class II MHC responses. The loci on chromosome 1q32 encode a common deletion of *CFHR3*

and *CFHR1* (*CFHR3-CFHR1* deletion). Chromosome 22q12 encodes *HORMAD2*, leukaemia inhibitory factor and oncostatin M, which are involved in the mucosal immune system. All polymorphisms in the detected loci were associated with a reduced risk of developing IgAN. Based on these five loci, a genetic risk score was devised, with risk of IgAN varying up to 10 fold between those with no polymorphisms in these alleles and those with polymorphisms in five or more alleles (Gharavi et al., 2011).

A further GWAS in a Chinese cohort replicated four of these loci (the locus on chromosome 22q12 and the three loci on chromosome 6p21) and identified two new loci on chromosome 17p23 (centred on TNFSF13, encoding a proliferation-inducing ligand (APRIL) which influences IgA-producing B lymphocytes) and chromosome 8p23 (*DEFA* gene cluster, encoding α-defensins) (Yu et al., 2012).

Recently, a fourth GWAS has been performed incorporating populations from all three previous GWAS and including additional populations from Europe and Asia (Kiryluk et al., 2014). Nine previously reported signals were replicated in this study (CFHR3-CFHR1 deletion, 4 from the *HLA-DR-HLA-DQ* region, *TAP2-PSMB9*, *HLA-DP*, *DEFA*, *TNFSF13* and *HORMAD2*), and six new associations were identified, four in *ITGAM-ITGAX*, *VAV3* and *CARD9*. Many of these newly reported loci are associated with risk of inflammatory bowel disease, or maintenance of the intestinal epithelial barrier and defence against mucosal pathogens.

1.2.3 Clinical course

Given the variety of histological patterns associated with IgAN (see Section 1.2.4), it is unsurprising that patients may present to clinical attention in a number of different ways. The mode of presentation largely differs according to the age at which patients present to clinical attention (Figure 5).

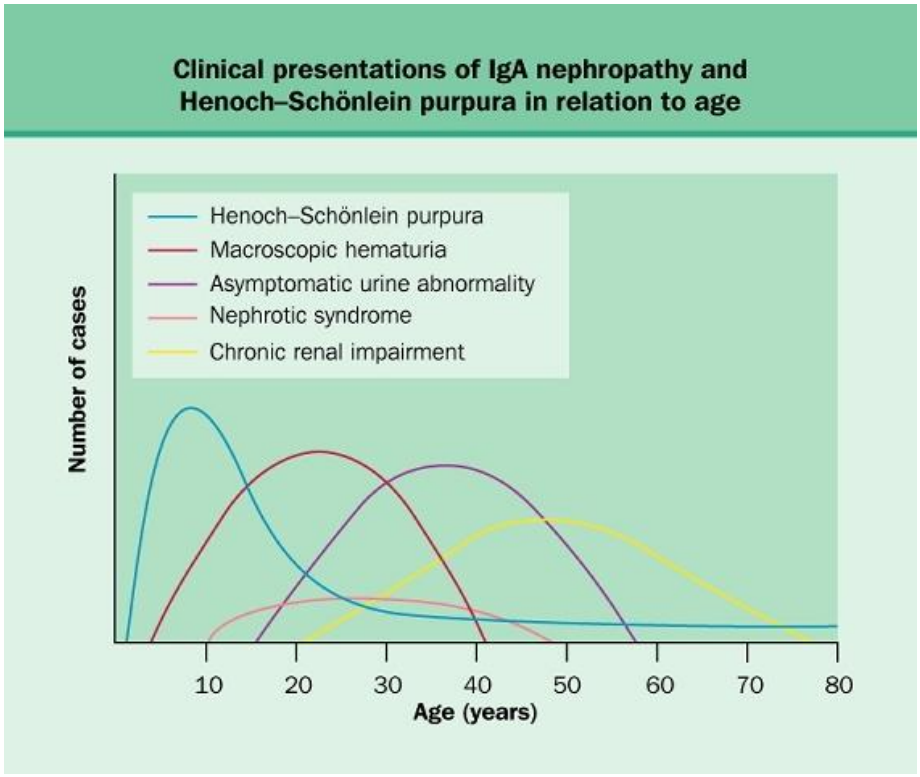

Figure 5: Clinical presentations of IgAN and Henoch-Schönlein purpura in relation to age. Differing modes of clinical presentation are more common in specific age groups. From Feehally and Floege, 2010.

1.2.3.1 Asymptomatic non-visible haematuria

The majority of patients present in this manner, and may be identified by urinalysis, for example via a screening programme, or during work-up for unexplained CKD, proteinuria or hypertension.

1.2.3.2 Visible haematuria

Approximately 30-40% of patients present with painless visible haematuria (Tumlin et al., 2007). This may coincide with a mucosal infection, most commonly an upper respiratory tract infection, but can also accompany a gastrointestinal infection or physical exercise (Eitner and Floege, 2012). This mode of presentation is more common in children and is infrequent in those over the age of 40 years. Recurrent flares of visible haematuria may occur, whereas it is rare for a patient who initially presents with non-visible haematuria to develop this, implying that these two modes of presentation represent different disease mechanisms (D'Amico, 1987).

1.2.3.3 Nephrotic syndrome

Although nephrotic range proteinuria in the context of IgAN is not uncommon, overt nephrotic syndrome is rare, affecting around 5% of patients. There may be evidence of minimal change disease on electron microscopy, with effacement of podocyte foot processes (Lai et al., 1986). Whether these two conditions can develop as part of the same disease process or represent two completely separate pathologies that co-exist is unclear.

1.2.3.4 Acute kidney injury (AKI)

AKI in the context of IgAN is rare, affecting less than 5% of patients, and occurs in the context of two presentations in IgAN: cast nephropathy due to intratubular red cell cast formation during episodes of visible haematuria, which is usually self-limiting, or a rapidly progressive glomerulonephritis, caused by crescentic disease. The latter is associated with a particularly poor prognosis and often does not respond to immunosuppression.

1.2.3.5 Secondary forms of IgAN

1.2.3.6 Henoch-Schönlein purpura

Henoch-Schönlein purpura (HSP) is a systemic small vessel vasculitis which mostly affects a younger age group than IgAN. It may affect the skin, joints, gut and kidneys leading to a characteristic set of symptoms of rash, arthralgia, abdominal pain and nephritis respectively. Renal histology is indistinguishable from IgAN, and therefore HSP has been likened to being a systemic form of IgAN (Waldo, 1988). Indeed, there are many links between these two conditions. Identical twins have been reported, where following an adenovirus infection, one developed HSP with systemic symptoms and the other developed IgAN with only renal-limited symptoms (Meadow and Scott, 1985). Both diseases have also been reported in the same patient (Ravelli et al., 1996). Between one and two thirds of cases of HSP are preceded by a mucosal infection (Haycock, 1992). Lastly, there is an elevated level of undergalactosylated IgA in the serum in HSP compared to controls, similar to that in IgAN (Kiryluk et al., 2011).

The main differences between these conditions are that HSP tends to affect a younger age group, with peak incidence being between 3 and 15 years, and secondly, presentation with AKI or heavy proteinuria is more common (Davin et al., 2001). The mechanisms that underlie these differences are unclear.

1.2.3.7 Other secondary forms of IgAN

IgAN is associated with a number of other conditions. In liver cirrhosis, impaired removal of IgA-immune complexes by Kupffer cells may lead to glomerular IgA deposition (Amore et al., 1994). In adults this occurs most often with alcoholic liver disease and less commonly viral hepatitis, and in children most often with alpha-1 antitrypsin deficiency and biliary atresia. However, progressive IgAN in such cases is rare. In HIV, there may be an increase in IgA production and subsequent IgA deposition, although there is often no other evidence of glomerular injury or disease. In coeliac disease, patients may have an increase in anti-gliadin IgA antibodies. Case reports have been published where in individuals diagnosed with both IgAN and coeliac disease, introduction of a gluten free diet led to resolution of haematuria, and improvement of renal function (Koivuviita et al., 2009; Woodrow et al., 1993).

1.2.4 Histology

IgAN is associated with a wide variety of histological patterns, and this is reflected in the variability of its clinical course. Patterns range from glomerular IgA deposition with no other evidence of histological change, to pathology that resembles minimal change disease (i.e. podocyte foot process effacement on electron microscopy), proliferative disease with mesangial and endocapillary hypercellularity, focal and segmental glomerulosclerosis, chronic kidney disease with glomerulosclerosis and tubulointerstitial fibrosis, crescentic glomerulonephritis with necrotising lesions, or a combination of the above.

Glomerular IgA deposition appears to be common and may, in some individuals, never reach clinical attention. From autopsy series, approximately 4-10% of individuals studied were found to have incidental histological evidence of mesangial IgA deposition (Sinniah, 1983; Varis et al., 1989; Waldherr et al., 1989). A study of donor kidneys, from individuals previously assessed and deemed suitable, found evidence of mesangial IgA deposition in as many as 16% at time of transplantation

(Suzuki et al., 2003). The number of cases that reach clinical attention has been referred to as the 'tip of an iceberg' (Waldherr et al., 1989).

The hallmark of IgAN on renal biopsy is dominant or co-dominant mesangial deposition of IgA, alone or with IgG, IgM, or both. IgA deposition is usually mesangial, although capillary wall IgA deposits may be present in up to one third of patients, where they are associated with greater mesangial and endocapillary hypercellularity, and worse renal outcome (Bellur et al., 2011; Roberts, 2014; Yoshimura et al., 1987). IgG co-deposition ranges between 15-85% in published series, and is reported as an independent risk factor for worse renal outcome (Jennette, 2007; Roberts, 2014). The complement component C3 is found in over 90% of cases, and components of the alternative pathway of complement activation properdin and Factor H may often be found (Roberts, 2014). In a study of renal biopsies from 60 patients with IgAN, one quarter had evidence of complement activation via the lectin pathway, with mannose-binding lectin (MBL), L-ficolin, MBL-associated serine proteases (MASP) and C4d deposition. These cases were associated with worse histological damage and greater proteinuria (Roos et al., 2006). Features of HSP are indistinguishable from those of IgAN on renal biopsy.

On light microscopy, glomerular features include mesangial matrix expansion, mesangial cell proliferation, focal necrosis, segmental glomerulosclerosis and/or crescent formation (Figure 6). Tubulointerstitial fibrosis may be present. Electron microscopy shows mesangial and paramesangial electron dense material corresponding to the immune deposits seen on immunofluorescence microscopy.

In 2009, the Working Group of the International IgA Nephropathy Network and the Renal Pathology Society proposed a new classification for histological features in IgAN. Histological features of IgAN were identified, that could be observed by independent pathologists with high reproducibility. Four of these, mesangial hypercellularity (M), endocapillary proliferation (E), segmental glomerulosclerosis (S) and tubular atrophy and interstitial fibrosis (T), were shown to have prognostic significance (Cattran et al., 2009).

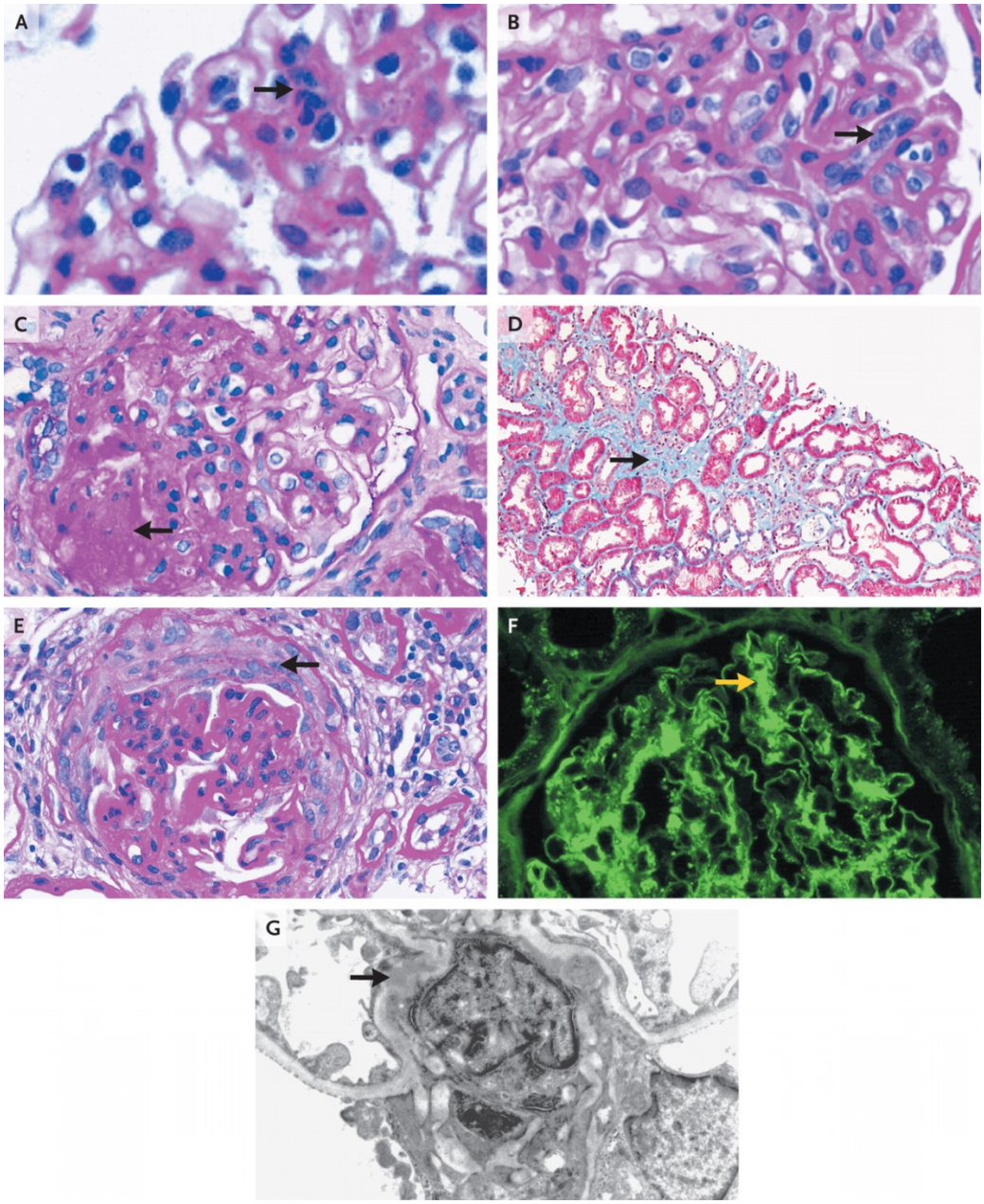

Figure 6: Pathological characteristics of IgAN. (A) Mesangial hypercellularity, with four or more cells per mesangial area (arrow). (B) Segmental endocapillary proliferation with occlusion of the capillary lumen (arrow). (C) Segmental glomerulosclerosis and adhesion, with focal accumulation of hyaline and obliteration of the capillary lumen (arrow). (D) Tubular atrophy and interstitial fibrosis with loss of tubules (arrow). (E) A glomerular crescent. (F) Diffuse mesangial staining for IgA (arrow). (G) Electron dense material in the mesangial area (arrow). (A – C, and E): Periodic acid-Schiff stains, (D) Masson's trichrome stain, (F) Immunofluorescence stain with fluorescein-conjugated anti-IgA antibodies, (G) Electron microscopy image. From Wyatt and Julian, 2013.

1.2.5 Prognosis and treatment

Despite modern treatment, approximately 20-40% of patients develop progressive CKD leading to ESRD within 20 years of diagnosis, necessitating renal replacement therapy (RRT) in the form of dialysis or transplantation which themselves are associated with far greater rates of death compared to the general population (D'Amico, 2004). Others may undergo a clinically indolent course with stabilisation or improvement of kidney function, and may or may not be affected by episodes of frank haematuria. Clinical factors independently associated with worse prognosis include impaired GFR at presentation, hypertension and proteinuria. Of these, proteinuria is the most accurate predictor of progression.

There are currently no specific treatments available to slow or stop progression of IgAN, other than anti-hypertensive and anti-proteinuric medications such as renin-angiotensin blockade with angiotensin converting enzyme inhibitors or angiotensin receptor blockers, in common with other glomerulonephritides. Registry data has demonstrated that reduction of proteinuria to <1g/24h results in significantly improved renal survival (Reich et al., 2007). A 6-month course of corticosteroids is suggested for patients with persistent proteinuria >1g/day and GFR > 50 mL/min per 1.73 m^2 who do not respond to the above measures ("Chapter 10: Immunoglobulin A nephropathy.," 2012).

1.3 Pathogenesis of IgA nephropathy

Observations that IgA deposition recurs in approximately 50% of kidneys after transplantation, and that kidneys with IgA deposits inadvertently used for transplantation were shown to be clear of deposits on follow up renal biopsy have led to the conclusion that the defect in IgAN is systemic and not confined to the kidney (Bumgardner et al., 1998; Sanfilippo et al., 1982; Silva et al., 1982).

It is believed that multiple 'hits' are required for development of the disease, including: (1) Increased galactose deficient IgA1 production, (2) Production of anti-glycan antibodies, (3) Formation of pathogenic IgA1-containing circulating immune complexes, and (4) Glomerular injury (Suzuki et al., 2011).

1.3.1 Characteristics of IgA in IgA nephropathy

Serum IgA in IgAN possesses a number of abnormalities. The most striking, believed to be central to the pathogenesis of IgAN, is that there is an increase in serum IgA1 with hinge region *O*-glycans that lack terminal galactose, and instead possess truncated forms with either terminal GalNac or sialylated GalNac (see Section 1.1.3 and Figure 2). These forms of IgA1 are interchangeably referred to in the literature as being galactose-deficient, undergalactosylated (or glycosylated), poorly galactosylated/glycosylated, or aberrantly galactosylated/ glycosylated. Other abnormalities include raised serum IgA levels, which are found in approximately 50% of patients, although there is no correlation with disease severity or risk of progression. There is an increase in the proportion of polymeric compared to monomeric serum IgA. Serum IgA in IgAN tends to be anionic, and there is an over-representation of lambda light chains. IgA eluted from mesangial deposits in IgAN in a number of studies reflects these changes, specifically that it is almost exclusively of the IgA1 isotype, and primarily undergalactosylated, polymeric, anionic, and with a predominance for lambda light chains (Allen et al., 2001; Conley et al., 1980; Giannakakis et al., 2007; Hiki et al., 2001; Mestecky et al., 2013; Monteiro et al., 1985). Therefore this form of IgA1 is believed to be particularly pathogenic in IgAN. Concurrent IgA2 deposition has also been reported infrequently, and was found in up to 50% of Japanese patients in one case series (André et al., 1980; Hisano et al., 2001).

Since IgD can be normally *O*-galactosylated in IgAN, the galactosylation defect does not appear to be a generic feature of B-lineage cells, and instead is thought to occur after class switching to IgA1 (Allen et al., 1995; Smith et al., 2006a). In patients, only a small proportion of IgA1 is undergalactosylated while the remainder may be normally galactosylated, suggesting that a subset of IgA1-committed B cells is responsible for synthesising this form of IgA (Barratt and Feehally, 2011). The main sites at which B cells that synthesise undergalactosylated IgA1 are produced and reside remain unclear. As hinge region undergalactosylation is more commonly associated with mucosal IgA1 rather than serum IgA1, IgA1 may be 'mis-homed' to the serum compartment following a mucosal antigen stimulus, although the mechanism behind this remains unclear (Barratt et al., 2009). Serum levels of galactose-deficient IgA1 were increased in response to the mucosal antigen *Helicobacter pylori* and mucosal vaccines in IgAN patients compared to healthy controls. In contrast, systemic antigen challenge was associated with production of IgA1 with increased terminal galactose residues (Barratt et al., 1999; Smith et al., 2006b).

1.3.2 Effects of undergalactosylated IgA1

Undergalactosylated IgA1 has a propensity for self-aggregation and for IgG or IgA autoantibody formation towards a hinge-region 'neo-epitope' (Suzuki et al., 2009; Tomana et al., 1999, 1997). Utilising EBV-transformed IgG secreting B lymphocytes from IgAN patients, IgG autoantibodies have been shown to have specificity for the GalNac epitopes within the undergalactosylated IgA1 hinge region (Suzuki et al., 2009; Tomana et al., 1999). Furthermore, in patients, levels of IgG directed against galactose-deficient IgA1 correlated with the degree of proteinuria (Suzuki et al., 2009). Together with GWAS data highlighting susceptibility loci within the MHC complex, these findings support an autoimmune disease model in IgAN, rather than a model of overproduction of IgA with reduced clearance. Recent structural studies conducted by analytical ultracentrifugation and X-ray/neutron scattering demonstrated that undergalactosylated monomeric IgA1 had a higher tendency to self-aggregate, but that there was no difference in solution structure compared to normally galactosylated IgA1 (Hui et al., 2015).

IgA-immune complexes have a strong affinity for the extracellular matrix components fibronectin and collagen (Coppo et al., 1993). IgA-IC have been shown

to preferentially bind and activate mesangial cells, leading to mesangial cell proliferation, extracellular matrix production, release of pro-inflammatory cytokines and growth factors, podocyte damage, and disruption of the glomerular filtration barrier and glomerular and tubulointerstitial scarring (Lai, 2012, 2003) (Figure 7). *In vitro* studies suggest that only IgA1-immune complexes >800kDa are responsible for mesangial cell proliferation (Novak et al., 2011, 2005). It is currently unclear whether immune complexes form in the serum prior to depositing in the mesangium in IgAN, or whether deposition of undergalactosylated IgA1 occurs first before formation of immune complexes *in situ* (Suzuki et al., 2011).

IgA may also form immune complexes with the soluble form of the myeloid FcαR1 or CD89 (sCD89). It has been proposed in IgAN that pIgA induces shedding of sCD89 from myeloid cells, contributing towards IgA immune complex formation and subsequent mesangial deposition.

The mechanism by which circulating IgA-IC escapes into and deposits in the mesangium remains unclear, and mesangial cell receptors for IgA are not well characterised. The IgA receptors (Section 1.1.5) CD89, polymeric Ig receptor and ASPG-R are not expressed by mesangial cells (Leung et al., 2000). The transferrin receptor (TfR; CD71) has however been found to be expressed by mesangial cells, and binds IgA, with a preference for galactose-deficient polymeric IgA1 (Moura et al., 2004, 2001). TfR is ubiquitously expressed by proliferating cell types, and therefore binding of IgA may create a positive feedback loop, with stimulation of cell proliferation and TfR expression (Moura et al., 2005).

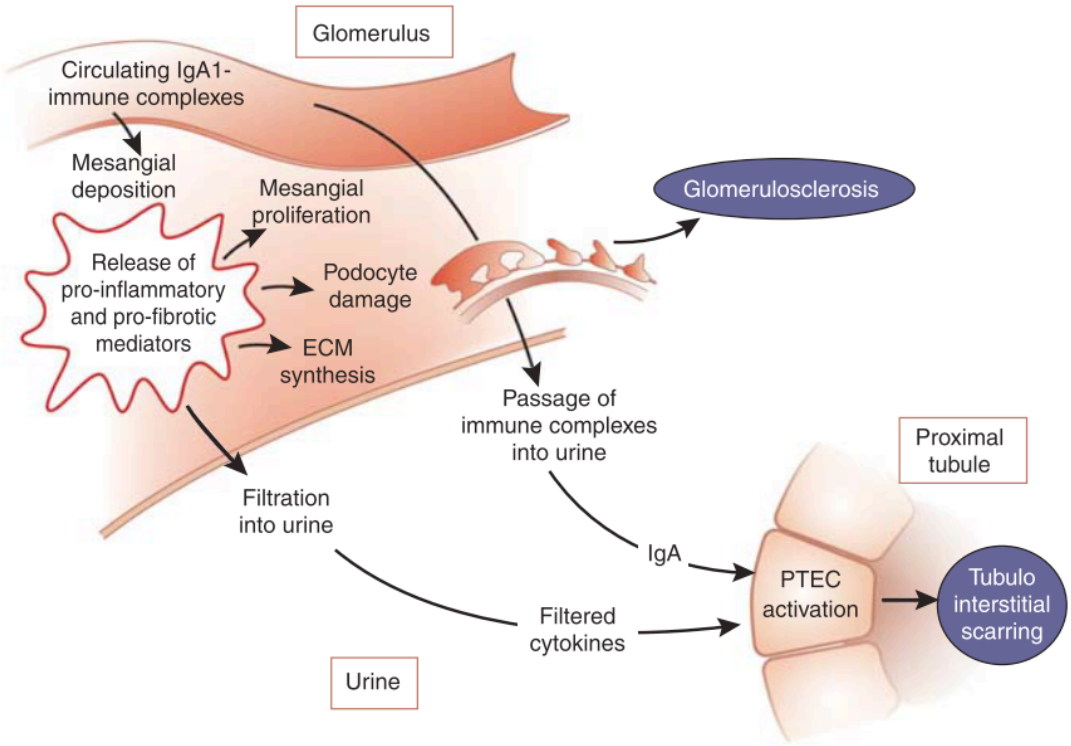

Figure 7: IgA immune complex deposition and triggering of glomerular and tubulointerstitial injury. IgA1 immune complexes deposit on to the mesangium and trigger release of pro-inflammatory and pro-fibrotic mediators, which lead to mesangial cell proliferation, podocyte damage, synthesis of extracellular matrix (ECM) components, and filtration of mediators into the proximal tubule. Continued IgA1 deposition results in progressive glomerulosclerosis due to ECM deposition. Damage to the glomerular filtration barrier also leads to increasing proteinuria, and filtration of albumin, mesangial-derived mediators and IgA1 immune complexes into the proximal tubule. These factors lead to pro-inflammatory and pro-fibrotic mediator release from PTEC into the interstitial space resulting in tubulointerstitial fibrosis. From Boyd et al., 2012.

1.3.3 Helix Aspersa agglutinin binding assay

The lectin *Helix Aspersa* agglutinin (HAA) is able to bind to terminal GalNac, and IgA1-HAA binding has been used as an ELISA based method by a number of laboratory groups to detect levels of galactose-deficient IgA1. IgA1 from healthy individuals may contain some galactose-deficient O-glycans, in particular at residues threonine 233 (Thr233) and Thr236 (Takahashi et al., 2012), and therefore an overlap in HAA-binding levels may be found between patients and healthy subjects, rendering this assay unsuitable currently as a diagnostic test. Recently, a monoclonal antibody has been developed against the galactose-deficient hinge region and tested on patient samples by ELISA, where results correlated well with the HAA-binding ELISA (Yasutake et al., 2015).

In North American Caucasian subjects, approximately 75% of patients with IgAN had levels of galactose-deficient IgA above the 90th percentile of healthy controls, as detected by an HAA-binding ELISA (Moldoveanu et al., 2007). This finding has been replicated in cohorts consisting of Italian and North American Caucasian adult IgAN patients (Camilla et al., 2011), adult Chinese patients (Zhao et al., 2012), adult Japanese patients (Shimozato et al., 2008) and in North American Caucasian or African-American children with either IgAN or HSP (Lau et al., 2007). Levels of galactose-deficient IgA have subsequently been shown to correlate with progressive IgAN in a cohort of Chinese patients (Zhao et al., 2012). A high proportion of first-degree relatives, up to 40% in one study, may have raised levels of galactose-deficient IgA1, suggesting that hereditary factors are likely to be an important factor in this process (Gharavi et al., 2008). However, the majority of these relatives had no manifestations of renal disease, implying that additional factors are required for the development of IgAN.

1.3.4 Mechanisms of tubulointerstitial injury in IgAN

IgAN is associated with a substantial risk of progressive kidney disease, with approximately 20% developing ESRD within 20 years of diagnosis (D'Amico, 2004). Despite mesangial IgA deposition being a defining feature of IgAN, there is no correlation between the degree of IgA deposition and subsequent tubulointerstitial inflammation, scarring and renal prognosis, indicating that tubular-specific processes may play a central role in driving progression. One of the strongest predictors of developing progressive IgAN and ESRD is the development of tubular atrophy and interstitial fibrosis (Cattran et al., 2009). However, the factors that link mesangial IgA deposition and the development of tubulointerstitial fibrosis are not well defined. Following mesangial IgA deposition, local inflammatory changes occur which lead to disruption of the glomerular filtration barrier. A number of mechanisms may then act independently or synergistically to promote the development of tubulointerstitial injury: proteinuria, monocyte or macrophage infiltration, direct toxic effects of filtered IgA on proximal tubular epithelial cells, and glomerulotubular cross talk (Lai et al., 2005).

In common with other glomerular diseases, a feature of progressive IgAN is the abnormal appearance of protein in the urine, due to disruption of the glomerular filtration barrier. Much recent attention has focused on the presence of proteinuria being not only a marker of kidney disease, but also a cause of progressive kidney scarring, by triggering pro-inflammatory cytokine and mediator release from PTEC (Abbate et al., 2006; Baines and Brunskill, 2011; Eddy, 2004). Clinically, the level of proteinuria is the single most important modifiable risk factor in the treatment of progressive IgAN (Reich et al., 2007).

A number of clinical observations indicate that proximal tubular cells (PTEC) are exposed to increased amounts of abnormally filtered IgA in IgAN, and that a correlation between filtered IgA and progressive CKD exists. Firstly, in a study of 98 patients, non-selective proteinuria (i.e. containing higher molecular weight proteins including immunoglobulins) was associated with worse outcome in IgAN, in terms of higher incidence of glomerulosclerosis, lower creatinine clearance and higher incidence of hypertension at four year follow up (Woo et al., 1989). Secondly, raised urinary IgA and IgG levels were observed in IgAN patients compared to patients with other glomerular and non-glomerular renal diseases and

healthy subjects (Galla et al., 1985; Matousovic et al., 2006). Urinary IgA levels also correlated with serum creatinine concentration and levels of proteinuria. Thirdly, levels of IgA-immune complexes containing undergalactosylated IgA1 were elevated in the urine in IgAN (Matousovic et al., 2006).

Experimentally, IgA1 from both IgAN patients and healthy subjects was found to bind to PTEC on assessment by flow cytometry, albeit with a lesser affinity than it does to mesangial cells (Chan et al., 2005). In this study, mRNA for known IgA receptors FcαR1, Fcα/μR, pIgR and ASPG-R were not expressed by PTEC. More recent evidence suggests that megalin, a member of the LDL receptor family and a multi-ligand endocytic scavenger receptor highly expressed on the apical surface of PTEC, may facilitate interaction between IgA and PTEC. Induction of non-selective proteinuria using an immunotoxin in megalin knockout mosaic mice, lacking expression of megalin in 60% of PTEC, led to uptake of IgA only in PTEC that expressed megalin, as well as albumin, immunoglobulin light chain, and IgG (Motoyoshi et al., 2008). It should be noted, however, that organised tubular deposits of IgA are infrequently observed in IgAN, featuring in 2 out of 51 cases in one series, without evidence of electron-dense deposits on electron microscopy (Frascà et al., 1982).

In vitro studies indicate that following stimulation by IgA, mesangial cells may release soluble factors, including cytokines, that have a stimulatory effect on PTEC, a mechanism termed glomerulo-tubular crosstalk (Lai et al., 2005). Increased proliferation and production of the inflammatory mediators tumour necrosis factor-α (TNF-α), macrophage migration inhibitory factor (MIF), soluble intercellular adhesion molecule 1 (ICAM-1) and angiotensin II were observed from primary PTEC after incubation with conditioned media from mesangial cells that had been stimulated with IgA from IgAN patients (Chan et al., 2005). These effects were not observed when PTEC were cultured with IgA directly. Stimulation of PTEC by the mesangial cell conditioned media was reduced by addition of neutralising antibodies to TNF-α, but not to IL-1β, TGF-β, or PDGF. However these studies were performed with IgA pooled from a number of patients with no data regarding whether they had progressive or non-progressive disease, and with no separation of IgA to monomeric and polymeric forms. Given that in mesangial cells, it has been established that polymeric galactose-deficient IgA1 has a particularly

stimulatory effect on mesangial cells, and as PTEC are likely to be continuously exposed to these forms of filtered IgA after glomerular filtration barrier damage has occurred (Matousovic et al., 2006), a further detailed study into whether particular forms of IgA have a directly toxic effect on PTEC is warranted and has direct clinical relevance.

1.3.5 Role of complement in IgAN

The complement system comprises a complex network of over 30 serum and cell-surface proteins that play a key role in mediating innate and adaptive immune responses, and provide defence against invading pathogens (Walport, 2001). The central converging event is stabilisation of a C3 convertase that cleaves C3, generating C3a, an anaphylatoxin, and C3b, an opsonin (Figure 8) (Cook, 2013). C3b may then form a C5 convertase that cleaves C5, generating C5a, an anaphylatoxin, and C5b. Both C3a and C5a are chemotactic factors that act in a synergistic manner (Wada and Nangaku, 2013). Production of C5b may subsequently lead to formation of C5b-9, termed membrane attack complex (MAC), that inserts into the lipid bilayer of cell membranes causing lysis of non-nucleated cells, e.g. erythrocytes. The amount of C5b-9 generated is usually insufficient to cause lysis of nucleated cells; however sublytic quantities are able to induce activation of resident cells, including in the kidney, promoting cytokine release, inflammation, and local tissue injury (Wada and Nangaku, 2013). Under normal circumstances, complement activation is tightly regulated by a number of regulatory proteins which act at several levels of this cascade, therefore limiting host tissue damage.

There are three main pathways of complement activation: the classical, lectin and alternative pathways (Figure 8). The classical pathway is triggered by interaction between IgG or IgM and antigen, and subsequent binding of the immune complex with C1q. C1qrs is subsequently formed and cleaves C2 and C4, to form C4bC2a, a C3 convertase. The lectin pathway is triggered by recognition of cell surface carbohydrates on pathogens by the plasma lectins mannan-binding lectin (MBL, also known as mannose-binding lectin), L-ficolin or H-ficolin. This leads to activation of MBL-associated serine proteases (MASP), which are present in a proenzymatic complex with these lectins. Activated MASP then leads to formation of the C3 convertase C4b2a. The alternative pathway is in a constant state of

activation (or 'tick-over') with spontaneous hydrolysis of C3 leading to formation of $C3(H_2O)Bb$, which cleaves C3 into C3a and C3b. Exposure and binding of C3b to an activating surface (e.g. bacterial surface) leads to cleavage of factor B, which in the presence of factor D and properdin, leads to formation of the alternative pathway C3 convertase, C3bBb. This C3 convertase is inherently unstable and has a short half-life of approximately 90 seconds. Properdin promotes the association between C3b and factor B, stabilising the C3 convertase and extending its half-life up to 10 fold, and acts as the only known positive regulator of the alternative pathway (Fearon and Austen, 1975). A number of negative regulators tightly regulate the alternative pathway, including circulating regulators (factor H and factor I), and cell membrane bound regulators (decay accelerating factor (DAF; CD55), membrane cofactor protein (CD46) and CD59) (Maillard et al., 2015). As discussed in Section 1.2.2.1, recent GWAS have shown that variations in complement regulator genes have an important effect regarding susceptibility to IgAN (Gharavi et al., 2011; Kiryluk et al., 2012).

There is evidence in IgAN that both the alternative and lectin pathways are commonly activated. The classical pathway is not believed to be involved, as C1q deposition occurs in less than 10% of cases, thought to be a non-specific consequence of progressive renal injury, and also IgA is unable to activate the classical pathway *in vitro*. Regarding the alternative pathway, mesangial C3 deposition may be found in over 90%, properdin is co-deposited with IgA and C3 in 75-100%, and factor H is found in up to 90% of cases (Maillard et al., 2015; Roberts, 2014). Serum levels of factor B, properdin, factor H and factor I are higher in IgAN patients compared to healthy subjects (Onda et al., 2007). Circulating alternative pathway-induced C3 breakdown products were found to be increased in IgAN patients, and were associated with subsequent decline in kidney function (Zwirner et al., 1997). In a cohort of 343 IgAN patients, low serum C3 levels (<90 mg/dl) at time of renal biopsy were found in 66 patients (19.2%), and this was associated with increased glomerular C3 deposition and worse renal outcome, defined by doubling of serum creatinine or reaching ESRD. Urinary MAC, factor H and properdin levels were also elevated in IgAN patients and correlated with worse kidney function, proteinuria, and glomerular and tubulointerstitial scarring (Onda et al., 2011). In proteinuric renal disease, properdin was shown to be deposited on the

brush border of PTEC, and *in vitro*, binds PTEC, promoting tubular deposition of C3 and generation of C5b-9 (Gaarkeuken et al., 2008).

Evidence of lectin pathway involvement was initially suspected following reports of glomerular C4 deposition in IgAN, in the absence of classical pathway activation, and with the finding of glomerular MBL deposition with IgA (Endo et al., 1998; Hisano et al., 2001; Matsuda et al., 1998). In a recent case series, 15 out of 60 IgAN patients had evidence of lectin pathway activation on renal biopsy, in terms of glomerular MBL, L-ficolin, MASP and C4d, and these patients had more pronounced renal damage and proteinuria compared to those who had no evidence of lectin pathway involvement (Roos et al., 2006). MBL is able to bind to polymeric IgA via its lectin domain, but not monomeric IgA, and results in activation of C3 and C4 (Roos et al., 2001). Urinary MBL levels were also elevated in IgAN patients, and correlated with worse renal function, proteinuria, hypertension, and more severe histological disease according to the Oxford classification (Liu et al., 2012).

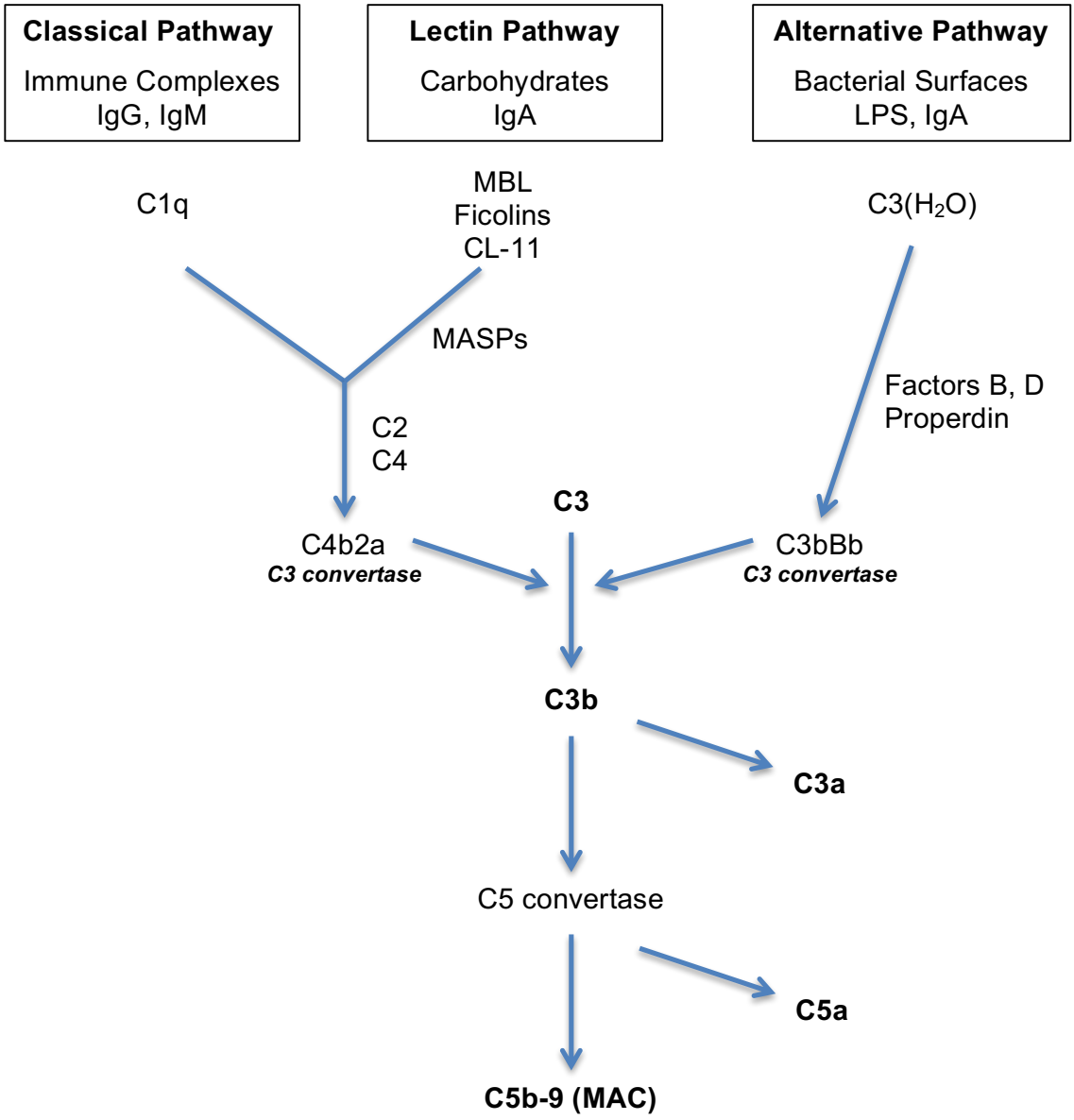

Figure 8: Schematic diagram depicting the complement system. The classical, lectin and alternative pathways of complement activation converge on the stabilisation of a C3 convertase that cleaves C3, leading to the generation of C3a, an anaphylotoxin, and C3b, an opsonin. C3b may then form a C5 convertase, leading to generation of C5a, an anaphylotoxin, and C5b, which then forms part of the membrane attack complex (MAC), C5b-9. Adapted from Berger et al., 2005.

1.4 Animal models of IgAN

Insights into the pathogenesis of IgAN have been hindered by the lack of a suitable rodent model that encompasses all the various characteristics of the human disease (Floege, 2011). This may be partly explained by differences between the structure of human and rodent IgA. Only humans and higher primates have two IgA isoforms, with IgA1 possessing a glycosylated hinge region. Murine IgA exists as one isoform, lacks an extended hinge region and structurally resembles human IgA2. Furthermore murine IgA exists predominantly as a polymer in the circulation, compared to human IgA which exists mainly in monomeric form. Mice lack a dominant hepatobiliary clearance system of IgA, which is a feature of human IgA metabolism. Mouse models may, however, provide useful information regarding the mesangial reaction to IgA deposition, and subsequent downstream responses.

Early models involved passive transfer of IgA-containing immune complexes (murine myeloma-derived IgA bound to bovine albumin) formed *ex vivo* into BALB/c mice. These mice developed diffuse granular mesangial IgA deposits with transient haematuria (Rifai et al., 1979). More recently, models involving mucosal immunisation have been developed, involving oral immunisation of a foreign inert protein antigen, followed by parenteral immunisation to form IgA antibodies that subsequently deposit in the mesangium. The earliest studies used bovine gamma globulin (BGG), chicken ovalbumin and horse spleen ferritin as antigens, with BGG giving the most consistent results (Emancipator et al., 1983a). This model results in mesangial IgA deposition, electron dense mesangial deposits, haematuria, proteinuria, but no change in serum creatinine, and has been studied previously in BALB/c mice, and Sprague-Dawley and Lewis rats (Emancipator et al., 1983a, 1983b; Gesualdo et al., 1990; Kuemmerle et al., 1999, 1998; Lai et al., 2011; Trachtman et al., 1996; Yi et al., 1996). Additionally, it has been reported that addition of a uninephrectomy after oral and parenteral BGG immunisation serves to augment renal damage and proteinuria in this model (Lai et al., 2011).

Spontaneous mouse models have also been developed in order to study mechanisms of pathogenesis in IgAN. The ddY outbred mouse strain, and the HIGA strain selectively bred from this colony that possess high circulating levels of IgA, carry a retrovirus (murine leukaemia virus) that cause mice to develop lymphomas and elevated levels of IgA and IgG2 by 40 weeks of age. These mice

develop strong IgA deposits, mesangial expansion and proliferation, and proteinuria but no haematuria or decline in renal function (Hashimoto et al., 2012; Miyawaki et al., 1997).

To investigate the putative role of CD89 (as discussed in Section 1.1.5), mouse models have been developed that express various components of the human IgA system. Transgenic mice, expressing human CD89 on monocytes and macrophages, displayed evidence of mouse IgA-human CD89 interaction on these cells, and spontaneous mesangial IgA deposition by 24 weeks (Launay et al., 2000). However, in a separate study, injection of human recombinant soluble CD89 did not induce mesangial IgA deposition (van der Boog, 2004). Subsequently, transgenic mice that express human IgA1 (α1KI mice), and both human IgA1 and human CD89 (α1KI-CD89Tg mice) have been described (Berthelot et al., 2012). α1KI mice developed endocapillary IgA1 deposits but no mesangial injury or renal dysfunction. In contrast, by 12 weeks, α1KI-CD89Tg mice developed extensive mesangial IgA1 and CD89 deposition, associated with glomerular macrophage infiltration ($CD11b^+$ and $F4/80^+$ cells), haematuria and proteinuria, and complement component (MBL and C3) deposition, suggesting that both components are required for glomerular disease to occur. Recently, a gluten free diet was shown to protect against mesangial IgA1 deposition and haematuria in α1KI-CD89Tg mice (Papista et al., 2015).

1.4.1 Studies of the proximal tubule

Investigations of proximal tubular physiology have ranged from cell culture experiments, to tissue preparations (e.g. isolated single tubules), through to studies of intact kidneys either *ex vivo* (perfusion studies) or in living animals (intravital studies). Various proximal tubular cell culture models have been used. These have included primary cell cultures, isolated from humans or other animals, or cell culture lines that have been immortalised. Although providing useful information regarding the metabolic characteristics of PTEC, isolated cell culture has certain disadvantages. PTEC may rapidly lose their phenotype in an *in vitro* setting, and display an altered metabolism, with an increase in anaerobic ATP generation, which does not occur *in vivo* (Gstraunthaler et al., 1999). Secondly, it may be difficult to replicate their anatomical polarity and therefore transport characteristics

may be greatly altered. Thirdly, the effect of neighbouring renal cell types and infiltrating cells cannot be easily studied.

1.4.1.1 HK-2 cells

HK-2 (human kidney 2) is a proximal tubular cell line previously isolated from normal adult kidney cortex, and immortalised by transfection with the human papilloma virus 16 (HPV-16) E6/E7 genes (Ryan et al., 1994). They have a phenotype characteristic of well differentiated PTEC, and express normal PTEC markers including cytokeratin. They retain characteristics including sodium-dependent, phlorizin-sensitive sugar transport, adenylate cyclase responsiveness to parathyroid but not antidiuretic hormone, and gluconeogenesis. They express the important PTEC endocytic receptors, megalin and cubulin. As such, they have been used extensively in models of drug-induced nephrotoxicity (Gunness et al., 2010). More recently, HK-2 cells were found to lack expression of members of the SLC22 drug transporter family, OAT1, OAT3 and OCT2, normally located at the basolateral surface of PTEC (Jenkinson et al., 2012). However, noting the caveats of using immortalised cell lines, HK-2 cells may provide useful information regarding human PTEC physiology.

1.4.1.2 Multiphoton microscopy

Advances in imaging techniques have led to their increased application in studies of renal physiology. The relatively recent advent of multiphoton microscopy (Denk et al., 1990) offers significant advantages over conventional single photon confocal microscopy, principally that its ability to obtain minimally invasive high-resolution images with increased depth of penetration, without causing significant photo-bleaching and injury to surrounding tissue structures, allows for visualisation of cellular and subcellular processes within living animals, which can be repeated over time (Molitoris and Sandoval, 2005). The kidney is particularly amenable to multiphoton imaging as it may be exteriorised without causing significant damage. Serial multiphoton imaging studies have revealed novel insights into important functions of the kidney, including glomerular filtration and proximal tubular handling of proteins, and the dynamic nature of podocyte motility and migration following glomerular injury (Hackl et al., 2013; Russo et al., 2007).

Multiphoton microscopy describes the simultaneous absorption of two (or more) photons simultaneously to cause fluorescence excitation, at half (or less) the wavelength and therefore energy of single photon microscopy (Figure 9). Multiphoton microscopy utilises long wavelength lasers, typically near the infrared range (700-1000 nm), which is of lower energy than the visible wavelengths used in standard confocal microscopy. As fluorophore excitation occurs only at the point where two photons arrive, the surrounding tissue is less affected by photo-toxicity than single photon confocal microscopy, where imaging of deeper structures can lead to significant photo-bleaching and tissue damage, and light scattering from out of focus planes. As such, multiphoton microscopy images can be obtained to a greater depth, currently up to around 200μm, whereas confocal microscopy is only able to reach a tissue depth of tens of microns (Dunn et al., 2002).

Munich Wistar Frömter (MWF) rats have been utilised in several multiphoton imaging studies, as they possess surface glomeruli, and allow imaging of the transition between the glomerulus and the S1 segment of the proximal tubule. Male MWF rats have an inherited deficit in nephron number, and spontaneously develop hypertension and albuminuria by around 8 weeks of age, which progresses later to overt proteinuria, focal segmental glomerulosclerosis and impaired GFR (Fassi et al., 1998). Female MWF rats also inherit the deficit in nephron number, and develop mild albuminuria, but no overt proteinuria or glomerular damage (Remuzzi et al., 1988). An alternative approach has been to induce hydronephrosis by ureteral ligation in mice, in order to study leucocyte recruitment in states of glomerular inflammation, although this approach may itself lead to tissue injury and fibrosis (Devi et al., 2012).

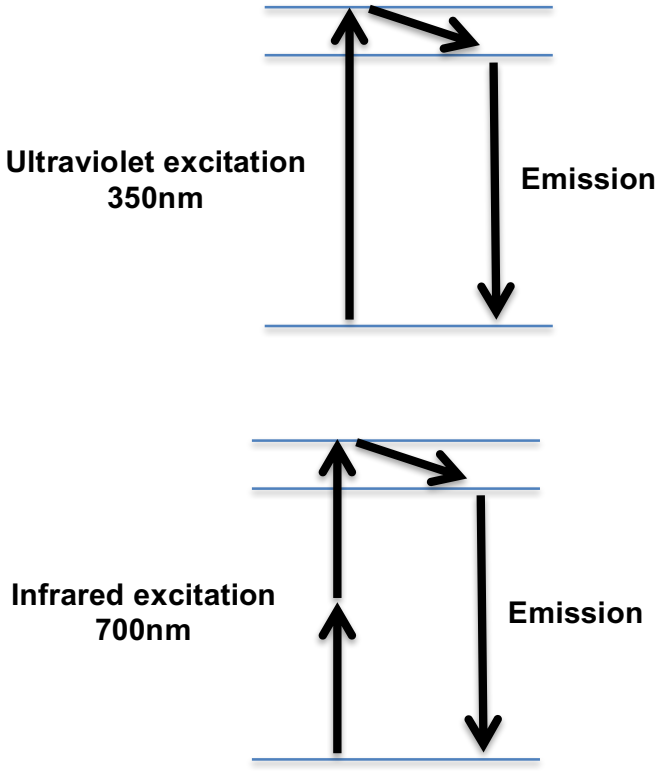

Figure 9: Principles of multiphoton microscopy. (A) In confocal microscopy, a single photon with higher energy (shorter wavelength) is required for electron excitation and light emission. (B) In multi-photon microscopy, simultaneous excitation by two or more photons with lower energy (longer wavelength) results in the identical excited state.

Aims and hypothesis

The overall aim of my thesis was to investigate mechanisms of progression of IgAN after mesangial deposition of IgA occurs, and whether filtration of IgA into the proximal tubule augments inflammation and fibrosis within the tubulointerstitial compartment.

The following hypothesis was tested: "A major factor determining the development of progressive renal failure in IgAN is the presence in the serum of IgA1 with PTEC-specific pro-inflammatory and pro-fibrotic activity. As non-selective proteinuria develops this IgA1 enters the proximal tubule and augments PTEC activation, accelerating renal scarring".

My specific aims were:

1. To investigate whether IgA interacts with PTEC *in vivo*, utilising multiphoton intravital microscopy, in wild-type animals and in models of proteinuria.
2. To investigate whether IgA has a stimulatory effect on PTEC *in vitro*.
3. To develop a mouse model of IgAN.
4. To assess whether genetic deficiency of components of the lectin pathway of complement protect against the development of glomerular and tubulointerstitial inflammation in the mouse model of IgAN.

Chapter 2: Materials and Methods

2.1 General materials

Unless otherwise stated, all reagents were purchased from Sigma-Aldrich (Poole, UK), and all plasticware and disposables from Fisher Scientific (Loughborough, UK).

2.2 Human subjects

Clinical samples were obtained from adult patients aged over 18 years with biopsy-proven IgAN, identified from nephrology outpatient clinics at the Leicester General Hospital, and from healthy subjects with no history of renal or systemic disease. Patients with Henoch-Schönlein purpura, systemic lupus erythematosus, diabetes mellitus, potential secondary causes of glomerular IgA deposition (e.g. liver disease, coeliac disease, inflammatory bowel disease, or HIV), an eGFR ≤ 30 mL/min/1.73m2, or on immunosuppression including corticosteroids were excluded. All subjects gave their written informed consent, and the following studies were approved by the Leicestershire, Northamptonshire and Rutland Research Ethics Committee.

2.2.1 Serum processing

Venous blood was collected and allowed to clot for 30 minutes at room temperature. Following this, serum was separated by centrifugation at 3000 rpm for 10 minutes at 18°C. Aliquots were stored at -80°C until required.

2.3 *In vitro* studies

2.3.1 Purification of IgA1

IgA1 was purified from the serum of patients with IgAN and healthy controls by Jacalin-agarose affinity chromatography based on a method described previously (Allen et al., 1999). High molecular weight proteins were precipitated from the serum with 45% saturated ammonium sulphate, the precipitate was washed three times with 45% saturated ammonium sulphate, and then resusupended in UltraPure 0.175M Tris HCl, pH 7.5 (Invitrogen, Thermo Fisher Scientific, Paisley, UK). The IgA1 was captured from the protein solution using Jacalin-agarose (Vector laboratories, Peterborough, UK). Unbound proteins were removed by extensive washing with 0.175M Tris HCl, pH 7.5, until the protein concentration of the eluate was <0.01 mg/mL, determined by absorbance at 280 nM using a spectrophotometer (NanoDrop 200, Thermo Scientific, Loughborough, UK). IgA1 was eluted from the Jacalin-agarose with 1M galactose in 0.175M Tris HCl. The IgA1 was dialysed overnight against phosphate-buffered saline (PBS), concentrated using a 50 kDa molecular weight cut off (MWCO) Amicon centrifugal filter unit (Millipore, Livingston, UK) to approximately 1 mg/mL, and stored in aliquots at -80°C until needed. IgA1 concentration was determined by absorbance at 280 nM. The purity of the IgA1 preparations was tested by SDS-PAGE and Coomassie blue staining.

2.3.2 Separation of polymeric and monomeric IgA1

Polymeric and monomeric IgA1 were separated by size exclusion chromatography using a HiLoad 16/600 Superdex 200 preparative grade column (GE Healthcare, Little Chalfont, UK) on an ÄKTA purifier (GE Healthcare). 1 mL aliquots of total IgA1 were applied to the column and separation carried out at 1 mL/min. Fractions were assessed for the presence of IgA by ELISA and Western blotting. On the basis of the elution profile, IgA-containing fractions were pooled into pIgA1 and mIgA1, and concentrated to approximately 1 mg/mL using a 100 kDa MWCO Amicon centrifugal filter for pIgA1, or a 50kDa MWCO Amicon centrifugal filter for mIgA1, chosen according to the manufacturer's recommendation that the MWCO size should be approximately three times smaller than the protein of interest.

2.3.3 Determination of endotoxin levels in IgA1 preparations

Endotoxin content of the IgA1 preparations was tested by the Limulus amoebocyte lysate (LAL) assay (Lonza, Slough, UK). Gram-negative bacterial endotoxin catalyses the activation of a pro-enzyme in LAL, and the activated enzyme then catalyses the release of pNA from the colourless substrate Ac-Ile-Glu-Ala-Arg-pNA. The free pNA may then be measured photometrically.

Standard endotoxin solutions were reconstituted from lyophilised E. Coli O111:B4 endotoxin, according to the manufacturer's instructions, into the following concentrations: 10, 5.0, 1.0, 0.5, 0.25 and 0.1 EU/mL. Standards and samples were mixed with LAL, and incubated at 37°C for 10 minutes. A chromogenic substrate solution was then added and incubated at 37°C for a further 6 minutes, before addition of the stop reagent, acetic acid. Absorbance of the samples and standards were determined at 405 nm, using an Infinite F50 plate reader (Tecan, Weymouth, UK). Preparations of IgA1 all contained less than 10 endotoxin units (EU)/mL.

2.3.3 SDS-polyacrylamide gel electrophoresis (SDS-PAGE)

Proteins were subjected to SDS-PAGE followed either by immunoblotting or in-gel staining with Coomassie blue. Electrophoresis was performed at 180 Volts.

For immunoblotting, proteins were electrophoretically transferred to a Hybond-C Super nitrocellulose membrane (GE Healthcare), at 30V overnight at 4°C for higher molecular weight proteins (≥100 kDa), or at 80V for 2 hours at room temperature for lower molecular weight proteins (<100 kDa). Following transfer, non-specific protein binding sites were blocked by incubation of the membrane in 5% w/v non-fat milk powder diluted in tris-buffered saline (TBS)/0.05% Tween 20 for 1 hour. Polyclonal rabbit anti-human IgA/HRP (Dako, Ely, UK) was diluted at a concentration of 1:2000 in TBS/Tween/2% non-fat milk powder, and applied to the membrane for 2 hours at room temperature. After washes, antibody binding was detected using SuperSignal West Pico Chemiluminescent substrate (Thermo Scientific) followed by exposure to X-ray film (Fujifilm Super RX, Fisher Scientific).

2.3.4 Coomassie blue staining

For Coomassie blue staining, gels were stained with Coomassie Brilliant Blue R-250, then placed in de-staining buffer. Once backgrounds were clear, the gels were soaked in equilibration buffer and placed on a gel dryer (BioRad Laboratories, Hemel Hempstead, UK).

2.3.5 Helix aspersa agglutinin (HAA) binding

Serum and purified IgA1 samples were tested for binding to Helix Aspersa agglutinin (HAA) which recognises terminal GalNac. Nunc Maxisorp polystyrene 96-well microtitre plates (Fisher Scientific) were coated with 10 µg/mL rabbit anti-human IgA (Dako) in a bicarbonate/carbonate buffer, and incubated overnight at 4°C. Plates were blocked with 2% bovine serum albumin (BSA) for one hour at room temperature. 11 serum samples of known IgA1-HAA binding, from very high (110 AU) to very low (10 AU) were used as standards. Each standard or sample was diluted 1:100 in PBS and applied to the plate in duplicate, and incubated overnight at 4°C. After removal of the samples, the plate was incubated with biotinylated HAA, followed by streptavidin-HRP (1:200), and developed with OPD. The OD at 492 nm was measured using a spectrophotometer.

2.3.6 Cell culture

The human proximal tubular cell line, HK-2, was originally obtained from the American Type Culture Collection (ATCC, Manassas, VA, USA). Stock cultures of HK-2 cells were confirmed to be mycoplasma-free by PCR. Cells were maintained in DMEM-F12 (Life Technologies, Paisley, UK) with 10% vol/vol heat inactivated fetal calf serum, 1% Glutamax (Gibco, Fisher Scientific), penicillin (10^2 IU/mL) and streptomycin (100 µg/mL), at 37°C in a humidified 5% CO_2 atmosphere. Cells were subcultured at 70-80% confluence using 0.05% trypsin/0.02% EDTA (Gibco, Fisher Scientific). For experiments, HK-2 cells were used between passages 10-20. 24-well plates were seeded at a density of 2.5 x 10^4 cells per well, and cells were used at 70% confluence.

Primary mesangial cells were obtained from a commercial supplier (Lonza), and maintained in mesangial cell growth medium (Lonza), supplemented with 5% fetal bovine serum according to the manufacturer's instructions. Cells were subcultured

at 70-80% confluence using trypsin/EDTA solution (Lonza). For experiments, cells between passages 5-8 were seeded in 6-well plates at a density of 2.5 x 10^5 cells per well, and used at 70% confluence.

2.3.7 PPAR Response element (PPRE) and cytokine analysis

To measure PPAR response element (PPRE) activity, HK-2 cells were transfected with the reporter plasmid pPPRE-TK-Luc (kindly provided by Dr M. Lazar, Philadelphia, PA, USA) using Fugene 6 (Roche Diagnostics, Lewes, UK) according to the manufacturer's instructions. Cells were placed in serum-free DMEM/F-12 for 24 hours, before being exposed to media and vehicle (PBS) alone, human serum albumin (100 μg/mL or 5 mg/mL), IgA1 (100 μg/mL) from healthy subjects and patients with IgAN, and IgM (100 μg/mL; Sigma-Aldrich). After 24 hours, the media was removed and cells lysed in a buffer consisting of 500 mmol/L HEPES, 1 mmol/L CaCl2, 1 mmol/L MgCl2 containing 2% Triton N101, pH 7.8. Cells were lysed for 10 minutes, then 100 μL aliquots of lysate were assayed for luciferase using a luminometer (Lumicount, Packard, Pangbourne, UK).

To determine cytokine release, HK-2 cells were placed in serum free media for 24 hours. They were then exposed to media and vehicle (PBS) alone, albumin (100 μg/mL or 5 mg/mL), IgA1 (100 μg/mL) from healthy subjects or patients with IgAN, IgG or IgM (both 100 μg/mL; Sigma-Aldrich) for the time period specified. Levels of IL-6, TGF-β1, and fibronectin in the cell culture supernatants were then determined by sandwich ELISA (R&D systems, Abingdon, UK) according to the manufacturer's instructions. Other serum cytokines were measured using a customised Luminex array (R&D systems) according to the manufacturer's instructions. The cytokine array was assayed and data analysis performed using the Bio-Plex MAGPIX Multiplex Reader (Bio-Rad).

2.4 Animal studies: intravital microscopy

2.4.1 Animal models

All intravital microscopy experiments were conducted at the O'Brien Center for Advanced Renal Microscopy and Analysis, Indiana University, in accordance with National Institutes of Health guidelines. Studies were approved by the Indiana University School of Medicine Institutional Animal Care and Use Committee.

Munich-Wistar Frömter (MWF) rats, which possess surface glomeruli, were derived from a colony previously provided by Dr Roland Blantz (University of California-San Francisco, San Diego, CA, USA), and maintained within the Indiana University School of Medicine. All animals were given free access to food and water throughout the studies.

2.4.1.1 Podocyte depletion model

hDTR-Pod/SG rats were generated previously in the Wiggins laboratory at the University of Michigan as follows. MWF rats were supplied by the Molitoris laboratory at Indiana University. They were crossed with human diphtheria toxin receptor (hDTR) transgenic Fischer 344 rats. A podocin promoter/hDTR construct had previously been inserted into this rat strain, resulting in podocyte-specific hDTR gene expression, and allows for podocyte depletion by injection of diphtheria toxin in a dose- and time-dependent manner (Wharram et al., 2005). After each crossing, the offspring were genotyped to select for the hDTR transgene and a kidney biopsy performed to select for those rats that had superficial glomeruli. After five generations of selection, rats were inbred to select for homozygosity of the hDTR transgene, using a Taqman PCR assay to quantify transgene copy number. This rat line, homozygous for the hDTR transgene and containing superficial glomeruli, was designated hDTR-Pod/SG, and has been established as a breeding colony since 2007 (Wagner et al., 2016).

hDTR-Pod/SG rats used for these experiments were confirmed to possess the hDTR transgene by PCR genotyping of genomic DNA, isolated from tail snips. Samples were lysed in DNA lysis buffer with 100 µg/mL proteinase K overnight at 55°C. The DNA was quantified by UV absorption using a spectrophotometer

(NanoDrop 2000), diluted to 25 ng/μL with distilled water, and heat inactivated for 15 minutes at 75°C. A PCR was then carried out, with each reaction tube containing the following: 1.25 μL DNA, 7.5 μL GoTaq Green Mastermix (Promega, Madison, WI, USA), 1.2 μL forward and reverse primers, 5 μL water. The following primer pair was used: 5',5'-ACCCGACGGTCTTTAGGG-3'; 3',5'-CCTTGTATTTCC-GAAGACATGGGT-3'. A 465 bp fragment was amplified when the transgene was present in rat genomic DNA.

PCR conditions

Denaturation	95°C	3 minutes
Amplification	95°C	45 seconds
	55°C	1 minute
	72°C	1 minute
	x 40 cycles	
Extension	72°C	10 minutes

Following PCR, the products were analysed by gel electrophoresis, in a 2% agarose gel in TAE buffer with 0.5 μg/mL ethidium bromide. 10 μL of each sample was mixed with 2 μL of loading dye and loaded on to the gel alongside a 1 kB plus DNA ladder (Thermo Fisher Scientific). The samples underwent electrophoresis in TAE buffer for 60 minutes at 80V. DNA was visualised using a transilluminator under UV light.

To induce podocyte depletion, diphtheria toxin (200 ng/kg in 0.9% sodium chloride) was administered via an intraperitoneal injection five days before imaging studies.

2.4.1.2 Ischaemic CKD model

For the ischaemic CKD model, wild type male MWF rats were anaesthetised by inhaled isofluorane, a midline incision made and ischaemic kidney injury induced by clamping the left renal pedicle for 50 minutes, following which the clamp was removed and the kidney observed to ensure complete reperfusion. 2 mL warm 0.9% sodium chloride was administered via an intraperitoneal injection to replace insensible and blood volume losses. This was followed by uninephrectomy of the right kidney 14 days later. Animals were imaged 2 weeks after these procedures. Previous studies indicated that this model results in increased proteinuria and

reduction in GFR, with histology showing evidence of chronic kidney disease, including tubular atrophy, interstitial mononuclear infiltration and oedema, peri-glomerular fibrosis, hyaline cast formation and generalised fibrosis (Campos-Bilderback et al., 2013).

2.4.2 Fluorescent IgA synthesis

2.4.2.1 Generation of rat IgA

Rat IgA was isolated from the 91C hybridoma cell line (kindly supplied by Professor Gerard Apodaca, University of Pittsburgh, PA, USA), which produces both polymeric and monomeric IgA, by the following method. 91C cells were cultured in DMEM with high glucose (D-5671, Sigma-Aldrich, St. Louis, MO, USA), 10% NCTC media, 20% fetal bovine serum, L-glutamine and penicillin/streptamicin. Ascites was generated by a commercial company (GenScript, Piscataway, NJ, USA) by injecting 20 nude mice with 1 x 10^6 cells each. This produced a total of 30 mL ascites, which was collected and pooled. The ascites fluid was centrifuged at 1500 x *g* to remove cell debris, the supernatant collected and stored at 4°C.

Pooled ascites fluid was dialysed into PBS, and sterilised through a 0.2 µm filter. The fluid was then passed through a HiTrap Protein L column (GE Healthcare, Pittsburgh, PA, USA) on an ÄKTA pure FPLC system (GE Healthcare) in 5 mL aliquots, before elution with 0.1M glycine buffer at pH 2.5. The eluate was immediately neutralised with 1M Tris pH 7.5, and pH adjusted to 7.5, before dialysing into PBS, and addition of 0.1% sodium azide. The solution was then stored as 1 mL aliquots at -80°C. A separate batch of rat IgA was obtained commercially (Life Technologies, Thermo Fisher Scientific) and separated into pIgA and mIgA by size exclusion chromatography, using a HiLoad 16/600 Superdex 200 preparative grade column (GE Healthcare) on an ÄKTA purifier FPLC system (GE Healthcare). The purity and IgA content of the IgA preparations was confirmed by SDS-PAGE, Coomassie blue staining and immunoblotting.

2.4.2.2 Fluorescent labelling of rat IgA

Aliquots of rat IgA were conjugated by the following method. IgA was dialysed into 100mM sodium bicarbonate at pH 8.3, using a 50 kDa MWCO dialysis membrane (Float-A-Lyzer, Spectrum Labs, Rancho Dominguez, CA, USA). The fluorophore,

Texas Red-X-succinimidyl ester (Molecular Probes, Life Technologies, Eugene, OR, USA), was prepared by the addition of 100 µl dimethylformamide (DMF; Sigma-Aldrich), and vortexed until the NHS ester was dissolved. The prepared fluorophore was then added to the IgA, and incubated for one hour on a shaker at room temperature, protected from light. The labelled IgA was then dialysed into 0.9% sodium chloride. The final stoichiometric ratio was approximately 8:1 moles dye:IgA.

2.4.3 Preparation of animals for imaging

For experiments with recovery, anaesthesia was induced by inhaled isofluorane. In experiments without recovery, in male MWF rats, anaesthesia was induced by intraperitoneal injection of thiobutabarbital sodium (130 mg/mL; Sigma-Aldrich) at a dose of 160 mg/kg. In female MWF rats, anaesthesia was induced by intraperitoneal injection of sodium pentobarbital (50 mg/mL; Ovation Pharmaceuticals, Deerfield, IL, USA) at a dose of 50 mg/kg. A jugular vein catheter was placed for delivery of fluorescent conjugates. A femoral artery catheter was inserted for monitoring of arterial blood pressure. The left kidney was externalised immediately before imaging via an incision on the left flank.

2.4.4 Two-Photon Microscopy

The animals were moved to the microscope stage, and the externalised kidney was placed in contact with a glass-bottomed dish filled with 0.9% sodium chloride (Figure 10). Blood pressure, heart rate and rectal temperature were continuously monitored during imaging using LabChart 6 (AD Instruments, Colorado Springs, CO, USA). Imaging was conducted using an Olympus FV1000 microscope adapted for two-photon microscopy with high-sensitivity gallium arsenide non-descanned 12-bit detectors with animal preparations. The 60x water immersion objective with a numerical aperture of 1.2 was heated using an objective heater (Warner Instruments, Hamden, CT, USA). Animals were covered by a water-circulating warming blanket in order to stabilise body temperature during imaging. In addition, the microscope stage was warmed using 2 ReptiTherm heating pads (Zoo Med Laboratories, San Luis Obispop, CA, USA), one under the upper torso/head and one under the lower abdomen. The temperature of the animal was maintained between 36.5 and 37.5°C. Blood pressure and hydration status was maintained by infusion of intravenous 0.9% sodium chloride. Twenty consecutive glomeruli and

surrounding tubules were imaged at 60x original magnification, and 10 cortical sections at 20x original magnification per animal. All images for a given study were collected at the same focal plane at a depth of 10-20 µm. Images were analysed using MetaMorph v.7.1 (Molecular Devices, Downington, PA, USA).

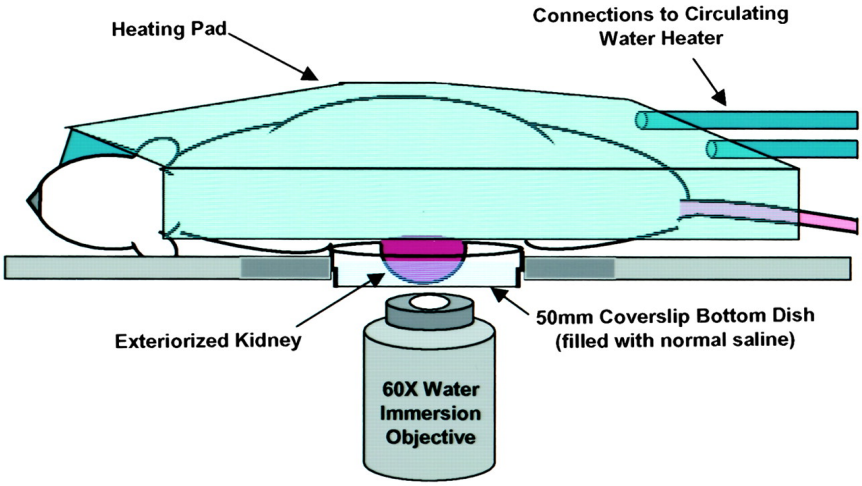

Figure 10: Experimental setup used for live intravital imaging of rat kidneys. Anaesthetised rats were placed on the stage of an inverted microscope, and the kidney was exposed and placed on to a cell culture dish and bathed in 0.9% sodium chloride. A heating pad was placed over the animal, and temperature was monitored by a rectal thermometer. Imaging was conducted using a Nikon 60x 1.2NA water-immersion objective. From Dunn et al., 2002.

2.4.5 Analysis of plasma and urine electrolytes

Urine samples were collected for 24 hours prior to imaging in individual metabolic cages. Whole blood was collected via the jugular vein catheter or by cardiac puncture under terminal anaesthesia, and placed into heparinised tubes. Plasma was isolated by centrifugation. Measurement of plasma and urine creatinine was performed by the modified Jaffe method with a Pointe 180 QT Quick Touch Analyzer and Creatinine reagent set C7539 (Pointe Scientific, Canton, MI, USA), according to the manufacturer's instructions. Urine total protein was measured using a Coomassie blue protein assay (Pierce Chemical, Rockford, IL, USA), and data acquisition was performed with SoftMax Pro 4.6 (Molecular Devices).

2.5 Animal studies: *in vivo* model

2.5.1 Animals

Wild type C57BL/6 and BALB/c mice were purchased from Charles River (Margate, UK). Mice were housed in individual ventilated cages, in a pathogen-free environment. All animal experiments were carried out with local ethics committee approval, and in accordance with the UK Animals Scientific Procedures Act 1986.

2.5.1.1 Generation of MASP-2 and CL-11 deficient mice

MASP-2$^{-/-}$ mice were generously provided by Professor Wilhelm Schwaeble, University of Leicester, and mice from the colony had been backcrossed on to a C57BL/6 background for at least 11 generations. MASP-2 deficient mice were generated by homologous recombination, using a gene targeting vector containing 3.8kb of *Masp2* genomic DNA, the neomycin resistance gene and the thymidine kinase gene, described previously (Schwaeble et al., 2011). Plasma MASP-2 levels are undetectable in MASP-2$^{-/-}$ mice, and there is no significant difference in plasma MBL-A, MBL-C, C3, ficolin A and Collectin-11 expression between MASP-2 deficient and wild type C57BL/6 mice. Both heterozygous and homozygous MASP-2 deficient mice are healthy and fertile, and show no gross abnormalities, with normal life expectancy (>18 months) compared to their wild type littermates.

CL-11$^{-/-}$ mice were also generously provided by Professor Wilhelm Schwaeble, and mice from the colony had been backcrossed on to a C57BL/6 background for at least 15 generations.

2.5.1.2 Genotyping of MASP-2 and CL-11 deficient mice

Genomic DNA was isolated from ear clippings. Samples were lysed in an EDTA/nuclei lysis solution with 10 µL of 20 mg/ml Proteinase K overnight at 55°C. 1.5 µL of RNAse A solution (4 mg/mL) was then added to the nuclear lysate, and samples were incubated for 30 minutes at 37°C. Following this, 100 µL of protein precipitation solution was added and the sample was vortexed vigorously. Samples were centrifuged for 4 minutes at 13000 rpm to precipitate the protein content. The supernatant containing the DNA was transferred to a new tube, and 300 µL isopropanol was added, before centrifuging for 5 minutes at 13000 rpm to

precipitate the DNA. Following a 70% ethanol wash, the DNA pellet was air dried before being resuspended in 500 µL Nanopure water.

A PCR was carried out, using the following primers:

MASP-2

1. M2_F1 CATCTATCCAAGTTCCTCAGA
2. Neo5_R1 CTGATCAGCCTCGACTGTGC
3. M2WTO_R1 AGCTGTAGTTGTCATTTGCTTGA

These amplified a 500-bp product from the disrupted allele and an 800-bp product from the wild-type allele.

CL-11

1. CL-11_wto-F1 CAGATTCTTGTCCCTGGCCTCA
2. Neo3a GCAGCGCATCGCCTTCTATC
3. CL-11_scr-R1 CTCAGTGTCAGCTGAATAAATGCCA

These amplified a 600-bp product from the disrupted allele and a 470-bp product from the wild-type allele (Figure 56).

Each reaction tube contained the following: 2 µL DNA, 12 µL MyTaq Red Mix (Bioline Reagents, London, UK), 4.5 µL primers, 5.5 µL distilled water.

PCR conditions

Denaturation	95°C	90 seconds
Amplification	95°C	30 seconds
	62°C	30 seconds
	72°C	15 seconds
	x 35 cycles	
Extension	72°C	5 minutes

Following PCR, the products were analysed by gel electrophoresis, in a 1% agarose gel in TAE buffer with 0.5 µg/mL ethidium bromide. 10 µL of each sample was mixed with 2 µL of loading dye and loaded on to the gel alongside a 1 kB plus DNA ladder (Thermo Fisher Scientific). The samples underwent electrophoresis in

TAE buffer for 45 minutes at 120V. DNA was visualised using a transilluminator under UV light.

2.5.2 Study protocol

For dosed animals, mice were fed 0.1% bovine gamma globulin (BGG) continuously in the drinking water. At the time points, doses and frequencies specified, mice were administered BGG diluted in 0.2mL sterile PBS by intravenous injection into the tail vein (Figure 11). For control animals, age, sex and strain-matched mice received normal drinking water, and were injected with vehicle (sterile PBS) only.

Before sacrifice, dosed and control mice were placed in individual metabolic cages for urine collection for 24 hours, with free access to food and water. At the time points specified, mice were subjected to terminal anaesthesia by inhaled isofluorothane. Blood samples were collected immediately by cardiac puncture, and kidneys were rapidly harvested, and sectioned longitudinally. For one kidney, one half was fixed with neutral buffered formalin overnight, transferred to 70% ethanol and subsequently embedded in paraffin for histological evaluation. The other half was embedded in OCT (Tissue-Tek OCT, Sakura, Netherlands) in a cryomold, and snap-frozen in an isopentane bath cooled with liquid nitrogen, and stored at -80°C for immunofluorescence studies. For the contralateral kidney, half the kidney was fixed in paraformaldehyde-lysine-periodate (PLP) fixative at 4°C for 4 hours, before being transferred to a 10% sucrose solution overnight at 4°C, then embedded in OCT in a cryomold, and snap-frozen in an isopentane bath cooled with liquid nitrogen. The remainder was dissected and snap frozen in liquid nitrogen and stored at -80°C for RNA and protein analysis. In some experiments, a small section of renal cortex was fixed in a gluteraldehyde /formaldehyde buffer (Section 2.5.5.3) for electron microscopy studies.

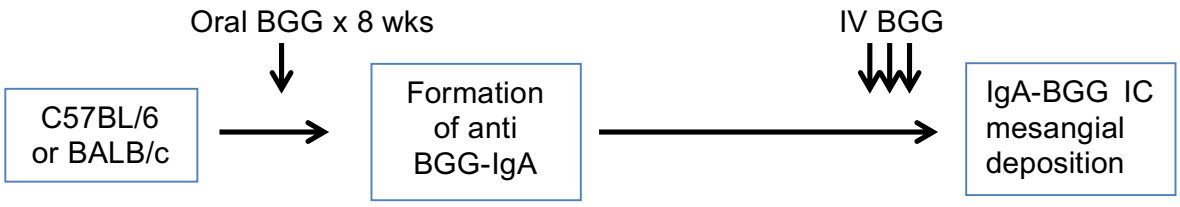

Figure 11: Schematic protocol for the mouse model of IgAN

2.5.3 Biochemical analysis of serum and urine samples

Blood samples were allowed to clot at room temperature, and then centrifuged at 3000 rpm for 10 minutes at 4°C for serum collection, before storage at -80°C until analysis. Serum urea and creatinine (enzymatic method), and urine creatinine were measured by an automated bioanalyzer (ADVIA 2400, Siemens Healthcare Diagnostics, Camberley, UK) in the Department of Pathology, Leicester Royal Infirmary. Urine protein was measured in triplicate by the Bio-Rad protein assay, based on the Bradford dye-binding method (Bradford, 1976) (Bio-Rad, Hertfordshire, UK). This method assays the colour change of Coomassie brilliant blue G-250 dye in response to protein concentration, with the dye binding to basic (especially arginine) and aromatic amino acid residues. Urine albumin was measured by a mouse albumin ELISA quantification kit according to the manufacturer's instructions (Bethyl Laboratories, Montgomery, TX).

2.5.4 Measurement of serum antibody responses

Serum IgA and IgG immune responses to BGG were determined by ELISA, based on a method previously described (Gesualdo et al., 1992). Nunc Maxisorp polystyrene 96-well microtitre plates (Fisher Scientific) were coated with 10 µg/mL BGG diluted in a bicarbonate/carbonate buffer, pH 9.6, and incubated overnight at room temperature. Serum samples diluted 1:40 in 1% BSA/PBS were then added (50 µl/well) to duplicate wells, and incubated for 2 hours at room temperature. HRP-conjugated goat anti-mouse IgA or IgG (Abcam, Cambridge, UK; 1:2000-1:4000 in 1% BSA/PBS) were then added for 2 hours before development with OPD.

2.5.5 Histological analysis

2 µm formalin fixed paraffin embedded (FFPE) kidney sections were stained with Periodic acid-Schiff (PAS) for morphological analysis and glomerular cell counting, and with Picosirius red and Masson's trichrome for analysis of glomerular and interstitial fibrosis.

2.5.5.1 Immunohistochemistry

For F4/80 and CD3, 4 µm FFPE kidney sections were deparaffinised in xylene and rehydrated through a graded series of ethanol. For CD68, 5 µm PLP fixed frozen

sections were used. Sections were blocked with 2.5% goat serum (Vector Laboratories), before being incubated with rat anti-mouse F4/80 (AbD Serotec, Kidlington, UK) 1:50 overnight at 4°C, rabbit anti-human/mouse CD3 (Dako) 1:200, or rat-anti mouse CD68 (AbD Serotec), both for 1 hour at room temperature. Following washing, sections were incubated with 3% hydrogen peroxide for 10 minutes for F4/80 and CD68, or 0.3% hydrogen peroxide for 30 minutes for CD3 to block endogenous peroxidase. This was followed by incubation with a peroxidase-conjugated secondary antibody (ImmPRESS reagent, Vector Laboratories) and signal development with diaminobenzamidine (DAB; Vector Laboratories). Sections stained for CD3 and CD68 were counterstained by briefly incubating with haematoxylin solution (Sigma-Aldrich). Counterstaining was omitted for sections stained for F4/80, due to potential interference with the image analysis software. Sections then underwent dehydration through a graded series of ethanol, cleared in xylene and mounted with DPX mounting media (Sigma-Aldrich). Negative control slides were included in each run, where the primary antibody was substituted by antibody diluent only.

2.5.5.2 Immunofluorescence

5 µm frozen kidney sections were cut using a cryostat and left to air-dry for 30 minutes before being stored at -80°C before use. For immunofluorescence staining, sections were thawed for 10 minutes before being fixed with ice-cold acetone for 10 minutes, air-dried, washed with PBS, then blocked with 10% goat serum for 30 minutes. Sections were then incubated with fluorescein isothiocyanate (FITC)-conjugated goat anti-mouse IgA (Southern Biotech, Cambridge Bioscience, Cambridge, UK; 1:50), goat anti-mouse IgG (Sigma-Aldrich; 1:100), or goat anti-mouse C3 (MP Biomedical, Fisher Scientific; 1:100). For C4, sections were incubated with rat anti-mouse C4 (16D2, Hycult Biotechnologies, Uden, Netherlands; 1:50) overnight at 4°C, washed with PBS and then incubated with Alexa Fluor 488-conjugated goat-anti rat IgG (Life Technologies; 1:1000) for 1 hour at room temperature. After washing the sections, slides were mounted with Permafluor (Thermo Scientific, UK). All antibodies were diluted in PBS.

Images were acquired with a fluorescent microscope (BX61, Olympus, Tokyo, Japan) using Volocity image analysis software (PerkinElmer, Waltham, MA, USA). For each section, images of 10 consecutive glomeruli were captured using a

ORCA-R2 C10600-10B digital CCD camera (Hamamatsu Photonics, Hamamatsu City, Japan). Images were analysed in Image J (Bethesda, MD, USA), and mean fluorescent intensity for each glomerulus was calculated after background subtraction. All sections for one experiment were stained at the same time and imaged in the same session.

All interpretations of the light microscopy and immunofluorescence images were verified by an independent consultant histopathologist.

2.5.5.3 Transmission electron microscopy

Kidney sections were fixed in 4% gluteraldehyde/2% paraformaldehyde in 0.1 M sodium cacodylate buffer with 2 mM calcium chloride (pH 7.4). Sections were dehydrated in a graded series of ethanol and embedded in Modified Spurr's low viscosity resin. Ultrathin 90 nm sections were collected onto copper mesh grids. The sections were counterstained for 2 minutes in Reynold's Lead citrate. Samples were viewed on the JEOL JEM-1400 (JEOL, Welwyn Garden City, UK) with an accelerating voltage of 80kV. Images were captured using an Olympus Megaview III digital camera with iTEM software (Olympus). Images were interpreted by an independent electron microscopy technician who was blinded to the treatment allocation.

2.6 Statistical analysis

Results are expressed as mean ± standard error of the mean (SEM), and were analysed using GraphPad Prism version 6.05 for Windows (GraphPad Software, La Jolla, CA, USA). Comparisons between means were made by the one-way analysis of variance (ANOVA) test, combined with Tukey's post-hoc test for normally distributed data, or Dunn's post hoc test for non-parametric data. The Spearman rank correlation coefficient was used to analyse correlations. A P value <0.05 was considered statistically significant.

Chapter 3: The effects of filtered IgA on the proximal tubule *in vivo*

3.1 Introduction

IgA nephropathy (IgAN) remains a significant cause of progressive chronic kidney disease (CKD) and end stage renal disease (ESRD), with 20-40% of patients developing ESRD within 20 years of diagnosis (D'Amico, 2000). Following mesangial IgA deposition and damage to the glomerular filtration barrier, the kidney may undergo a process of progressive tubulointerstitial inflammation and fibrosis, in common with many other forms of CKD. During this phase, the proximal tubule is exposed to a number of potentially toxic factors within the glomerular ultrafiltrate, including proteins such as albumin, mesangial cell and podocyte-derived cytokines and IgA itself. Urinary levels of IgA, IgA-IgG immune complexes and poorly galactosylated IgA are all reported to be increased in patients with IgAN compared to those with other kidney diseases or healthy individuals (Galla et al., 1985; Matousovic et al., 2006). Non-selective proteinuria, defined by the presence of higher molecular weight proteins including immunoglobulins, is associated with worse renal function and prognosis in IgAN (Woo et al., 1989).

These observations suggest that the proximal tubule is exposed to increased amounts of filtered IgA in IgAN that pass abnormally through the damaged glomerular filtration barrier, before its final excretion into the urine. However, an alternative explanation is that this urinary IgA may undergo basolateral to apical transcytosis through tubular epithelial cells within the kidney or distally within the urinary tract, thus bypassing the glomeruli, and that the increased amounts of urinary IgA observed are simply a consequence of the higher serum IgA levels found in IgAN. Basolateral to apical transcytosis of IgA is a well-characterised process that occurs in many epithelial cell types, most notably in intestinal plasma cells, and involves the binding of pIgA to the polymeric Ig receptor (pIgR) at the basolateral surface, and transportation to the apical surface, where pIgR is cleaved to form secretory IgA, comprising of dIgA and the secretory component, derived from the pIgR (Apodaca et al., 1994; Pabst, 2012). Secretory IgA performs a number of essential roles at mucosal surfaces as part of the immune host defence (Pabst, 2012).

In this chapter, multiphoton intravital microscopy was utilised to determine whether filtered IgA, that passes across the glomerular filtration barrier, interacts with the apical surface of PTEC. The proximal tubule plays a vital role in the reabsorption of filtered proteins to maintain homeostasis, and PTEC, especially within the S1 segment, possess specialised mechanisms to facilitate protein reclamation, which include receptor-mediated clathrin-dependent endocytosis and fluid-phase endocytosis (Dickson et al., 2014). Several lines of *in vitro* and *in vivo* data indicate that proteins, including albumin and immunoglobulin light chains, may lead to deleterious PTEC signalling, and release of proinflammatory and profibrotic cytokines into the renal interstitium (Abbate et al., 2006; Baines and Brunskill, 2011; Basnayake et al., 2011). The stimulus for the switch between normal homeostatic reclamation and deleterious signalling is a focus of much investigation. One line of enquiry suggests that changes in protein structure may lead to different signalling and transport pathways being triggered. For example, changes in albumin glycation or carbamylation may lead it to be trafficked towards lysosomal degradation instead of being reabsorbed via the basolateral membrane (Dickson et al., 2014).

Modern multiphoton microscopy techniques allow for high resolution imaging of cellular and subcellular processes in live animals, due to its ability to achieve greater tissue penetration with lower amounts of phototoxicity and damage to surrounding structures compared to conventional single photon confocal microscopy. The kidney is particularly amenable to imaging as it can be externalised without causing significant disruption or injury, and this form of imaging has now been used extensively in studies of renal physiology and disease, including the filtration and proximal tubular handling of albumin and dextrans of varying molecular sizes (Dunn et al., 2002; Russo et al., 2007; Sandoval et al., 2012; Wagner et al., 2016), podocyte migration and dynamics (Hackl et al., 2013), mitochondrial function (Hall et al., 2013), and to assess delivery of vectors containing small interfering RNA (siRNA) for therapeutic purposes (Corridon et al., 2013).

In the following studies, the Munich Wistar Frömter (MWF) rat strain was used as they possess numerous surface glomeruli that allow for direct visualisation of their structure and their connection to the proximal tubular S1 segment by multiphoton

microscopy (Peti-Peterdi and Sipos, 2010; Sandoval and Molitoris, 2008). Male MWF rats develop focal glomerulosclerosis and progressive albuminuria with age, while females are protected from these effects (Schulz et al., 2008). Two models of proteinuria were studied in this rat strain, to study tubular handling of filtered fluorescently labelled IgA. Firstly, a transgenic rat colony was used that expresses the human diphtheria toxin (DT) receptor specifically on podocytes, under the control of the podocyte-specific promoter podocin (hDTR-Pod/SG). In this strain, under physiological conditions, urinary albumin excretion is normal, but administration of diphtheria toxin leads to selective and dose-dependent podocyte death and depletion, and increased filtration of proteins across the glomerular filtration barrier (Wagner et al., 2016; Wharram et al., 2005). Secondly, a model of CKD was studied analgous to ischaemic acute tubular necrosis (ATN) without recovery, by inducing renal ischaemia-reperfusion injury followed by uninephrectomy of the contralateral kidney, which leads to progressive proteinuria, reduction in GFR, and histological changes of tubular atrophy, interstitial mononuclear cell infiltration and oedema, periglomerular fibrosis, hyaline droplet formation and generalised fibrosis (Campos-Bilderback et al., 2013).

Utilising multiphoton microscopy to study renal handling of fluorescently labelled IgA in the MWF rat, the aim of these studies was to establish:

1. Whether IgA is able to cross the glomerular filtration barrier, or if urinary IgA originates solely from basolateral to apical transcytosis.
2. In two distinct models of proteinuria, induced by podocyte depletion, or by ischaemic-ATN induced CKD, whether renal handling of IgA differs, and specifically whether the amount of filtered IgA increases.
3. Whether filtered IgA is able to interact with proximal tubular epithelial cells (PTEC) *in vivo*.

3.2 Results

3.2.1 Purification and separation of rat IgA

To perform these studies, rat IgA was purified for fluorescent labelling and intravenous injection. Rat IgA was generated from mouse ascites induced by the hybridoma cell line, 91C. IgA was then purified from the ascites fluid by using a Protein L column, which has a high binding affinity and specificity for kappa light chains.

The elution profile of the ascites fluid from the Protein L column demonstrated a well-defined peak (Figure 12), from which fractions were obtained, pooled, concentrated by centrifugal filtration and dialysed into PBS. Samples were subjected to SDS-PAGE and Western blotting, which demonstrated that the IgA purified contained both polymeric and monomeric forms, with minimal contamination (Figure 13). Multiple bands were observed after staining with Coomassie blue. These bands were all detected by Western blotting using an anti-rat IgA antibody, suggesting that they represented IgA that had undergone post-translational modification. A sample was subjected to gel filtration, which demonstrated that the majority of the IgA was polymeric (approximately 75% of the total solution).

The same samples were also analysed by Western blotting using an anti-rat IgG antibody to test for the presence of contaminating IgG, and no bands were detected (data not shown).

Pooled IgA was aliquoted and subsequently labelled with the fluorophore Texas Red-X-succinimidyl ester immediately before administration and imaging studies.

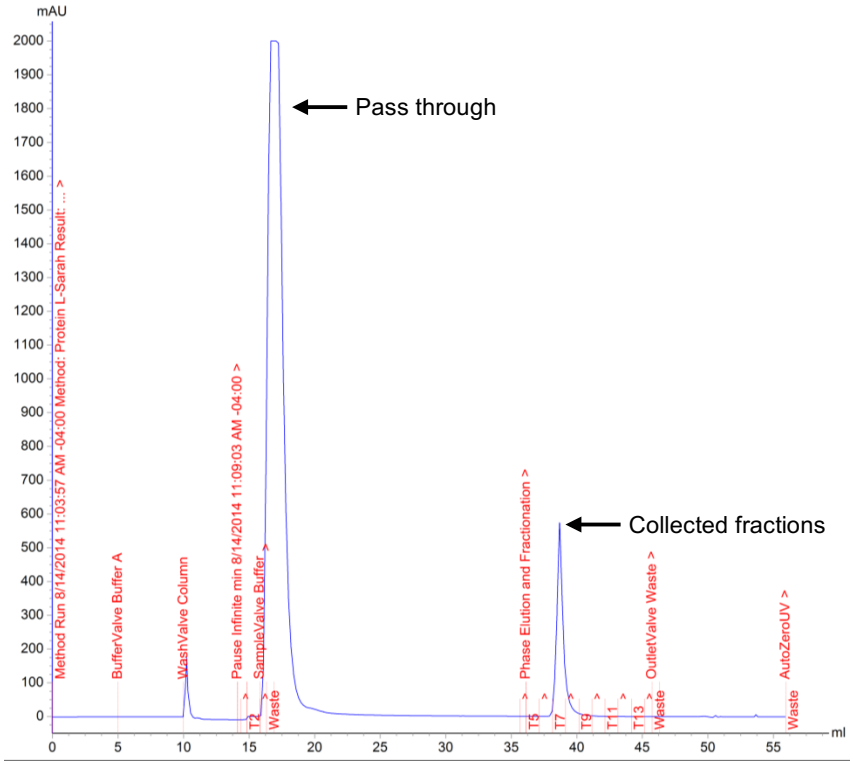

Figure 12: Elution profile of ascites fluid generated by the 91C cell line, from the Protein L column. A single peak was obtained at approximately 38mL elution volume. Fractions from this peak were collected and pooled. The first larger peak represents pass through that did not bind to the column, consisting of other proteins contained within the ascites fluid.

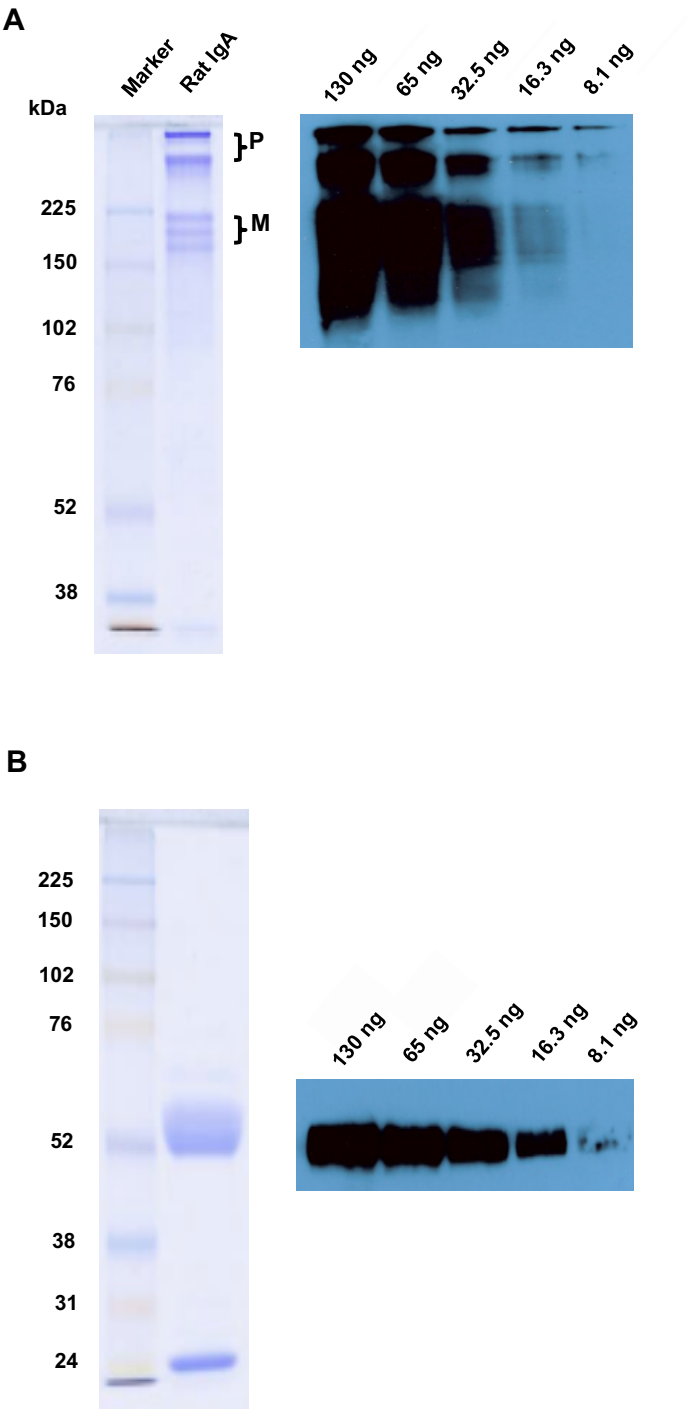

Figure 13: Analysis of purified rat IgA by SDS-PAGE, Coomassie blue staining and Western blotting. (A) Non-reduced sample, demonstrating monomeric (M) and polymeric (P) forms of rat IgA. (B) Reduced sample showing protein bands at approximately 55 kDa (α heavy chains), and at approximately 25 kDa (light chains). IgA remained detectable at very low levels (8ng) of total protein by Western blotting.

3.2.2 Genotyping of the hDTR-Pod/SG rat line

The hDTR-Pod/SG rat line has been established as a breeding colony at Indiana University since 2007. To confirm presence of the hDTR transgene, tail snips were taken from four rats, for genomic DNA extraction, and these samples were then subjected to PCR for the hDTR transgene. A 465 bp fragment, confirming presence of the transgene, was present in all the samples tested (Figure 14).

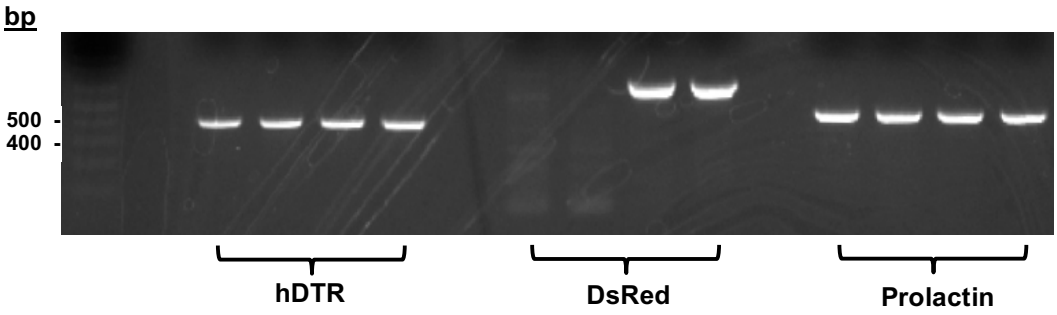

Figure 14: Genotyping of hDTR-Pod/SG rats. Genomic DNA was tested from four rats from the colony, and subjected to PCR. A 465-bp product was isolated from all rats, confirming presence of the hDTR transgene. Some rats from the colony also possessed dsRed-labelled podocytes, and the two rats that were negative for this transgene were used in these experiments. Prolactin was used as a positive control.

3.2.3 Characteristics of the animal models

Initial studies were performed to assess the characteristics of the animal models utilised in subsequent imaging analyses. Three groups were studied: female wild-type (*wt*) MWF rats, transgenic male MWF rats expressing the human DT receptor on podocytes (hDTR-Pod/SG), that had undergone injection of DT to induce podocyte depletion, and male *wt* MWF rats that had undergone ischaemic-ATN induced CKD (n=2 in each group). Wt female MWF rats were used to obtain baseline observations, to eliminate the potential contribution of age-related focal glomerulosclerosis and progressive proteinuria that occurs spontaneously in males (Schulz et al., 2008).

Body weight, 24-hour urine volume, plasma creatinine concentration, spot urine creatinine concentration, spot urine protein concentration and glomerular filtration rate (Creatinine clearance) are displayed in Table 1 and Figure 15. Female *wt* MWF rats displayed mild levels of proteinuria (69.6 ± 10.1 mg/24h). This was slightly increased in the DT group (109.2 ± 14.2 mg/24h) and greatly elevated in the CKD group (238.9 ± 49.7 mg/24h). GFR was greater in the DT group compared to the other two groups. Consistent with previous reports (Campos-Bilderback et al., 2013), the CKD group had a low GFR, with increased urinary volume, and reduced urinary creatinine measurements. These findings were consistent with tubular injury occurring in the CKD model, with impaired urine concentrating ability, leading to the passing of large volumes of dilute urine.

Histological features of the models are shown in Figure 16, from perfused-fixed kidneys retrieved immediately after completion of the imaging studies. *wt* MWF rats had normal renal architecture. Podocyte depleted rats displayed evidence of disrupted glomerular architecture, with expansion of capillary loops, and tubular vacuole formation. In the ischaemic-ATN CKD rats, gross disruption of the renal cortex was observed, with evidence of tubular atrophy, interstitial mononuclear cell infiltration, protein cast formation, and fibrous intimal thickening, and increased interstitial collagen deposition as detected by the Masson's trichrome stain.

Model	BWt g	U Vol ml/24h	Pl Cr mg/dL	U Cr mg/dL	U Prot mg/24hr	GFR ml/min/100g BWt
wt	198.5 ± 4.5	12.3 ± 1.5	0.53 ± 0.01	27.7 ± 0.7	69.6 ± 10.1	0.23 ± 0.03
DT	378.0 ± 0.6	10.7 ± 0.03	0.45 ± 0.05	117.0 ± 3.0	109.2 ± 14.2	0.50 ± 0.02
CKD	226.5 ± 14.5	41.2 ± 11.2	2.50 ± 0.02	6.8 ± 2.2	238.9 ± 49.7	0.03 ± 0.004

Table 1: Summary of characteristics of the rat models used in intravital studies. BWt: body weight, U Vol: Urine volume, Pl Cr: Plasma creatinine, U Cr: Urine creatinine, U Prot: Urine protein, GFR: glomerular filtration rate. Mean ± SEM, n=2 rats per group.

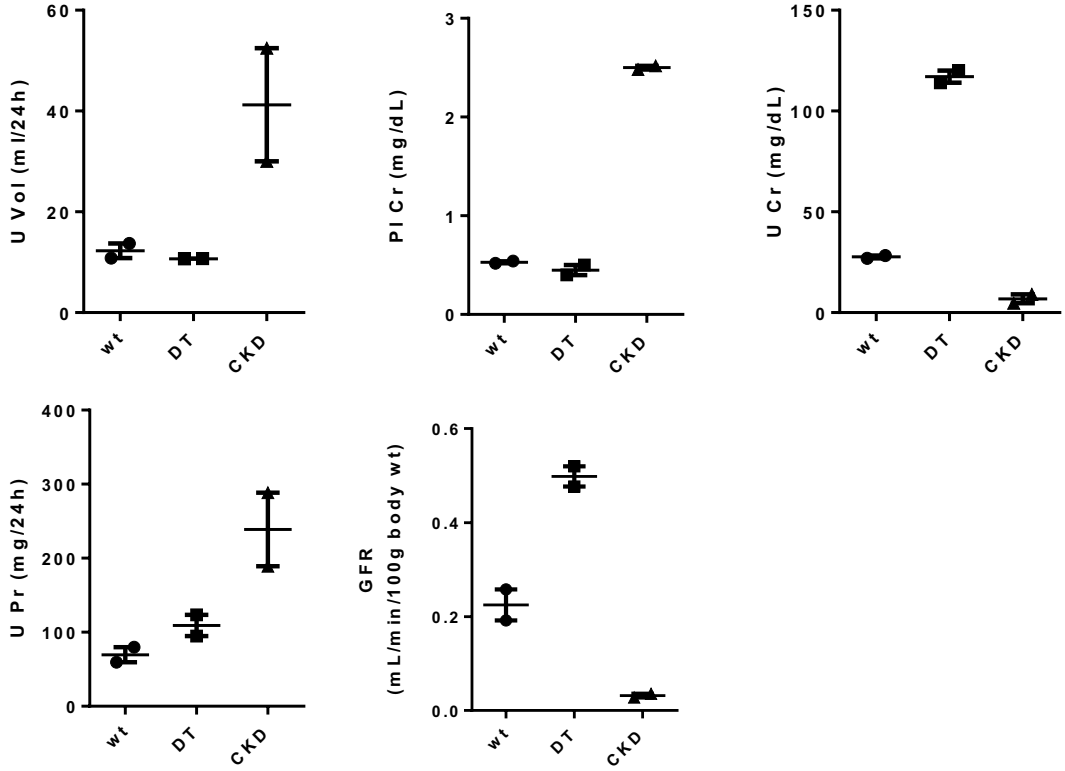

Figure 15: Characteristics of the rat models used in intravital studies. Samples were taken at the time of imaging. Each point represents an individual animal. Creatinine and protein concentrations were measured in duplicate, and a mean value was calculated. Horizontal lines represent the mean of each group, and vertical lines represent SEM. n=2 rats per group.

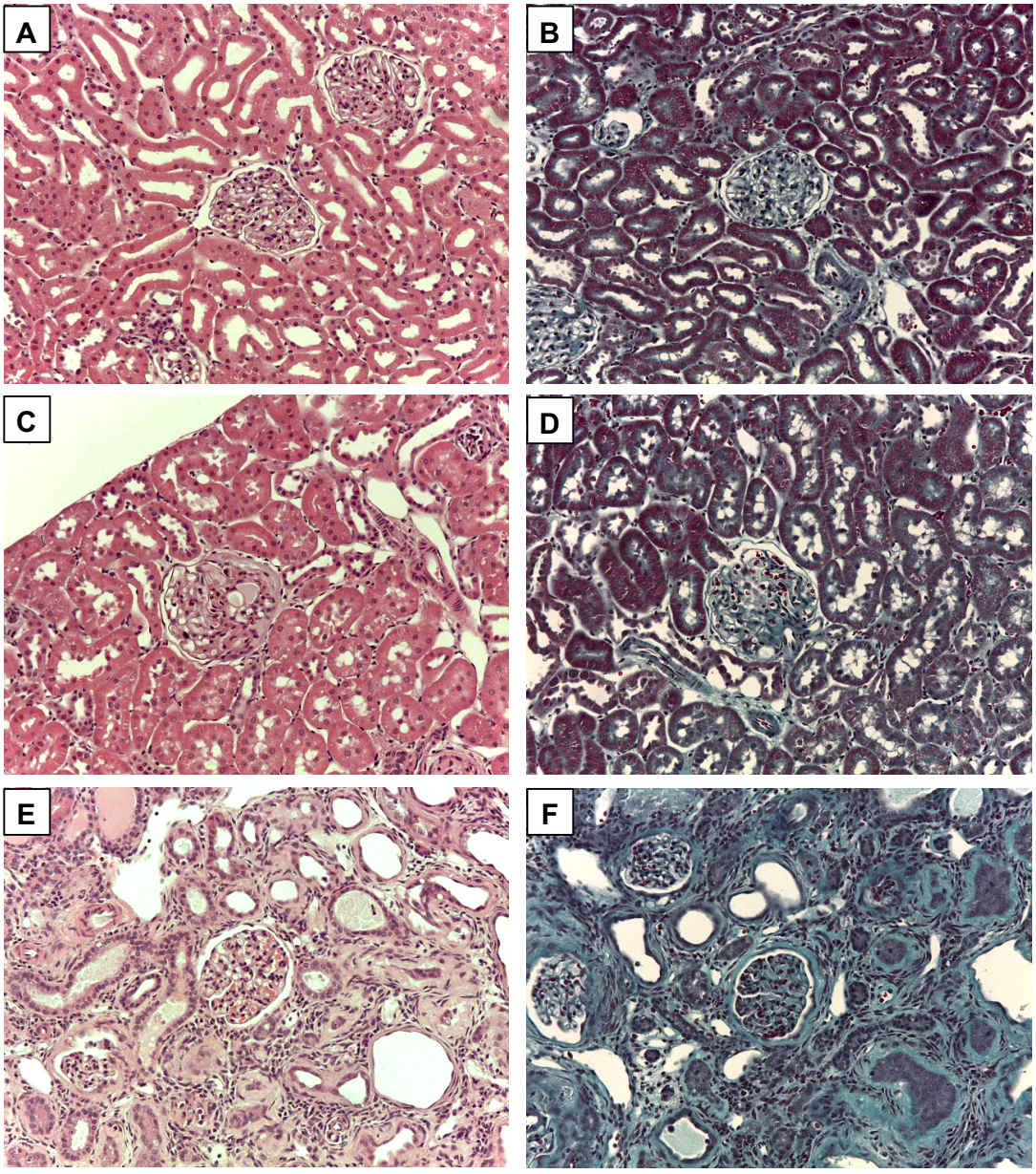

Figure 16: Histological features of the animal models used for intravital multiphoton microscopy. (A) H&E and (B) Masson's trichrome stain of a kidney section from a *wt* MWF rat, displaying normal renal architecture. (C) H&E of a kidney section from a podocyte depleted rat, displaying expansion of glomerular capillary loops, and vacuole formation within the tubules, and (D) Masson's trichrome stain displaying no increase in collagen deposition. (E) H&E stain of a kidney section from an ischaemic-ATN CKD rat, displaying tubular atrophy, interstitial mononuclear cell infiltration, protein cast formation, and (F) extensive interstitial and periglomerular collagen deposition (stained blue) on Masson's trichrome staining. Original magnification x200.

3.2.4 IgA is filtered and endocytosed by PTEC in wild type MWF rats

Initial studies were performed to evaluate the distribution and uptake of Texas Red labelled rat IgA (TR-IgA) in the kidney following its intravenous administration into a 15-week-old male MWF rat (not included in Table 1 or Figure 15). Imaging was performed up to 2.5 hours following administration (Figure 17). IgA was observed to filter across the glomerular filtration barrier and undergo endocytosis by PTEC by 40 minutes, via their apical surface. IgA accumulated within PTEC over the time studied, mainly in the S1 segments. No basolateral uptake of labelled IgA from peritubular capillaries was observed. By the end of the experiment, labelled IgA had merged with autofluorescent lysosomes, suggesting that the IgA had undergone lysosomal uptake and processing within PTEC. In addition, extracapillary deposits of IgA had started to organise within glomeruli, a characteristic not observed previously with experiments involving labelled albumin.

In order to better visualise intracellular lysosomal uptake, in subsequent experiments, a 3kDa Cascade Blue-labelled dextran was administered intravenously 24 hours prior to imaging. This lysosomal marker is freely filtered by the glomerulus, and labels PTEC lysosomes (Figure 18). Uptake of labelled rat IgA was studied in two 16 week old female *wt* MWF rats. Imaging was performed at 2h, 4h and 24 hours. IgA was again observed to be filtered across the glomerular filtration barrier, and undergo PTEC endocytosis. Merging of TR-IgA with the Cascade Blue labelled PTEC lysosomes was observed by 2 hours. By 24 hours, the merged IgA-lysosomes had trafficked towards the basolateral aspect of PTEC. A time series showed that the intensity of IgA had reduced by the 24 hour time point.

Finally, to ensure that the above observations were not phenomena isolated to surface glomeruli in the MWF strain, following sacrifice of the animals at 24 hours, the kidneys were immediately extracted, bisected longitudinally, and *ex vivo* images were obtained. These demonstrated that TR-IgA was visible within PTEC at a greater depth of up to 300 microns below the surface of the kidney, and that uptake was not confined to surface glomeruli and their connecting proximal tubules (Figure 18).

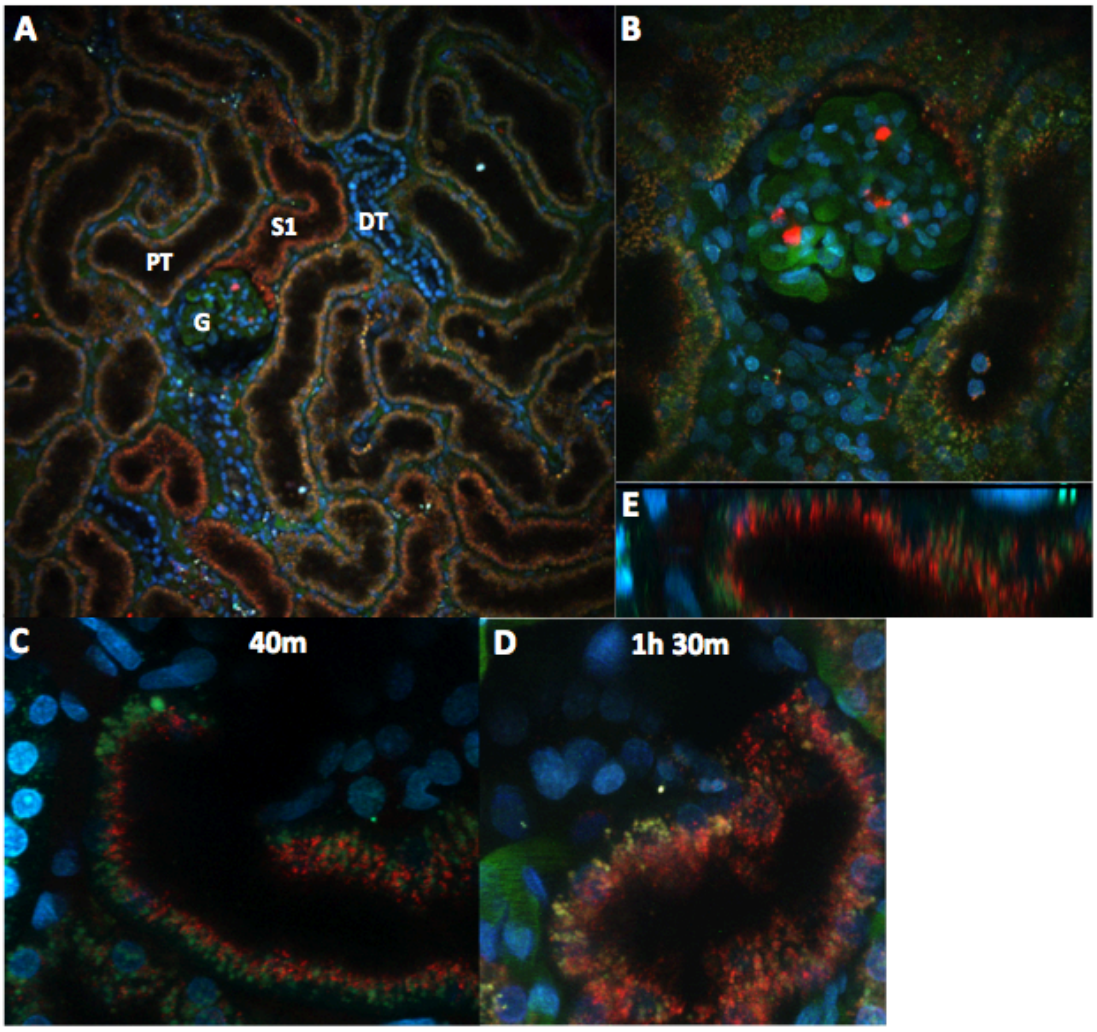

Figure 17: Glomerular filtration and proximal tubular uptake of rat IgA in a live male MWF rat, visualised by intravital multiphoton microscopy. (A) Image at 2h 30 mins demonstrating landmarks after labelling with a 150kDa fluorescein dextran (green) and the nuclear dye Hoechst 33342 (blue). G: Glomerulus, S1: S1 segment of the proximal tubule, PT: Proximal tubule, DT: Distal tubule. TR-IgA was observed mainly within PTEC of the S1 segment of the proximal tubule. PTEC can be identified by their autofluorescence (green), in contrast to distal tubular cells (B) IgA was observed to accumulate in extracapillary deposits within glomeruli by 2 hours. (C) Image at 40 minutes demonstrates IgA uptake by the apical surface of the proximal tubule. (D) By 1h 30 mins, IgA was observed to merge (yellow) with autofluorescent lysosomes, suggesting lysosomal uptake. (E) Orthogonal view of apical proximal tubule IgA uptake.

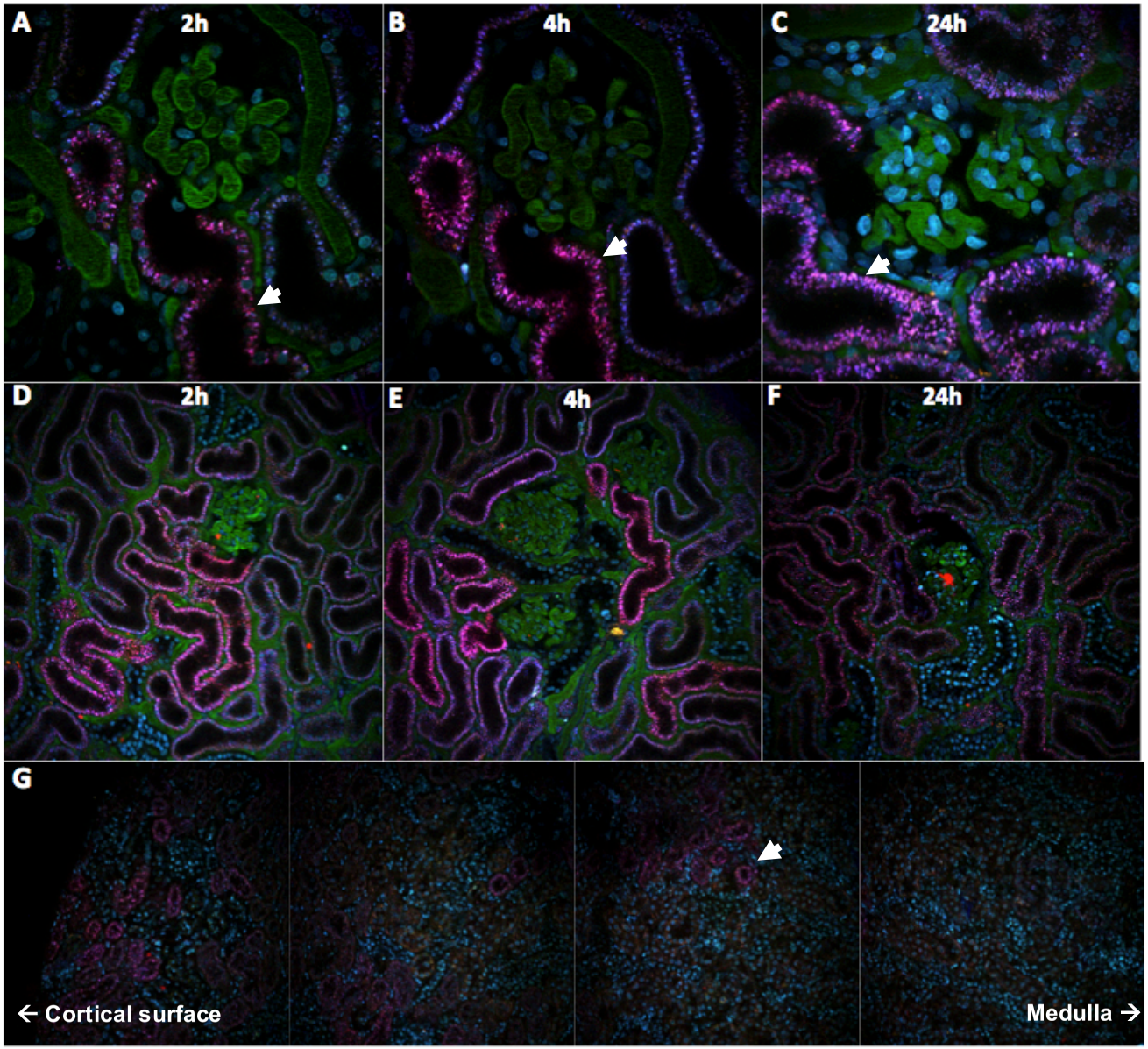

Figure 18: Glomerular filtration and proximal tubular uptake of rat IgA in female MWF rats, visualised by intravital multiphoton microscopy. (A) Image at 2h demonstrated initial uptake by the proximal tubule, with free TR-IgA being seen (arrowhead). (B) At 4h, increased uptake was observed, with merging of Texas Red-IgA with Cascade Blue-labelled lysosomes (arrowhead). (C) By 24h, most of the merged purple signal was evident at the basolateral surface of the proximal tubular cells (arrowhead). (D-F) Time series over 2h, 4h and 24h respectively. Peak signal was seen at 4h, with the signal fading by 24h. (G) Ex vivo images of the kidney, removed, bisected longitudinally and imaged after sacrifice. TR-IgA was seen at a depth of around 300 microns (arrowhead signifies deepest level where TR-IgA observed), indicating that proximal tubular endocytosis of IgA was not confined to the surface glomeruli of the MWF rat.

3.2.5 Glomerular deposition, filtration and proximal tubular endocytosis of IgA are increased in a rat model of podocyte depletion

A model of podocyte depletion was used to determine whether disruption to the glomerular filtration barrier and increasing the amount of filtered IgA had an effect on its interaction with the proximal tubule. Podocyte depletion in transgenic adult male hDTR-Pod/SG rats was induced by administration of 200 ng diphtheria toxin by subcutaneous injection five days before imaging studies took place, a dosage established from previous studies (Wagner et al., 2016; Wharram et al., 2005).

By 2 hours after intravenous injection of TR-IgA, uptake of IgA by proximal tubules was greatly increased compared to the same time point in *wt* MWF rats (Figure 19). The degree of proximal tubular IgA uptake was not uniform and appeared to correlate with the amount of IgA deposition observed in the connecting glomerulus. The fluorescent signal from TR-IgA within PTEC remained present at 24 hours, and had localised to peri-nuclear regions by this time point.

Ex vivo images again demonstrated PTEC uptake of TR-IgA to a depth of approximately 300 μm below the cortical surface (data not shown).

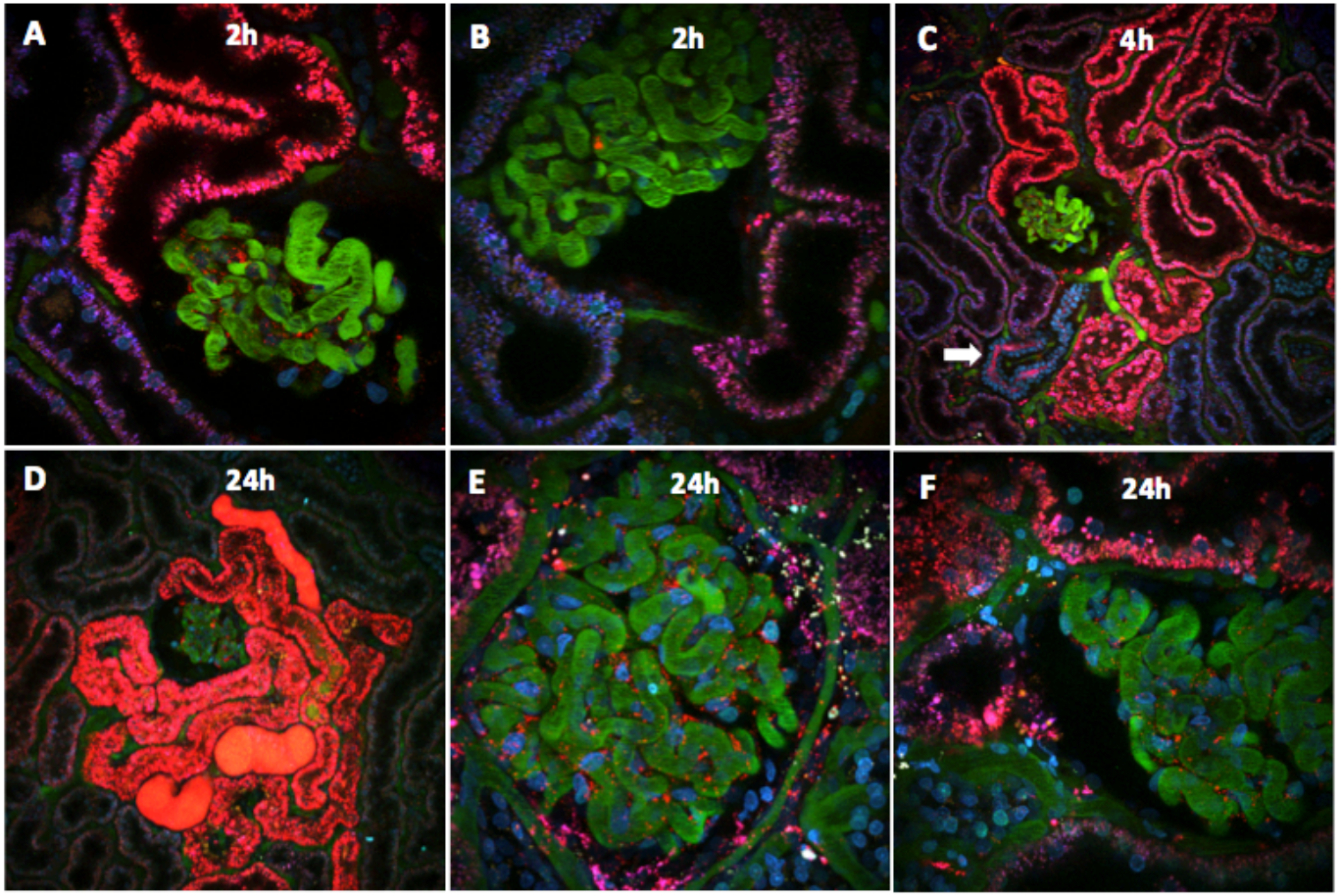

Figure 19: Glomerular filtration and proximal tubular uptake of rat IgA in podocyte injured rats. (A) By 2 hours, proximal tubular uptake of TR-IgA was already greatly upregulated compared to the same time point in wild type MWF rats. (B) A separate proximal tubule and glomerulus from the same rat showing less IgA uptake. The degree of uptake was not uniform across all proximal tubules, and appeared to be related to the degree of glomerular IgA deposition, and therefore the amount of IgA that had escaped across the glomerular filtration barrier. (C) 20x magnification of IgA uptake in a podocyte depleted rat. Note that some IgA was also seen in the distal tubule (arrow). (D) The fluorescent signal from the IgA was still visible at 24h. Note the presence of protein casts which contained TR-IgA. (E) Glomerular deposition of IgA was increased and remained visible at 24h. (F) By 24h, IgA was localised to the perinuclear and basolateral aspects of PTEC.

3.2.6 IgA is not endocytosed by the proximal tubule in a model of ischaemic ATN induced chronic kidney disease

CKD was induced in adult male *wt* MWF rats by renal ischaemia reperfusion injury followed two weeks later by contralateral uninephrectomy, to determine whether TR-IgA uptake by PTEC would be affected by the tubular injury known to occur in this model. Imaging took place two weeks after the uninephrectomy.

In contrast to the findings observed with *wt* MWF rats, and with the podocyte depleted rats, in this model of ischaemic ATN induced CKD, minimal to absent proximal tubule uptake of TR-IgA was observed at all the time points studied up to 24 hours (Figure 20). However, total proteinuria levels were over three times higher than in *wt* MWF rats (Table 1).

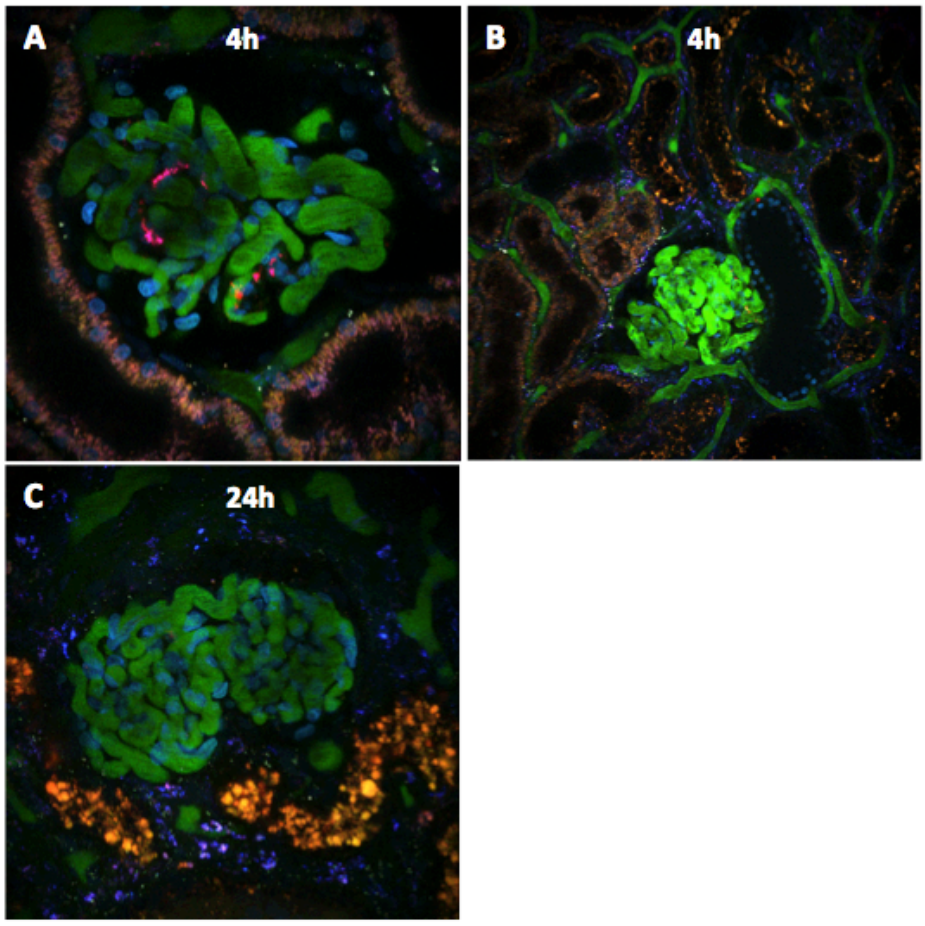

Figure 20: Renal handling of IgA in a rat model of ATN induced chronic kidney disease. (A) IgA deposition was observed within occasional glomeruli and proximal tubules, but this was markedly reduced compared to the wild type and podocyte depleted rats. Furthermore, proximal tubule lysosomal uptake of the Cascade Blue dextran was also reduced. Proximal tubules are demonstrated by autofluorescence. (B) 20x magnification image showing no uptake of IgA in the glomerulus or tubules. (C) This absence persisted up to 24h.

3.3 Conclusions

This series of intravital multiphoton microscopy studies demonstrated that in *wt* MWF rats, serum IgA can be filtered through the glomerular filtration barrier into the urinary space, and undergoes endocytosis by the proximal tubule. This process was greatly increased in a model of podocyte depletion with compromise to the glomerular filtration barrier, that results in increased glomerular extracapillary deposition, filtration and proximal tubular uptake of IgA. In a model of ischaemia-reperfusion induced ATN and CKD, the processes of glomerular deposition and proximal tubular uptake were reduced. These experiments provide, for the first time, *in vivo* evidence that IgA interacts with the apical surface of PTEC.

Despite induction of podocyte depletion in the hDTR-Pod/SG rat strain, and a clear increase in the filtration of IgA and its uptake by PTEC, total proteinuria levels were only modestly increased compared to wild type animals (109.2 ± 14.2 *vs* 69.6 ± 10.1 mg/24h respectively). This finding lends support to the hypothesis that the proximal tubule is able to endocytose considerable amounts of protein after its leakage through a damaged glomerular filtration barrier, preventing loss into excreted urine. Recent multiphoton microscopy studies suggest a role for both glomerular filtration and tubular uptake in determining the final level of proteinuria in disease (Wagner et al., 2016).

In contrast, minimal uptake of IgA by PTEC was observed in the ischaemic ATN-induced CKD model. This model, induced by ischaemia-reperfusion injury to one kidney followed by contralateral uninephrectomy, is analogous to the clinical scenario of ischaemic acute tubular necrosis (ATN) without recovery. The ability of the proximal tubule in this model to reabsorb filtered IgA was greatly diminished, and indeed total proteinuria was increased, both likely due to the tubular injury induced. This suggests that endocytosis of IgA by PTEC requires healthy tubules, and is likely to be an active process.

Although tubular staining for IgA is not a common feature of IgAN, filtered IgA may be endocytosed and processed by PTEC meaning that organised IgA-containing immune deposits do not accumulate in IgAN. From the current studies, filtered IgA was rapidly processed by the proximal tubules, with evidence of uptake and lysosomal processing within 2 hours, and basolateral accumulation occurring within

24 hours. These processes may then lead to catabolism, and therefore deposits of IgA may not have the chance to organise, and thus not be detectable by standard immunohistochemical techniques, which have a lower sensitivity compared to the methods used in this chapter.

The glomerular filtration of TR-IgA in *wt* rats was unexpected, especially as the majority of IgA purified was high molecular weight polymeric IgA, as seen in Figure 13. The *wt* MWF rats studied had mild levels of proteinuria, which may have resulted in small amounts of IgA passing through the glomerular filtration barrier. The 150 kDa fluorescein dextran had a lower molecular weight than the IgA administered, and was not filtered. This is likely due to the difference in their tertiary structures, dextran being essentially a linear carbohydrate, compared to the more globular structure of IgA. Indeed, dextrans of lower molecular weight (70 kDa) have been used in clinical medicine as colloids for the purposes of plasma volume expansion. Whether both pIgA and mIgA are able to pass through the glomerular filtration barrier in the MWF rat is unknown and would be an interesting area for future study.

MWF rats were used for these studies as they possess glomeruli in close proximity to the cortical surface, and enable anatomical details to be visualised such as transition from the glomerulus to the S1 segment of the proximal tubule. The working distance of the Nikon 60x water immersion objective used limits imaging to a maximum of approximately 200 μm depth into tissue. The dynamics of deeper glomeruli and tubules are currently not visible by intravital multiphoton microscopy. Humans do not possess surface glomeruli, and therefore a limitation to the applicability of this model is whether the surface glomeruli and their connected tubules behave in the same way as deeper structures. To address this, *ex vivo* sections were studied, where it was demonstrated that proximal tubular uptake of IgA could be observed up to around 300 μm depth, approaching the cortico-medullary junction. This was observed in both wild type and podocye depleted rats, implying that proximal tubular uptake of IgA was not a phenomenon solely limited to surface glomeruli. In another intravital imaging study focusing on mouse glomerular IgA deposition and utilising confocal microscopy, IgA from the ddY mouse strain, but not from *wt* BALB/c mice, deposited along mouse glomerular capillaries in a focal and segmental manner as early as 1 minute after injection, and then

diminished after 2 hours. However, in order to image the glomeruli, the investigators had to dissect the lower pole of the kidney before imaging, and this trauma may have had significant effects on normal physiological processes (Yamaji et al., 2014).

A podocyte depletion model was studied in order to test whether disruption of the glomerular filtration barrier led to an increase in filtered IgA and its subsequent processing. In patients with IgAN, podocyte loss was found to correlate with the extent of glomerulosclerosis, impairment of permselectivity and loss of GFR (Lemley et al., 2002). In a separate study of patients with IgAN, urinary podocyte mRNA, indicative of acute podocyte loss, correlated with glomerular lesions (segmental glomerulosclerosis and extracapillary proliferation) (Fukuda et al., 2015). Furthermore, a reduction in glomerular podocyte nuclear density was associated with tubular atrophy/interstitial fibrosis, reduction in eGFR and proteinuria (Fukuda et al., 2015). In children with either IgAN or HSP, persistent urinary podocyte excretion was associated with glomerulosclerosis and progression of disease. Although conflicting data exists regarding the direct effects of IgA on podocytes, glomerular expression of the podocyte markers nephrin and ezrin were shown to be downregulated in response to IgA-mesangial cell conditioned medium, prepared by culturing human mesangial cells with pIgA from IgAN patients (Lai et al., 2009, 2008; Wang et al., 2009). Podocyte loss may therefore be an important early step in the progression of IgAN, linking mesangial IgA deposition with disruption of the glomerular filtration barrier and subsequent increase in protein filtration.

Labelled rat IgA was used in these studies to model a homologous situation to human disease. Although the structure and function of rat IgA has not been completely characterised, there are important differences between human and rat IgA which should be noted. Hepatobiliary transport of rat polymeric IgA occurs to a greater extent than in mice or humans (Delacroix et al., 1982; Jackson et al., 1978). Also, rodent IgA differs from human IgA in that there is only a single isotype, and rodent IgA lacks the elongated O-glycosylated hinge region found in humans (Woof, 2013). Interestingly, in the current study, rat IgA was deposited in the mesangium at an early time point, a phenomenon not previously observed in studies of fluorescently labelled rat serum albumin or dextrans, suggesting that the

absence of the elongated hinge region did not affect rat IgA glomerular deposition. How the rat handles labelled human IgA and whether this differs from the current observations would be an area of interest for further study.

In summary, these intravital multiphoton microscopy studies have provided evidence for the first time that IgA can undergo filtration and proximal tubular endocytosis, and that this is increased in a model of proteinuria of glomerular origin.

Chapter 4: The effects of IgA1 on proximal tubular epithelial cells

4.1 Introduction

It remains unclear why a certain proportion of patients with IgAN develop progressive CKD and ESRD, while the remainder may have stable kidney function. From histological features, severity of mesangial IgA deposition does not correlate with the risk of disease progression or renal prognosis, but rather tubulointerstitial fibrosis is the strongest predictor of progression (Cattran et al., 2009). This implies that tubular-specific factors are important in the pathogenesis of progressive IgAN. In common with other glomerular diseases, glomerular and tubulointerstitial inflammation with infiltration of mononuclear cells including macrophages, monocytes, and T cells into both compartments plays a key role in driving glomerular and tubulointerstitial fibrosis in IgAN (Alexopoulos et al., 1989; Arrizabalaga et al., 1997; Sabadini et al., 1988). Local production of cytokines, chemokines, adhesion molecules, growth factors and extracellular matrix subsequently contribute to the process of fibrogenesis.

Patients with IgAN possess characteristic abnormalities in their immune system. Serum IgA levels are raised in approximately 50% of patients, and there are elevated levels of pIgA compared to healthy individuals (van der Boog et al., 2005). Patients have elevated levels of serum IgA that is undergalactosylated in its hinge region (Moldoveanu et al., 2007). Eluates of mesangial IgA deposits are almost exclusively of the IgA1 isotype, polymeric, undergalactosylated, and anionic in nature, implying that these structural alterations confer specific pathogenicity (Allen et al., 2001; Conley et al., 1980; Monteiro et al., 1985). In a cohort of patients from Asia, the degree of IgA hinge region undergalactosylation, determined by HAA binding, correlated with worse renal prognosis (Zhao et al., 2012). *In vitro*, undergalactosylated IgA had a greater effect on mesangial cell proliferation compared to normally galactosylated IgA (Novak et al., 2005). Undergalactosylated IgA therefore appears to play a central role in the pathogenesis of IgAN. However, this is not the sole requirement, as first degree relatives of patents with IgAN, who themselves display no evidence of renal disease, may also possess raised levels of

undergalactosylated IgA1, implying that other susceptibility factors are important (Gharavi et al., 2008; Suzuki et al., 2011).

The links between undergalactosylated serum IgA, glomerular IgA deposition and disease progression are incompletely understood. Following IgA deposition and induction of glomerular disease, there are a number of potential mechanisms by which the tubular compartment may be affected, which may act independently or synergistically. Firstly, IgA may trigger release of soluble mediators from glomerular cells, e.g. mesangial cells or podocytes, which subsequently filter through the glomerular filtration barrier and interact with tubular cells. This process has previously been glomerulo-tubular crosstalk (Lai et al., 2005). *In vitro*, pIgA has been demonstrated to produce a stimulatory effect on mesangial cells, resulting in release of a number of pro-inflammatory cytokines, including TNF-α, MCP-1, IL-8, IFN-10, MIF, and TGF-β (Lai, 2003; Leung et al., 2008, 2003; Oortwijn et al., 2006; Tam et al., 2009).

Secondly, disruption to the glomerular filtration barrier may result in proteinuria. Albumin itself may be a trigger for PTEC stimulation, and has been the focus of many recent studies (Baines and Brunskill, 2011). It should be noted, however, that progressive interstitial fibrosis is an uncommon finding in minimal change disease, a form of glomerulonephritis where there may be heavy proteinuria restricted to lower molecular weight proteins such as albumin (Waldman et al., 2007).

Thirdly, IgA may pass through the damaged glomerular filtration barrier in IgAN, and cause direct damage to PTEC. IgA is filtered into the proximal tubule and ultimately into the urine in increased amounts in IgAN. Levels of urinary IgA-IgG immune complexes and undergalactosylated IgA were increased in IgAN compared to other renal diseases and healthy individuals, implying that the proximal tubule is exposed to these in IgAN (Matousovic et al., 2006). Additionally, non-selective proteinuria, defined by the presence of higher molecular weight proteins such as immunoglobulins, was associated with worse renal function and prognosis in IgAN (Woo et al., 1989). However, to date, the effects of IgA on PTEC have not been explored in detail.

The aims of this chapter were to ascertain:

1. Whether total IgA has an effect on human PTEC cytokine release
2. The structural properties of IgA required for this effect
3. The differential effects of conditioned media from IgA-stimulated mesangial cells, compared to IgA itself, on PTEC cytokine release

Initial studies focussed on PTEC release of TGF-β1, as a cytokine widely implicated in renal fibrosis and released in increased quantities by mesangial cells in response to pIgA1 (Lai, 2003; Loeffler and Wolf, 2014), and IL-6, implicated in several inflammatory renal conditions, and found in increased levels in the urine of patients with IgAN (Harada et al., 2002). Stimulation of Peroxisome proliferator-activated receptor (PPAR) response element (PPRE) was examined as an indicator of PPAR transcription factor activity, given its importance in PTEC intracellular signalling as a response to other proteins including albumin, and previous evidence from an *in vivo* model of IgAN, demonstrating that the PPAR-γ inhibitor rosiglitazone had an anti-inflammatory effect in reducing renal expression of TGF-β1, angiotensin II receptor subtype-1 and ICAM-1 (Baines and Brunskill, 2011; Lai et al., 2011).

4.2 Results

4.2.1 Purification and separation of IgA1

Human IgA1 was purified by Jacalin-agarose affinity chromatography. Samples were concentrated to between 1 to 2 mg/mL by centrifugal filtration. To determine purity, non-reduced and reduced IgA1 samples were separated by SDS-PAGE, and stained with Coomassie blue (Figure 21), which revealed minimal contamination.

Total IgA1 was then separated by gel filtration (Figure 22). Distinct peaks were observed which, according to previous reports, were consistent with polymeric (pIgA1), dimeric (dIgA1), and monomeric (mIgA1) forms of IgA1 (Almogren and Kerr, 2008; Oortwijn et al., 2006). Individual fractions obtained were analysed and confirmed to contain IgA by ELISA (Figure 23), and separated by SDS-PAGE for analysis by staining with Coomassie blue and by Western blotting (Figure 24).

Fractions containing mIgA1 and pIgA1 were pooled as indicated, and concentrated to approximately 1 mg/mL by centrifugal filtration. Pooled total IgA1, mIgA1 and pIgA1 samples were subjected to Western blotting, which confirmed separation of these fractions (Figure 25).

During optimisation experiments, IgA1, purified from historically collected serum samples that had been subjected to repeat freeze-thaw cycles, was found to contain a much higher proportion of pIgA compared to IgA1 purified from serum that had not been frozen. The proportion of pIgA was also found to increase if the total IgA1 preparation had been concentrated to over 2 mg/mL. Therefore IgA appeared to self-aggregate depending on freeze-thaw cycles and working concentration. Care was taken in all subsequent experiments to minimise freeze-thaw cycles and to maintain the working concentration of purified IgA to less than 2 mg/mL.

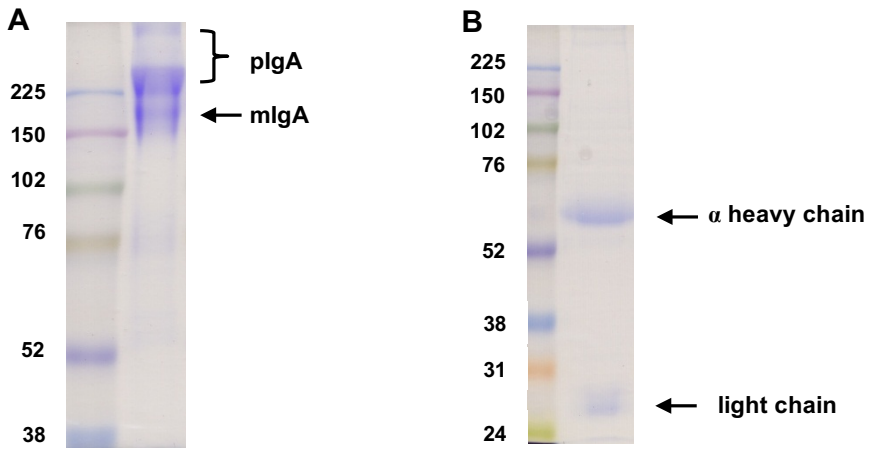

Figure 21: Analysis of total IgA1 after separation by SDS-PAGE and staining with Coomassie Blue. Total IgA1 was prepared from serum from a healthy subject by Jacalin-affinity chromatography. (A) Non-reduced sample, showing separation of mIgA1 from pIgA1 and (B) Reduced sample, showing a single protein band at approximately 55 kDa representing α heavy chains, and a smaller band at approximately 25 kDa, which represent the light chains.

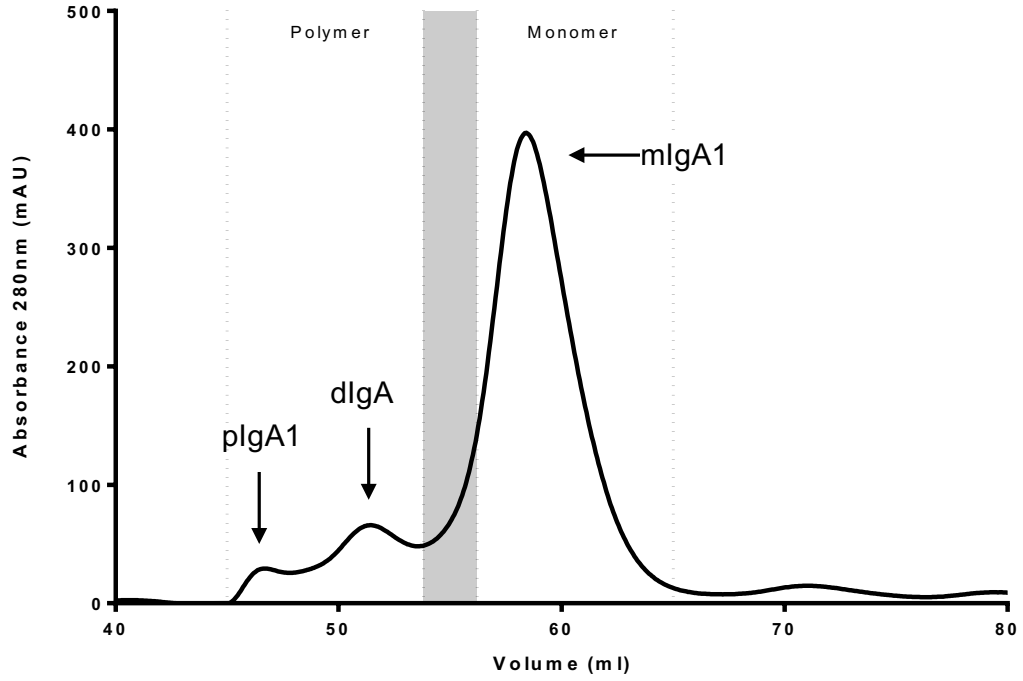

Figure 22: Example separation of purified IgA1 by gel filtration on a HiLoad 16/600 Superdex 200 preparative grade column (GE Healthcare). The line indicates the elution profile of a purified total IgA1 sample. pIgA1: polymeric IgA1, dIgA1: dimeric IgA1, mIgA1: monomeric IgA1.

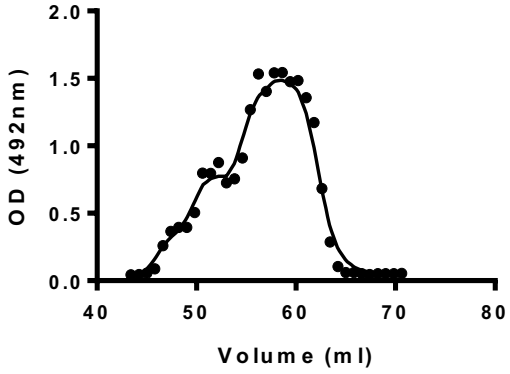

Figure 23: IgA content of purified fractions separated by gel filtration. IgA was detected in samples collected in mIgA1 and pIgA1 fractions by ELISA, and not in other fractions.

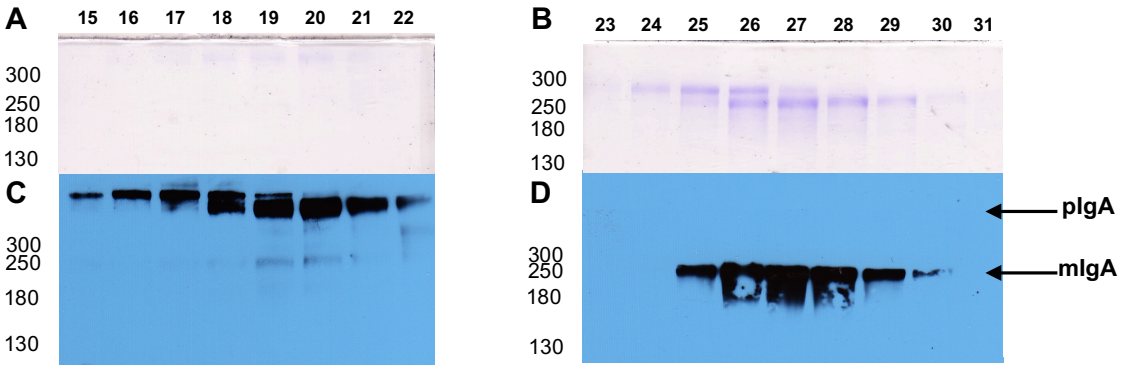

Figure 24: Characterisation of purified IgA1 fractions. (A & B) 8% SDS-PAGE under non-reducing conditions stained with Coomassie blue to determine purity of each fraction. (C & D) Western blot of IgA containing fractions, showing separation of fractions according to molecular weight.

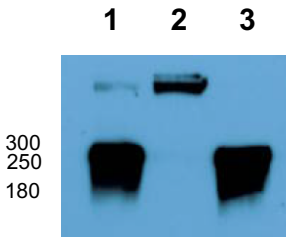

Figure 25: Western blot of IgA1 samples pooled and concentrated after separation by gel filtration. Samples were separated on 8% SDS-PAGE under non-reducing conditions and probed with an anti-human IgA antibody. Lane 1: Total IgA1, Lane 2: Polymeric IgA1, Lane 3: Monomeric IgA1.

4.2.2 Total IgA1 stimulates PTEC PPRE activity and pro-inflammatory (IL-6) and pro-fibrotic (TGF-β1) cytokine production by HK-2 PTEC

To assess whether IgA1 had a stimulatory effect on cultured human PTEC, HK-2 PTEC were incubated with total IgA1 pooled from patients with IgAN, or from healthy subjects at a concentration of 100 μg/mL, and compared to incubation with albumin at 100 μg/mL or 5 mg/mL, IgG or IgM, both at 100 μg/mL, for 24 hours.

PPAR response element (PPRE)-luciferase activity was significantly upregulated by IgA1 from the IgAN patients by approximately 1.5 fold compared to media alone (Figure 26). Of the other conditions, PPRE-luciferase activity was also significantly upregulated by the albumin at 5 mg/mL only. Albumin at 100 μg/mL, IgA1 from healthy subjects, and IgM had no significant effect.

TGF-β1 release by PTEC was also significantly upregulated by IgA1. There was no difference observed between cells stimulated with IgA1 isolated from patients with IgAN compared to healthy subjects. IL-6 release from PTEC was significantly upregulated by IgA1 from the IgAN patients and by albumin at 5 mg/mL. Although there was an increase in fibronectin release from PTEC stimulated with IgA1, this was not statistically significant.

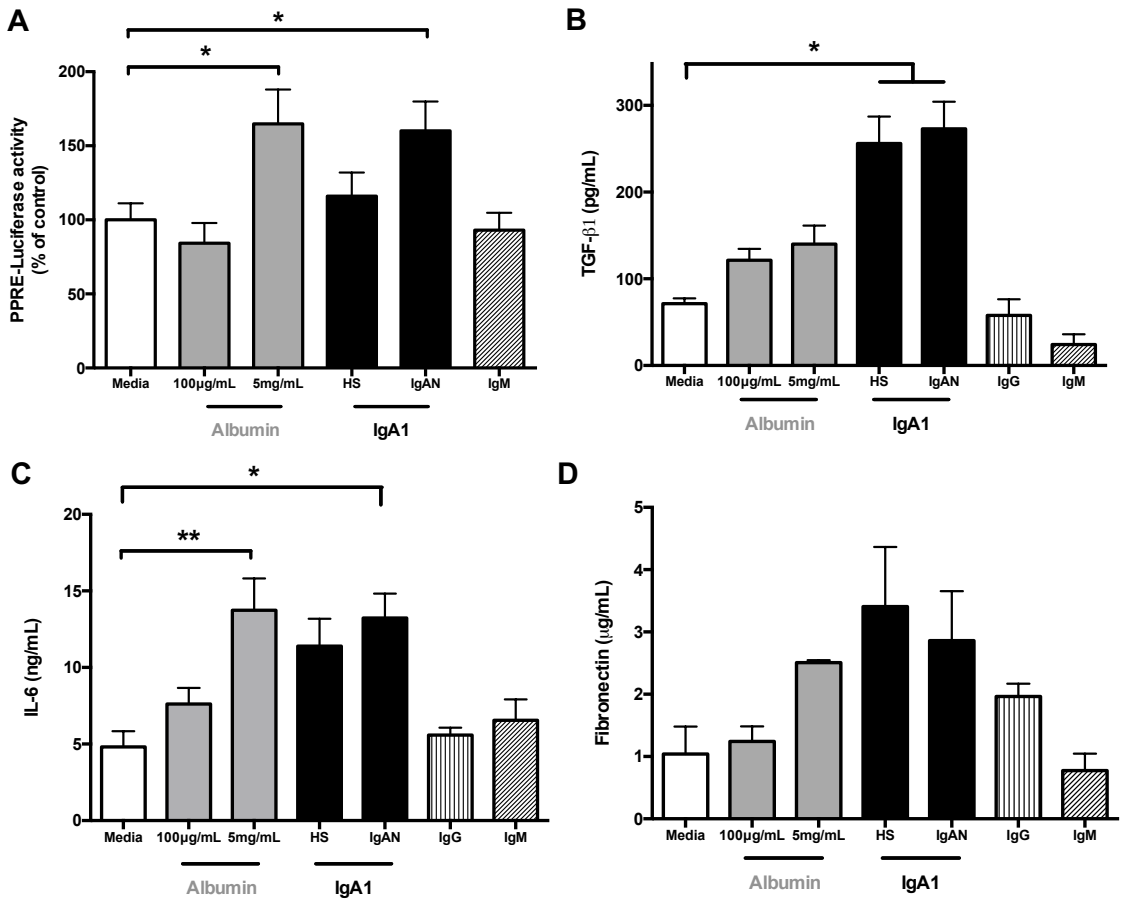

Figure 26: PPRE activity and cytokine release from PTEC stimulated with total IgA1. (A) PPRE-luciferase activity was significantly increased in HK-2 PTEC treated with albumin at 5 mg/mL or IgA1 from IgAN patients at 24 hours (n=4) * *P* <0.05. (B) TGF-β1 release from PTEC was increased by IgA1 from both healthy subjects (HS) and IgAN patients (n=5) * *P*<0.05. (C) IL-6 release was increased by albumin at 5 mg/mL and IgA1 from IgAN patients (n=5) ** *P* <0.01, * *P* <0.05. (D) No significant increase in fibronectin release was observed.

4.2.3 TGF-β1 production is significantly increased by pIgA1 and mIgA1

The differing effects of mIgA1 and pIgA1 on HK-2 PTEC cytokine production were compared. HK-2 cells were stimulated with mIgA1, pIgA1 (both 100 μg/mL), or vehicle only (PBS) for 48 hours, the optimal time point established after pilot time course experiments, before supernatants were collected for analysis.

pIgA1 had a greater effect on TGF-β1 release than mIgA1 (Figure 27A). There was no significant difference in the effects observed between IgA1 preparations from healthy subjects and IgAN patients. An increase in TGF-β1 mRNA expression, expressed as a ratio compared to the housekeeping gene RPL37A, was also observed in HK-2 cells stimulated by pIgA1, although this only reached statistical significance from the pIgA1 from healthy subjects (Figure 27B).

To ensure IgA1-induced TGF-β1 release by PTEC could not be explained by low levels of endotoxin contamination, in a separate experiment, HK-2 PTEC were stimulated with lipopolysaccharide (LPS) from *E Coli*. No increase in TGF-β1 was observed at concentrations of LPS up to 10 ng/mL (all levels below the limit of detection, data not shown). Additionally, there was no significant difference in HK-2 cell lysate total protein content between the different conditions tested, implying that differences in TGF-β1 production could not be explained by variations in cell proliferation. Correcting TGF-β1 production for cell lysate protein concentration produced the same findings as above.

In contrast, IL-6 production by PTEC was not increased by mIgA1 or pIgA1 compared to vehicle alone (Figure 27C).

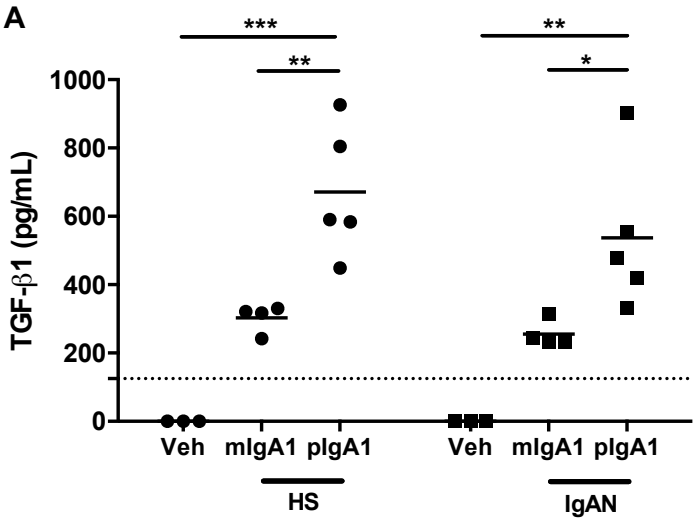
A
***
**
**
*
1000
800
600
400
200
0
TGF-β1 (pg/mL)
Veh
mIgA1
pIgA1
Veh
mIgA1
pIgA1
HS
IgAN

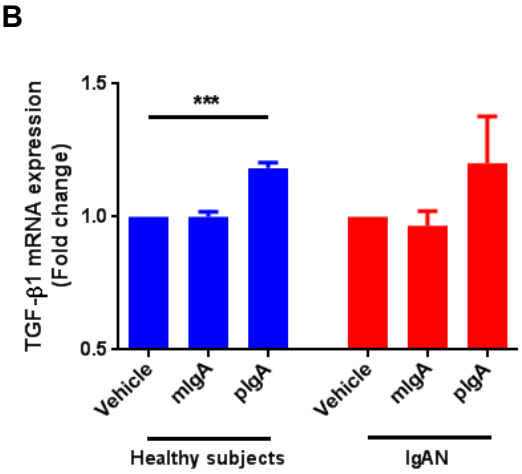
B
***
1.5
1.0
0.5
TGF-β1 mRNA expression
(Fold change)
Vehicle
mIgA
pIgA
Vehicle
mIgA
pIgA
Healthy subjects
IgAN

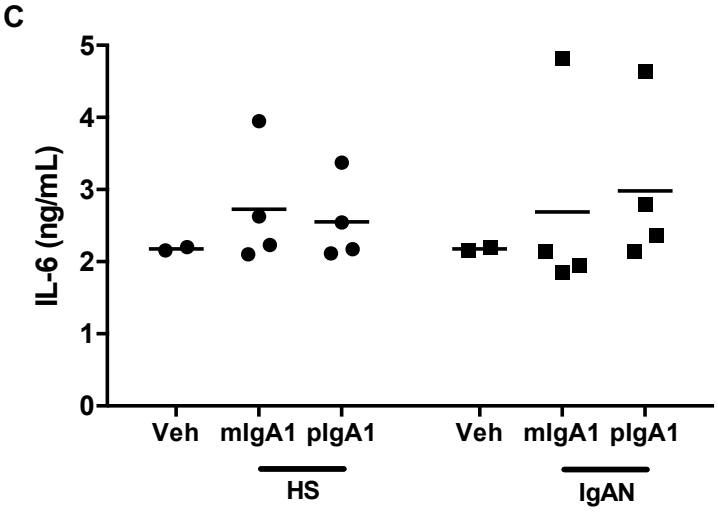
C
5
4
3
2
1
0
IL-6 (ng/mL)
Veh
mIgA1
pIgA1
Veh
mIgA1
pIgA1
HS
IgAN

Figure 27: HK-2 cell cytokine release in response to mIgA1 and pIgA1. (A) TGF-β1 release by HK-2 cells. TGF-β1 production was increased by both mIgA1 and pIgA1. No significant difference was observed between IgA preparations from healthy subjects (HS) or IgAN patients. (B) Relative HK-2 cell mRNA levels of TGF-β1/RPL37A stimulated by IgA1. An increase in TGF-β1/RPL37A mRNA was observed in cells treated by pIgA1 from HS only. (C) IL-6 release by HK-2 cells. No significant increase in IL-6 production was observed in cells treated with mIgA1 or pIgA1. Horizontal lines represent the mean. Points represent HK-2 cells stimulated by IgA1 from an individual patient or control, with each experiment was performed in duplicate and the mean calculated. In (B), data are presented as a grouped analysis. * $P < 0.05$, ** $P < 0.01$, *** $P < 0.001$.

4.2.4 pIgA1 is undergalactosylated when compared to mIgA1

As undergalactosylated IgA1 is believed to be particularly pathogenic, the galactosylation status of mIgA1 and pIgA1 preparations from 5 individual patients with IgAN and 5 healthy controls was tested by *Helix Aspersa* agglutinin (HAA) binding. pIgA1 preparations had significantly higher HAA binding levels compared to the mIgA1 preparations, indicating that pIgA1 was enriched for IgA1 that was galactose-deficient. No difference in HAA binding was apparent between IgA1 isolated from patients with IgAN and healthy subjects.

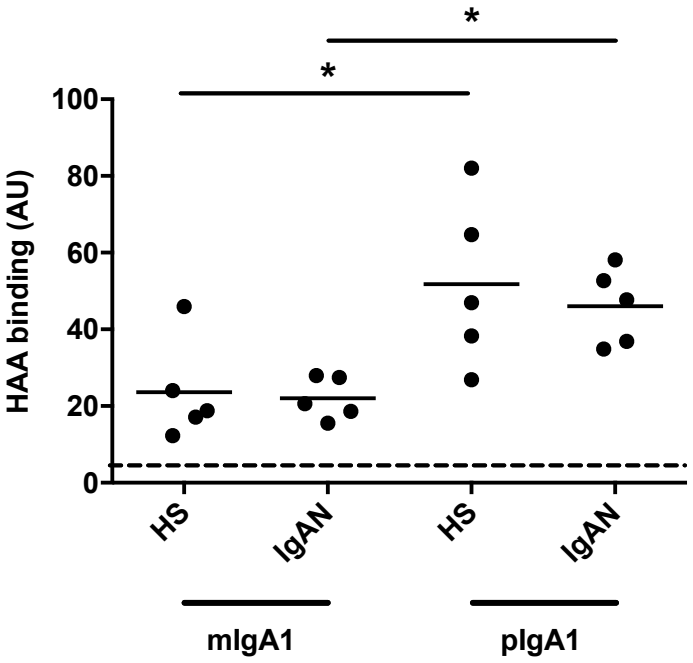

Figure 28: Helix Aspersa agglutinin (HAA) binding to IgA1 samples. HAA binding was significantly higher in pIgA1 from both healthy subjects (HS) and patients with IgAN compared to mIgA1, indicating reduced IgA1-hinge region galactosylation. Horizontal lines represent the mean, each sample was tested in duplicate. * $P < 0.05$. HS: Healthy subjects. AU: Arbitrary units.

4.2.5 TGF-β1 production by IgA1 stimulated HK-2 cells correlates with IgA1 galactosylation status.

The galactosylation status of individual IgA1 preparations was tested and compared to its effect on TGF-β1 release. HK-2 TGF-β1 release correlated with HAA-IgA1 binding, indicating that there was a relationship between TGF-β1 production and the degree of IgA1-hinge region undergalactosylation. This effect was most pronounced with galactose-deficient pIgA1 (GdpIgA1) (Figure 29A). No correlation was observed between IL-6 production and IgA1-HAA binding (Figure 29B).

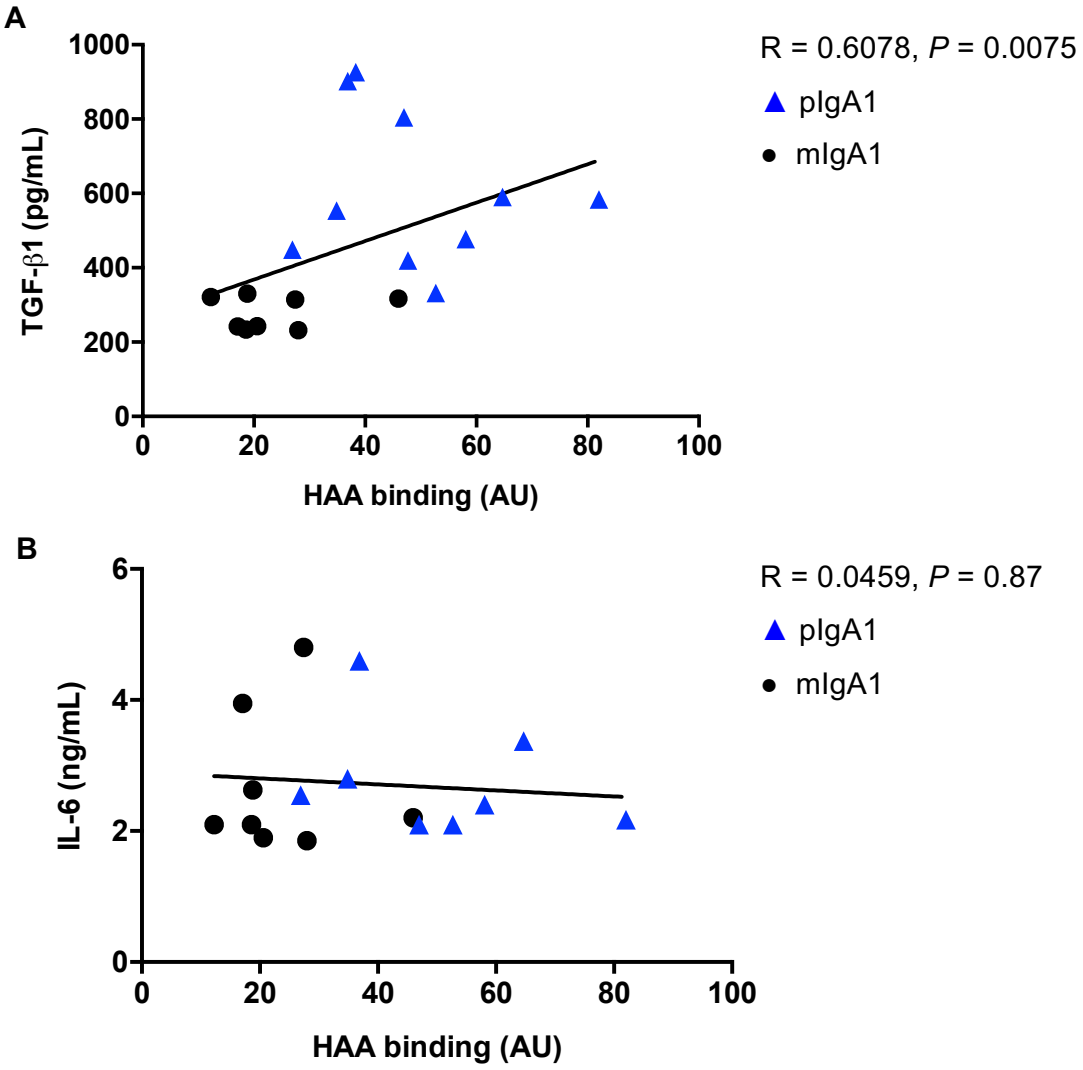

Figure 29: Effects of IgA1 galactosylation status and HK-2 cytokine production. (A) Correlation between TGF-β1 production and HAA binding of individual IgA1 preparations. IgA1 preparations that possessed higher HAA binding produced greater TGF-β1 release from HK-2 cells. (B) Correlation between IL-6 production and HAA binding of individual IgA1 preparations. No correlation was observed between HK-2 cell IL-6 release and HAA-IgA1 binding.

4.2.6 The effects of IgA1 and IgA1-mesangial cell derived conditioned media on PTEC cytokine release

In vivo, PTEC are likely to be exposed simultaneously to both filtered IgA1 and glomerular-derived cytokines produced from IgA1-stimulated mesangial cells. PTEC were therefore incubated with IgA1 alone, IgA1-human mesangial cell derived conditioned medium (HMC-CM), or a combination of the two. To generate HMC-CM, primary human mesangial cells were incubated with pIgA1 (100 µg/mL) from individual patients with IgAN or a healthy subject for 48 hours before collecting the conditioned media. PTEC were then incubated with vehicle (PBS), HMC-CM (diluted 1:4 in DMEM/F12 media), or mIgA1 or pIgA1, alone or together with HMC-CM diluted 1:4 (final concentration of IgA1 125 µg/mL) generated using pIgA1 from the same patient or control (Figure 30). After 48 hours, supernatants were collected and the presence of a panel of pro-inflammatory and pro-fibrotic cytokines and growth factors, known to play a role in progressive interstitial fibrosis, was quantified using a customised multiplex array (Table 2) (Abbate et al., 2006; Baines and Brunskill, 2011).

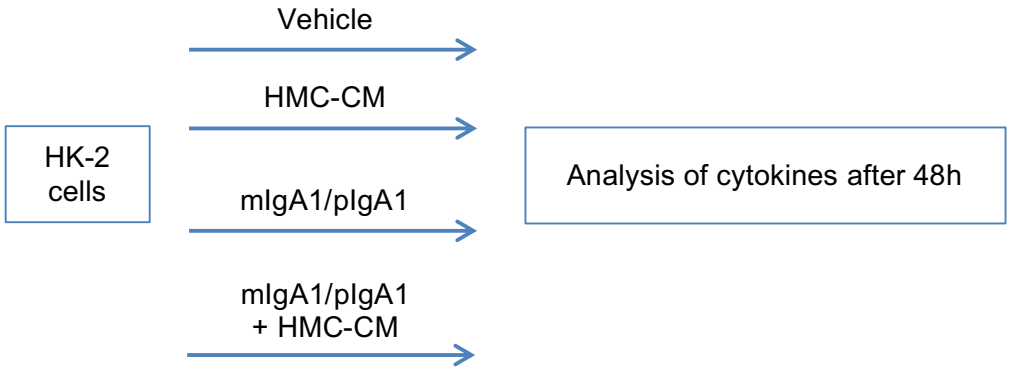

Figure 30: Experimental plan for the comparison of the effects of IgA1 and HMC-CM on PTEC cytokine release.

• BMP-2	• IL-1α	• Lipocalin-2	• PDGF-AA
• C5a	• IL-1β	• MCP-1	• PDGF-BB
• Collagen IVα	• IL-2	• MCP-2	• RANTES
• EGF	• IL-6	• MCP-3	• TNF-α
• Endothelin-1	• IL-8	• MIF	
• Fas Ligand	• IL-10	• MMP-1	
• GDF-15	• IL-17A	• MMP-2	
• GM-CSF	• IL-18BPa	• MMP-3	
• GRO-α	• IP-10	• MMP-7	
• ICAM-1	• KIM-1	• PAI-1	

Table 2: The customised panel of pro-inflammatory and pro-fibrotic cytokines tested for in the cell culture supernatants by multiplex array. TGF-β1 was tested separately by ELISA.

mIgA1 and pIgA1 was purified from two individual patients and one healthy control for these experiments. Patient 1 had IgAN and medium HAA binding. Patient 2 had IgAN and high HAA binding. The healthy control had medium HAA binding.

4.2.6.1 Effect of HMC-CM on PTEC

IL-6, MCP-1 and MMP-2 release were significantly increased by HMC-CM compared to vehicle (PBS), with no significant increase found with mIgA1 or pIgA1 alone compared to vehicle, or with mIgA1 or pIgA1 with HMC-CM compared to HMC-CM alone (Figure 31). The greatest increase in the release of these cytokines was observed from HK-2 cells stimulated with the HMC-CM from Patient 1. IL-6 release was increased significantly only for HMC-CM purified from Patient 1, while MCP-1 and MMP-2 release were increased for HMC-CM from both IgAN patients and the healthy subject.

4.2.6.2 Effect of IgA1 alone on PTEC

GM-CSF, PDGF-AA and GDF-15 release was increased by pIgA1 alone, and not by HMC-CM alone, or by the IgA1 preparations in addition to HMC-CM compared to HMC-CM alone (Figure 32). GM-CSF and PDGF-AA were increased by the pIgA1 from Patient 2 only, whilst, GDF-15 release was increased by the pIgA1 from Patient 2 and the healthy subject.

TGF-β1 release was increased by pIgA1 from both IgAN patients and the healthy subject, but not by mIgA1. TGF-β1 release was also increased by HMC-CM from the IgAN patients only and not from the healthy subject. The combination of IgA1 and HMC-CM did not produce any significant increase in TGF-β1 release over HMC-CM alone.

4.2.6.3 Effect of IgA1 and HMC-CM on HK-2 PTEC

Both mIgA1 and pIgA1 from Patient 2, and mIgA1 from the healthy subject caused an increase in MMP-9 release, alone and in combination with HMC-CM (Figure 33). HMC-CM from both patients but not the healthy individual caused an increase in MMP-9 release, with the strongest effect from Patient 2. mIgA1 from both patients but not the healthy subject resulted in an increase in NGAL, both alone and with the HMC-CM. HMC-CM alone did not result in an increase in NGAL release from PTEC.

4.2.6.4 Effect of lectin binding status on PTEC cytokine release

Serum from Patient 2 displayed the highest HAA-binding and therefore contained the most undergalactosylated IgA1. mIgA1 and pIgA1 isolated from Patient 2 had the strongest effect on PTEC GM-CSF, PDGF-AA, TGF-β1, and MMP-9 release compared to preparations from the other subjects.

4.2.6.5 Other findings

The remaining cytokines assayed were below the level of detection for all conditions tested: TNF-α, IL-1α, IL-1β, IL-10, IL-18BPa, IP-10, IFN-γ, RANTES, C5a, MCP-2, MCP-3, Endothelin-1, CXCL1/GRO α. PAI-1/serpin E1 was above the maximum level of detection for all conditions, including for cells stimulated with vehicle alone. No significant difference between any of the conditions was found regarding release of IL-1ra, IL-2, IL-17, MIF, MMP2, MMP7, BMP2, Collagen IVA, EGF or Fas ligand.

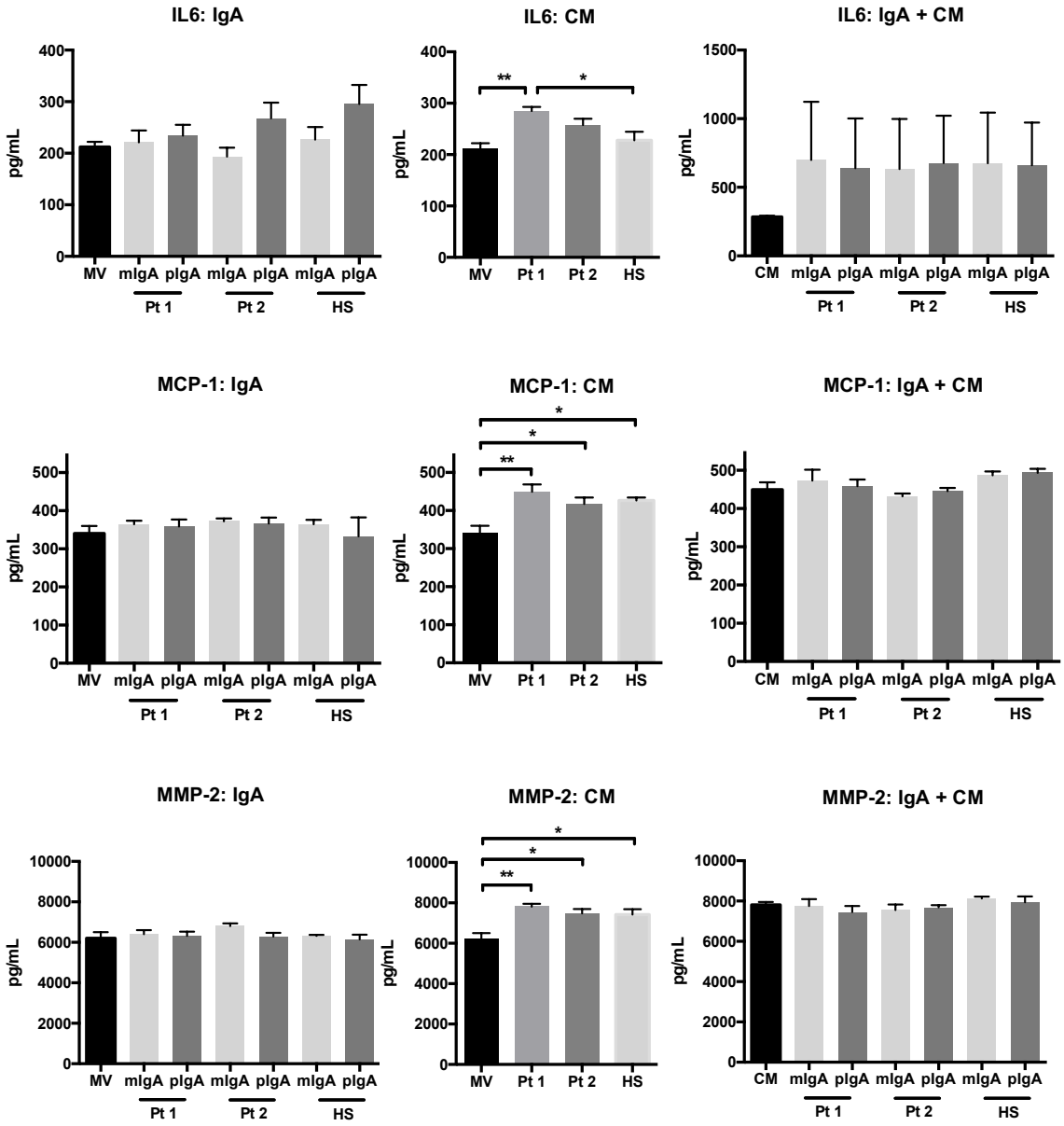

Figure 31: Effects of IgA1, HMC-CM, and IgA1 with HMC-CM on HK-2 PTEC IL-6, MCP-1 and MMP-2 release. IL-6, MCP-1 and MMP-2 were increased by HMC-CM, but not by IgA directly. Addition of HMC-CM to IgA produced no significant increase over HMC-CM alone. n=4. * $p < 0.05$, ** $p < 0.01$.

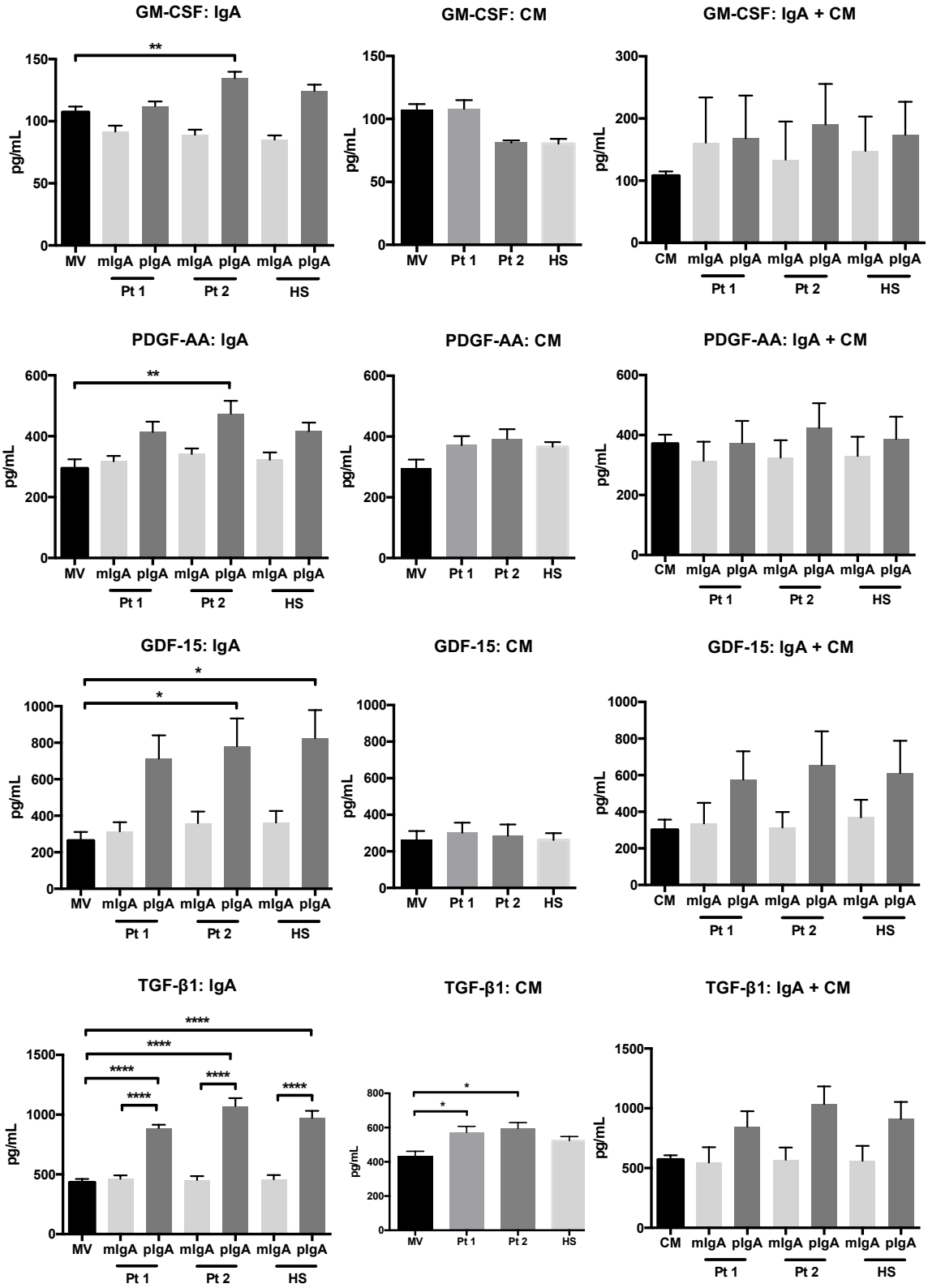

Figure 32: Effects of IgA1, HMC-CM, and IgA1 with HMC-CM on HK-2 PTEC GM-CSF, PDGF-AA, GDF-15, and TGF-β1 release. GM-CSF and PDGF-AA were significantly increased by pIgA1 from Patient 2, with the addition of HMC-CM, or HMC-CM alone producing no significant effect. GDF-15 release was increased by pIgA1 from Patient 2 and the healthy subject. TGF-β1 release was increased by all pIgA1 preparations, and by the HMC-CM from the IgAN patients, but not the healthy subject. n=4. * $p < 0.05$, ** $p < 0.01$, **** $p<0.0001$.

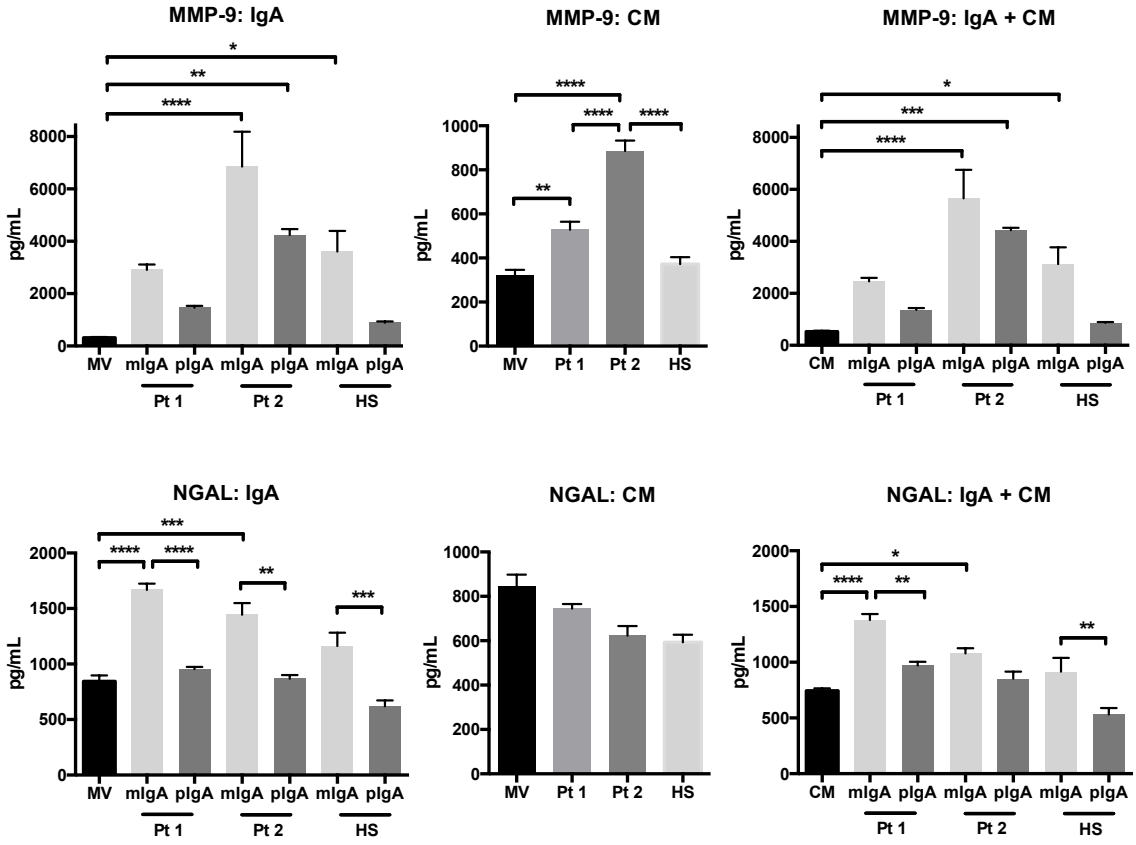

Figure 33: Effects of IgA1, HMC-CM, and IgA1 with HMC-CM on HK-2 PTEC MMP-9 and NGAL release. MMP-9 was significantly increased by both mIgA1 and pIgA1 from Patient 2, and by mIgA1 from the healthy subject, both with IgA1 alone compared to vehicle, or with the addition of HMC-CM. The HMC-CM from both patients caused an increase in MMP-9 release. NGAL was increased by mIgA1 from both patients, both alone and in combination with the HMC-CM. HMC-CM alone had no effect on NGAL release. n=4. * $p < 0.05$, ** $p < 0.01$, *** $p < 0.001$, **** $p < 0.0001$.

4.3 Conclusion

This series of *in vitro* experiments demonstrate for the first time that total IgA1 had stimulatory effects on human HK-2 PTEC, resulting in transcription factor (PPRE) activation, and pro-inflammatory (IL-6) and pro-fibrotic (TGF-β1) cytokine release. pIgA1 was found to be undergalactosylated in comparison to mIgA1. Incubating HK-2 cells with pIgA1 resulted in significantly increased TGF-β1 release compared to mIgA1 or vehicle alone, but there was no effect on IL-6 release in contrast to findings with total IgA1. TGF-β1 release correlated inversely with the galactosylation status of the IgA1 preparation used to stimulate the PTEC, with galactose-deficient pIgA1 (GdpIgA1) having the most effect. On testing the effects of individual mIgA1 and pIgA1 preparations on PTEC compared to mesangial cell conditioned medium (HMC-CM) generated by pIgA1 from the same patient or control, pIgA1 resulted in increased release of GM-CSF, GDF-15, PDGF-AA, and TGF-β1 with no additional effect observed with the HMC-CM. IL-6, MCP-1, and MMP-2 release were increased by HMC-CM, but not directly by mIgA1 or pIgA1. MMP-9 and NGAL release were mainly increased by mIgA1.

Taken together, these results indicate that incubation of human PTEC with IgA1 resulted in release of a number of pro-inflammatory and pro-fibrotic mediators, with galactose deficient pIgA1 (GdpIgA1) having the strongest effect on TGF-β1 release. IgA1 appears to be able to stimulate PTEC cytokine release, both directly and indirectly via generation of human mesangial cell derived signalling factors. The PTEC cytokine response from these two different stimuli was distinct. IgA1 generated HMC-CM promoted pro-inflammatory (IL-6, MCP-1) cytokine release consistent with previous reports, while IgA promoted both pro-inflammatory (GM-CSF, PDGF-AA) and pro-fibrotic (TGF-β1, GDF-15) responses from PTEC (Xiao et al., 2009). In addition, IgA1 isolated from the patient with the highest HAA-binding, and therefore most undergalactosylated IgA1, had the strongest effect on PTEC GM-CSF, PDGF-AA, TGF-β1, and MMP-9 release, although further replicate experiments are required to confirm these observations. IgA1 may therefore act in both a direct and indirect manner to stimulate PTEC cytokine release that drives tubulointerstitial fibrosis in progressive IgAN.

At normal physiological levels, TGF-β plays vital roles in organ development and repair and has important anti-inflammatory effects (Loeffler and Wolf, 2014).

However, overexpression of TGF-β1 has been implicated as a key factor in promoting both glomerulosclerosis and tubulointerstitial fibrosis (Kitamura and Sütö, 1997; Loeffler and Wolf, 2014). An increase in TGF-β gene, protein, and signal transduction pathway expression has been demonstrated after incubation of human mesangial cells with pIgA1, and this effect was significantly higher than that observed with mIgA1 (Lai, 2003). IL-6 has both anti- and pro-inflammatory effects, and promotes inflammation by augmenting lymphocyte activation and proliferation, B cell differentiation, leucocyte recruitment and induction of acute phase protein synthesis by the liver (Pecoits-Filho et al., 2003). Urinary IL-6 levels were reported to be raised in IgAN patients compared to healthy control subjects, and were associated with risk of progression at up to 8 years follow up (Dohi et al., 1991; Harada et al., 2002). GM-CSF acts via the signal transducer and activator of transcription STAT5, and is produced by a number of cell types, including PTEC (Huen et al., 2014). It plays an important role in the derivation of granulocyte and macrophage populations from bone marrow derived precursor cells, and differentiation of macrophages into the M1 phenotype, serving a pro-inflammatory effect. GDF-15 is a more recently described member of the TGF-β superfamily and is induced in many tissues in response to stress. It was shown to be upregulated after induction of renal ischaemia-reperfusion injury or 5/6 nephrectomy in mice (Zimmers et al., 2005). The role of GDF-15 in renal injury is less well established, with *in vitro* effects on immune cell modulation and activation of epithelial cell apoptosis having been reported (Zimmers et al., 2005). The PDGFs play an important role in mesangial cell proliferation, and also contribute towards tubulointerstitial damage, although the precise role for PDGF-AA is less well defined compared to PDGF-BB and –DD (Boor et al., 2014; Floege, 2011; Floege et al., 2014).

Despite observational data demonstrating that urinary IgA levels are increased in IgAN (Galla et al., 1985; Matousovic et al., 2006), inferring that the proximal tubule is exposed to increased amounts of IgA, the direct effects of IgA on the proximal tubule have been relatively under-studied. Chan *et al* reported that IgA is able to bind to PTEC, although with lesser affinity than to mesangial cells (Chan et al., 2005). However, incubation of PTEC with IgA did not result in upregulation of TNF-α, MIF or sICAM-1 release, whereas release of these cytokines was upregulated by IgA-mesangial cell conditioned media, utilising IgA from patients with IgAN. In this

current study, IgA was purified further, and its effects on different cytokines was examined, with GdpIgA1 having the strongest effect on TGF-β1 release. The differences in these findings may therefore be explained by the additional purification steps undertaken in this study, and the different cytokines tested.

In the current study, pIgA1 had stronger stimulatory effects on PTEC than mIgA1. There appear to be important structural differences between these forms of IgA. pIgA1 displayed significantly higher HAA binding compared to mIgA1, implying that pIgA1 is enriched in galactose deficient IgA (GdIgA), potentially due to its propensity to self-aggregate (Hui et al., 2015). The findings presented in this chapter are consistent with a previous study by Oortwijn et al, where IgA was purified by a different method, using an anti-IgA column, before separation into polymeric and monomeric forms (Oortwijn et al., 2006). GdIgA is believed to possess specific nephritogenic properties. Mesangial deposits of IgA contain a high proportion of GdIgA in IgAN, and GdIgA produces a stimulatory effect on mesangial cell proliferation, compared to IgA that is normally galactosylated (Novak et al., 2005). Furthermore, autoantibodies against the undergalactosylated IgA1 hinge region are found in increased quantities in IgAN from the serum and also in urine (Berthoux et al., 2012; Tam et al., 2009). pIgA, compared to mIgA, exhibited increased binding to mannose-binding lectin (MBL), a circulating C-type lectin containing several carbohydrate recognition domains, that plays a central role in the activation of the lectin pathway of the complement system (Ip et al., 2009). The precise nature and constituents of pIgA and high molecular weight containing IgA immune complexes remain uncertain, but could explain their increased ability to stimulate PTEC cytokine production in comparison to mIgA, and is therefore worthy of further investigation.

Observational clinical data also provide evidence that GdIgA plays a central role in the pathogenesis of progressive IgAN. Serum GdIgA1 levels were reported to be elevated in patients with IgAN (Moldoveanu et al., 2007). A prospective study of 275 IgAN patients followed for a median of 47 months showed that higher levels of GdIgA1 were independently associated with a greater risk of deterioration of renal function, and reduced rates of renal survival (Zhao et al., 2012).

Similar to findings by Oortwijn et al, in the current study, no significant difference was observed between IgA from patients with IgAN and healthy subjects in their ability to stimulate production of certain cytokines. Under normal healthy physiological conditions, PTEC exposure to IgA is likely to be minimal. Following glomerular damage in IgAN, leakage of IgA into the urinary space, with other factors including mesangial cell derived cytokines and/or other filtered proteins, may contribute towards activation of PTEC and production of pro-fibrotic cytokines. Although tubular staining for IgA is not a common feature of IgAN, filtered IgA may be endocytosed and processed by PTEC meaning that organised immune deposits do not accumulate in IgAN.

Potential receptors for PTEC IgA receptors remain unclear. Chan et al found that PTEC did not express mRNA for the IgA receptors FcαR, the polymeric Ig receptor (pIgR) and Fcα/μR (Chan et al., 2005). Transferrin receptor (TfR) was expressed by PTEC although this is expressed at low levels by many cell types, and its expression is increased in cells which are actively proliferating. A potential IgA receptor of interest is megalin, a multi-ligand scavenger receptor belonging to the low-density lipoprotein receptor family, which is highly expressed on the apical surface of PTEC. In a megalin mosaic knockout mouse model that lacked megalin expression in 60% of PTEC, induction of non-selective proteinuria by the toxin NEP25, resulting in podocyte injury, led to endocytosis and accumulation of IgA into PTEC, but only in cells that expressed megalin (Motoyoshi et al., 2008).

In conclusion, GdpIgA1 appears to have particular direct stimulatory properties on PTEC. In IgAN, after damage to the glomerular filtration barrier occurs, exposure of PTEC to this form of IgA may be particularly pathogenic. Identifying the receptors and signalling pathways involved in the interaction between GdpIgA1 and PTEC may reveal novel therapeutic targets, which may be targeted to disrupt its pro-fibrotic effects.

Chapter 5: Establishing a mouse model of IgA nephropathy, by the oral and intravenous administration of bovine gamma globulin

5.1 Introduction

Advances in the understanding of the mechanisms that underlie IgAN have been hindered by the lack of a suitable animal model that accurately replicates features of the human disease (Eitner et al., 2010). This is perhaps unsurprising, since IgAN displays marked heterogeneity in its clinical phenotype, and as the factors responsible for the variability in its prognosis are currently poorly understood.

In vitro studies have provided key insights into the pathogenesis of IgAN. Work involving the elution and characterisation of mesangial IgA deposits has established that these consist primarily of galactose-deficient pIgA1 (GdpIgA1) (Allen et al., 2001; Monteiro et al., 1985). Applying this particular form of IgA to mesangial cells results in a strong stimulatory response, involving cell proliferation and cytokine release (Novak et al., 2005). The data presented in Chapter 4 demonstrates that IgA also has a stimulatory effect on PTEC, with GdpIgA1 having particularly strong effects.

However, *in vitro* models have important limitations. The cell culture environment is vastly different to the cell's native *in vivo* environment, where they are surrounded by other cell types, and, under certain circumstances, are exposed to infiltrating cells and a multitude of cytokines and other signalling factors in their local milieu. Cells cultured *in vitro* also behave differently compared to when in their usual *in vivo* microenvironment, with differences in their rates of endocytosis and proliferation. These effects are particularly pronounced in transformed cell lines, although primary cells may also undergo rapid phenotypic alterations in cell culture environments. Furthermore, it is difficult to accurately replicate the cell's usual polarity *in vitro*, which is a particular issue when modelling the exposure of filtered proteins to the apical surface of PTEC. Therefore, although *in vitro* models may provide key insights into physiological mechanisms, their applicability and relevance are limited by these caveats.

Various animal models have been developed that replicate at least part of the IgAN disease process. The most frequently studied have included either the passive administration, or the active *in vivo* generation, of IgA-containing immune complexes. Rifai et al first developed a murine model in the BALB/c strain, which involved the formation of IgA-bovine serum albumin (BSA) complexes. These were formed either by generating the immune complexes *in vitro* and administering them parenterally, or by pre-administering anti-dinitrophenol (DNP) IgA secreting plasma cells to mice, then injecting BSA coupled to DNP. This model resulted in mild mesangial IgA deposition, C3 deposition and transient haematuria (Rifai et al., 1979). Isaacs and Miller subsequently reported a model that involved the intravenous administration of various dextran preparations, resulting in IgA and IgM mesangial deposits, mesangial expansion and proliferation (Isaacs et al., 1981). The relevance of this model has been questioned in a more recent study, where administering dextran preparations to Lewis rats led to similar glomerular changes, but with the mesangial deposition of IgG, and not IgA, suggesting that the changes observed were not IgA-dependent.

Viral immunisation models to replicate the upper respiratory tract mucosal infection that may precede glomerular injury and haematuria in IgAN have been studied, most notably by the intranasal administration of the Sendai virus (also known as murine parainfluenza virus type 1) in BALB/c mice, which resulted in a high serum IgA (and IgG) anti-virus immune response and glomerular IgA deposition (Yamashita et al., 2007). Murine models of secondary IgA deposition have also been studied, for example by bile duct ligation-induced cholestasis (Gormly et al., 1981), or carbon tetrachloride-induced liver cirrhosis (Emancipator et al., 1983c), that resulted in the reduced hepatic clearance and subsequent glomerular deposition of IgA immune complexes.

More recently, a model was developed by Emancipator et al, who observed that administering various xenoantigens (chicken egg albumin or ovalbumin, bovine gamma globulin (BGG), horse spleen ferritin) to BALB/c mice led to the development of mesangial IgA deposition (Emancipator et al., 1983b). Of these, BGG and ovalbumin had the most consistent effect (Emancipator, 2001). The purpose of the oral immunisation was to exploit the propensity of gut mucosal associated lymphoid tissue (MALT) to produce antibodies of the IgA subclass

directed against the xenoantigen. Over around a six-week period, a switch from an IgM-, to IgG-, to IgA-dominant serum antibody response was observed. By ten to fourteen weeks, the serum antibody response became almost exclusively IgA, although as some IgG co-deposition was required to produce a glomerular response, the optimum time course for oral administration was around six to eight weeks in duration. Administration of intravenous boluses of the same antigen served to augment the immune response, providing a 'burst' of antigen (Emancipator, 2001). Haematuria was present in ~80% of immunised mice, as quantified by microscopy, but at a level too low to be reliably detected by urine dipstick. No change in renal function or proteinuria was observed, indicating that this was a model of early disease which does not progress to cause chronic damage i.e. tubulointerstitial fibrosis. This model has since been used by a number of research groups, in BALB/c mice (Emancipator et al., 1983a, 1983b; Gesualdo et al., 1990), Sprague-Dawley rats (Kuemmerle et al., 1998) and Lewis rats (Gesualdo et al., 1992; Kuemmerle et al., 1999; Lai et al., 2011; Trachtman et al., 1996; Yi et al., 1996). A uninephrectomy was incorporated in one study, to increase the severity of IgA deposition and subsequent glomerular pathology (Lai et al., 2011).

The objective of this chapter was to establish, characterise and optimise a murine model of IgAN, based on the original method described by Emancipator et al (Emancipator, 2001) by the oral and intravenous immunisation of bovine gamma globulin (BGG). Regarding previously published studies on mice, successful use of this immunisation method had been reported in the Th2 prone BALB/c strain only. However, as mouse and human studies also suggest a role for Th1 cytokines in IgAN, an initial aim was to assess whether the model could be induced in the Th1 prone C57BL/6 mouse strain (Lai et al., 1994; Lim et al., 2001; Suzuki et al., 2007).

The aims of this chapter were therefore to assess the following:

1. Whether a model of IgAN could be induced in both the C57BL/6 and BALB/c mouse strains, and whether the disease phenotype and severity differed between these strains.
2. Whether glomerular and/or interstitial inflammation were increased in this model.
3. Whether IgA undergoes glomerular filtration in increased amounts in this model and can be detected in the urine.

As the experiments presented in this chapter represent a series of optimisation experiments, the number of animals used was minimised, and therefore it was not possible to perform a statistical analysis for all the parameters measured.

5.2 Experiment 1: Establishing the model in the C57BL/6 mouse strain

As this model had only been described in mice of the BALB/c strain previously, the aim of the first experiment was to assess whether a model of IgAN, involving oral and parenteral immunisation of BGG, could be induced in C57BL/6 mice. 6-week-old female C57BL/6 mice were divided into dosed (n=2) and control (n=2) groups. Dosed animals received 0.1% BGG continuously in the drinking water for 6 weeks, followed by intravenous injections of 1 mg BGG diluted in 0.2 mL PBS daily for 3 days. Control animals received standard drinking water and IV injections of vehicle (PBS) only at the same frequency. Animals were sacrificed 48 hours after the last injection.

5.2.1 Protocol

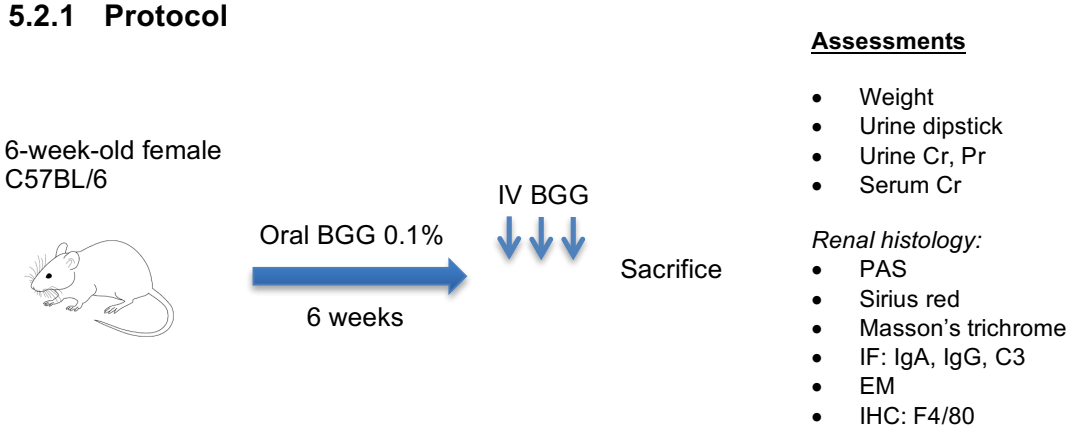

5.2.2 Results

All mice gained weight consistently, with no difference observed between the control and dosed groups (Figure 34). By the end of the experiment, one of the dosed mice developed non-visible haematuria, detectable by urine dipstick (2+), while one of the control group developed trace haematuria (Table 3). Urine protein:creatinine ratio (PCR) was higher in the dosed group, although this difference was not statistically significant (Figure 35). Serum creatinine was lower in the dosed group, although this was also not statistically significant. All serum creatinine measurements were within normal reference values for adult mice (normal range 8.8 – 17.7 µmol/L).

Immunofluorescence staining of frozen sections, displayed increased glomerular deposition of IgA, IgG and complement component C3 in dosed mice compared to

controls (Figure 36). Glomerular IgA and C3 deposits were occasionally observed in control animals but these were of lower intensity compared to the dosed group. Glomerular IgG deposition was not detected in the control mice. Electron microscopy revealed small well-defined electron dense deposits in the mesangial areas of the dosed animals, corresponding to immune deposits (Figure 37). No electron dense deposits were detected in sections from the control animals.

There was no significant increase in cell number per glomerular cross section (gcs) between control and dosed mice (control 31.3 ± 2.3 *vs* dosed 36.5 ± 0.7 cells/gcs; p = 0.16) (Figure 38). Sirius red staining demonstrated an increase in glomerular staining in the dosed mice (Figure 39). No interstitial fibrosis was observed on the Masson's trichrome stain in either the control or dosed groups. An increase in infiltrating F4/80^{+} tubulointerstitial macrophages was observed in the dosed animals (Figure 40).

Together these data indicate that mice of the C57BL/6 strain could be induced to generate mesangial IgA deposition, after oral and parenteral administration of BGG.

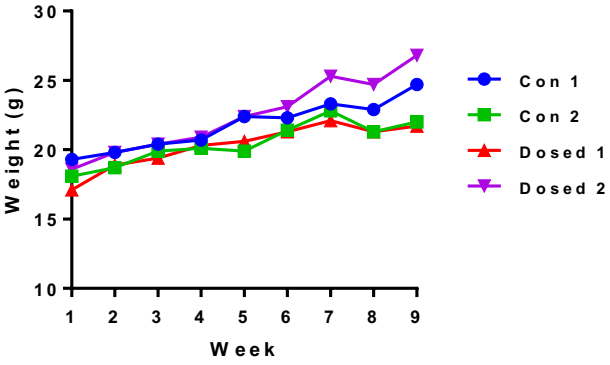

Figure 34: Changes in body weight throughout the experimental course. All mice gained weight consistently, with no difference observed between the control and dosed groups.

	Blood	Prot
Con 1	-	Tr
Con 2	Tr	-
Dosed 1	-	1+
Dosed 2	2+	-

Table 3: Urine dipstick results for control and dosed mice. One dosed mouse and one control mouse developed non-visible haematuria.

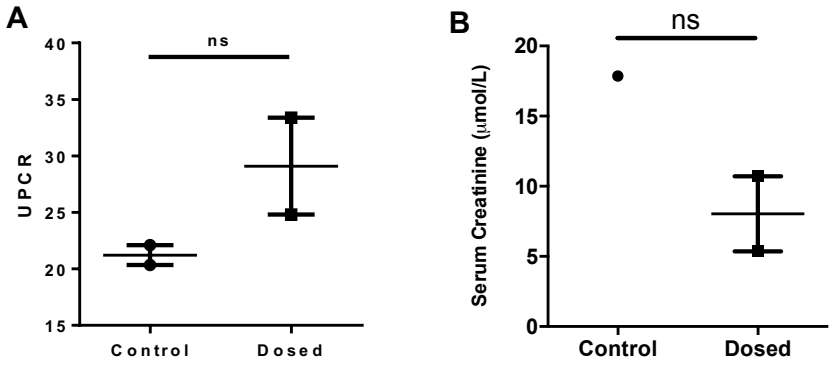

Figure 35: (A) Urine Protein:Creatinine ratio (UPCR) and (B) Serum Creatinine. No significant change was observed between control and dosed mice. n=2 for both groups, apart from serum creatinine measurement for the control group, where only one sample was suitable for analysis. Horizontal bars indicate the mean, and error bars indicate the SEM.

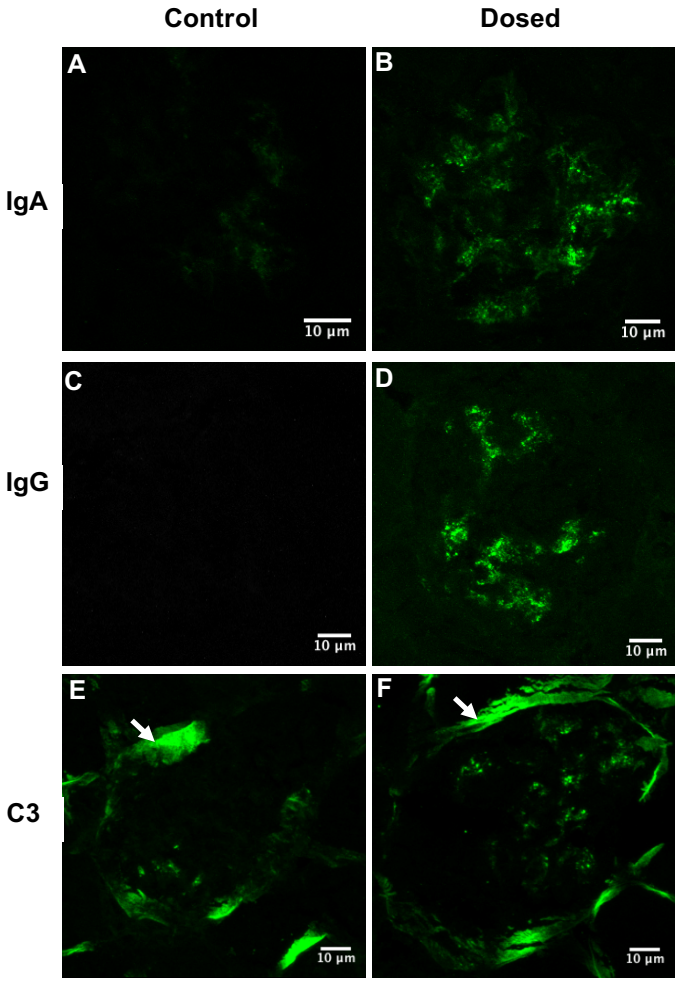

Figure 36: Glomerular IgA, IgG and C3 deposition in control and dosed mice. All were increased in the glomeruli of the dosed compared to control mice. For C3, arrows indicate background complement activation in the periglomerular capillaries, found normally in wild-type C57BL/6 mice.

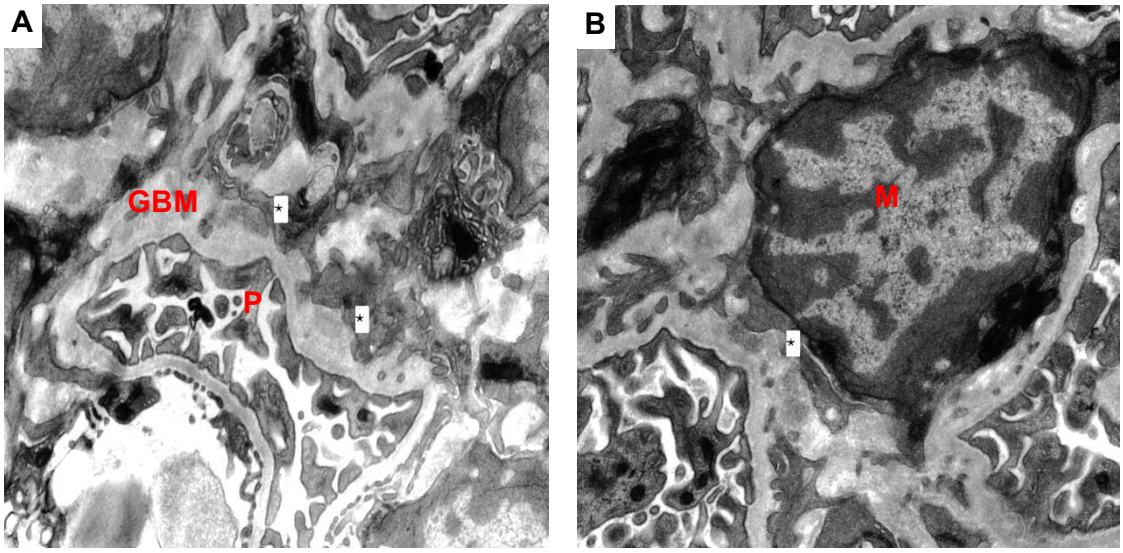

Figure 37: Electron microscopy images of kidney sections taken from a dosed mouse. * indicates the electron dense areas, corresponding to the IgA mesangial deposits. GBM: glomerular basement membrane, P: podocyte foot process, M: mesangial cell.

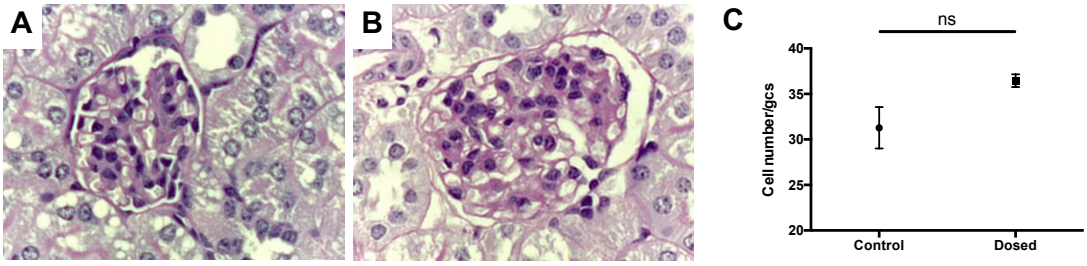

Figure 38: Glomerular cell count in control and dosed mice. Representative PAS-stained kidney sections from a (A) control mouse and (B) dosed mouse are displayed. Original magnification x 400. (C) Cell number per glomerular cross section (gcs) from control and dosed groups. Cell counts were performed from 25 consecutive glomeruli, and are expressed as mean ± SEM. No significant difference was found between the two groups.

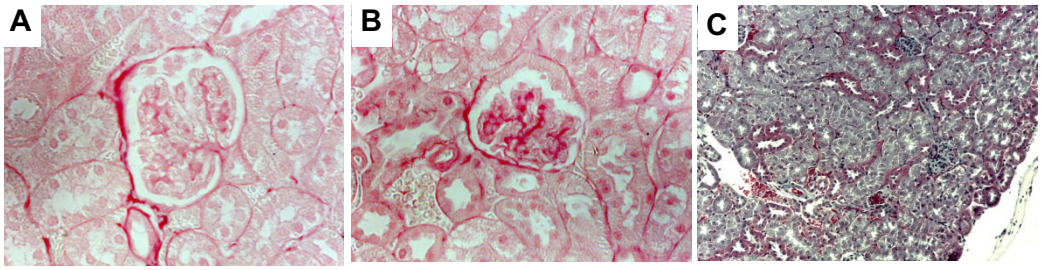

Figure 39: Sirius red staining and Masson's trichrome staining of kidney sections from control and dosed mice. Representative sections from a (A) control and (B and C) dosed mouse are displayed. Increased Sirius red staining was observed in the glomeruli from dosed mice. No increase in interstitial fibrosis was observed in either group. Original magnification (A and B) x 400, (C) x 200.

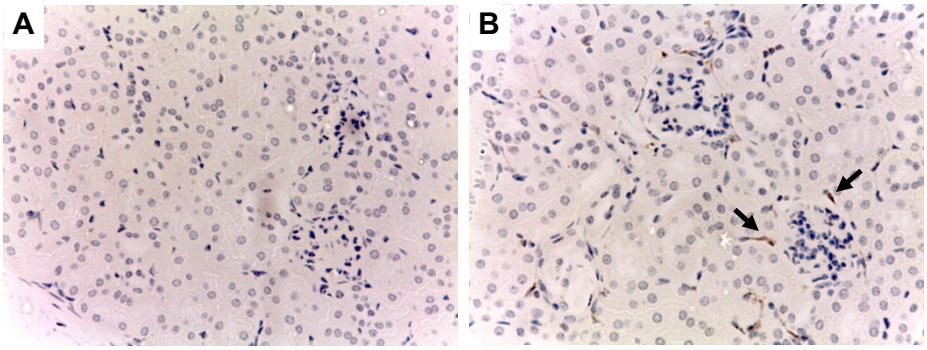

Figure 40: Renal interstitial macrophage infiltration in control and dosed mice. Sections were immunostained for the macrophage marker F4/80. Representative sections from a (A) control mouse and (B) dosed mouse are displayed. An increase in $F4/80^{+}$ cells (arrows) was observed in the interstitial compartment of the dosed mice, compared to control mice. No glomerular $F4/80^{+}$ cells were detected. Original magnification x 200.

5.3 Experiment 2: Time-course optimisation

In the second experiment, a time-course experiment was designed to assess whether continuation of oral BGG immunisation following the 3 IV injections increased the intensity of IgA immune deposition and glomerular injury.

5.3.1 Protocol

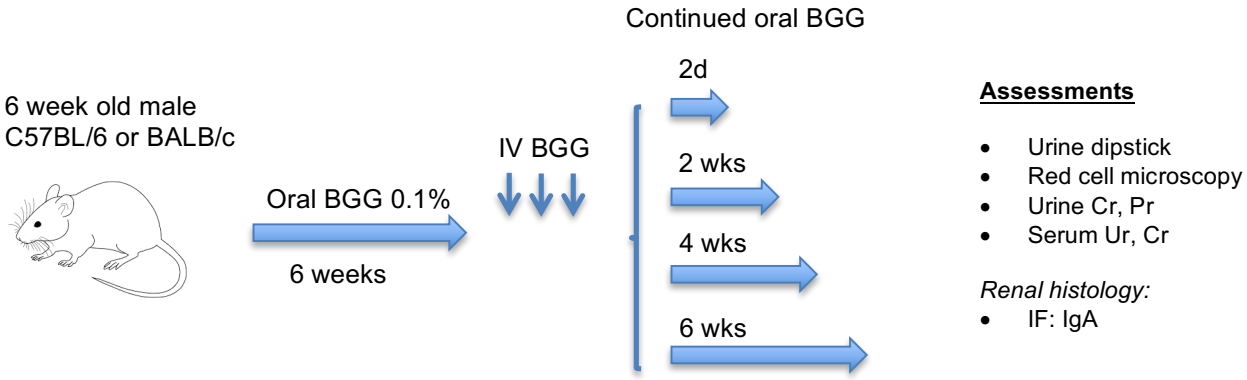

5.3.2 Results

In both BALB/c and C57BL/6 mice, no increase in the intensity of IgA deposition was observed after extending the oral immunisation course beyond 48 hours post IV injections (Figure 41 and Figure 44). Intensity of the immune deposits in both strains decreased with increased duration following the IV injections. Deposition of IgA was observed more consistently in dosed mice of the BALB/c strain compared to the C57BL/6 strain. IgA deposits were also observed in some of the control animals, especially in the C57BL/6 group. Urinary red cells, quantified by microscopy, were increased in the dosed animals. Haematuria was not detectable by urine dipstick in any of the mice. No changes in kidney function (serum urea or creatinine), or in urinary albumin or protein excretion were observed in either group (Figure 42, Figure 43, Figure 45 and Figure 46).

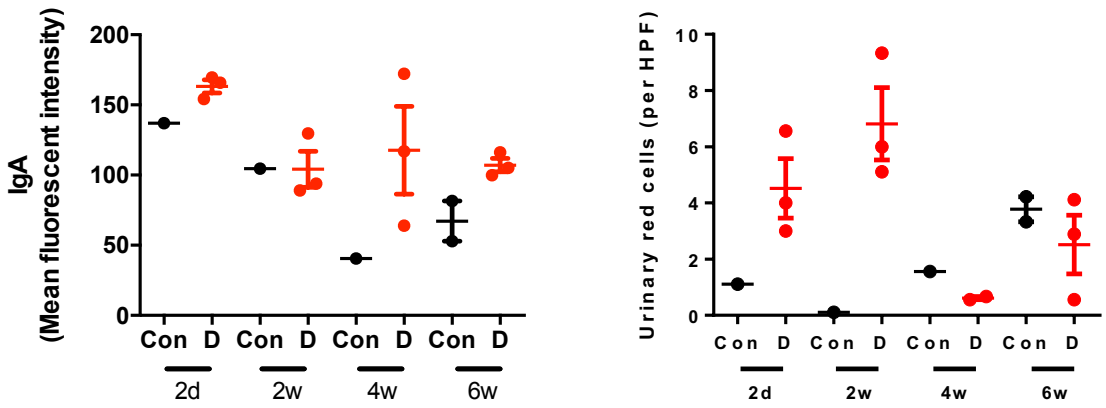

Figure 41: Immunofluorescence staining for IgA, and urine red cell count in BALB/c mice from the time course experiment. Intensity of IgA deposition decreased with increased duration following the IV injections. Urine red cells were increased in the dosed mice, and diminished by 4 weeks following the IV injections. HPF: High power field.

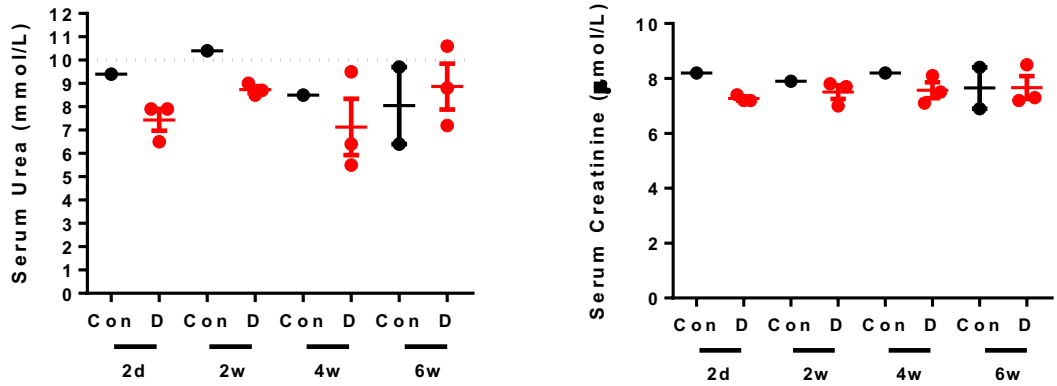

Figure 42: Serum urea and creatinine in BALB/c mice from the time course experiment. No difference was observed between control and dosed animals, and all values were within normal limits.

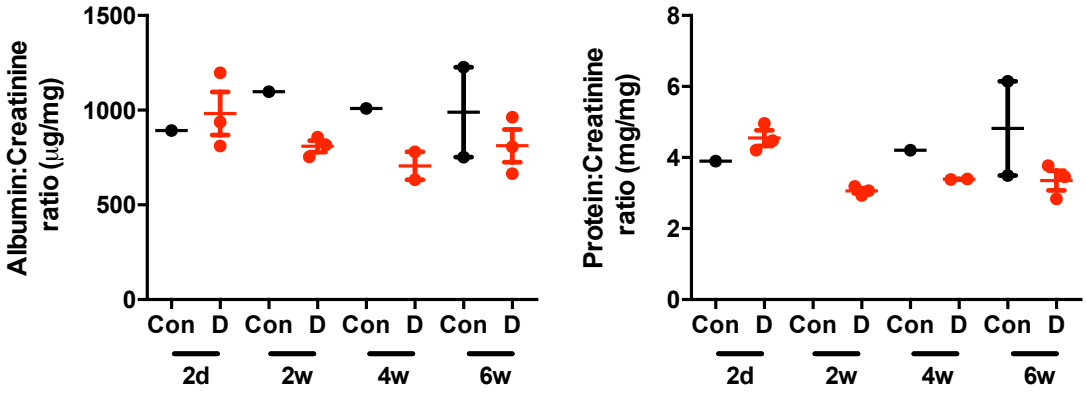

Figure 43: Urine albumin:creatinine and protein:creatinine ratio in BALB/c mice from the time course experiment. No difference was observed between control and dosed animals.

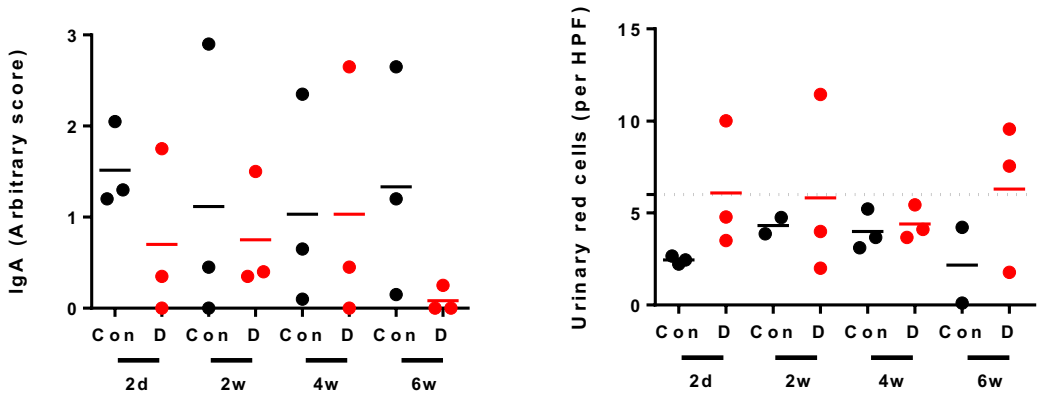

Figure 44: Immunofluorescence staining for IgA, and urine red cell count in C57BL/6 mice from the time course experiment. Deposition of IgA was observed less consistently in the dosed mice in this experiment, and a number of control mice had evidence of glomerular IgA deposition. Urine red cells were increased in the dosed animals. HPF: High power field.

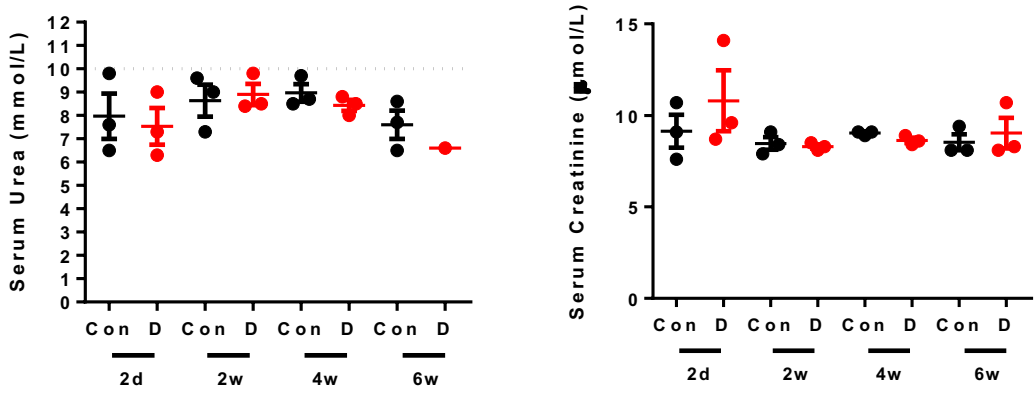

Figure 45: Serum urea and creatinine in C57BL/6 mice from the time course experiment. No difference was observed between control and dosed mice, and all values were within normal limits.

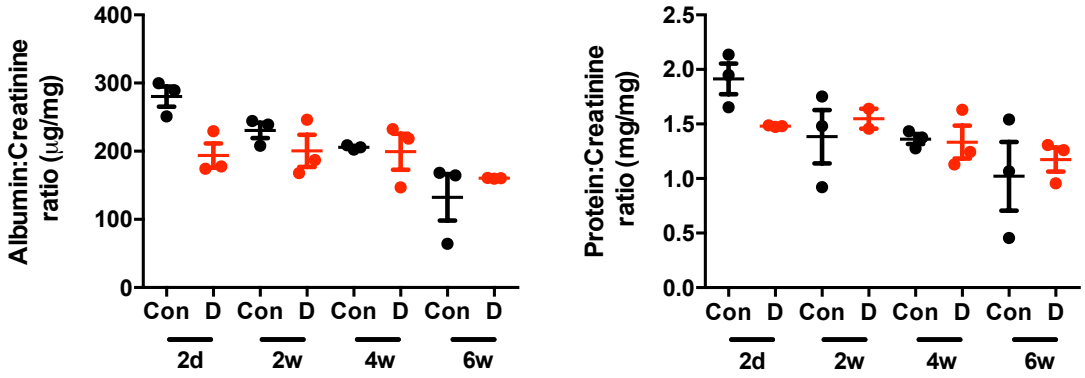

Figure 46: Urine albumin:creatinine and protein:creatinine ratio in C57BL/6 mice from the time course experiment. No difference was observed between control and dosed animals.

5.4 Experiment 3: Dose-response optimisation and phenotype of the model

In the third experiment, a dose-response protocol was designed, to test the optimum number of IV injections needed to elicit glomerular IgA deposition. After personal communication with Professor Steven Emancipator who described the original model, 8-week-old male mice were used, an age at which they are considered to possess a fully mature immune system. Oral BGG dosing was continued for 8 weeks instead of the original 6 weeks, before administering IV injections. The dose of BGG administered intravenously was increased to 2 mg per dose. Mice were sacrificed 72 hours following the last IV injection.

5.4.1 Protocol

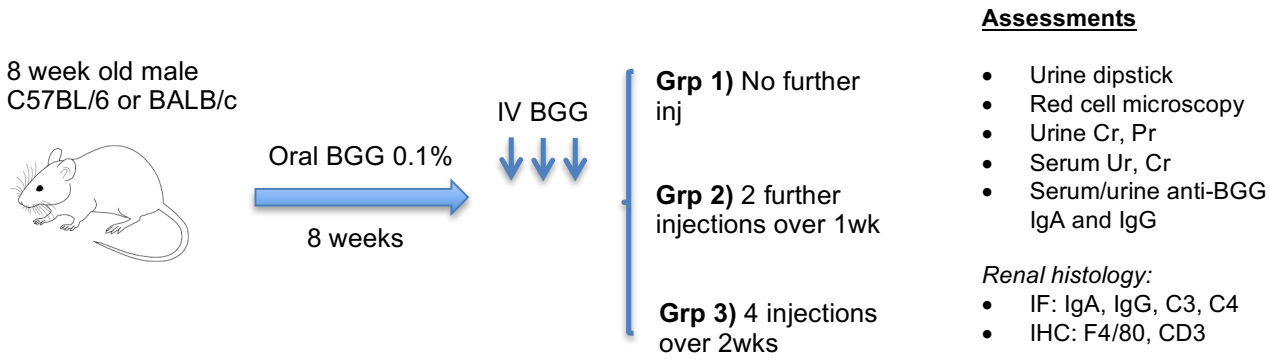

5.4.2 Results

The increase in the dose of BGG administered by IV injection, from 1 mg to 2 mg, was tolerated without any ill effects displayed. 3 mice died before completion of the experimental course due to husbandry or technical issues: one BALB/c mouse from Group 2 (culled due to fight wounds, before receiving any IV injections), and two C57BL/6 mice from Group 2 (one died before receiving the 1st IV injection in the restrainer, and one died before receiving the 5th IV injection in the restrainer. Tissue from the last mouse was harvested post-mortem and analysed as part of Group 2, however collection of urine was not possible).

Immunofluorescence staining of frozen sections demonstrated that the strongest glomerular IgA deposition was found in the C57BL/6 mice from Group 2 (those that received 1 or 2 additional IV injections of BGG after the initial 3 injections) (Figure 47). This corresponded with stronger glomerular IgG deposition compared to the

other groups. An increase in glomerular C3 deposition was observed in Groups 1 and 2 of the C57BL/6 mice but not in Group 3. Glomerular C4 deposition was observed in both control and dosed animals.

These findings corresponded with the immune responses, where the highest serum anti-BGG IgA titres were found in the C57BL/6 mice from Group 2 (Figure 48). Serum anti-BGG IgG titres were raised in all dosed animals compared to controls, and in the C57BL/6 mice, the anti-BGG IgG titre was highest in Group 3. Anti-BGG IgA and IgG were also detected in the urine at increased levels in the dosed mice. C57BL/6 mice in Group 2 demonstrated the highest urine anti-BGG IgA titres, while urine anti-BGG IgG was highest in Group 3.

Dipstick haematuria (2+) was observed in 2 of the dosed C57BL/6 mice in Group 1, but none of the other groups. Regarding measurements of kidney function (serum urea and creatinine) and urinary protein excretion, no differences were observed between control and dosed animals (Figure 49).

Inflammatory cell infiltration was assessed on renal histology. An increase in $F4/80^{+}$ tubulointerstitial macrophage infiltration was evident in dosed animals compared to control groups (Figure 50). In addition, there was a greater number of infiltrating glomerular $CD3^{+}$ T-lymphocytes in the dosed C57BL/6 mice (Figure 51).

Analysis of urine protein excretion demonstrated that urine IgA excretion was increased in the single available sample, from the C57BL/6 mouse in Group 2 (Figure 52). Repeated experiments are required to confirm this observation. The pattern of protein excretion, as assessed by SDS-PAGE, was broadly similar between control and dosed animals, although a protein of approximately 31kDa molecular weight was absent from two of the dosed mice (Figure 53). The identity of this protein is unknown and has been submitted for sequencing.

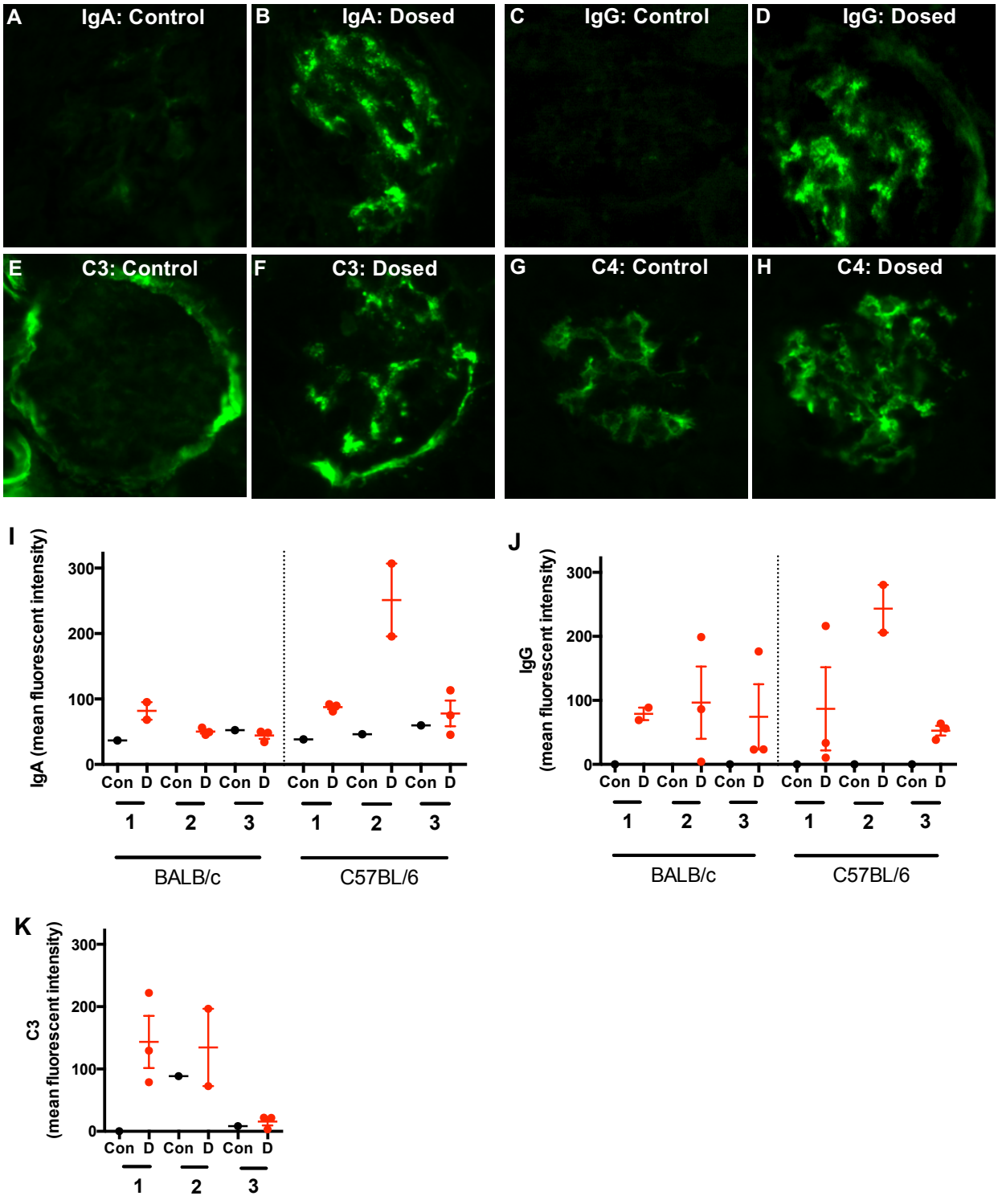

Figure 47: Immunofluorescence staining for IgA, IgG, C3 and C4. (A-H) Representative images shown from control and dosed C57BL/6 mice from Group 2, which demonstrated the strongest staining for all components in the dosed group. (I-K) Mean fluorescent intensity for IgA, IgG and C3. Quantification for C3 is shown for the C57BL/6 group only.

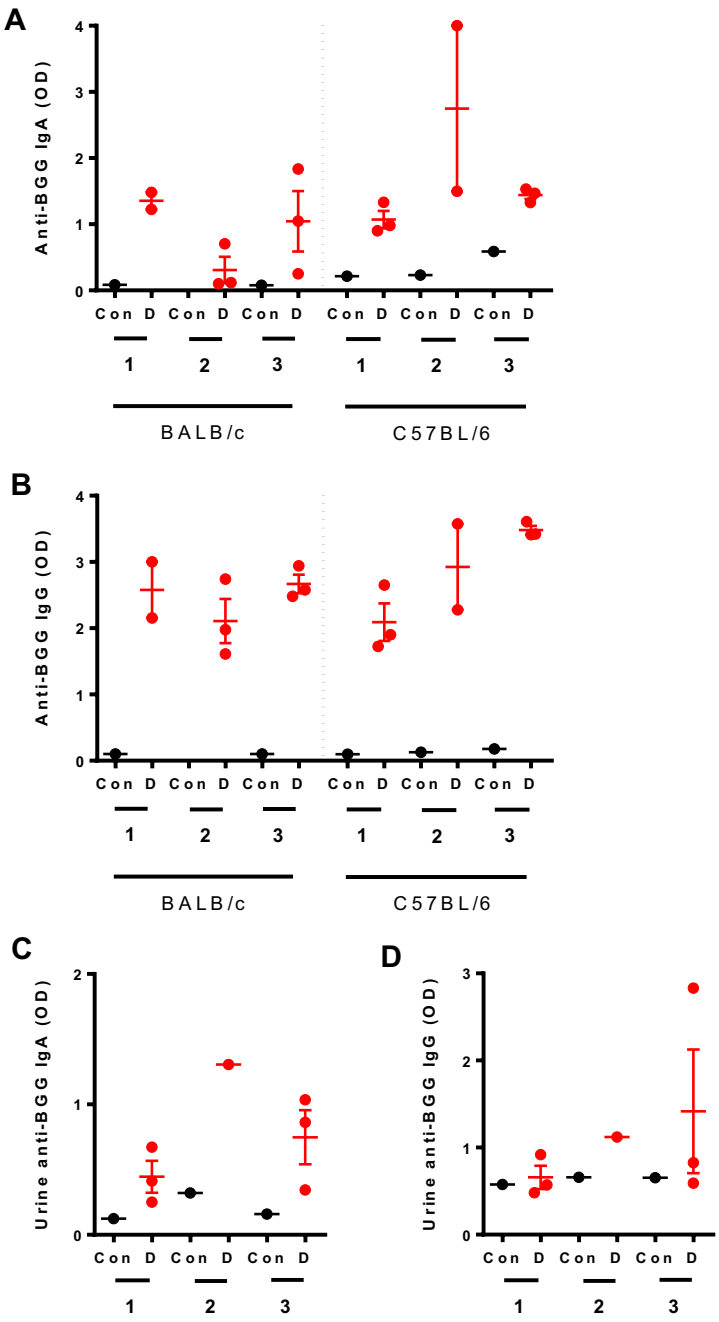

Figure 48: Serum and urine anti-BGG immune responses. (A and B) Serum anti-BGG IgA and IgG levels. Serum anti-BGG IgA levels were highest in Group 2 from C57BL/6 mice, while serum anti-BGG IgG levels were highest in Group 3 from C57BL/6 mice (C and D) Urine anti-BGG IgA and IgG levels, from C57BL/6 mice only. The strongest urine anti-BGG IgA response was observed from Group 2, while urine anti-BGG IgG was highest in Group 3.

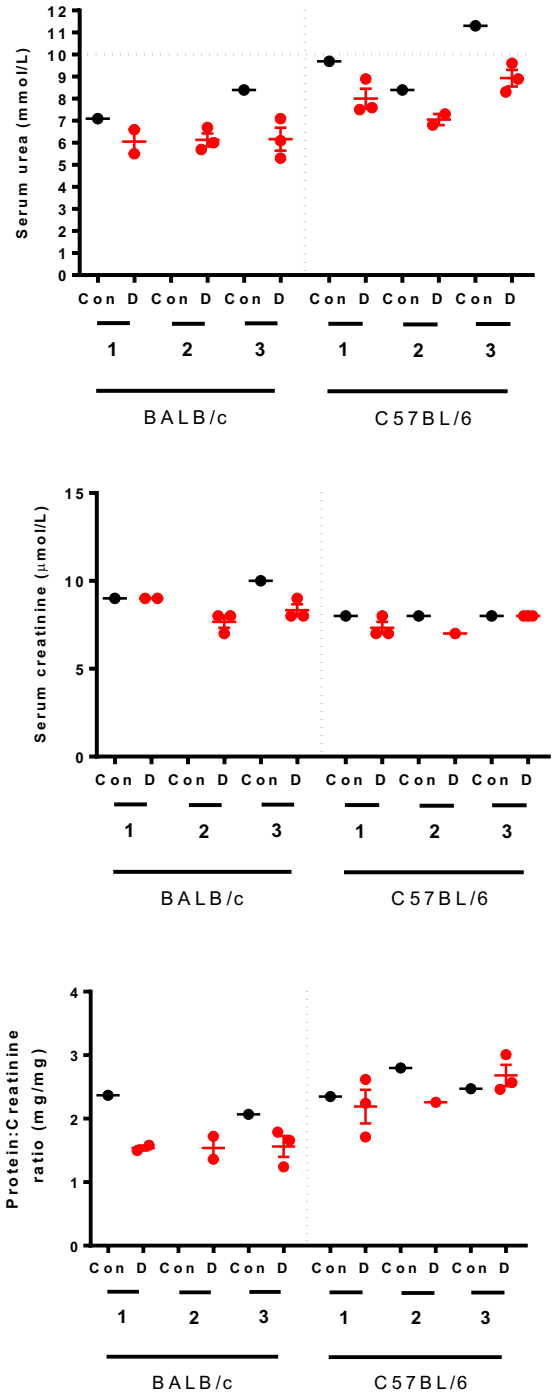

Figure 49: Serum urea and creatinine levels, and urine protein:creatinine ratio. No differences were observed between control and dosed mice regarding kidney function or proteinuria levels. All serum urea and creatinine measurements were within normal reference values.

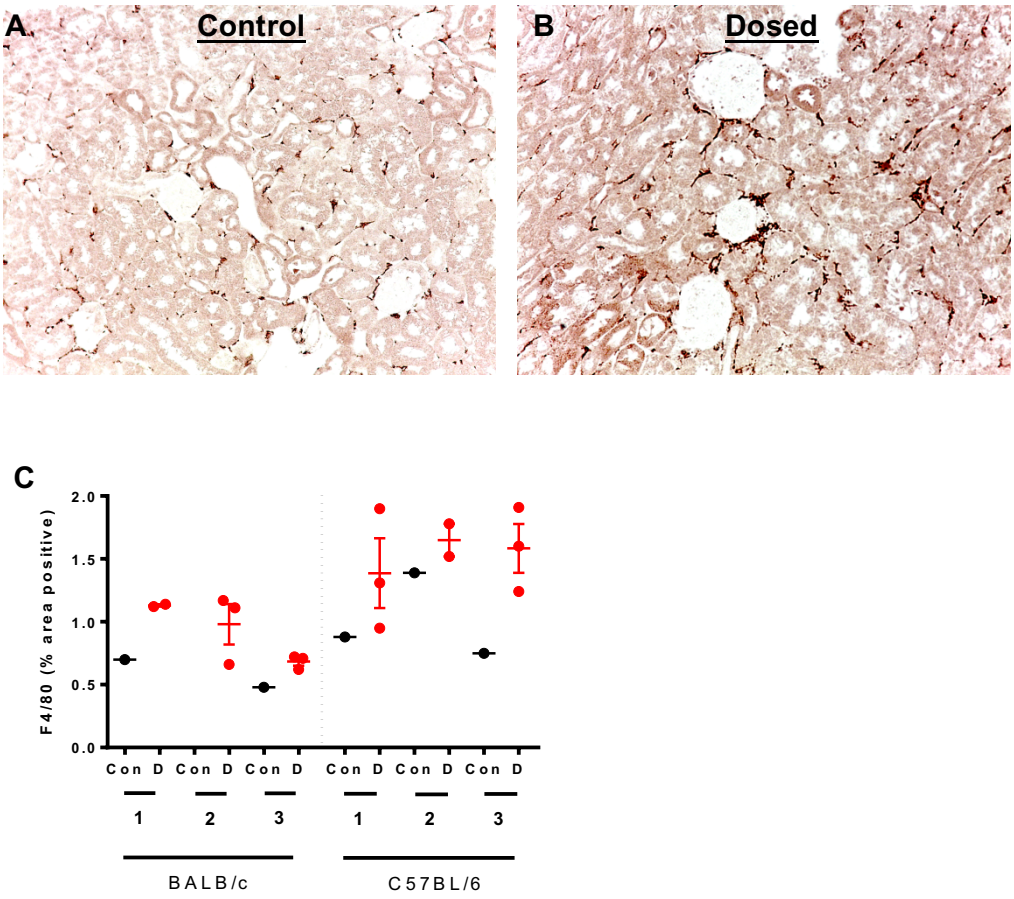

Figure 50: Immunohistochemistry for F4/80^{+} tubulointerstitial macrophage infiltration. Representative images demonstrating immunostaining for F4/80^{+} cells are displayed for a (A) Control and (B) Dosed C57BL/6 mouse from Group 2. (C) Quantification of F4/80^{+} cells was performed by automated analysis in Image J, from 30 randomly selected cortical fields captured at 200 x original magnification. Dosed mice displayed a greater number of F4/80^{+} cells.

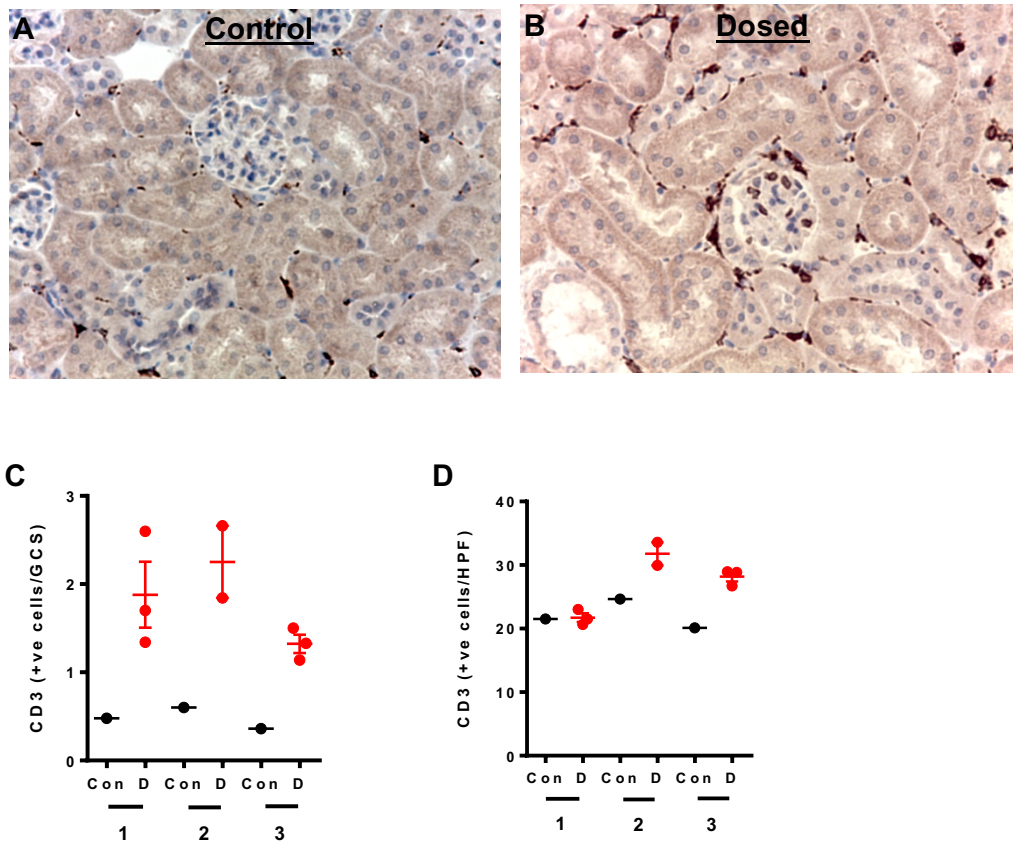

Figure 51: Immunohistochemistry for $CD3^+$ T cell infiltration in control and dosed C57/BL6 mice. Representative images demonstrating immunostaining for $CD3^+$ cells are displayed for a (A) Control and (B) Dosed C57BL/6 mouse from Group 2. Quantification of $CD3^+$ cells was performed manually by counting positive cells in (C) 25 consecutive glomeruli (x 400 original magnification) or (D) 30 consecutive cortical fields (x 200 original magnification). Dosed mice displayed an increase in glomerular T cells. GCS: Glomerular cross section. HPF: High power field.

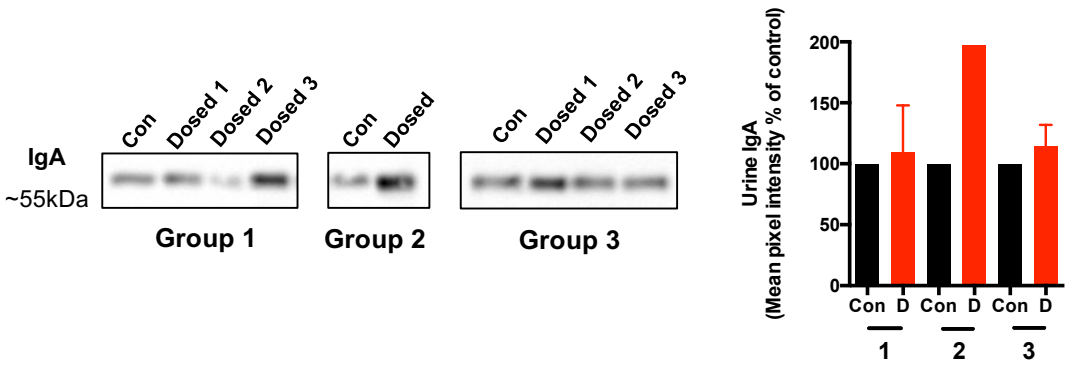

Figure 52: Western blot for urine IgA excretion between control and dosed groups. Urine samples, with loaded quantities standardised to urinary creatinine, were resolved by 10% SDS-PAGE, and immunoblotted with an anti-IgA antibody. Urine excretion of IgA was increased in dosed mice, particularly from Group 2.

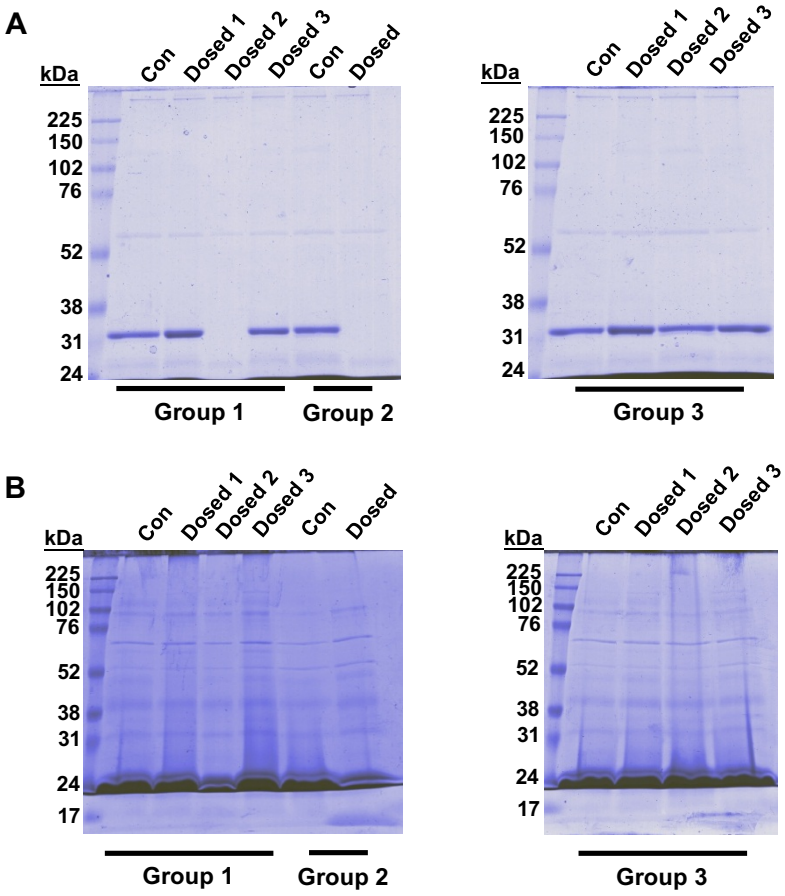

Figure 53: Urine protein excretion. (A) Non-reduced and (B) Reduced urine samples, with loaded quantities standardised to urine creatinine, were resolved by 8% or 10% SDS-PAGE respectively, and stained with Coomassie blue. The pattern of protein excretion between control and dosed mice was broadly similar. A band of approximately 31kDa was missing from two of the dosed mice, which has been submitted for sequencing.

5.5 Conclusions

The main finding from this chapter was that a model of IgAN, based on oral and intravenous immunisation with BGG, could be induced in both BALB/c and C57BL/6 mouse strains. The experimental protocol was optimised through a series of time-course and dose-response experiments. Through these experiments, a dosing scheme of 8 weeks of continuous oral BGG followed by 3 IV injections of BGG daily, and a 4^{th} injection 72 hours after the 3^{rd} injection, was optimal in inducing an anti-BGG immune response and glomerular IgA deposition in C57BL/6 mice, with subsequent glomerular (CD3) and tubulointerstitial (F4/80) inflammatory cell infiltration. Extending the duration of oral immunisation beyond the initial course of IV injections or increasing the number of injections beyond 2 additional doses did not result in any increase in the intensity of IgA deposition, presumably due to tolerance to the antigen and clearance of the immune deposits.

The BALB/c and C57BL/6 mouse strains are amongst the most commonly used laboratory inbred strains. C57BL/6 and BALB/c mice are regarded as being Th1 and Th2 prone respectively, due to their T cells preferentially producing either Th1-type cytokines (IL-2, IFN-γ) or Th2-type cytokines (IL-4, IL-5, IL-10) in response to pathogenic stimuli (Mills et al., 2000; Watanabe et al., 2004). Macrophage responses from these two strains also differ, with C57BL/6 macrophages displaying augmented cytokine responses (TNF-α, IL-12) after stimulation with LPS or the TLR-ligand MALP-2, and increased bactericidal activity, which was reflected in the improved survival of C57BL/6 compared to BALB/c mice after induction of a septic peritonitis model by cecal ligation and puncture (Watanabe et al., 2004).

BALB/c mice were used in the original reports to induce this model, as Th2 responses are believed to play an important role in the initiation of IgAN. PBMCs isolated from IgAN patients produced more IL-4 compared to those isolated from healthy controls, after stimulation with phytohaemagglutinin or phorbol myristate acetate (Lai et al., 1991; Scivittaro et al., 1994). Stimulation of B cells with both IL-4 and IL-5 led to altered glycosylation of IgA produced from murine lymphoma cells (Chintalacharuvu and Emancipator, 1997). However, there is emerging evidence that Th1 responses may also play a significant role in IgAN. mRNA for both Th1 (IL-2, IFN-γ) and Th2 cytokines (IL-4, IL-5) was increased in circulating $CD4^+$ T cells from patients with IgAN compared to healthy controls (Lai et al., 1994). In the

spontaneous ddY mouse model of IgAN, spleen cell cytokines from early-onset disease mice demonstrated polarisation towards Th1 responses (IFN-γ production) compared to those from mice with quiescent disease, which were biased towards a Th2 response (IL-4 production). Furthermore, IFN-γ production increased progressively in diseased mice, from 20 to 40 weeks, and correlated with disease severity (Suzuki et al., 2007). In a study of intrarenal cytokine gene expression from whole IgAN renal biopsies, expression of Th1 cytokine mRNA (IFN-γ) was associated with glomerulosclerosis, while expression of Th2 cytokine mRNA (IL-10) was related to the degree of tubulointerstitial fibrosis (Lim et al., 2001). Additionally, the ratio of Th1/Th2 cytokine (IFN-γ/IL-10) mRNA increased with worsening renal function. Therefore, both Th1 and Th2 cytokines may play a role in the initiation and progression of the disease phenotype. The data presented in this chapter suggests that a model of IgAN can be induced in the C57BL/6 Th1 prone mouse, and that subsequent inflammatory responses, in terms of tubulointerstitial $F4/80^{+}$ cell infiltration, are upregulated.

Glomerular IgA deposition was occasionally noted in the control animals, particularly in Experiment 2. This has been noted by others, and attributed to fecophagia or commensal contamination of food or water (Emancipator, 2001). In their studies, IgA deposits found in the control animals were not accompanied by deposits of complement, haematuria or electron dense mesangial deposits that were seen in the dosed animals. For the experiments performed in the following chapter, housing of mice was reduced from 3 to 2 per cage to account for this potential contributory factor.

Important differences exist between the murine and human IgA systems, that may in part explain the difficulty of modelling all aspects of human IgAN. Mice possess only one form of IgA that more closely resembles IgA2 than IgA1, in that it lacks the extended hinge region that is variably glycosylated in IgAN. Only humans and higher primates (e.g. chimpanzee, gorilla) possess these two separate forms of IgA. In humans, serum IgA mainly exists in monomeric form, whereas in rodents, it is mainly polymeric. Mice lack the equivalent of the human FcαR1 receptor (Monteiro and Van De Winkel, 2003). Lastly, mouse polymeric IgA undergoes hepatobiliary transport and clearance to a far greater extent than human IgA (Delacroix et al., 1985). Despite these differences, it appears that mouse IgA

undergoes glomerular deposition in this model, and that subsequent glomerular and tubulointersitial changes occur. This data, together with the multiphoton microscopy observations from Chapter 3, suggest that IgA has a propensity for glomerular deposition that is conserved between humans and rodents. The model established here may prove useful for studying events *in vivo* that occur subsequent to the deposition of IgA, for example the development of glomerular and tubulointerstitial inflammation.

In an attempt to address some of the differences between species, Monteiro et al recently reported a model that incorporates components of the human IgA system into the mouse. A double transgenic knock-in model was developed that expresses both human IgA1 and the human myeloid FcαR1 (CD89). In this model, both components were required to produce the disease phenotype, with IgA1-CD89 complexes being formed and deposited in the mesangium, leading to haematuria, proteinuria and impairment of kidney function. This interaction was dependent upon another IgA1 receptor, transferrin 1 (TfR1/CD71) and the cross-linking enzyme tissue transglutaminase 2. Mice that expressed human IgA1 only developed IgA deposits in an endocapillary distribution without other evidence of glomerular injury. However, further validation of this model is required, especially as few studies have demonstrated the presence of CD89 in renal biopsies from patients with IgAN.

In summary, in this chapter, a model of IgAN was induced and optimised in C57BL/6 mice, with co-deposition of IgG and C3 and subsequent inflammatory changes, in the form of glomerular T cell infiltration, and tubulointerstitial macrophage infiltration.

Chapter 6: The contribution of the lectin pathway of complement activation to a mouse model of IgA nephropathy

6.1 Introduction

The hypothesis examined in this thesis is that in IgAN, filtered IgA contributes to tubulointerstitial inflammation, and therefore disease progression. The previous chapters established the following: filtered IgA is recognised and endocytosed at the apical surface of PTEC *in vivo*; IgA1 and IgA1-induced mesangial cell cytokines elicit a pro-inflammatory and pro-fibrotic phenotypic transformation in cultured human PTEC; and a mouse model of IgAN, that developed glomerular IgA and IgG deposition, and complement (C3) activation and deposition, resulted in both glomerular (T-lymphocyte infiltration) and tubulointerstitial (macrophage infiltration) inflammation. The final chapter in my thesis focuses on the role of the lectin pathway in mediating both glomerular and tubulointerstitial inflammation in the mouse model of IgAN studied, and specifically whether mice genetically deficient in either MASP-2 or Collectin-11, key initiators of the lectin pathway, were protected against the development of renal inflammation.

The complement system consists of a complex network of over 30 proteins that mediate both adaptive and innate immune responses, resulting in an amplification cascade of effector responses. There are three main mechanisms of activation, termed the classical, alternative and lectin pathways. In IgAN, there is evidence that both the alternative and lectin pathways are commonly activated, and play an important role in disease initiation and progression. C3 deposits are found together with mesangial IgA in over 90% of cases, indicative of complement activation (Maillard et al., 2015). C1q is rarely deposited, implying that the classical pathway does not play a major role. Regarding the alternative pathway, properdin, a positive amplifier which stabilises the normally labile C3 convertase C3bBb, and Factor H, a negative regulator which acts at multiple levels, are commonly detected within glomeruli in IgAN (Maillard et al., 2015). In addition, two separate genome wide association studies (GWAS) identified that a single nucleotide polymorphism (SNP) in the *CFH*/*CFHR* locus, resulting in deletion of Complement factor-H related protein-1 and -3 (CFHR-1 and CFHR-3), protected against the risk of developing IgAN (Gharavi et al., 2011; Kiryluk et al., 2012). CFHR-1 and CFHR-3 compete with

the binding of Factor H to C3, and their deletion results in uninhibited Factor H-C3 binding, and down-regulation of the alternative pathway. Increased urinary excretion of C5b-9, Factor H and properdin have been identified in IgAN, implying that tubular epithelial cells are exposed to these factors (Onda et al., 2011). Therefore complement may be a factor that links glomerular and tubulointerstitial inflammatory disease in IgAN.

Activation of the lectin pathway may play an important contribution in the progression of IgAN. Glomerular deposition of C4 and C4-binding protein were first reported over 20 years ago in a subgroup of patients with IgAN, but was originally thought to result from classical pathway activation (Miyazaki et al., 1984). However, as C1q is usually absent, and following the more recent description of the lectin pathway, this finding is currently believed to represent lectin pathway activation. Deposits of the lectin pathway components MBL, L-ficolin, MBL-associated protein (MASP)-1/3 and MASP-2, C4d and C4-binding protein, but not C1q, were identified in 25% of IgAN renal biopsies, and these cases were associated with more severe histological injury (mesangial proliferation, extracapillary proliferation, glomerular sclerosis and interstitial fibrosis), increased proteinuria, and impairment of kidney function (Roos et al., 2006). In another biopsy series, around one third of IgAN patients had evidence of mesangial C4d deposition, and these patients had a marked reduction in 10-year renal survival (C4d +ve 43.9% *vs* C4d –ve 90.9%) (Espinosa et al., 2009).

In humans, activation of the lectin pathway is initiated by five known molecules that bind to pathogen-associated molecular patterns: mannose binding lectin 2 (MBL2), the ficolins: H-ficolin, L-ficolin and M-ficolin, and the more recently discovered C-type lectin, Collectin-11 (CL-11), also known as Collectin kidney-1 due to its high expression in the kidney, specifically by mesangial cells and in the brush border of the proximal tubules (Motomura et al., 2008). Following activation, these recognition molecules form complexes with MASP-1, -2, and/or -3, promoting further complement activation and stabilisation of the lectin pathway C3 convertase C4b2a (Figure 8). Of these, MASP-1 and -3 are derived from the same gene MASP1/3, by alternative splicing (Stover et al., 2003; Thiel, 2007). In mice, two separate forms of MBL exist, MBL-A and MBL-C, which along with L-ficolin and CL-11 may complex with MASP-1/3 or MASP-2 to trigger complement activation. It is

thought that only MASP-2 is absolutely required for mouse lectin pathway activation, as mice deficient in MASP1/3 demonstrate normal lectin pathway activity (Schwaeble et al., 2011). MASP-2 deficient mice were protected from the injurious effects of myocardial and gatrointerstinal ischaemic-reperfusion (Schwaeble et al., 2011).

The exact mechanism of interaction between IgA and the lectin pathway is yet to be fully elucidated. Polymeric IgA, but not monomeric IgA, was demonstrated to bind to the carbohydrate recognition domain of MBL and induced C4 and C3 activation (Roos et al., 2001). Binding was not inhibited by GalNac, suggesting that the presence of an undergalactosylated IgA1 hinge region was not a requirement for this interaction.

Given the central role of MASP-2 to lectin pathway activation, and its potential ability to link IgA deposition to complement activation and subsequent renal inflammation, the first aim of this chapter was to ascertain whether mice genetically deficient in MASP-2 were protected from the development of glomerular and tubulointersititial inflammation after induction of the mouse model of IgA nephropathy. As CL-11 is highly expressed within the kidney and may play a role in initiating IgA-induced lectin pathway activation, especially regarding the potential interaction between filtered IgA and CL-11 expressed at the brush border of the proximal tubule, the second aim of this chapter was to assess whether mice genetically deficient in this lectin pathway initiator were protected against these effects.

6.2 Protocol

Three groups of 8-week-old male mice were tested in the following protocol: wild-type (wt) C57BL/6, CL-11$^{-/-}$ and MASP-2$^{-/-}$. Mice received 0.1% BGG continuously in the drinking water, before receiving three intravenous injections of 1mg BGG via the tail vein on consecutive days, a further IV injection of 1mg BGG after 48 hours, and were then sacrificed after 48 hours. A control group of wt C57BL/6 mice received normal drinking water and intravenous injections of vehicle (PBS) at the same volume and frequency as the dosed experimental groups. 8 mice were included in each group. One of the CL-11$^{-/-}$ mice died overnight after receiving the first injection of BGG, but all other mice completed the experimental protocol.

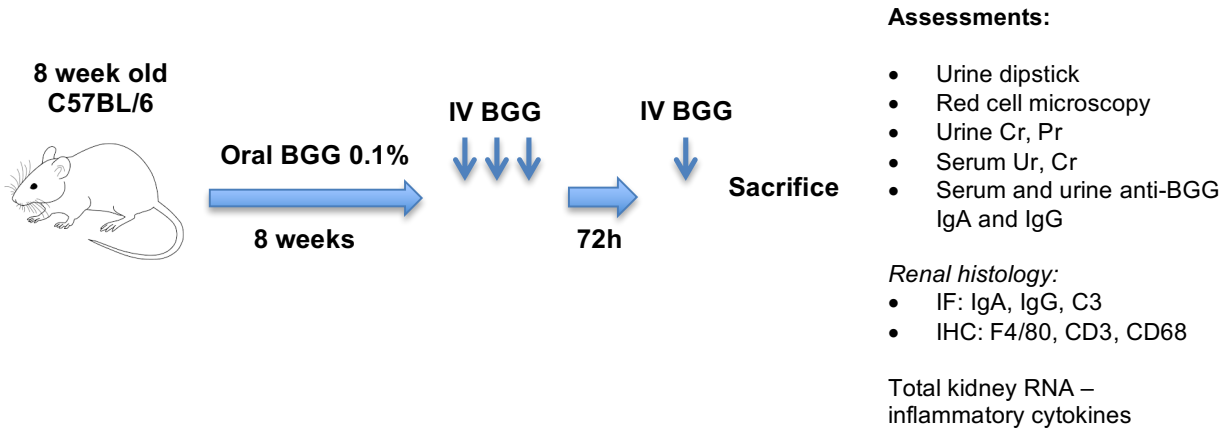

Figure 54: Experimental protocol utilised in this chapter. C57BL/6 mice were orally immunised with BGG followed by 4 intravenous injections of BGG, and were then sacrificed after 48 hours.

Comparisons were made between wt control and wt dosed groups, and between the wt dosed and either the CL-11$^{-/-}$ or MASP-2$^{-/-}$ groups.

6.3 Results

6.3.1 Genotyping of MASP-2 and Collectin-11 deficient mice

MASP-2$^{-/-}$ mice were generously provided by Professor Wilhelm Schwaeble, University of Leicester, and mice from the colony had been backcrossed on to a C57BL/6 background for at least 11 generations (Schwaeble et al., 2011). Mice were genotyped by PCR using the following three primers: M2_F1 (CATCTATCCAAGTTCCTCAGA), Neo5_R1 (CTGATCAGCCTCGACTGTGC), and m2WTO_R1 (AGCTGTAGTTGTCATTTGCTTGA). These amplified a 500-bp product from the disrupted allele and an 800-bp product from the wild-type allele (Figure 55).

The CL-11 deficient mouse line was also generously provided by Professor Wilhelm Schwaeble, and mice from the colony had been backcrossed on to a C57BL/6 background for at least 15 generations. Mice were genotyped using the following three primers: CL-11_wto-F1 (CAGATTCTTGTCCCTGGCCTCA), Neo3a (GCAGCGCATCGCCTTCTATC), and CL-11_scr-R1 (CTCAGTGTCAGCTGAATA-AATGCCA). These amplified a 600-bp product from the disrupted allele and a 470-bp product from the wild-type allele (Figure 56).

All MASP-2$^{-/-}$ and CL-11$^{-/-}$ mice were confirmed to be homozygous for the disrupted allele prior to being used in the subsequent experiments.

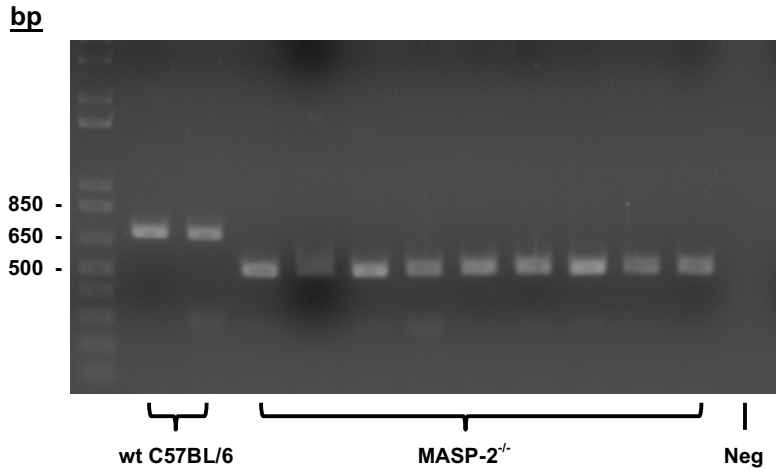

Figure 55: Genotyping of MASP-2$^{-/-}$ mice. Genomic DNA was extracted from ear clippings from 2 wild type C57BL/6 mice and 9 MASP-2$^{-/-}$ mice, and subjected to PCR. An 800-bp product was demonstrated from the wild type allele, and a 500-bp product from the disrupted allele.

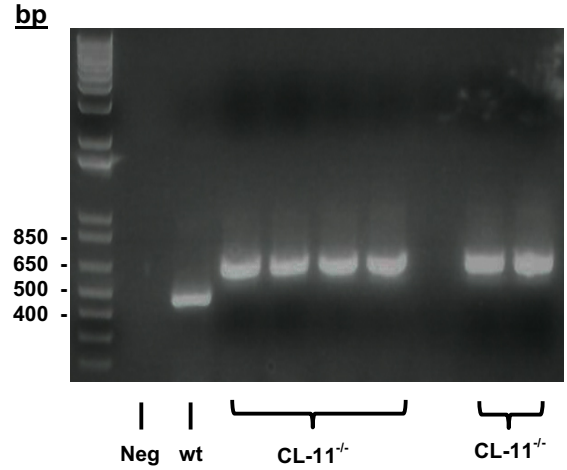

Figure 56: Genotyping of CL-11$^{-/-}$ mice. Genomic DNA was tested from 1 wt C57BL/6 mouse and 6 CL-11-/- mice (the other 2 CL-11$^{-/-}$ mice in the group were analysed separately), and subjected to PCR. A 470-bp product was demonstrated from the wild type allele, and a 600-bp product from the disrupted allele.

6.3.2 Characteristics of the animal models

Mice from all experimental groups were matched for age and sex, and were dosed with the same amount of oral and intravenous BGG. Mice were weighed before being placed in the metabolic cages for the final 24 hours of the experimental course. As shown in Figure 57, experimental groups were well matched for weight, with the only significant difference observed being between mice from the wt control group (mean ± SEM, 31.95 ± 0.62 g) and the CL-11$^{-/-}$ group (26.70 ± 1.33 g; p=0.02). No significant difference was observed between the three dosed groups, with the mean weight of the wt dosed group being 30.00 ± 2.37 g and the MASP-2$^{-/-}$ group being 29.06 ± 0.58 g.

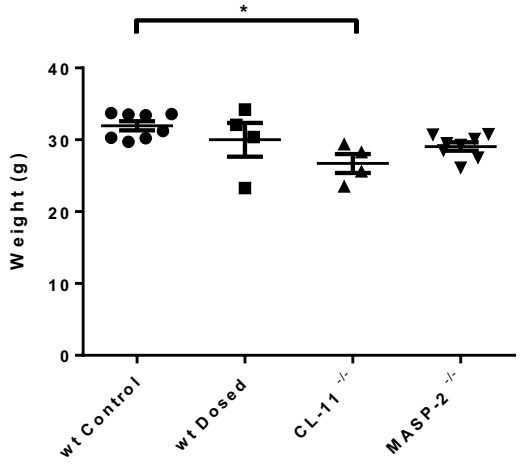

Figure 57: Mean weight of the mice at the end of the experimental course, measured before placement into the metabolic cages. A significant difference was observed only between mice from the wt control and CL-11$^{-/-}$ groups, with no difference between the three dosed groups. Weights from only four mice from the wt dosed and the CL-11$^{-/-}$ groups were available for analysis. Data points represent each individual mouse, horizontal lines represent the mean, and error bars represent the SEM. * P<0.05.

6.3.3 Serum and urine measurements

Blood was collected under terminal anaesthesia and analysed for serum urea and creatinine. 24-hour collections of urine, obtained prior to sacrifice using individual metabolic cages, were analysed for protein excretion. Fresh collections of urine, obtained at the end of the experimental course, were analysed for haematuria by urine dipstick and by microscopy.

No significant difference was observed between the experimental groups regarding measurements of kidney function (serum urea and creatinine) and urinary protein excretion, quantified by the protein:creatinine ratio (PCR) (Figure 58). A number of the mice from the CL-11$^{-/-}$ and MASP-2$^{-/-}$ groups had a borderline raised urea (normal reference range <10 mmol/L). All serum creatinine measurements were within normal reference values.

Regarding measurements of haematuria, in the wt dosed group, 3/8 mice developed haematuria detectable by urine dipstick, compared to 1/8 in the wt control group, 1/7 in the CL-11$^{-/-}$ group, and 1/8 in the MASP-2$^{-/-}$ group, all at 1+ intensity. On quantification by microscopy, a significant increase was observed in urinary red cells in the wt dosed (7.0 ± 1.1 x 10^4 RBC/mL) compared to the wt control groups (2.4 ± 0.8 x 10^4 RBC/mL; p=0.005; Figure 59). Although a trend towards a reduction in urinary red cells was observed in the CL-11$^{-/-}$ group (4.0 ± 1.3 x 10^4 RBC/mL) compared to the wt dosed group, this did not reach statistical significance. No significant difference was observed between the wt dosed group and the MASP-2$^{-/-}$ group (8.3 ± 2.3 x 10^4 RBC/mL).

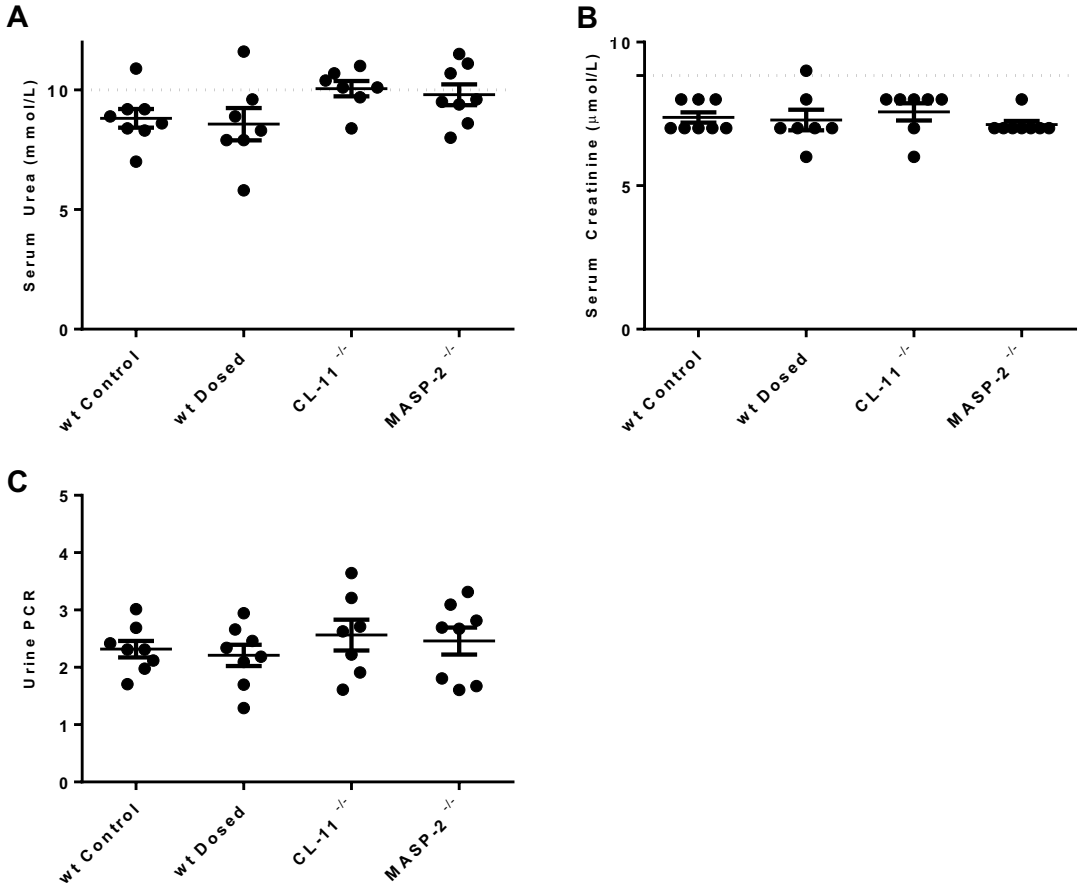

Figure 58: Measurements of kidney function and proteinuria. No significant difference was observed between the experimental groups regarding (A) serum urea, (B) creatinine, and (C) urine protein:creatinine ratio (PCR). Data points represent each individual mouse, horizontal lines represent the mean, and error bars represent the SEM.

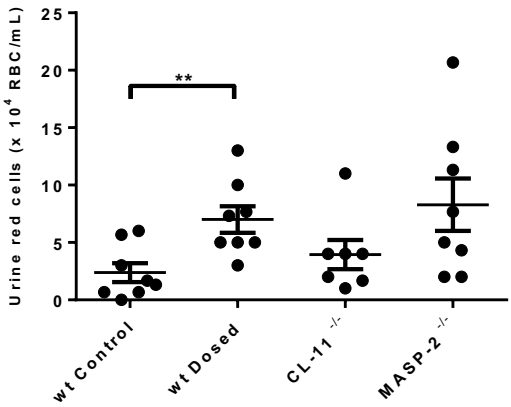

Figure 59: Urinary red cells in the experimental groups. A significant increase was observed in the wt dosed group compared to the wt control group. No significant difference was observed between the other experimental groups. Data points represent each individual mouse, horizontal lines represent the mean, and error bars represent the SEM. ** $p<0.01$.

6.3.4 Immune responses

To quantify the immune response against BGG, serum anti-BGG IgA and IgG levels were measured by ELISA. Plates were coated with 10 µg/mL BGG in coating buffer overnight, before being blocked with 1% BSA/PBS. Samples were added to the wells at a 1/40 dilution in 1% BSA/PBS, following which a goat anti-IgA or anti-IgG HRP antibody was applied, at 1/2000 and 1/4000 dilution respectively. Plates were developed using OPD.

The serum anti-BGG IgA response was significantly higher in the wt dosed compared to the wt control group (0.37 ± 0.13 *vs* 0.03 ± 0.01 OD, p=0.019; Figure 60). In addition, serum anti-BGG IgA responses were significantly higher in both the CL-11$^{-/-}$ (1.21 ± 0.37 OD; p=0.04) and the MASP-2$^{-/-}$ (1.02 ± 0.24 OD; p=0.03) groups compared to the wt dosed group. Urine anti-BGG IgA was detectable in all the dosed groups. No significant difference was observed in the urinary anti-BGG IgA levels between the experimental groups, although a trend towards an increase was observed in the dosed animals, especially in the MASP-2$^{-/-}$ group.

Regarding serum anti-BGG IgG responses, there was a trend towards a higher response in the wt dosed (0.26 ± 0.13 OD) compared to the wt control animals (0.02 ± 0.004 OD), although this was not statistically significant. An increase in serum anti-BGG IgG levels was observed in both the CL-11$^{-/-}$ (0.81 ± 0.15 OD) and the MASP-2$^{-/-}$ (0.78 ± 0.23 OD) groups, with the CL-11$^{-/-}$ group reaching statistical significance (p=0.01). No alteration was observed in urine anti-BGG IgG levels between the experimental groups, compared to the wt control group.

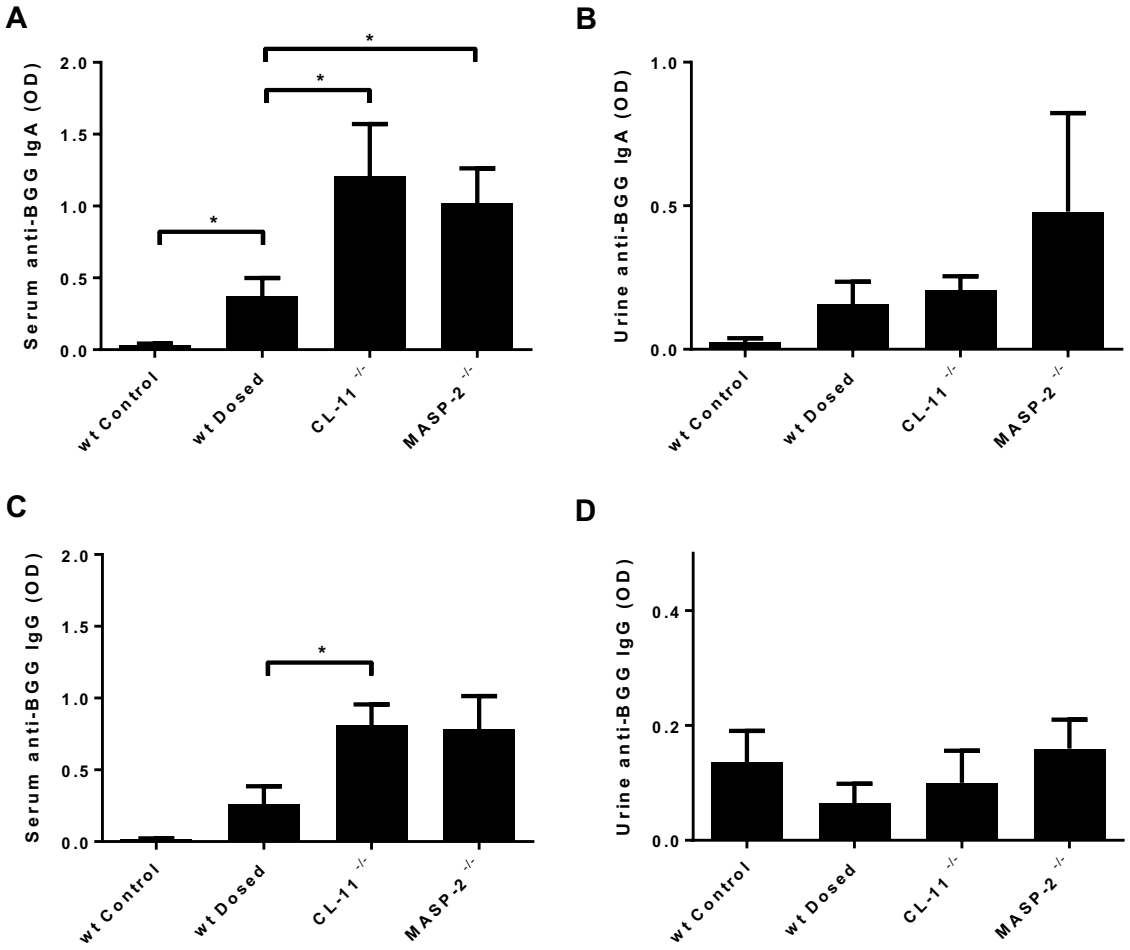

Figure 60: Immune responses in the experimental groups. (A) Serum anti-BGG IgA levels were increased in the wt dosed mice compared to the wt controls, and furthermore were significantly higher in the CL-11$^{-/-}$ and MASP-2$^{-/-}$ mice than in the wt dosed mice. (B) A similar increase was observed in the urine anti-BGG IgA levels in the three dosed mice groups compared to the wt control group, although there was no statistically significant difference between the groups. (C) Serum anti-BGG IgG levels followed a similar pattern, with levels in the CL-11$^{-/-}$ mice being significantly higher than the wt dosed mice. (D) No increase in urinary anti-BGG IgG levels was observed in any of the three dosed groups compared to the wt control group. Mean and SEM are displayed. * $p<0.05$.

6.3.5 Immunofluorescence

Immunofluorescence staining for IgA, IgG and C3 was performed on frozen kidney sections, and the mean intensity of staining from 10 consecutive glomeruli was quantified in Image J.

Glomerular IgA staining was significantly increased in the wt dosed compared to the wt control group (Figure 61). No significant difference in glomerular IgA staining was observed between either the dosed CL-11$^{-/-}$ or MASP-2$^{-/-}$ mice and the wt dosed mice. A trend towards increased glomerular IgG staining in the CL-11$^{-/-}$ and the wt dosed groups compared to wt control group was observed, but this did not reach statistical significance (Figure 62). In contrast, dosed MASP-2$^{-/-}$ mice displayed significantly increased glomerular IgG staining compared to wt controls, but not compared to wt dosed animals. Glomerular C3 deposition was increased in the wt dosed mice compared to the wt controls (Figure 63). This was significantly lower in the CL-11$^{-/-}$ group in comparison to both the wt dosed and control groups. A trend towards reduced glomerular C3 staining was observed in the MASP-2$^{-/-}$ group compared to the wt dosed group, but this did not reach significance.

6.3.5.1 IgA

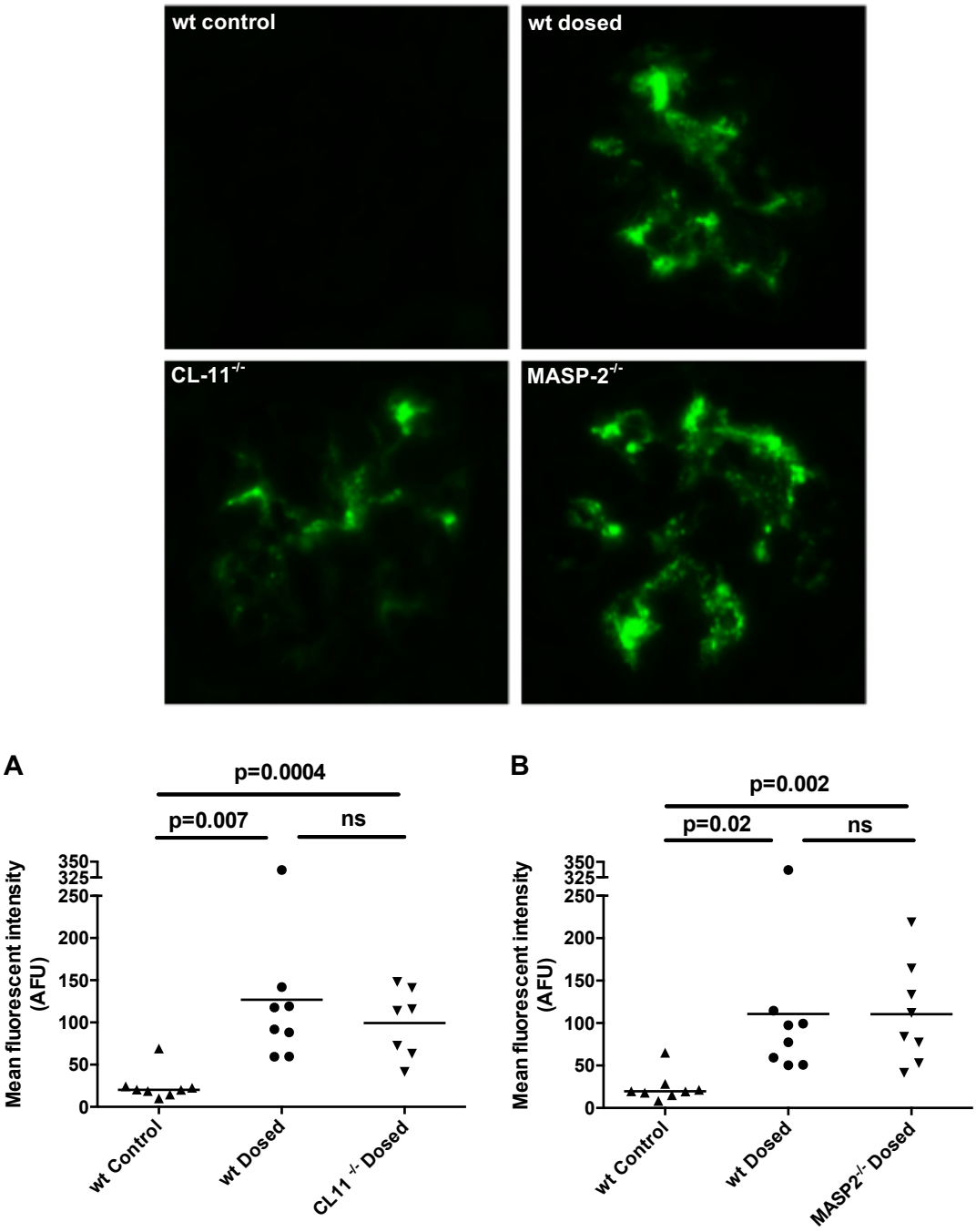

Figure 61: Immunohistochemistry for IgA-FITC in frozen kidney sections. Glomerular IgA staining was increased in the wt dosed group, and both the (A) CL-11$^{-/-}$ and (B) MASP-2$^{-/-}$ groups compared to the wt controls. Data points represent the mean fluorescent intensity from ten consecutive glomeruli from each individual mouse, horizontal bars signify the mean for each group.

6.3.5.2 IgG

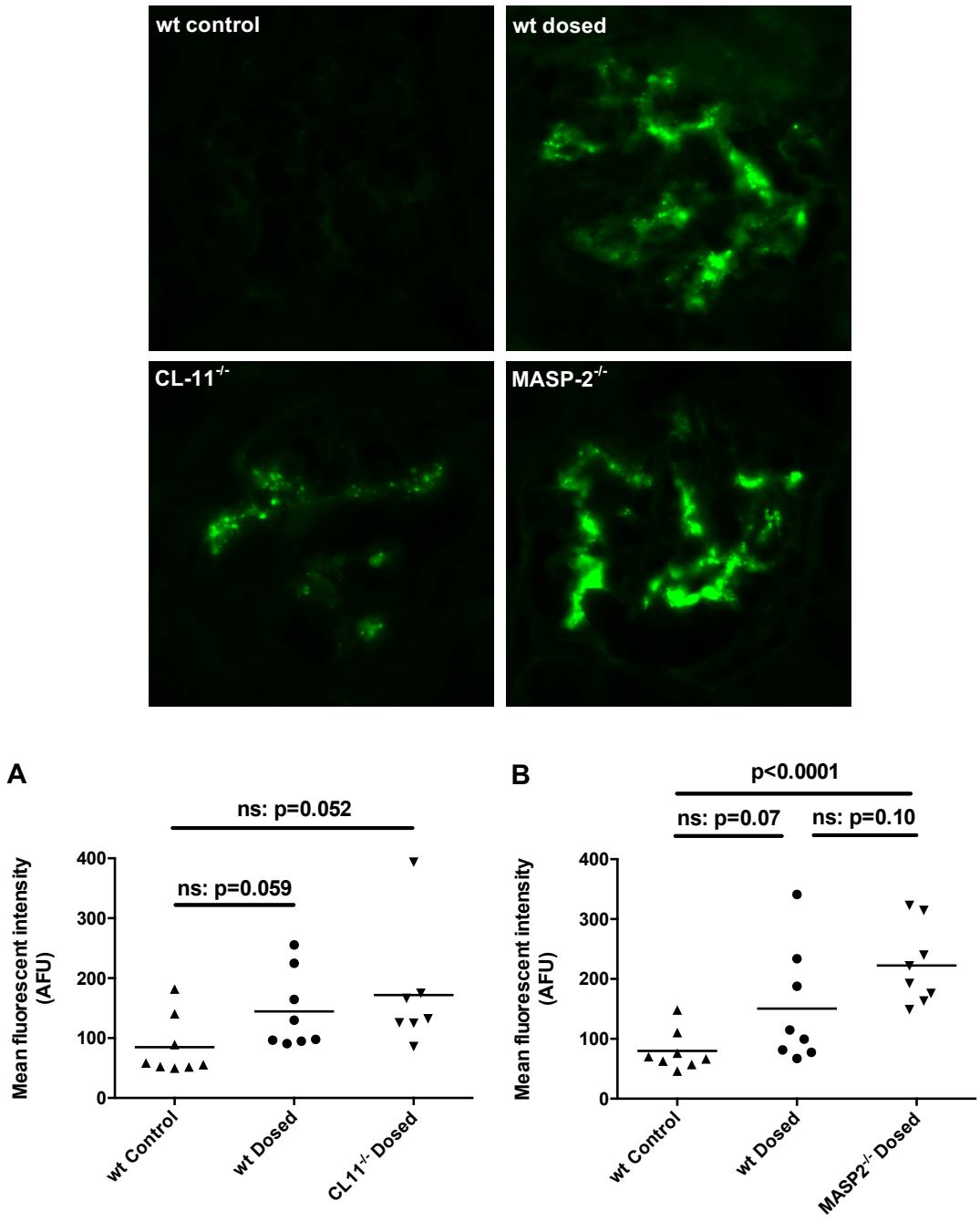

Figure 62: Immunohistochemistry for IgG-FITC in frozen kidney sections. (A) A non-significant trend towards increased glomerular IgG staining was observed in the wt dosed and the CL-11$^{-/-}$ groups compared to the wt controls. (B) MASP-2$^{-/-}$ dosed mice had significantly increased glomerular IgG staining compared to the wt controls. Data points represent the mean fluorescent intensity from ten consecutive glomeruli from each individual mouse, horizontal bars signify the mean for each group.

6.3.5.3 C3

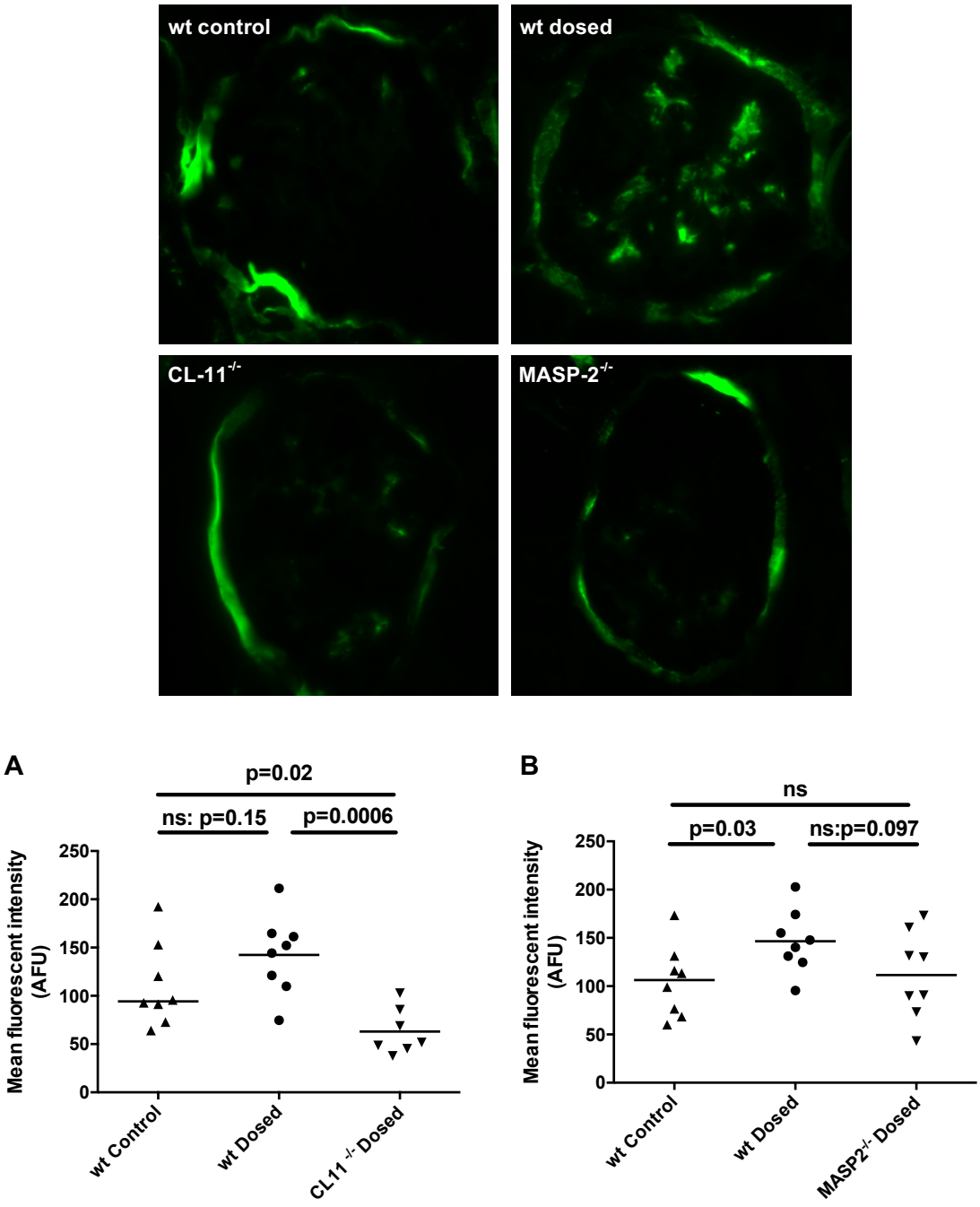

Figure 63: Immunohistochemistry for C3-FITC in frozen kidney sections. (A) Glomerular C3 staining was increased in the wt dosed group compared to the wt controls. C3 deposition was significantly decreased in the CL-11$^{-/-}$ mice compared to both the wt dosed and wt control groups. (B) There was a non-significant reduction of glomerular C3 staining in the MASP-2$^{-/-}$ dosed group compared to the wt dosed group. Data points represent the mean fluorescent intensity from ten consecutive glomeruli from each individual mouse, horizontal bars signify the mean for each group.

6.3.6 Glomerular cell count

Total cell counts were performed from 25 consecutive glomeruli. Wt dosed mice had a significantly higher glomerular cell count compared to wt control animals (31.96 ± 1.1 *vs* 26.32 ± 0.55; p = 0.0004; Figure 64). CL-11$^{-/-}$ mice had a significantly lower glomerular cell count (23.68 ± 0.58; p < 0.0001) compared to the wt dosed mice. There was no difference in glomerular cell count between the wt dosed and the MASP-2$^{-/-}$ (29.1 ± 1.51; p = 0.15) groups.

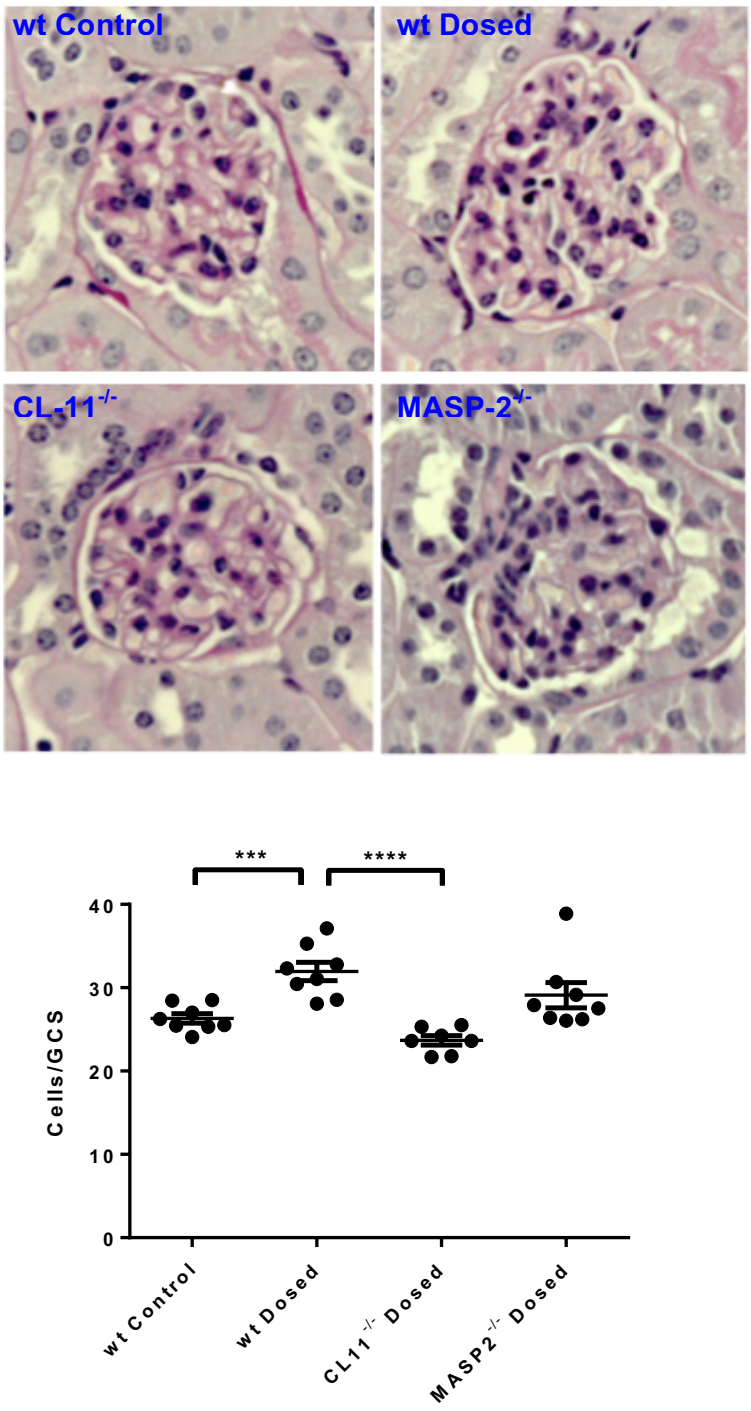

Figure 64: Glomerular cell counts across the experimental groups. Cells were counted manually from 25 consecutive glomeruli in Periodic Acid Schiff stained kidney sections. An increase in glomerular cell count was observed in the wt dosed compared to the wt control mice. CL-11$^{-/-}$ mice had a lower glomerular cell count compared to wt dosed mice. There was no difference in glomerular cell count between wt dosed and MASP-2$^{-/-}$ dosed mice. Data points represent the mean cell count from each individual mouse. Horizontal bars represent the mean and error bars represent the SEM for each group.

6.3.7 Immunohistochemistry for macrophage and T cell infiltration

Immunohistochemistry was performed on FFPE kidney sections for the macrophage marker, F4/80. 35 consecutive cortical areas were imaged and positive areas calculated using Image J. Wt dosed animals displayed significantly increased F4/80^{+} staining compared to wt controls, indicative of increased macrophage infiltration. Furthermore, F4/80^{+} staining was significantly increased in both the CL-11$^{-/-}$ and MASP-2$^{-/-}$ groups compared to both the wt control and dosed groups (Figure 65).

As the F4/80 antigen may not be readily detected in intraglomerular macrophages (Masaki et al., 2003), immunostaining against an alternative macrophage marker, CD68, was performed in paraformaldehyde lysine periodate (PLP) fixed frozen kidney sections. Positive cells were manually counted in 25 consecutive glomeruli. No significant difference in the number of intraglomerular CD68^{+} cells was detected between the groups (Figure 66).

Immunohistochemistry was also performed against the pan-T cell marker, CD3, in FFPE kidney sections. Positive cells were manually counted in 25 consecutive glomeruli. A significant increase in intraglomerular CD3^{+} cells was detected in the wt dosed group compared to the wt controls, and compared to both the CL-11$^{-/-}$ and MASP-2$^{-/-}$ groups (Figure 67).

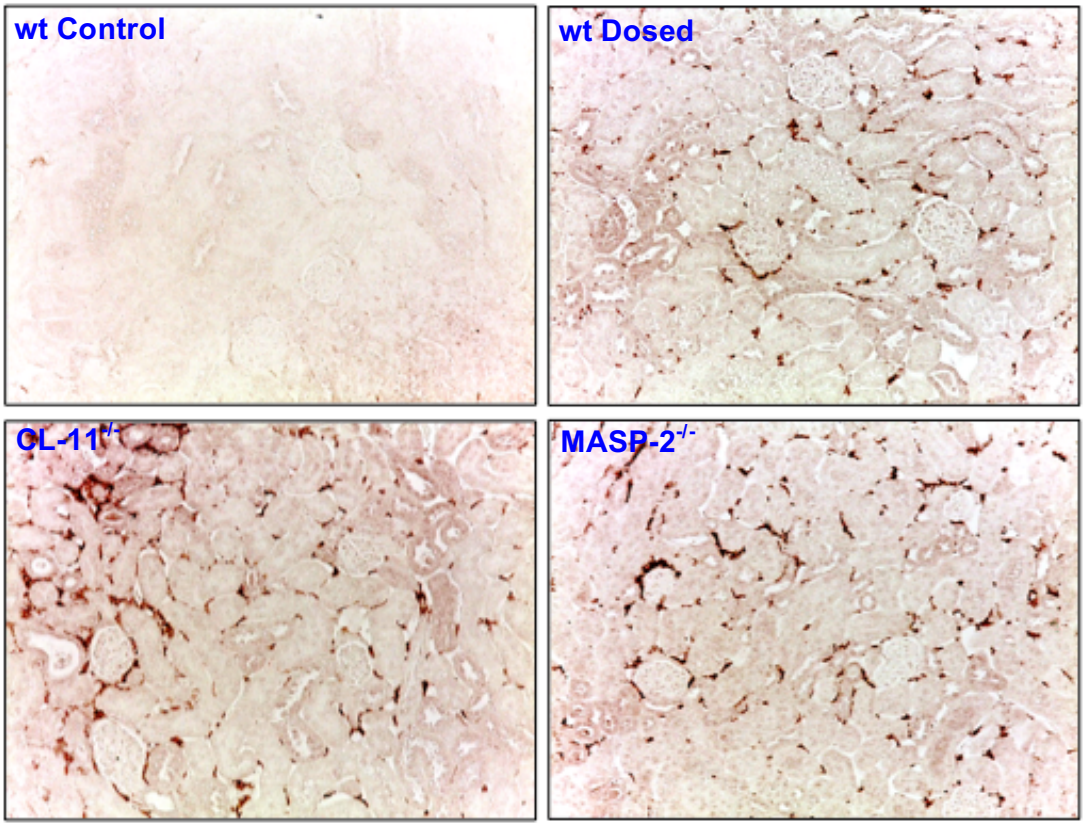

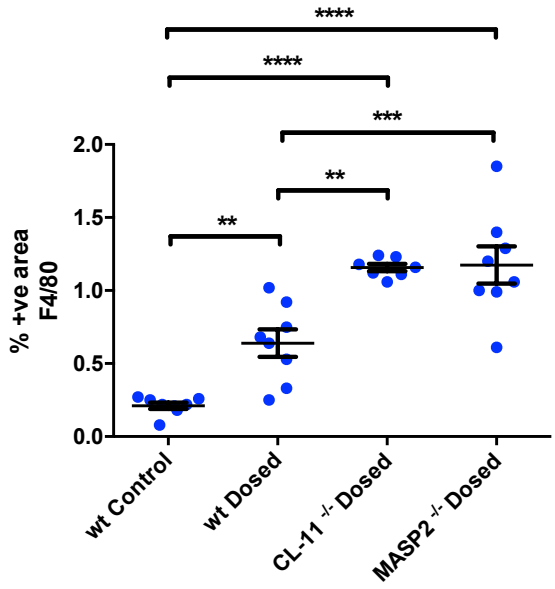

Figure 65: Renal cortical macrophage ($F4/80^{+}$) infiltration in the experimental groups. $F4/80^{+}$ staining was increased in wt dosed compared to wt control mice, and in both $CL\text{-}11^{-/-}$ and $MASP\text{-}2^{-/-}$ compared to wt dosed mice. Data points represent the mean positive F4/80 stained area from 30 consecutive cortical areas from an individual mouse. Horizontal bars represent the mean and error bars represent the SEM from each group. ** $p<0.01$, *** $p<0.001$, **** $p<0.0001$.

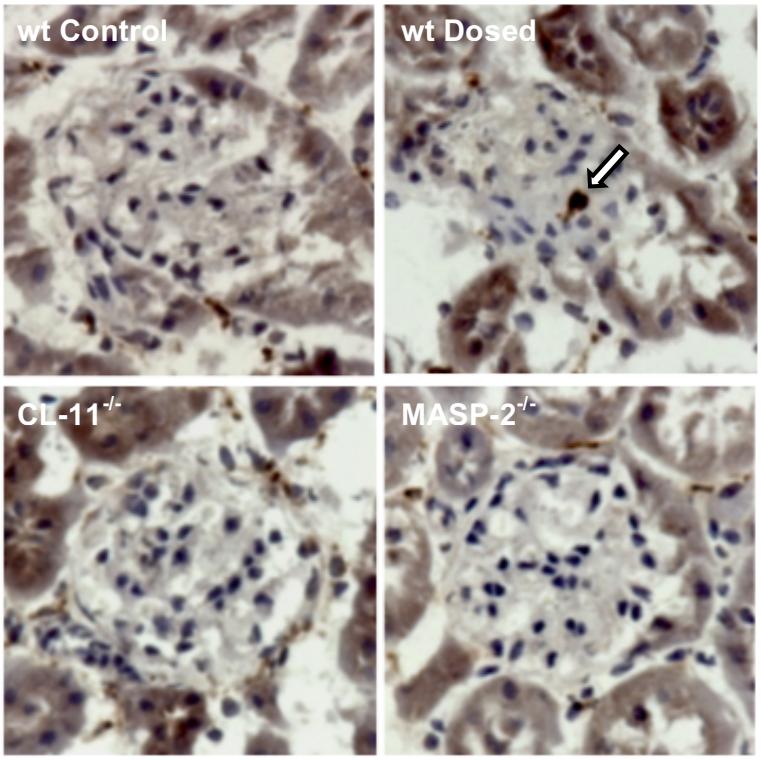

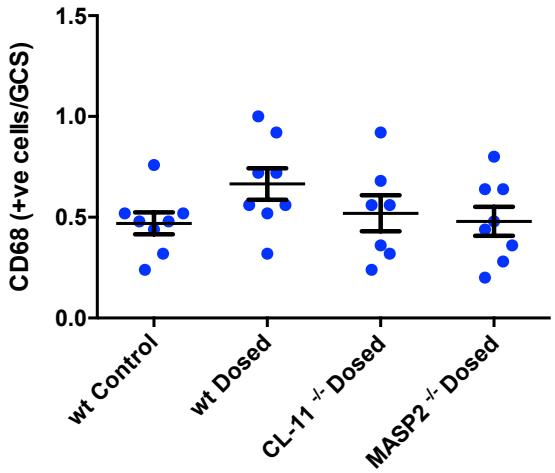

Figure 66: Intraglomerular macrophage infiltration across the experimental groups. CD68 staining was performed on paraformaldehyde lysine periodate (PLP) fixed frozen sections. No significant difference was observed between the experimental groups. Arrow indicates a positively stained cell. Positive cells were quantified from 25 consecutive glomeruli. Points represent the mean cell count for an individual mouse, mean ± SEM for each group are displayed.

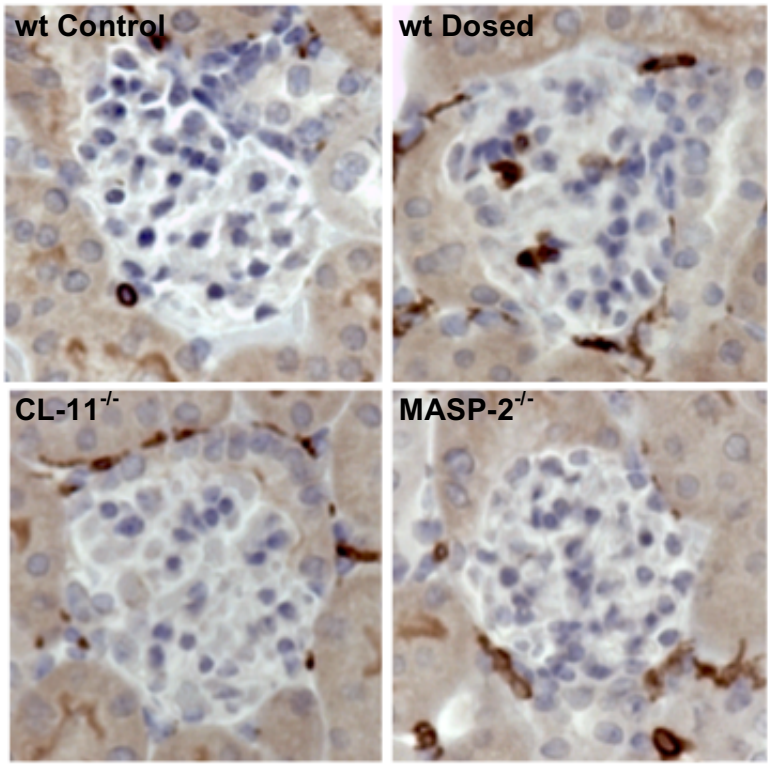

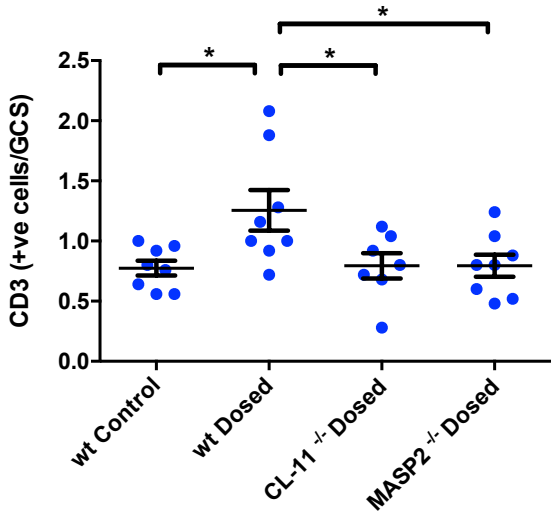

Figure 67: Intraglomerular T cell infiltration across the experimental groups. Staining was performed for the pan T cell marker CD3 in formalin fixed paraffin embedded kidney sections, and positive cells were quantified from 25 consecutive glomeruli. Positively stained cells are demonstrated in the section from the wt dosed animal above (top right). An increase in intraglomerular T cells was observed in wt dosed mice compared to all other groups. Points represent the mean cell count for an individual mouse, mean ± SEM for each group are displayed.

6.3.8 Pro-inflammatory and pro-fibrotic gene expression

Finally, RNA was extracted from individual total kidney samples, and analysed for the gene expression for six different pro-inflammatory or pro-fibrotic mediators: complement factor *C3*, interleukin-6 (*IL6*), tumor necrosis factor (*TNF*), chemokine ligand 2 (*CCL2*, also known as monocyte chemotactic protein 1 (MCP1)), fibronectin (*Fn*), and transforming growth factor beta 1 (*TGFB1*). Gene expression was analysed as a comparison to the housekeeping gene cyclophilin. Statistical comparisons were performed between wt control and wt dosed groups, wt dosed and CL-11$^{-/-}$ dosed groups, and wt dosed and MASP-2$^{-/-}$ dosed groups.

There was a significant reduction in *TNF* gene expression in the wt dosed compared to the wt control animals, but no other significant change in the other genes tested (Figure 68). In the dosed CL-11$^{-/-}$ mice, there was a significant increase in TNF expression, and a significant reduction in *CCL2* and *TGFB1* expression compared to the wt dosed animals. In the dosed MASP-2$^{-/-}$ mice, there was a significant reduction in *Fn* and *TGFB1* gene expression compared to the wt dosed animals.

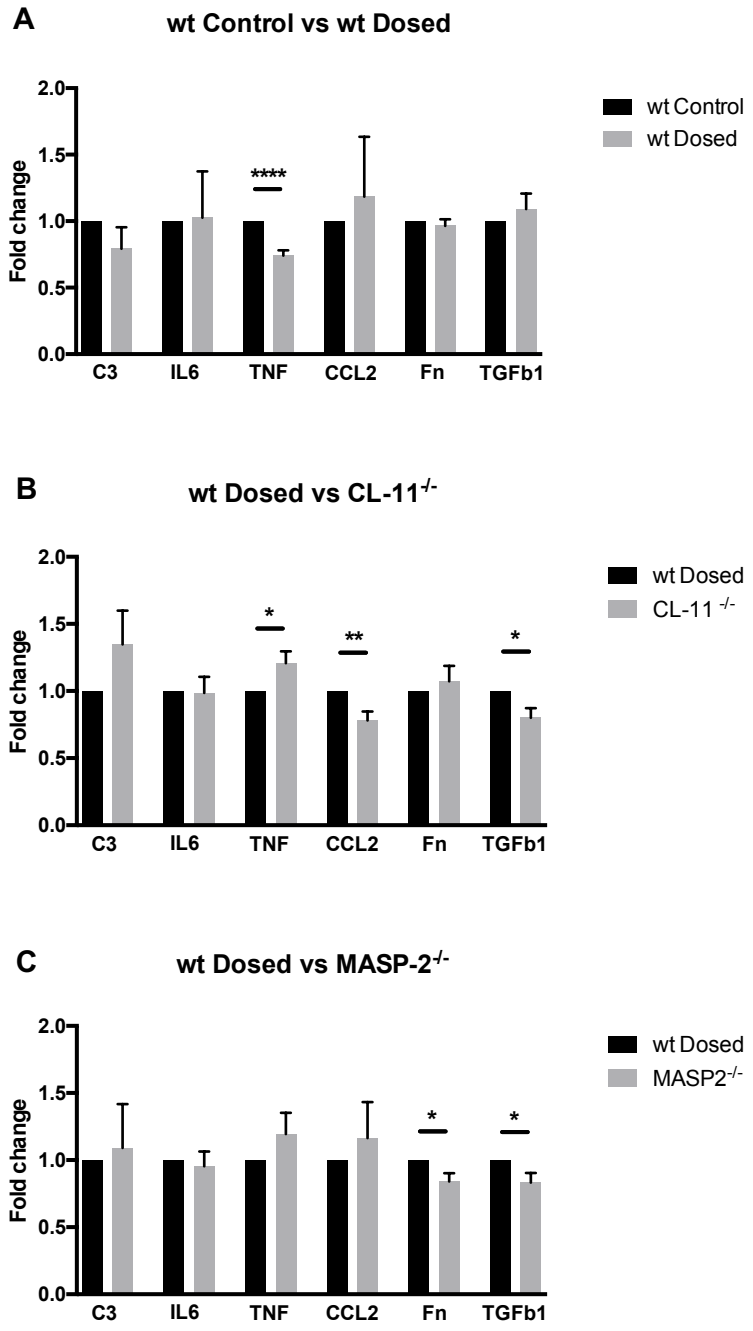
A
wt Control vs wt Dosed
Fold change
2.0
1.5
1.0
0.5
0.0
****
C3
IL6
TNF
CCL2
Fn
TGFb1
wt Control
wt Dosed
B
wt Dosed vs CL-11-/-
Fold change
*
**
*
wt Dosed
CL-11 -/-
C
wt Dosed vs MASP-2-/-
Fold change
*
*
wt Dosed
MASP2-/-

Figure 68: Pro-inflammatory and pro-fibrotic gene expression across the experimental groups. RNA from individual total kidney samples was analysed for the gene expression of six different pro-inflammatory or pro-fibrotic mediators by quantitative real time PCR. Gene expression was quantified as a ratio to the housekeeping gene cyclophilin using the delta delta CT method, and expressed as fold change compared to the control group. (A) Gene expression in the wt dosed group compared to the wt control group. A significant reduction in *TNF* gene expression was found in the wt dosed mice compared to the wt controls. No other significant changes were found in the other genes tested. (B) Gene expression in the dosed CL-11$^{-/-}$ group compared to the wt dosed group. A significant increase in *TNF*, and decreases in *CCL2* and *TGFB1* gene expression were observed in the CL-11$^{-/-}$ group. (C) Gene expression in the dosed MASP-2$^{-/-}$ group compared to the wt dosed group. Significant reductions in *Fn* and *TGFB1* gene expression were observed in the MASP-2-/- mice. Bars represent the mean ± SEM for each group. * $p<0.05$, ** $p<0.01$, **** $p<0.0001$.

6.4 Conclusion

The data in this chapter demonstrates that a model of IgA nephropathy was successfully induced in wt, CL-11$^{-/-}$ and MASP-2$^{-/-}$ C57BL/6 mice, by the oral and parenteral administration of BGG. Induction of the model led to generation of a serum anti-BGG IgA and IgG immune response, and the presence of anti-BGG IgA in the urine. Immune responses were consistently stronger in the CL-11$^{-/-}$ and MASP-2$^{-/-}$ groups compared to wt dosed animals. Glomerular IgA deposition was equivalent across the dosed groups, and there was a trend towards stronger IgG deposition in the MASP-2$^{-/-}$ mice. Consistent with these findings, interstitial macrophage infiltration was increased in the CL-11$^{-/-}$ and MASP-2$^{-/-}$ groups compared to wt mice. Overall, the model appeared to be more strongly induced in the CL-11$^{-/-}$ and MASP-2$^{-/-}$ groups. Deficiencies in these components of the lectin pathway did not protect against the interstitial inflammatory responses generated by this disease model, and conversely, these responses may have been exacerbated, possibly due to compensatory effects of other pro-inflammatory pathways.

Some differences in glomerular pathology were observed between the groups. Although there was no alteration in kidney function or levels of proteinuria, there was a trend towards a reduction in haematuria in the CL-11$^{-/-}$ mice, associated with a reduction in glomerular cell count in this group. A significant reduction in glomerular T cell infiltration, and a trend towards reduction in glomerular macrophages were observed in the CL-11$^{-/-}$ and MASP-2$^{-/-}$ groups, compared to wt dosed animals. Absence of these lectin pathway components may therefore have a protective effect against aspects of the glomerular pathology induced by this model.

Interestingly, CL-11$^{-/-}$ mice had reduced glomerular C3 deposition compared to both wt control and dosed animals, suggesting that this effect was independent of the model. It would be of major interest to investigate this characteristic further by inducing other models of renal disease in CL-11$^{-/-}$ mice where glomerular C3 deposition occurs to a greater extent.

No notable increase in renal pro-inflammatory and pro-fibrotic cytokine gene expression was detected in the model in wt mice compared to control animals. Although some reductions in CL-11$^{-/-}$ and MASP-2$^{-/-}$ mice were observed compared

to the wt dosed mice, the relevance of these findings is unclear given that the expression of these genes was not induced in the model. It would be interesting to examine whether relative gene expression differs according to specific renal cortical compartments (i.e. glomerular or tubulo-interstitial areas) by techniques such as laser capture microdissection or *in situ* hybridisation, since changes within individual regions may become undetectable when total renal tissue is analysed. For example, differences in proteoglycan gene expression between glomerular and tubulointerstitium areas, thought to be important for extracellular matrix production and cell signalling, have been identified from biopsies from patients with IgAN (Ebefors et al., 2011). Differences in gene expression between individual renal compartments may explain the apparent discrepancy between the increase in interstitial inflammation and reduction in glomerular pathology observed in the genetically deficient mice.

It remains unclear whether the lectin pathway of complement is activated in this model. There does appear to be complement activation, evidenced by the increased glomerular deposition of C3. In human IgAN, the complement system is most commonly activated via the alternative and lectin pathways (Maillard et al., 2015). Further efforts are currently underway to establish whether complement components from each of these pathways are generated and deposited in increased amounts in this model. However, as complement activation may lead only to transient soluble component formation, the activation of these pathways cannot be ruled out by the absence of such deposits. An interesting proposition is a potential link between MASP1/3 and the alternative pathway, so that the increased tubulointerstitial macrophage infiltration observed in the MASP-2$^{-/-}$ mice may be attributable to an increase in MASP1/3 activity driving alternative pathway activation (Degn et al., 2012; Sekine et al., 2013). Current efforts are underway to elucidate the links between these two pathways of complement activation.

Of note, studies of human IgAN have indicated that the lectin pathway is activated in only a subset of patients with IgAN, and its activation is associated with a more aggressive form of the disease (Espinosa et al., 2009; Roos et al., 2006). There have been limited *in vitro* studies to date that examine the interaction between IgA and the lectin pathway (Roos et al., 2001). Recognition molecules that act as initiators of the lectin pathway may respond to specific oligosaccharide patterns,

and the undergalactosylated IgA1 hinge region, a feature of human IgAN not replicated in the mouse IgA system, may prove to be an important trigger for lectin pathway activity.

There are certain limitations to this model. Despite efforts to optimise the dosing schedule, some of the mice did not respond strongly to the antigen, both in terms of a serum immune response, and the deposition of IgA, which in some cases was mild-moderate in nature. This heterogeneity of response is consistent with previous reports (Emancipator, 2001; Emancipator et al., 1983a). These findings may be reflected in the degree of inflammatory cell infiltration, and the finding that no renal dysfunction or proteinuria occurred. Additionally there is no evidence from this study or from previous reports that renal fibrosis occurs in this model. Together, these findings mean that the model is more representative of an early stage of human IgA nephropathy. Non-affected littermates would have served as a more optimal control to the genetically deficient animals, to fully control for both the genetic background and environmental factors (Holmdahl and Malissen, 2012). However, these were unavailable for this study.

Previously, other investigators have incorporated a uninephrectomy immediately following the parenteral administration of BGG in order to induce a more severe phenotype, and have reported fibrosis and increased proteinuria in this model (Lai et al., 2011). However, it would be important to ensure that these effects are not due to the uninephrectomy itself, rather than the immunisation of BGG. Another approach may be the incorporation of an adjuvant together with BGG immunisation, to stimulate a stronger IgA response. The intranasal delivery of Cholera toxin (CT) and its non-toxic B subunit, CTB, has been shown to strongly stimulate both mucosal and serum IgA responses (Czerkinsky et al., 1991). Use of CTB and oral immunisation with ovalbumin have been reported in a mouse model of IgAN (Yamanaka et al., 2016).

In summary, in this mouse model of IgA nephropathy, genetic deficiency of MASP-2 or CL-11 did not protect against the tubulointerstitial inflammation observed in the form of interstitial macrophage recruitment. Further studies should focus on the role of the alternative pathway and whether this is activated in the model.

Chapter 7: Final discussion

7.1 Summary of results

The aim of this thesis was to investigate mechanisms of progression of IgAN following mesangial deposition of IgA, and to ascertain whether IgA has a direct effect on the proximal tubule, that contributes towards tubulointerstitial inflammation and fibrosis. The following hypothesis was tested “A major factor determining the development of progressive renal failure in IgAN is the presence in the serum of IgA1 with PTEC-specific pro-inflammatory and pro-fibrotic activity. As non-selective proteinuria develops this IgA1 enters the proximal tubule and augments PTEC activation, accelerating renal scarring”.

Since only limited studies had been performed to date that examined the interaction between IgA and PTEC, the first study concentrated on this interaction *in vivo*, utilising multiphoton microscopy. Serum IgA that was filtered across the glomerular filtration barrier was found to interact with PTEC and undergo endocytosis in wild type MWF rats. Induction of podocyte injury and compromise of the glomerular filtration barrier led to a large increase in the filtration of IgA, and its uptake by PTEC. A model of ischaemic-ATN induced CKD, resulting in tubular injury, led to greatly diminished endocytosis of IgA by PTEC, suggesting that this interaction requires healthy tubules and is therefore an active process.

The second study focused on the effects of human IgA on PTEC cytokine release. Total IgA1 had a stimulatory effect on human PTEC, leading to transcription factor (PPRE) activation, and pro-inflammatory (IL-6) and pro-fibrotic (TGF-β1) responses. pIgA1 had a particularly strong effect on TGF-β1 release. The strongest response was observed with galactose-deficient pIgA1 (gdpIgA1), the fraction of IgA1 that is increased in IgAN patients and found within glomerular mesangial IgA deposits. IgA1 was found to have effects on PTEC pro-inflammatory and pro-fibrotic cytokine release both directly, and via IgA1-human mesangial cell stimulated conditioned media. Therefore IgA1, especially gdpIgA1, may have potent stimulatory properties on PTEC cytokine release that contribute towards the process of tubulointerstitial fibrosis in IgAN.

In the third study, a mouse model of IgAN, involving oral and parenteral immunisation with bovine gamma globulin, was developed and optimised. The model was established in both BALB/c and C57BL/6 mouse strains. Through this series of experiments, it was shown that the model of IgAN was associated with both glomerular (T cell) and tubulointerstitial (macrophage) inflammatory cell infiltration. These effects were broadly equivalent across the two mouse strains.

In the fourth study, the contribution of the lectin pathway of complement activation towards glomerular and tubulointerstitial inflammation was studied in the mouse model of IgAN. The model was induced in mice genetically deficient in key components of the lectin pathway, MASP-2, and the recognition molecule Collectin-11. The model was more strongly induced in both genetically deficient mice compared to wild type animals, with equivalent IgA deposition, stronger IgG deposition, and an increase in tubulointerstitial inflammatory (macrophage) cell infiltration. However, some protective effects on glomerular inflammatory (T cell) cell infiltration were noted, implying that the lectin pathway may have differing effects according to specific renal compartment. Overall, however, it appeared that deficiency of these lectin pathway components did not protect against the development of tubulointerstitial inflammation. Indeed, the increased effects observed could possibly be due to the compensatory effects of other pro-inflammatory pathways, although this remains to be shown.

7.2 Limitations of the thesis

7.2.1 Limitations of the multiphoton microscopy studies

Although the multiphoton microscopy studies demonstrated uptake of fluorescently labelled IgA by the proximal tubule, and that the proximal tubule has capacity for increased endocytosis following damage to the glomerular filtration barrier, it remains to be demonstrated whether this process occurs in humans. Although intravital imaging offers key advantages, specifically the ability to assess the handling of filtered proteins in their native environment, differences exist between the structure of human and rat IgA. Live imaging of the renal handling of filtered proteins within the human kidney is not possible, although binding of IgA to human PTEC has been previously demonstrated by flow cytometry (Chan et al., 2005). More detailed studies, for example by confocal microscopy, to examine IgA-PTEC binding would be helpful to confirm this interaction. It would also be helpful to

confirm the multiphoton imaging findings by staining the kidney sections generated at the end of the experiment for the presence and location of IgA.

7.2.2 Limitations to the *in vitro* studies

Further work is required to detail the potentially important and clinically significant interaction between human IgA1 and PTEC. The release of a number of pro-inflammatory and pro-fibrotic cytokines was demonstrated from PTEC after incubation with IgA1. Isolation of IgA1 from serum is technically challenging, and a number of different approaches have been reported previously, each with their own advantages and limitations.

In these studies, jacalin was used to isolate IgA1 from ammonium sulphate precipitated serum. There remains a possibility that some of the effects observed may be in part attributable to other unknown proteins that have either bound to jacalin, or were carried over during the isolation process. Care was taken to minimise these effects as far as possible. Jacalin has a high affinity for O-glycosylated peptides. IgA1, IgD and C1 esterase inhibitor are the main O-glycosylated proteins within serum, and of these IgA1 is by far the most abundant. Jacalin has strong affinity for both T and Tn antigen (Figure 2). Sialylation of the Tn antigen inhibits binding of Jacalin, excluding this particular fraction of IgA1 from the isolate, while the sialylation of the T antigen does not affect binding (Tachibana et al., 2006). The use of jacalin may therefore not isolate all forms of IgA1 contained within serum.

Other groups have performed affinity chromatography using an anti-IgA column (Oortwijn et al., 2006), although this approach isolates both IgA1 and IgA2, the latter being of less relevance in IgAN. In addition, this method requires the use of an acidic glycine-HCl buffer to elute the IgA, which may potentially affect and degrade IgA-containing immune complexes. Another approach has been the generation of IgA by EBV-immortalised B cell lines, isolated from both patients with IgAN and healthy subjects (Suzuki et al., 2008). This method has been used to characterise differences in the galactosylation processing of IgA1 in IgAN patients, although the generation of enough IgA required for cell culture experiments may prove to be technically challenging. Furthermore, patients with IgAN possess a variety of circulating IgA1 molecules with heterogeneity in their glycosylation states

at any one time. Although experiments performed with clonal populations of IgA1 would be of interest to understand underlying mechanisms, they would not model the clinical situation accurately.

7.2.3 Limitations to the mouse model of IgAN

A major limitation to developing mouse models of IgAN is the difference in the structure between human and mouse IgA. Mouse IgA exists as one isoform, and more closely resembles human IgA2 in that it lacks an extended hinge region. A central feature of IgAN is the undergalactosylation of this hinge region, which is thought to confer specific nephritogenic properties. Currently, no mouse model exists that encompasses all aspects of human IgAN, ranging from the mesangial deposition of galactose deficient IgA1, mesangial and podocyte activation, glomerular damage and eventually, the development of haematuria, proteinuria and progression of tubulointerstitial fibrosis (Eitner et al., 2010). Progressive IgAN typically develops over a number of years, making it difficult to accurately model in a practical manner.

In this thesis, I have used a model that examines the early events in IgAN, specifically the glomerular deposition of IgA and the glomerular and tubulointerstitial reactions that occur subsequently. My results from Chapter 5 demonstrate that deposition of IgA in this model is a transient phenomenon, and that the deposits clear if the model is extended beyond around 2 weeks following parenteral immunisation. The inflammatory processes that occur, although significantly altered from control animals, are relatively mild compared to those found in other mouse models of inflammatory kidney disease. Although this is in keeping with the pathological changes observed in IgAN, these mild phenotypical alterations mean that it is more difficult for an intervention to achieve a significant effect.

Transgenic mouse studies have provided many key insights into disease processes. However, deletion of genes may have unintended effects away from the target organ of interest. While there was no significant weight difference between wt and genetically deficient dosed mice, the CL-11$^{-/-}$ mice weighed significantly less than wt control mice by the end of the study. This finding suggests that, although there were no other clear phenotypic differences, that the CL-11$^{-/-}$ mice may not

have gained weight and developed in a normal manner. The use of littermate controls would have been a better control to account for all genetic and environmental factors. However, these were not available for this study, and commercially obtained C57BL/6 mice were used instead.

7.3 Hypothesis

The work performed in this thesis suggests that IgA, particularly galactose deficient pIgA1, contributes to the activation and generation of cytokines by PTEC that are known to drive the process of tubulointerstitial inflammation and fibrosis, and that passage of this form of IgA1 through a damaged glomerular filtration barrier contributes towards the progression of IgAN (Figure 69).

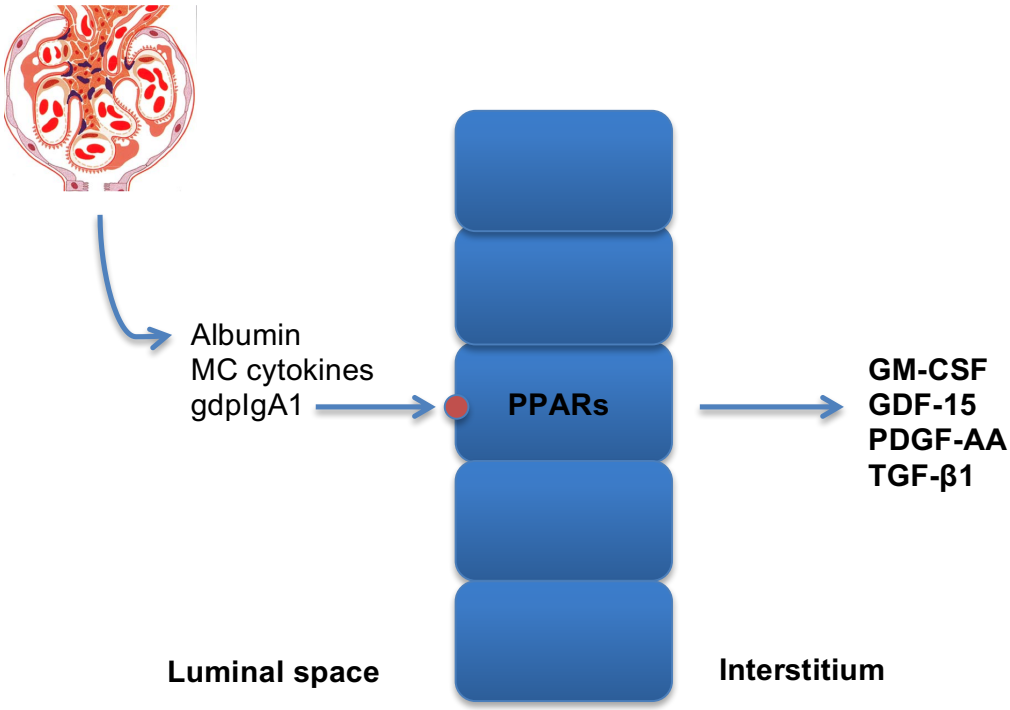

Figure 69: Schematic diagram demonstrating the proposed effects of filtered IgA on the proximal tubule. Following mesangial IgA deposition and damage to the glomerular filtration barrier in IgAN, IgA that filters through may interact with a PTEC receptor, undergo endocytosis, and activate PPARs. This interaction, in a synergistic manner with other components of the ultrafiltrate including albumin and mesagial cell derived cytokine, may trigger the release of a number of pro-inflammatory and pro-fibrotic cytokines, including GM-CSF, GDF-15, PDGF-BB and TGF-β1, that favour the development of progressive interstitial fibrosis.

The first study demonstrated for the first time *in vivo*, that IgA that traverses a damaged glomerular filtration barrier is able to interact and be endocytosed by PTEC. The PTEC receptor for IgA is unknown. A previous study showed that RNA for the known IgA receptors, FcαR, the polymeric Ig receptor (pIgR) and Fcα/μR, was not expressed by primary human PTEC (Chan et al., 2005). However, the multiligand receptor megalin, highly expressed on the apical surface of PTEC, may be a potential receptor for IgA. Utilising a megalin mosaic knockout mouse where megalin was expressed by approximately 40% of PTEC, induction of podocyte injury by the toxin NEP25, causing non-selective proteinuria, led to uptake of IgA by PTEC, but only in those cells that expressed megalin (Motoyoshi et al., 2008). In addition, preliminary studies in our laboratory performed by Dr Richard Baines have shown that an IgA-stimulated PTEC lysate was able to phosphorylate a megalin-cytoplasmic tail GST fusion protein. Therefore megalin is a potential receptor of interest for this interaction.

The second study demonstrated that total IgA1 had stimulatory effects on PTEC, leading to transcription factor (PPRE) activation and cytokine production. pIgA1 appeared to have the most effects, leading to GM-CSF, GDF-15, PDGF-AA and TGF-β1 release. TGF-β1 has well-established roles in contributing towards both glomeruloscerosis and tubulointerstitial fibrosis (Kitamura and Sütö, 1997; Loeffler and Wolf, 2014). TGF-β1 gene, protein expression and its associated signalling protein, SMAD, were also upregulated by human mesangial cells in response to pIgA1 (Lai, 2003). GDF-15 is also part of the TGF-β superfamily, and is induced by many tissues as a response to stress. It has been shown to be upregulated in mouse models of renal ischaemia-reperfusion injury and 5/6 nephrectomy, although its role in renal injury is currently unclear (Zimmers et al., 2005). GM-CSF acts via the signal transducer and activator of transcription STAT5, and plays a central role in the derivation of granulocyte and macrophage populations from bone marrow derived precursor cells, and the differentiation of macrophages into the M1 phenotype, overall having a pro-inflammatory effect (Huen et al., 2014). The PDGFs have roles in mesangial cell proliferation and tubulointerstitial injury, although the role of PDGF-AA is less well defined compared to –BB and –DD (Boor et al., 2014; Floege, 2011; Floege et al., 2014). Overall, release of these cytokines over time may contribute towards a pro-inflammatory and pro-fibrotic interstitial

microenvironment, leading to progression of tubulointerstitial damage and chronic kidney disease in IgAN.

Following damage to the glomerular filtration barrier, other components in the ultrafiltrate may play a synergistic role in driving the progressive interstitial damage seen in IgAN. The role for albumin in the progression of tubulointerstitial fibrosis has been the focus of many studies (Abbate et al., 2006; Baines and Brunskill, 2011). In addition, IgA has a number of effects on mesangial cells, leading to release of a number of pro-inflammatory cytokines, including TNF-α, MCP-1, IL-8, IFN-10, MIF and TGF-β, which may filter through the glomerular filtration barrier and have a stimulatory effect on PTEC, in a process termed glomerulo-tubular crosstalk (Lai, 2003; Leung et al., 2008, 2003; Oortwijn et al., 2006; Tam et al., 2009).

Of note, approximately two thirds of patients with IgAN do not develop progressive disease, despite mesangial IgA deposition, and the severity of mesangial IgA deposition is not a prognostic indicator in IgAN (Cattran et al., 2009). A differentiating factor appears to be the amount of circulating galactose deficient IgA1, which may have specific effects on mesangial cell activation (Zhao et al., 2012). Development of non-selective proteinuria appears to be a trigger for the development of progression of chronic kidney disease in IgAN (Woo et al., 1989). The data in the current study suggests that this event may lead to the filtration of galactose deficient IgA1, which may then have particularly strong effects on PTEC to drive the process of tubulointerstitial fibrosis in IgAN (Figure 70).

Data from the mouse model of IgAN demonstrated a link between glomerular IgA deposition, IgG and C3 deposition, and the development of tubulointerstitial inflammation. The factors that link glomerular IgA deposition and tubulointerstitial inflammation in this model are currently unclear, and an increase in proteinuria was not observed. Activation of the complement pathway is a major area of interest, given the increased filtration of complement components in IgAN (Onda et al., 2011), and interactions between complement and the apical surface of the proximal tubule in other glomerular diseases (Gaarkeuken et al., 2008). The current studies suggest that MASP-2 and CL-11 do not play a major role in promoting interstitial macrophage infiltration in this model, given that the deficiency of these initiators of

pathway did not protect against this event. Further studies should focus on the role and activity of the alternative pathway of complement pathway activation in this model.

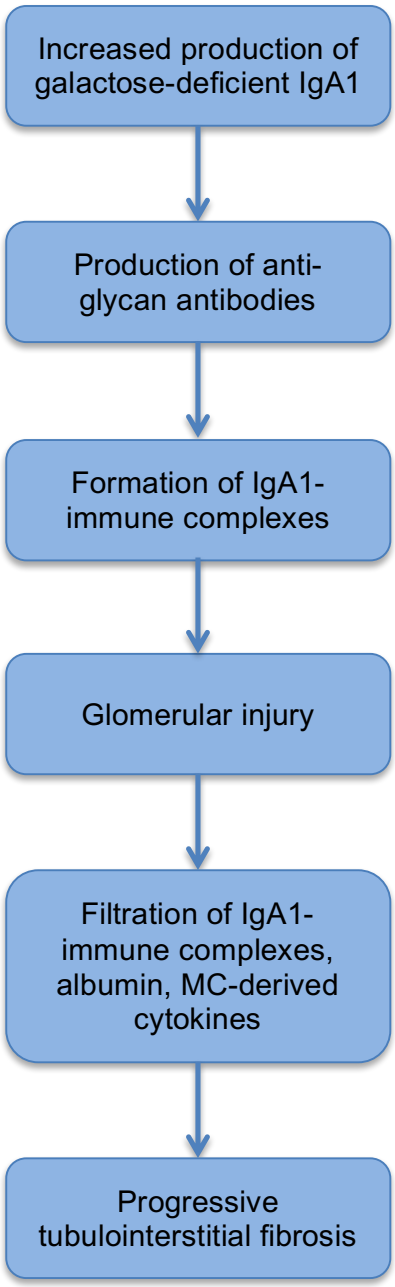

Figure 70: Proposed extension to the “multiple-hit hypothesis” in IgAN. Patients with IgAN possess increased amounts of galactose-deficient IgA1 (gdIgA1), which triggers the formation of anti-gdIgA1 antibodies. These complexes deposit in the renal mesangium resulting in mesangial cell activation, podocyte injury and damage to the glomerular filtration barrier. Loss of permselectivity leads to increasing amounts of filtered albumin, mesangial cell derived cytokines and gdIgA1-containing immune complexes which play a synergistic role in driving the progression of tubulointerstitial fibrosis.

7.4 Future work

7.4.1 *In vivo* imaging studies

Further work is planned to increase the numbers of rats studied so that quantitation of IgA-PTEC endocytosis can be performed, in wild-type MWF rats compared to the model of podocyte depletion. Total IgA has been separated into mIgA and pIgA forms by gel filtration, and these will be labelled with different fluorochromes, to assess the differences in their renal handling in these two models. A comparison between IgA and albumin will be of interest, to assess whether the difference in their molecular sizes makes a difference in the kinetics of their handling by the kidney. Given the differences in structure between rodent and human IgA, it would also be of interest to assess how human IgA is handled by the rat kidney, and whether mesangial deposition and PTEC endocytosis differs for galactose deficient compared to normally galactosylated IgA.

7.4.2 *In vitro* studies

It is of major interest to define and characterise the binding between IgA and PTEC. Confocal microscopy studies would help in studying this interaction. As megalin is a PTEC receptor of interest, immunofluorescence microscopy and flow cytometry studies, performed with and without receptor associated protein (RAP), a 39kDa high-affinity chaperone-like ligand for megalin that inhibits ligand binding, would help establish the importance of megalin in IgA-PTEC interaction, its endocytosis and subsequent PTEC cytokine release. It would be interesting to characterise the activity of other intracellular signalling pathways, for example MAPK/ERK, following incubation of IgA with PTEC. Given the issues with IgA isolation discussed earlier, using IgA that has been isolated by a different method would be helpful to confirm the findings above. The constituents of pIgA remain unclear, with previous reports indicating that circulating IgA1-immune complexes exist that contain IgG, fibronectin and/or C3 (Oortwijn et al., 2006; Suzuki et al., 2009; Tam et al., 2009; van der Boog et al., 2005). A study to characterise the constituents of pIgA, for example involving mass spectrometry and immunoprecipitation studies, may help to provide further understanding regarding the specific effects of pIgA1 on PTEC stimulation. Lastly, the precise nature of interaction between IgA and initiators of the complement pathway remains poorly understood, and is worthy of further study.

7.4.3 *In vivo* studies

Given that the alternative pathway of complement activation is almost universally activated in IgAN, and the increase in glomerular C3 deposition observed in the mouse model studied, it would be of importance to establish whether other complement components, from either the alternative or lectin pathways, are deposited in this model. These may lead to further *in vivo* studies that target either other parts of the lectin pathway (e.g. MASP1/3) or the alternative pathway (Factor B or properdin), for their contributions towards the inflammatory effects observed. Given the variability and mild renal damage observed in the model, pilot experiments to accelerate renal damage, for example by uninephrectomy or administration of an adjunct such as cholera toxin subunit b, may help to optimise the model.

7.5 Concluding remarks

The work from this thesis suggests that following the deposition of IgA in IgAN, mesangial cell activation and damage to the glomerular filtration barrier, the filtration of IgA, particularly galactose-deficient pIgA1, leads to a deleterious effect on PTEC, resulting in activation, and pro-inflammatory and pro-fibrotic cytokine release. Over time, this is likely to play a contributory role to the progression of IgAN. Understanding this interaction further, and the intracellular signalling pathways that are triggered, may lead to the identification of novel therapeutic targets in this disease.

A mouse model of IgAN was developed, that demonstrated a link between mucosal immunisation, glomerular IgA deposition and the development of interstitial inflammation. Deficiencies in initiators of the lectin pathway of complement did not protect against the development of interstitial macrophage recruitment, and further studies should focus on the role of the alternative pathway of complement in this model.

Appendix: Buffers and Solutions

General buffers

Phosphate buffered saline (PBS)

8 g NaCl, 1.15 g anhydrous Na_2HPO_4, 0.2 g KCl, 0.2 g KH_2PO_4

Dissolved in 1 L distilled water, adjusted to pH 7.4

Tris buffered saline (TBS)

6.06 g Tris base, 8.77 g NaCl

Dissolved in 1 L distilled water, adjusted to pH 7.6

Saturated ammonium sulphate (4.1M)

21.67 g ammonium sulphate in 40 mL PBS

ELISA

Coating buffer (0.05M carbonate/bicarbonate, pH 9.6)

0.189 g Sodium hydrogen carbonate, 0.027 g Sodium carbonate

Dissolved in 50 mL distilled water

Wash buffer (PBS/0.3M NaCl/0.1% Tween 20)

20.75 g NaCl, 1 mL Tween-20

Dissolved in 1 L PBS

OPD substrate

2 OPD tablet (o-phenylenediamine dihydrochloride) (Dako) in 6 mL distilled water.

2.5 µL hydrogen peroxide solution 30% (w/w) added immediately before use.

SDS-PAGE

Resolving and Stacking gel (quantities per gel):

Component	8% Resolving gel	10% Resolving gel	Stacking gel
Water	4.6 mL	4.1 mL	3.03 mL
30% Acrylamide	2.7 mL	3.3 mL	0.65 mL
1.5M Tris HCl, pH 8.8	2.5 mL	2.5 mL	-
0.5M Tris HCl, pH 6.8	-	-	1.25 mL
10% SDS (w/v)	0.1 mL	0.1 mL	0.05 mL
10% APS [1]	0.1 mL	0.05 mL	0.025 mL
TEMED [2]	0.006 mL	0.005 mL	0.005 mL

[1] APS: Ammonium persulphate

[2] TEMED: N,N,N',N'- Tetramethylene diamine

Sample buffer, 8 mL

4 mL water, 1 mL 0.5M Tris-HCl pH 6.8, 0.8 mL Glycerol, 1.6 mL 10% (w/v) SDS, 0.4mL β-mercaptoethanol, 0.05% (w/v) Bromophenol blue.

Running buffer (10x), 1 L

30.3 g Tris Base, 144 g Glycine, 10 g SDS, dissolved in 1 L distilled water.

Transfer buffer (10x), 1 L

30.3 g Tris Base, 144 g Glycine, dissolved in 1 L distilled water.

De-staining buffer

40% methanol, 10% acetic acid, 50% water

Equilibration buffer

40% methanol, 10% acetic acid, 3% glycerol, 47% water

PLP fixative

Lysine solution

0.2 M lysine monohydrochloride (3.65g/100mL) added to an equal volume of 0.1M disodium hydrogen orthophosphate (1.41g/100mL). Adjusted to pH 7.4, stored at 4°C.

4% Paraformaldehyde

Paraformaldehyde dissolved in distilled water at 4 g/100 mL, with stirring at 60°C in a fume hood. The solution was cleared by the addition of a few drops of 1M NaOH, adjusted to pH 7.4, and stored at 4°C.

Immediately prior to use, 1 volume of 4% paraformaldehyde was added to 3 volumes of lysine stock solution, and sodium metaperiodate (0.214g/100mL (10mM) was added.

PCR

TAE buffer:

2 M Tris-HCl, 50 mM EDTA-Na_2, 1 mM glacial acetic acid

References

Abbate, M., Zoja, C., Remuzzi, G., 2006. How does proteinuria cause progressive renal damage? J Am Soc Nephrol 17, 2974–84.

Alexopoulos, E., Seron, D., Hartley, R.B., Nolasco, F., Cameron, J.S., 1989. The role of interstitial infiltrates in IgA nephropathy: a study with monoclonal antibodies. Nephrol Dial Transplant 4, 187–95.

Allen, A.C., Harper, S.J., Feehally, J., 1995. Galactosylation of N- and O-linked carbohydrate moieties of IgA1 and IgG in IgA nephropathy. Clin Exp Immunol 100, 470–4.

Allen, A.C., 1999. Methodological approaches to the analysis of IgA1 O-glycosylation in IgA nephropathy. J Nephrol 12, 76–84.

Allen, A.C., Bailey, E.M., Barratt, J., Buck, K.S., Feehally, J., 1999. Analysis of IgA1 O-glycans in IgA nephropathy by fluorophore-assisted carbohydrate electrophoresis. J Am Soc Nephrol 10, 1763–71.

Allen, A.C., Bailey, E.M., Brenchley, P.E., Buck, K.S., Barratt, J., Feehally, J., 2001. Mesangial IgA1 in IgA nephropathy exhibits aberrant O-glycosylation: observations in three patients. Kidney Int 60, 969–73.

Almogren, A., Senior, B.W., Kerr, M.A., 2007. A comparison of the binding of secretory component to immunoglobulin A (IgA) in human colostral S-IgA1 and S-IgA2. Immunology 120, 273–280.

Almogren, A., Kerr, M.A., 2008. Irreversible aggregation of the Fc fragment derived from polymeric but not monomeric serum IgA1--implications in IgA-mediated disease. Mol Immunol 45, 87–94.

Amore, A., Coppo, R., Roccatello, D., Piccoli, G., Mazzucco, G., Gomez-Chiarri, M., Lamm, M.E., Emancipator, S.N., 1994. Experimental IgA nephropathy secondary to hepatocellular injury induced by dietary deficiencies and heavy alcohol intake. Lab Invest 70, 68–77.

André, C., Berthoux, F.C., André, F., Gillon, J., Genin, C., Sabatier, J.C., 1980. Prevalence of IgA2 deposits in IgA nephropathies: a clue to their pathogenesis. N Engl J Med 303, 1343–6.

Apodaca, G., Katz, L.A., Mostov, K.E., 1994. Receptor-mediated transcytosis of IgA in MDCK cells is via apical recycling endosomes. J Cell Biol 125, 67–86.

Arnold, J.N., Wormald, M.R., Sim, R.B., Rudd, P.M., Dwek, R.A., 2007. The impact of glycosylation on the biological function and structure of human immunoglobulins. Annu Rev Immunol 25, 21–50.

Arrizabalaga, P., Solé, M., Quintó, I.L., Ascaso, C., 1997. Intercellular adhesion molecule-1 mediated interactions and leucocyte infiltration in IgA nephropathy. Nephrol Dial Transplant 12, 2258–62.

Baines, R.J., Brunskill, N.J., 2011. Tubular toxicity of proteinuria. Nat Rev 7, 177–180.

Barratt, J., Bailey, E.M., Buck, K.S., Mailley, J., Moayyedi, P., Feehally, J., Turney, J.H., Crabtree, J.E., Allen, A.C., 1999. Exaggerated systemic antibody response to mucosal Helicobacter pylori infection in IgA nephropathy. Am J Kidney Dis 33, 1049–57.

Barratt, J., Greer, M.R., Pawluczyk, I.Z., Allen, A.C., Bailey, E.M., Buck, K.S., Feehally, J., 2000. Identification of a novel Fcalpha receptor expressed by human mesangial cells. Kidney Int 57, 1936–48.

Barratt, J., Smith, A.C., Feehally, J., 2007. The pathogenic role of IgA1 O-linked glycosylation in the pathogenesis of IgA nephropathy. Nephrology (Carlton) 12, 275–84.

Barratt, J., Harris, K., Topham, P. (Eds.), 2008. Oxford Desk Reference: Nephrology. Oxford University Press, pp. 100–105.

Barratt, J., Eitner, F., Feehally, J., Floege, J., 2009. Immune complex formation in IgA nephropathy: a case of the “right” antibodies in the “wrong” place at the “wrong” time? Nephrol Dial Transplant 24, 3620–3.

Barratt, J., Feehally, J., 2011. Pathogenesis of IgA nephropathy, in: Glassock, R.J. (Ed.), UpToDate. Waltham, MA.

Barratt, J., Feehally, J., 2013. Clinical Presentation and Diagnosis of IgA Nephropathy, in: Glassock, R.J. (Ed.), UpToDate. Waltham, MA.

Basnayake, K., Stringer, S.J., Hutchison, C.A., Cockwell, P., 2011. The biology of immunoglobulin free light chains and kidney injury. Kidney Int 79, 1289–1301.

Bellur, S.S., Troyanov, S., Cook, H.T., Roberts, I.S.D., 2011. Immunostaining findings in IgA nephropathy: Correlation with histology and clinical outcome in the Oxford classification patient cohort. Nephrol Dial Transplant 26, 2533–2536.

Berger, J., Hinglais, N., 1968. [Intercapillary deposits of IgA-IgG]. J Urol Nephrol (Paris) 74, 694–5.

Berger, S.P., Roos, A., Daha, M.R., 2005. Complement and the kidney: What the nephrologist needs to know in 2006? Nephrol Dial Transplant 20, 2613–2619.

Berthelot, L., Papista, C., Maciel, T.T., Biarnes-Pelicot, M., Tissandie, E., Wang, P.H.M., Tamouza, H., Jamin, A., Bex-Coudrat, J., Gestin, A., Boumediene, A., Arcos-Fajardo, M., England, P., Pillebout, E., Walker, F., Daugas, E., Vrtosvnik, F., Flamant, M., Benhamou, M., Cogné, M., Moura, I.C., Monteiro, R.C., Cogne, M., Moura, I.C., Monteiro, R.C., 2012. Transglutaminase is essential for IgA nephropathy development acting through IgA receptors. J Exp Med 209, 793–806.

Berthoux, F., Suzuki, H., Thibaudin, L., Yanagawa, H., Maillard, N., Mariat, C., Tomino, Y., Julian, B.A., Novak, J., 2012. Autoantibodies Targeting Galactose-Deficient IgA1 Associate with Progression of IgA Nephropathy. J Am Soc Nephrol 23, 1579–1587.

Boor, P., Ostendorf, T., Floege, J., 2014. PDGF and the progression of renal disease. Nephrol Dial Transplant 29 Suppl 1, i45–i54.

Boyd, J.K., Barratt, J., 2010. Immune complex formation in IgA nephropathy: CD89 a “saint” or a “sinner”? Kidney Int 78, 1211–3.

Boyd, J.K., Cheung, C.K., Molyneux, K., Feehally, J., Barratt, J., 2012. An update on the pathogenesis and treatment of IgA nephropathy. Kidney Int 81, 833–43.

Bradford, M.M., 1976. A rapid and sensitive method for the quantitation of microgram quantities of protein utilizing the principle of protein-dye binding. Anal Biochem 72, 248–254.

Bumgardner, G.L., Amend, W.C., Ascher, N.L., Vincenti, F.G., 1998. Single-center long-term results of renal transplantation for IgA nephropathy. Transplantation 65, 1053–1060.

Camilla, R., Suzuki, H., Daprà, V., Loiacono, E., Peruzzi, L., Amore, A., Ghiggeri, G.M., Mazzucco, G., Scolari, F., Gharavi, A.G., Appel, G.B., Troyanov, S., Novak, J., Julian, B.A., Coppo, R., 2011. Oxidative stress and galactose-deficient IgA1 as markers of progression in IgA nephropathy. Clin J Am Soc Nephrol 6, 1903–1911.

Campos-Bilderback, S.B., Desiree, M.D., Sandoval, R.M., Wean, S.E., Molitoris, B.A., 2013. Mechanisms of Proteinuria in a Chronic Kidney Disease (CKD) Model following Ischemic Injury [Abstract]. J Am Soc Nephrol 24, 420A.

Cattran, D.C., Coppo, R., Cook, H.T., Feehally, J., Roberts, I.S.D., Troyanov, S., Alpers, C.E., Amore, A., Barratt, J., Berthoux, F., Bonsib, S., Bruijn, J.A., D'Agati, V., D'Amico, G., Emancipator, S., Emma, F., Ferrario, F., Fervenza, F.C., Florquin, S., Fogo, A., Geddes, C.C., Groene, H.-J., Haas, M., Herzenberg, A.M., Hill, P.A., Hogg, R.J., Hsu, S.I., Jennette, J.C., Joh, K., Julian, B.A., Kawamura, T., Lai, F.M., Leung, C.B., Li, L.-S., Li, P.K.T., Liu, Z.-H., Mackinnon, B., Mezzano, S., Schena, F.P., Tomino, Y., Walker, P.D., Wang, H., Weening, J.J., Yoshikawa, N., Zhang, H., 2009. The Oxford classification of IgA nephropathy: rationale, clinicopathological correlations, and classification. Kidney Int 76, 534–545.

Chan, L.Y.Y., Leung, J.C.K., Tsang, A.W.L., Tang, S.C.W., Lai, K.N., 2005. Activation of tubular epithelial cells by mesangial-derived TNF-alpha: glomerulotubular communication in IgA nephropathy. Kidney Int 67, 602–12.

Chapter 10: Immunoglobulin A nephropathy, 2012. Kidney Int Suppl 2, 209–217.

Chintalacharuvu, K.R., Raines, M., Morrison, S.L., 1994. Divergence of human alpha-chain constant region gene sequences. A novel recombinant alpha 2 gene. J Immunol 152, 5299–304.

Chintalacharuvu, S.R., Emancipator, S.N., 1997. The glycosylation of IgA produced by murine B cells is altered by Th2 cytokines. J Immunol 159, 2327–33.

Conley, M.E., Cooper, M.D., Michael, A.F., 1980. Selective deposition of immunoglobulin A1 in immunoglobulin A nephropathy, anaphylactoid purpura nephritis, and systemic lupus erythematosus. J Clin Invest 66, 1432–1436.

Cook, H.T., 2013. Complement and kidney disease. Curr Opin Nephrol Hypertens 22, 295–301.

Coppo, R., Amore, A., Gianoglio, B., Reyna, A., Peruzzi, L., Roccatello, D., Alessi, D., Sena, L.M., 1993. Serum IgA and macromolecular IgA reacting with mesangial matrix components. Contrib Nephrol 104, 162–71.

Corridon, P.R., Rhodes, G.J., Leonard, E.C., Basile, D.P., Gattone, V.H., Bacallao, R.L., Atkinson, S.J., 2013. A method to facilitate and monitor expression of exogenous genes in the rat kidney using plasmid and viral vectors. Am J Physiol Renal Physiol 304, F1217–29.

Coulon, S., Dussiot, M., Grapton, D., Maciel, T.T., Wang, P.H.M., Callens, C., Tiwari, M.K., Agarwal, S., Fricot, A., Vandekerckhove, J., Tamouza, H., Zermati, Y., Ribeil, J.-A., Djedaini, K., Oruc, Z., Pascal, V., Courtois, G., Arnulf, B., Alyanakian, M.-A., Mayeux, P., Leanderson, T., Benhamou, M., Cogné, M., Monteiro, R.C., Hermine, O., Moura, I.C., 2011. Polymeric IgA1 controls erythroblast proliferation and accelerates erythropoiesis recovery in anemia. Nat Med 17, 1456–65.

Czerkinsky, C., Svennerholm, A.M., Quiding, M., Jonsson, R., Holmgren, J., 1991. Antibody-producing cells in peripheral blood and salivary glands after oral cholera vaccination of humans. Infect Immun 59, 996–1001.

D'Amico, G., 1987. The commonest glomerulonephritis in the world: IgA nephropathy. Q J Med 64, 709–27.

D'Amico, G., 2000. Natural history of idiopathic IgA nephropathy: role of clinical and histological prognostic factors. Am J Kidney Dis 36, 227–37.

D'Amico, G., 2004. Natural history of idiopathic IgA nephropathy and factors predictive of disease outcome. Semin Nephrol 24, 179–196.

Davin, J.C., Ten Berge, I.J., Weening, J.J., 2001. What is the difference between IgA nephropathy and Henoch-Schönlein purpura nephritis? Kidney Int 59, 823–34.

Degn, S.E., Jensen, L., Hansen, A.G., Duman, D., Tekin, M., Jensenius, J.C., Thiel, S., 2012. Mannan-binding lectin-associated serine protease (MASP)-1 is crucial for lectin pathway activation in human serum, whereas neither MASP-1 nor MASP-3 is required for alternative pathway function. J Immunol 189, 3957–69.

Delacroix, D.L., Hodgson, H.J.F., McPherson, A., 1982. Selective transport of polymeric immunoglobulin A in bile. Quantitiative relationships of monomeric and polymeric immunoglobulin A, immunoglobulin M, and other proteins in serum, bile, and saliva. J Clin Invest 70, 230–241.

Delacroix, D.L., Malburny, G.N., Vaerman, J.P., 1985. Hepatobiliary transport of plasma IgA in the mouse: contribution to clearance of intravascular IgA. Eur J Immunol 15, 893–9.

Denk, W., Strickler, J.H., Webb, W.W., 1990. Two-photon laser scanning fluorescence microscopy. Science 248, 73–6.

Devi, S., Li, A., Westhorpe, C.L. V, Lo, C.Y., Abeynaike, L.D., Snelgrove, S.L., Hall, P., Ooi, J.D., Sobey, C.G., Kitching, A.R., Hickey, M.J., 2012. Multiphoton imaging reveals a new leukocyte recruitment paradigm in the glomerulus. Nat Med 19, 107–112.

Dickson, L.E., Wagner, M.C., Sandoval, R.M., Molitoris, B.A., 2014. The proximal tubule and albuminuria: really! J Am Soc Nephrol 25, 443–53.

Dohi, K., Iwano, M., Muraguchi, A., Horii, Y., Hirayama, T., Ogawa, S., Shiiki, H., Hirano, T., Kishimoto, T., Ishikawa, H., 1991. The prognostic significance of urinary interleukin 6 in IgA nephropathy. Clin Nephrol 35, 1–5.

Dunn, K.W., Sandoval, R.M., Kelly, K.J., Dagher, P.C., Tanner, G.A., Atkinson, S.J., Bacallao, R.L., Molitoris, B.A., 2002. Functional studies of the kidney of living animals using multicolor two-photon microscopy. Am J Physiol Cell Physiol 283, C905–16.

Ebefors, K., Granqvist, A., Ingelsten, M., Mölne, J., Haraldsson, B., Nyström, J., 2011. Role of glomerular proteoglycans in IgA nephropathy. PLoS One 6, e18575.

Eddy, A.A., 2004. Proteinuria and interstitial injury. Nephrol Dial Transplant 19, 277–281.

Eitner, F., Boor, P., Floege, J., 2010. Models of IgA nephropathy. Drug Discov Today Dis Model 7, 21–26.

Eitner, F., Floege, J., 2012. In search of a better understanding of IgA nephropathy-associated hematuria. Kidney Int 82, 513–5.

Emancipator, S.N., Gallo, G.R., Lamm, M.E., 1983a. IgA-immune complex renal disease induced by mucosal immunization. Ann N Y Acad Sci 409, 171–6.

Emancipator, S.N., Gallo, G.R., Lamm, M.E., 1983b. Experimental IgA nephropathy induced by oral immunization. J Exp Med 157, 572–82.

Emancipator, S.N., Gallo, G.R., Razaboni, R., Lamm, M.E., 1983c. Experimental cholestasis promotes the deposition of glomerular IgA immune complexes. Am J Pathol 113, 19–26.

Emancipator, S.N., 2001. Animal models of IgA nephropathy. Curr Protoc Immunol Chapter 15, Unit 15.11.

Endo, M., Ohi, H., Ohsawa, I., Fujita, T., Matsushita, M., 1998. Glomerular deposition of mannose-binding lectin (MBL) indicates a novel mechanism of complement

activation in IgA nephropathy. Nephrol Dial Transplant 13, 1984–90.

Espinosa, M., Ortega, R., Gómez-Carrasco, J.M., López-Rubio, F., López-Andreu, M., López-Oliva, M.O., Aljama, P., 2009. Mesangial C4d deposition: A new prognostic factor in IgA nephropathy. Nephrol Dial Transplant 24, 886–891.

Fanger, M.W., Shen, L., Pugh, J., Bernier, G.M., 1980. Subpopulations of human peripheral granulocyes and monocytes express receptors for IgA. Proc Natl Acad Sci U S A 77, 3640–4.

Fassi, A., Sangalli, F., Maffi, R., Colombi, F., Mohamed, E.I., Brenner, B.M., Remuzzi, G., Remuzzi, A., 1998. Progressive glomerular injury in the MWF rat is predicted by inborn nephron deficit. J Am Soc Nephrol 9, 1399–406.

Fearon, D.T., Austen, K.F., 1975. Properdin: binding to C3b and stabilization of the C3b-dependent C3 convertase. J Exp Med 142, 856–63.

Feehally, J., Farrall, M., Boland, A., Gale, D.P., Gut, I., Heath, S., Kumar, A., Peden, J.F., Maxwell, P.H., Morris, D.L., Padmanabhan, S., Vyse, T.J., Zawadzka, A., Rees, A.J., Lathrop, M., Ratcliffe, P.J., 2010. HLA has strongest association with IgA nephropathy in genome-wide analysis. J Am Soc Nephrol 21, 1791–7.

Feehally, J., Floege, J., 2010. IgA Nephropathy and Henoch-Schönlein Nephritis, in: Floege, J., Johnson, R. J., Feehally, J. (Eds.), Comprehensive Clinical Nephrology. St. Louis: Elsevier, pp. 270–281.

Flanagan, J.G., Rabbitts, T.H., 1982. Arrangement of human immunoglobulin heavy chain constant region genes implies evolutionary duplication of a segment containing gamma, epsilon and alpha genes. Nature 300, 709–713.

Floege, J., 2011. The pathogenesis of IgA nephropathy: what is new and how does it change therapeutic approaches? Am J Kidney Dis 58, 992–1004.

Floege, J., Moura, I.C., Daha, M.R., 2014. New insights into the pathogenesis of IgA nephropathy. Semin Immunopathol 36, 431–42.

Frasca, G.M., Vangelista, A., Biagini, G., Bonomini, V., 1982. Immunological tubulo-interstitial deposits in IgA nephropathy. Kidney Int 22, 184–91.

Frasca, G.M., Soverini, L., Gharavi, A.G., Lifton, R.P., Canova, C., Preda, P., Vangelista, A., Stefoni, S., 2004. Thin basement membrane disease in patients with familial IgA nephropathy. J Nephrol 17, 778–785.

Fukuda, A., Sato, Y., Iwakiri, T., Komatsu, H., Kikuchi, M., Kitamura, K., Wiggins, R.C., Fujimoto, S., 2015. Urine podocyte mRNAs mark disease activity in IgA nephropathy. Nephrol Dial Transplant 30, 1140–50.

Gaarkeuken, H., Siezenga, M.A., Zuidwijk, K., van Kooten, C., Rabelink, T.J., Daha, M.R., Berger, S.P., 2008. Complement activation by tubular cells is mediated by properdin binding. Am J Physiol Renal Physiol 295, F1397–403.

Galla, J.H., Spotswood, M.F., Harrison, L.A., Mestecky, J., 1985. Urinary IgA in IgA nephropathy and Henoch-Schoenlein purpura. J Clin Immunol 5, 298–306.

Gesualdo, L., Lamm, M.E., Emancipator, S.N., 1990. Defective oral tolerance promotes nephritogenesis in experimental IgA nephropathy induced by oral immunization. J Immunol 145, 3684–91.

Gesualdo, L., Emancipator, S.N., Kesselheim, C., Lamm, M.E., 1992. Glomerular hemodynamics and eicosanoid synthesis in a rat model of IgA nephropathy. Kidney Int 42, 106–14.

Gharavi, A.G., Moldoveanu, Z., Wyatt, R.J., Barker, C. V, Woodford, S.Y., Lifton, R.P., Mestecky, J., Novak, J., Julian, B.A., 2008. Aberrant IgA1 glycosylation is

inherited in familial and sporadic IgA nephropathy. J Am Soc Nephrol 19, 1008–14.

Gharavi, A.G., Kiryluk, K., Choi, M., Li, Y., Hou, P., Xie, J., Sanna-Cherchi, S., Men, C.J., Julian, B.A., Wyatt, R.J., Novak, J., He, J.C., Wang, H., Lv, J., Zhu, L., Wang, W., Wang, Z., Yasuno, K., Gunel, M., Mane, S., Umlauf, S., Tikhonova, I., Beerman, I., Savoldi, S., Magistroni, R., Ghiggeri, G.M., Bodria, M., Lugani, F., Ravani, P., Ponticelli, C., Allegri, L., Boscutti, G., Frasca, G., Amore, A., Peruzzi, L., Coppo, R., Izzi, C., Viola, B.F., Prati, E., Salvadori, M., Mignani, R., Gesualdo, L., Bertinetto, F., Mesiano, P., Amoroso, A., Scolari, F., Chen, N., Zhang, H., Lifton, R.P., 2011. Genome-wide association study identifies susceptibility loci for IgA nephropathy. Nat Genet 43, 321–7.

Giannakakis, K., Feriozzi, S., Perez, M., Faraggiana, T., Muda, A.O., 2007. Aberrantly glycosylated IgA1 in glomerular immune deposits of IgA nephropathy. J Am Soc Nephrol 18, 3139–3146.

Gormly, A.A., Smith, P.S., Seymour, A.E., Clarkson, A.R., Woodroffe, A.J., 1981. IgA glomerular deposits in experimental cirrhosis. Am J Pathol 104, 50–4.

Gorter, A., Hiemstra, P.S., Leijh, P.C., van der Sluys, M.E., van den Barselaar, M.T., van Es, L.A., Daha, M.R., 1987. IgA- and secretory IgA-opsonized S. aureus induce a respiratory burst and phagocytosis by polymorphonuclear leucocytes. Immunology 61, 303–9.

Gstraunthaler, G., Seppi, T., Pfaller, W., 1999. Impact of culture conditions, culture media volumes, and glucose content on metabolic properties of renal epithelial cell cultures. Are renal cells in tissue culture hypoxic? Cell Physiol Biochem 9, 150–72.

Gunness, P., Aleksa, K., Kosuge, K., Ito, S., Koren, G., 2010. Comparison of the novel HK-2 human renal proximal tubular cell line with the standard LLC-PK1 cell line in studying drug-induced nephrotoxicity. Can J Physiol Pharmacol 88, 448–55.

Hackl, M.J., Burford, J.L., Villanueva, K., Lam, L., Suszták, K., Schermer, B., Benzing, T., Peti-Peterdi, J., 2013. Tracking the fate of glomerular epithelial cells in vivo using serial multiphoton imaging in new mouse models with fluorescent lineage tags. Nat Med 19, 1661–1666.

Hall, A.M., Rhodes, G.J., Sandoval, R.M., Corridon, P.R., Molitoris, B.A., 2013. In vivo multiphoton imaging of mitochondrial structure and function during acute kidney injury. Kidney Int 83, 72–83.

Hall, Y.N., Fuentes, E.F., Chertow, G.M., Olson, J.L., 2004. Race/ethnicity and disease severity in IgA nephropathy. BMC Nephrol 5, 10.

Harada, K., Akai, Y., Kurumatani, N., Iwano, M., Saito, Y., 2002. Prognostic value of urinary interleukin 6 in patients with IgA nephropathy: an 8-year follow-up study. Nephron 92, 824–6.

Hashimoto, A., Suzuki, Y., Suzuki, H., Ohsawa, I., Brown, R., Hall, S., Tanaka, Y., Novak, J., Ohi, H., Tomino, Y., 2012. Determination of severity of murine IgA nephropathy by glomerular complement activation by aberrantly glycosylated IgA and immune complexes. Am J Pathol 181, 1338–47.

Haycock, G.B., 1992. The nephritis of Henoch-Schönlein purpura, in: Cameron, S., Davison, A., Grünfeld, J. (Eds.), Oxford Textbook of Clinical Nephrology. Oxford, pp. 595–612.

Herr, A.B., Ballister, E.R., Bjorkman, P.J., 2003. Insights into IgA-mediated immune responses from the crystal structures of human FcalphaRI and its complex with IgA1-Fc. Nature 423, 614–620.

Hiki, Y., Odani, H., Takahashi, M., Yasuda, Y., Nishimoto, A., Iwase, H., Shinzato, T., Kobayashi, Y., Maeda, K., 2001. Mass spectrometry proves under-O-glycosylation of glomerular IgA1 in IgA nephropathy. Kidney Int 59, 1077–1085.

Hisano, S., Matsushita, M., Fujita, T., Endo, Y., Takebayashi, S., 2001. Mesangial IgA2 deposits and lectin pathway-mediated complement activation in IgA glomerulonephritis. Am J Kidney Dis 38, 1082–8.

Holmdahl, R., Malissen, B., 2012. The need for littermate controls. Eur J Immunol 42, 45–7.

Huen, S.C., Huynh, L., Marlier, A., Lee, Y., Moeckel, G.W., Cantley, L.G., 2015. GM-CSF Promotes Macrophage Alternative Activation after Renal Ischemia/Reperfusion Injury. J Am Soc Nephrol 26, 1334–45.

Hui, G.K., Wright, D.W., Vennard, O.L., Rayner, L.E., Pang, M., Yeo, S.C., Gor, J., Molyneux, K., Barratt, J., Perkins, S.J., 2015. The solution structures of native and patient monomeric human IgA1 reveal asymmetric extended structures: implications for function and IgAN disease. Biochem J 471, 167–85.

Ip, W.K.E., Takahashi, K., Ezekowitz, R.A., Stuart, L.M., 2009. Mannose-binding lectin and innate immunity. Immunol Rev 230, 9–21.

Isaacs, K., Miller, F., Lane, B., 1981. Experimental model for IgA nephropathy. Clin Immunol Immunopathol 20, 419–26.

Izzi, C., Ravani, P., Torres, D., Prati, E., Viola, B.F., Guerini, S., Foramitti, M., Frascà, G., Amoroso, A., Ghiggeri, G.M., Schena, F.P., Scolari, F., 2006. IgA Nephropathy: The Presence of Familial Disease Does Not Confer an Increased Risk for Progression. Am J Kidney Dis 47, 761–769.

Izzi, C., Sanna-Cherchi, S., Prati, E., Belleri, R., Remedio, A., Tardanico, R., Foramitti, M., Guerini, S., Viola, B.F., Movilli, E., Beerman, I., Lifton, R., Leone, L., Gharavi, A., Scolari, F., 2006. Familial aggregation of primary glomerulonephritis in an Italian population isolate: Valtrompia study. Kidney Int 69, 1033–1040.

Jackson, G.D.F., Lemaitre-Coelho, I., Vaerman, J.P., Bazin, H., Beckers, A., 1978. Rapid disappearance from serum of intravenously injected rat myeloma IgA and its secretion into bile. Eur J Immunol 8, 123–126.

Jenkinson, S.E., Chung, G.W., van Loon, E., Bakar, N.S., Dalzell, A.M., Brown, C.D.A., 2012. The limitations of renal epithelial cell line HK-2 as a model of drug transporter expression and function in the proximal tubule. Pflugers Arch 464, 601–11.

Jennette, J.C., 2007. Heptinstall's Pathology of the Kidney, Volume 1. Lippincott Williams & Wilkins.

Johnson, R.J., Hurtado, A., Merszei, J., Rodriguez-Iturbe, B., Feng, L., 2003. Hypothesis: dysregulation of immunologic balance resulting from hygiene and socioeconomic factors may influence the epidemiology and cause of glomerulonephritis worldwide. Am J Kidney Dis 42, 575–81.

Johnston, P.A., Brown, J.S., Braumholtz, D.A., Davison, A.M., 1992. Clinico-pathological correlations and long-term follow-up of 253 United Kingdom patients with IgA nephropathy. A report from the MRC Glomerulonephritis Registry. Q J Med 84, 619–627.

Julian, B.A., Woodford, S.Y., Baehler, R.W., McMorrow, R.G., Wyatt, R.J., 1988. Familial clustering and immunogenetic aspects of IgA nephropathy. Am J Kidney Dis 12, 366–370.

Kadaoui, K.A., Corthésy, B., 2007. Secretory IgA mediates bacterial translocation to

dendritic cells in mouse Peyer's patches with restriction to mucosal compartment. J Immunol 179, 7751–7757.

Kerr, M.A., 1990. The structure and function of human IgA. Biochem J 271, 285–96.

Kiryluk, K., Julian, B.A., Wyatt, R.J., Scolari, F., Zhang, H., Novak, J., Gharavi, A.G., 2010. Genetic studies of IgA nephropathy: past, present, and future. Pediatr Nephrol 25, 2257–68.

Kiryluk, K., Moldoveanu, Z., Sanders, J.T., Eison, T.M., Suzuki, H., Julian, B.A., Novak, J., Gharavi, A.G., Wyatt, R.J., 2011. Aberrant glycosylation of IgA1 is inherited in both pediatric IgA nephropathy and Henoch-Schönlein purpura nephritis. Kidney Int 80, 79–87.

Kiryluk, K., Li, Y., Sanna-Cherchi, S., Rohanizadegan, M., Suzuki, H., Eitner, F., Snyder, H.J., Choi, M., Hou, P., Scolari, F., Izzi, C., Gigante, M., Gesualdo, L., Savoldi, S., Amoroso, A., Cusi, D., Zamboli, P., Julian, B.A., Novak, J., Wyatt, R.J., Mucha, K., Perola, M., Kristiansson, K., Viktorin, A., Magnusson, P.K., Thorleifsson, G., Thorsteinsdottir, U., Stefansson, K., Boland, A., Metzger, M., Thibaudin, L., Wanner, C., Jager, K.J., Goto, S., Maixnerova, D., Karnib, H.H., Nagy, J., Panzer, U., Xie, J., Chen, N., Tesar, V., Narita, I., Berthoux, F., Floege, J., Stengel, B., Zhang, H., Lifton, R.P., Gharavi, A.G., 2012. Geographic differences in genetic susceptibility to IgA nephropathy: GWAS replication study and geospatial risk analysis. PLoS Genet 8, e1002765.

Kiryluk, K., Li, Y., Scolari, F., Sanna-Cherchi, S., Choi, M., Verbitsky, M., Fasel, D., Lata, S., Prakash, S., Shapiro, S., Fischman, C., Snyder, H.J., Appel, G., Izzi, C., Viola, B.F., Dallera, N., Del Vecchio, L., Barlassina, C., Salvi, E., Bertinetto, F.E., Amoroso, A., Savoldi, S., Rocchietti, M., Amore, A., Peruzzi, L., Coppo, R., Salvadori, M., Ravani, P., Magistroni, R., Ghiggeri, G.M., Caridi, G., Bodria, M., Lugani, F., Allegri, L., Delsante, M., Maiorana, M., Magnano, A., Frasca, G., Boer, E., Boscutti, G., Ponticelli, C., Mignani, R., Marcantoni, C., Di Landro, D., Santoro, D., Pani, A., Polci, R., Feriozzi, S., Chicca, S., Galliani, M., Gigante, M., Gesualdo, L., Zamboli, P., Battaglia, G.G., Garozzo, M., Maixnerová, D., Tesar, V., Eitner, F., Rauen, T., Floege, J., Kovacs, T., Nagy, J., Mucha, K., Pączek, L., Zaniew, M., Mizerska-Wasiak, M., Roszkowska-Blaim, M., Pawlaczyk, K., Gale, D., Barratt, J., Thibaudin, L., Berthoux, F., Canaud, G., Boland, A., Metzger, M., Panzer, U., Suzuki, H., Goto, S., Narita, I., Caliskan, Y., Xie, J., Hou, P., Chen, N., Zhang, H., Wyatt, R.J., Novak, J., Julian, B. A., Feehally, J., Stengel, B., Cusi, D., Lifton, R.P., Gharavi, A.G., 2014. Discovery of new risk loci for IgA nephropathy implicates genes involved in immunity against intestinal pathogens. Nat Genet 46, 1187–1196.

Kiryluk, K., Novak, J., 2014. The genetics and immunobiology of IgA nephropathy. J Clin Invest 124, 2325–2332.

Kitamura, M., Sütö, T.S., 1997. TGF-β and glomerulonephritis: Anti-inflammatory versus prosclerotic actions. Nephrol Dial Transplant 12, 669–679.

Koivuviita, N., Tertti, R., Heiro, M., Metsarinne, K., 2009. A case report: a patient with IgA nephropathy and coeliac disease. Complete clinical remission following gluten-free diet. Clin Kidney J 2, 161–163.

Korbet, S.M., Genchi, R.M., Borok, R.Z., Schwartz, M.M., 1996. The racial prevalence of glomerular lesions in nephrotic adults. Am J Kidney Dis 27, 647–651.

Kuemmerle, N.B., Chan, W., Krieg, R.J., Norkus, E.P., Trachtman, H., Chan, J.C., 1998. Effects of fish oil and alpha-tocopherol in immunoglobulin A nephropathy in the rat. Pediatr Res 43, 791–7.

Kuemmerle, N.B., Krieg, R.J., Chan, W., Trachtman, H., Norkus, E.P., Chan, J.C.,

1999. Influence of alpha-tocopherol over the time course of experimental IgA nephropathy. Pediatr Nephrol 13, 108–12.

Lai, K.N., Lai, F.M., Ho, C.P., Chan, K.W., 1986. Corticosteroid therapy in IgA nephropathy with nephrotic syndrome: a long-term controlled trial. Clin Nephrol 26, 174–80.

Lai, K.N., Leung, J.C., Li, P.K., Lui, S.F., 1991. Cytokine production by peripheral blood mononuclear cells in IgA nephropathy. Clin Exp Immunol 85, 240–5.

Lai, K.N., Ho, R.T., Lai, C.K., Chan, C.H., Li, P.K., 1994. Increase of both circulating Th1 and Th2 T lymphocyte subsets in IgA nephropathy. Clin Exp Immunol 96, 116–21.

Lai, K.N., 2003. Polymeric IgA1 from Patients with IgA Nephropathy Upregulates Transforming Growth Factor- Synthesis and Signal Transduction in Human Mesangial Cells via the Renin-Angiotensin System. J Am Soc Nephrol 14, 3127–3137.

Lai, K.N., Chan, L.Y.Y., Leung, J.C.K., 2005. Mechanisms of tubulointerstitial injury in IgA nephropathy. Kidney Int Suppl 67, S110–S115.

Lai, K.N., Leung, J.C.K., Chan, L.Y.Y., Saleem, M.A., Mathieson, P.W., Lai, F.M., Tang, S.C.W., 2008. Activation of podocytes by mesangial-derived TNF-alpha: glomerulo-podocytic communication in IgA nephropathy. Am J Physiol Renal Physiol 294, F945–F955.

Lai, K.N., Leung, J.C.K., Chan, L.Y.Y., Saleem, M.A., Mathieson, P.W., Tam, K.Y., Xiao, J., Lai, F.M., Tang, S.C.W., 2009. Podocyte injury induced by mesangial-derived cytokines in IgA nephropathy. Nephrol Dial Transplant 24, 62–72.

Lai, K.N., Chan, L.Y., Guo, H., Tang, S.C., Leung, J.C., 2011. Additive effect of PPAR-gamma agonist and ARB in treatment of experimental IgA nephropathy. Pediatr Nephrol 26, 257–266.

Lai, K.N., 2012. Pathogenesis of IgA nephropathy. Nat Rev Nephrol 8, 275–83.

Lau, K.K., Wyatt, R.J., Moldoveanu, Z., Tomana, M., Julian, B.A., Hogg, R.J., Lee, J.Y., Huang, W.Q., Mestecky, J., Novak, J., 2007. Serum levels of galactose-deficient IgA in children with IgA nephropathy and Henoch-Schönlein purpura. Pediatr Nephrol 22, 2067–2072.

Launay, P., Grossetête, B., Arcos-Fajardo, M., Gaudin, E., Torres, S.P., Beaudoin, L., Patey-Mariaud de Serre, N., Lehuen, A., Monteiro, R.C., 2000. Fcalpha receptor (CD89) mediates the development of immunoglobulin A (IgA) nephropathy (Berger's disease). Evidence for pathogenic soluble receptor-IgA complexes in patients and CD89 transgenic mice. J Exp Med 191, 1999–2009.

Lemley, K. V., Lafayette, R.A., Safai, M., Derby, G., Blouch, K., Squarer, A., Myers, B.D., 2002. Podocytopenia and disease severity in IgA nephropathy. Kidney Int 61, 1475–1485.

Leung, J.C., Tsang, A.W., Chan, D.T., Lai, K.N., 2000. Absence of CD89, polymeric immunoglobulin receptor, and asialoglycoprotein receptor on human mesangial cells. J Am Soc Nephrol 11, 241–9.

Leung, J.C.K., Tang, S.C.W., Chan, L.Y.Y., Tsang, A.W.L., Lan, H.Y., Lai, K.N., 2003. Polymeric IgA increases the synthesis of macrophage migration inhibitory factor by human mesangial cells in IgA nephropathy. Nephrol Dial Transplant 18, 36–45.

Leung, J.C.K., Tang, S.C.W., Chan, L.Y.Y., Chan, W.L., Lai, K.N., 2008. Synthesis of TNF-alpha by mesangial cells cultured with polymeric anionic IgA--role of MAPK and NF-kappaB. Nephrol Dial Transplant 23, 72–81.

Levy, M., 1989. [Familial cases of Berger's disease or of Berger's disease and rheumatoid purpura. Cooperative study of the Société Française de Néphrologie]. Néphrologie 10, 175–82.

Lim, C.S., Zheng, S., Kim, Y.S., Ahn, C., Han, J.S., Kim, S., Lee, J.S., Chae, D.W., Koo, J.R., Chun, R.W., Noh, J.W., 2001. Th1/Th2 predominance and proinflammatory cytokines determine the clinicopathological severity of IgA nephropathy. Nephrol Dial Transpl 16, 269–275.

Liu, L.L., Jiang, Y., Wang, L.N., Liu, N., 2012. Urinary mannose-binding lectin is a biomarker for predicting the progression of immunoglobulin (Ig)A nephropathy. Clin Exp Immunol 169, 148–155.

Loeffler, I., Wolf, G., 2014. Transforming growth factor-β and the progression of renal disease. Nephrol Dial Transplant 29 Suppl 1, i37–i45.

Maillard, N., Wyatt, R.J., Julian, B. a., Kiryluk, K., Gharavi, a., Fremeaux-Bacchi, V., Novak, J., 2015. Current Understanding of the Role of Complement in IgA Nephropathy. J Am Soc Nephrol 1–10.

Masaki, T., Chow, F., Nikolic-Paterson, D.J., Atkins, R.C., Tesch, G.H., 2003. Heterogeneity of antigen expression explains controversy over glomerular macrophage accumulation in mouse glomerulonephritis. Nephrol Dial Transplant 18, 178–181.

Matousovic, K., Novak, J., Yanagihara, T., Tomana, M., Moldoveanu, Z., Kulhavy, R., Julian, B.A., Konecny, K., Mestecky, J., 2006. IgA-containing immune complexes in the urine of IgA nephropathy patients. Nephrol Dial Transplant 21, 2478–2484.

Matsuda, M., Shikata, K., Wada, J., Sugimoto, H., Shikata, Y., Kawasaki, T., Makino, H., 1998. Deposition of mannan binding protein and mannan binding protein-mediated complement activation in the glomeruli of patients with IgA nephropathy. Nephron 80, 408–413.

Maxwell, P.H., Wang, Y., 2009. Genetic contribution to IgA nephropathy, in: Lai, K.N. (Ed.), Recent Advances in IgA Nephropathy. World Scientific, pp. 21–36.

McQuarrie, E.P., MacKinnon, B., Young, B., Yeoman, L., Stewart, G., Fleming, S., Robertson, S., Simpson, K., Fox, J., Geddes, C.C., 2009. Centre variation in incidence, indication and diagnosis of adult native renal biopsy in Scotland. Nephrol Dial Transplant 24, 1524–1528.

McQuarrie, E.P., Mackinnon, B., McNeice, V., Fox, J.G., Geddes, C.C., 2014. The incidence of biopsy-proven IgA nephropathy is associated with multiple socioeconomic deprivation. Kidney Int 85, 198–203.

Meadow, S.R., Scott, D.G., 1985. Berger disease: Henoch-Schönlein syndrome without the rash. J Pediatr 106, 27–32.

Mestecky, J., Raska, M., Julian, B.A., Gharavi, A.G., Renfrow, M.B., Moldoveanu, Z., Novak, L., Matousovic, K., Novak, J., 2013. IgA nephropathy: molecular mechanisms of the disease. Annu Rev Pathol 8, 217–40.

Mills, C.D., Kincaid, K., Alt, J.M., Heilman, M.J., Hill, A.M., 2000. M-1/M-2 macrophages and the Th1/Th2 paradigm. J Immunol 164, 6166–73.

Miyawaki, S., Muso, E., Takeuchi, E., Matsushima, H., Shibata, Y., Sasayama, S., Yoshida, H., 1997. Selective breeding for high serum IgA levels from noninbred ddY mice: isolation of a strain with an early onset of glomerular IgA deposition. Nephron 76, 201–7.

Miyazaki, R., Kuroda, M., Akiyama, T., Otani, I., Tofuku, Y., Takeda, R., 1984. Glomerular deposition and serum levels of complement control proteins in patients

with IgA nephropathy. Clin Nephrol 21, 335–40.

Moldoveanu, Z., Wyatt, R.J., Lee, J.Y., Tomana, M., Julian, B.A., Mestecky, J., Huang, W.-Q., Anreddy, S.R., Hall, S., Hastings, M.C., Lau, K.K., Cook, W.J., Novak, J., 2007. Patients with IgA nephropathy have increased serum galactose-deficient IgA1 levels. Kidney Int 71, 1148–54.

Molitoris, B.A., Sandoval, R.M., 2005. Intravital multiphoton microscopy of dynamic renal processes. Am J Physiol Renal Physiol 288, F1084–9.

Monteiro, R.C., Halbwachs-Mecarelli, L., Roque-Barreira, M.C., Noel, L.H., Berger, J., Lesavre, P., 1985. Charge and size of mesangial IgA in IgA nephropathy. Kidney Int 28, 666–71.

Monteiro, R.C., Van De Winkel, J.G.J., 2003. IgA Fc receptors. Annu Rev Immunol 21, 177–204.

Morton, H.C., van den Herik-Oudijk, I.E., Vossebeld, P., Snijders, A., Verhoeven, A.J., Capel, P.J., van de Winkel, J.G., 1995. Functional association between the human myeloid immunoglobulin A Fc receptor (CD89) and FcR gamma chain. Molecular basis for CD89/FcR gamma chain association. J Biol Chem 270, 29781–7.

Motomura, W., Yoshizaki, T., Ohtani, K., Okumura, T., Fukuda, M., Fukuzawa, J., Mori, K., Jang, S.-J., Nomura, N., Yoshida, I., Suzuki, Y., Kohgo, Y., Wakamiya, N., 2008. Immunolocalization of a novel collectin CL-K1 in murine tissues. J Histochem Cytochem 56, 243–52.

Motoyoshi, Y., Matsusaka, T., Saito, A., Pastan, I., Willnow, T.E., Mizutani, S., Ichikawa, I., 2008. Megalin contributes to the early injury of proximal tubule cells during nonselective proteinuria. Kidney Int 74, 1262–1269.

Moura, I.C., Centelles, M.N., Arcos-Fajardo, M., Malheiros, D.M., Collawn, J.F., Cooper, M.D., Monteiro, R.C., 2001. Identification of the transferrin receptor as a novel immunoglobulin (Ig)A1 receptor and its enhanced expression on mesangial cells in IgA nephropathy. J Exp Med 194, 417–25.

Moura, I.C., Arcos-Fajardo, M., Sadaka, C., Leroy, V., Benhamou, M., Novak, J., Vrtovsnik, F., Haddad, E., Chintalacharuvu, K.R., Monteiro, R.C., 2004. Glycosylation and size of IgA1 are essential for interaction with mesangial transferrin receptor in IgA nephropathy. J Am Soc Nephrol 15, 622–34.

Moura, I.C., Arcos-Fajardo, M., Gdoura, A., Leroy, V., Sadaka, C., Mahlaoui, N., Lepelletier, Y., Vrtovsnik, F., Haddad, E., Benhamou, M., Monteiro, R.C., 2005. Engagement of transferrin receptor by polymeric IgA1: evidence for a positive feedback loop involving increased receptor expression and mesangial cell proliferation in IgA nephropathy. J Am Soc Nephrol 16, 2667–76.

Novak, J., Tomana, M., Matousovic, K., Brown, R., Hall, S., Novak, L., Julian, B. A., Wyatt, R.J., Mestecky, J., 2005. IgA1-containing immune complexes in IgA nephropathy differentially affect proliferation of mesangial cells. Kidney Int 67, 504–13.

Novak, J., Raskova Kafkova, L., Suzuki, H., Tomana, M., Matousovic, K., Brown, R., Hall, S., Sanders, J.T., Eison, T.M., Moldoveanu, Z., Novak, L., Novak, Z., Mayne, R., Julian, B. A., Mestecky, J., Wyatt, R.J., 2011. IgA1 immune complexes from pediatric patients with IgA nephropathy activate cultured human mesangial cells. Nephrol Dial Transplant 26, 3451–7.

Onda, K., Ohi, H., Tamano, M., Ohsawa, I., Wakabayashi, M., Horikoshi, S., Fujita, T., Tomino, Y., 2007. Hypercomplementemia in adult patients with IgA nephropathy. J Clin Lab Anal 21, 77–84.

Onda, K., Ohsawa, I., Ohi, H., Tamano, M., Mano, S., Wakabayashi, M., Toki, A., Horikoshi, S., Fujita, T., Tomino, Y., 2011. Excretion of complement proteins and its activation marker C5b-9 in IgA nephropathy in relation to renal function. BMC Nephrol 12, 64.

Oortwijn, B.D., Roos, A., Royle, L., van Gijlswijk-Janssen, D.J., Faber-Krol, M.C., Eijgenraam, J.W., Dwek, R.A., Daha, M.R., Rudd, P.M., van Kooten, C., 2006. Differential glycosylation of polymeric and monomeric IgA: a possible role in glomerular inflammation in IgA nephropathy. J Am Soc Nephrol 17, 3529–3539.

Pabst, O., 2012. New concepts in the generation and functions of IgA. Nat Rev Immunol 12, 821–32.

Papista, C., Lechner, S., Ben Mkaddem, S., LeStang, M.-B., Abbad, L., Bex-Coudrat, J., Pillebout, E., Chemouny, J.M., Jablonski, M., Flamant, M., Daugas, E., Vrtovsnik, F., Yiangou, M., Berthelot, L., Monteiro, R.C., 2015. Gluten exacerbates IgA nephropathy in humanized mice through gliadin–CD89 interaction. Kidney Int 88, 276–285.

Pasquier, B., Launay, P., Kanamaru, Y., Moura, I.C., Pfirsch, S., Ruffié, C., Hénin, D., Benhamou, M., Pretolani, M., Blank, U., Monteiro, R.C., 2005. Identification of FcalphaRI as an inhibitory receptor that controls inflammation: dual role of FcRgamma ITAM. Immunity 22, 31–42.

Pecoits-Filho, R., Lindholm, B., Axelsson, J., Stenvinkel, P., 2003. Update on interleukin-6 and its role in chronic renal failure. Nephrol Dial Transplant 18, 1042–1045.

Peti-Peterdi, J., Sipos, A., 2010. A high-powered view of the filtration barrier. J Am Soc Nephrol 21, 1835–41.

Rambausek, M., Hartz, G., Waldherr, R., Andrassy, K., Ritz, E., 1987. Familial glomerulonephritis. Pediatr Nephrol 1, 416–418.

Ravelli, A., Carnevale-Maffe, G., Ruperto, N., Ascari, E., Martini, A., 1996. IgA nephropathy and Henoch-Schonlein syndrome occurring in the same patient. Nephron 72, 111–12.

Reich, H.N., Troyanov, S., Scholey, J.W., Cattran, D.C., 2007. Remission of proteinuria improves prognosis in IgA nephropathy. J Am Soc Nephrol 18, 3177–83.

Remuzzi, A., Puntorieri, S., Mazzoleni, A., Remuzzi, G., 1988. Sex related differences in glomerular ultrafiltration and proteinuria in Munich-Wistar rats. Kidney Int 34, 481–6.

Rifai, A., Small, P.A., Teague, P.O., Ayoub, E.M., 1979. Experimental IgA nephropathy. J Exp Med 150, 1161–73.

Roberts, I.S.D., 2014. Pathology of IgA nephropathy. Nat Rev Nephrol 10, 445–54.

Robinson, J.K., Blanchard, T.G., Levine, A.D., Emancipator, S.N., Lamm, M.E., 2001. A mucosal IgA-mediated excretory immune system in vivo. J Immunol 166, 3688–3692.

Roos, A., Bouwman, L.H., van Gijlswijk-Janssen, D.J., Faber-Krol, M.C., Stahl, G.L., Daha, M.R., 2001. Human IgA activates the complement system via the mannan-binding lectin pathway. J Immunol 167, 2861–8.

Roos, A., Rastaldi, M.P., Calvaresi, N., Oortwijn, B.D., Schlagwein, N., van Gijlswijk-Janssen, D.J., Stahl, G.L., Matsushita, M., Fujita, T., van Kooten, C., Daha, M.R., 2006. Glomerular activation of the lectin pathway of complement in IgA nephropathy is associated with more severe renal disease. J Am Soc Nephrol 17, 1724–34.

Russo, L.M., Sandoval, R.M., McKee, M., Osicka, T.M., Collins, A.B., Brown, D., Molitoris, B.A., Comper, W.D., 2007. The normal kidney filters nephrotic levels of albumin retrieved by proximal tubule cells: retrieval is disrupted in nephrotic states. Kidney Int 71, 504–13.

Ryan, M.J., Johnson, G., Kirk, J., Fuerstenberg, S.M., Zager, R.A., Torok-Storb, B., 1994. HK-2: an immortalized proximal tubule epithelial cell line from normal adult human kidney. Kidney Int 45, 48–57.

Sabadini, E., Castiglione, A., Colasanti, G., Ferrario, F., Civardi, R., Fellin, G., D'Amico, G., 1988. Characterization of interstitial infiltrating cells in Berger's disease. Am J Kidney Dis 12, 307–15.

Sakamoto, N., Shibuya, K., Shimizu, Y., Yotsumoto, K., Miyabayashi, T., Sakano, S., Tsuji, T., Nakayama, E., Nakauchi, H., Shibuya, A., 2001. A novel Fc receptor for IgA and IgM is expressed on both hematopoietic and non-hematopoietic tissues. Eur J Immunol 31, 1310–6.

Sandoval, R.M., Molitoris, B.A., 2008. Quantifying endocytosis in vivo using intravital two-photon microscopy. Methods Mol Biol 440, 389–402.

Sandoval, R.M., Wagner, M.C., Patel, M., Campos-Bilderback, S.B., Rhodes, G.J., Wang, E., Wean, S.E., Clendenon, S.S., Molitoris, B.A., 2012. Multiple factors influence glomerular albumin permeability in rats. J Am Soc Nephrol 23, 447–57.

Sanfilippo, F., Croker, B.P., Bollinger, R.R., 1982. Fate of four cadaveric donor renal allografts with mesangial IgA deposits. Transplantation 33, 370–6.

Schaffer, F.M., Monteiro, R.C., Volanakis, J.E., Cooper, M.D., 1991. IgA deficiency. Immunodefic Rev 3, 15–44.

Schena, F.P., Scivittaro, V., Ranieri, E., 1993. IgA nephropathy: pros and cons for a familial disease. Contrib Nephrol 104, 36–45.

Schena, F.P., Cerullo, G., Rossini, M., Lanzilotta, S.G., D'Altri, C., Manno, C., 2002. Increased risk of end-stage renal disease in familial IgA nephropathy. J Am Soc Nephrol 13, 453–460.

Schmitt, R., 2012. Studies of the pathogenesis of IgA nephropathy and Henoch-Schönlein purpura , with special reference to Streptococcus pyogenes infections and complement. Lund University, Sweden.

Schulz, A., Hansch, J., Kuhn, K., Schlesener, M., Kossmehl, P., Nyengaard, J.R., Wendt, N., Huber, M., Kreutz, R., Hänsch, J., Kuhn, K., Schlesener, M., Kossmehl, P., Nyengaard, J.R., Wendt, N., Huber, M., Kreutz, R., 2008. Nephron deficit is not required for progressive proteinuria development in the Munich Wistar Fromter rat. Physiol Genomics 35, 30–35.

Schwaeble, W.J., Lynch, N.J., Clark, J.E., Marber, M., Samani, N.J., Ali, Y.M., Dudler, T., Parent, B., Lhotta, K., Wallis, R., Farrar, C.A., Sacks, S., Lee, H., Zhang, M., Iwaki, D., Takahashi, M., Fujita, T., Tedford, C.E., Stover, C.M., 2011. Targeting of mannan-binding lectin-associated serine protease-2 confers protection from myocardial and gastrointestinal ischemia/reperfusion injury. Proc Natl Acad Sci U S A 108, 7523–8.

Scivittaro, V., Gesualdo, L., Ranieri, E., Marfella, C., Schewn, S.A., Emancipator, S.N., Schena, F.P., 1994. Profiles of immunoregulatory cytokine production in vitro in patients with IgA nephropathy and their kindred. Clin Exp Immunol 96, 311–6.

Scolari, F., Amoroso, A., Savoldi, S., Mazzola, G., Prati, E., Valzorio, B., Viola, B.F., Nicola, B., Movilli, E., Sandrini, M., Campanini, M., Maiorca, R., 1999. Familial clustering of IgA nephropathy: further evidence in an Italian population. Am J

Kidney Dis 33, 857–865.

Sehic, A.M., Gaber, L.W., Roy, S., Miller, P.M., Kritchevsky, S.B., Wyatt, R.J., 1997. Increased recognition of IgA nephropathy in African-American children. Pediatr Nephrol 11, 435–437.

Sekine, H., Takahashi, M., Iwaki, D., Fujita, T., 2013. The role of MASP-1/3 in complement activation. Adv Exp Med Biol 735, 41–53.

Shibuya, A., Sakamoto, N., Shimizu, Y., Shibuya, K., Osawa, M., Hiroyama, T., Eyre, H.J., Sutherland, G.R., Endo, Y., Fujita, T., Miyabayashi, T., Sakano, S., Tsuji, T., Nakayama, E., Phillips, J.H., Lanier, L.L., Nakauchi, H., 2000. Fc alpha/mu receptor mediates endocytosis of IgM-coated microbes. Nat Immunol 1, 441–6.

Shimozato, S., Hiki, Y., Odani, H., Takahashi, K., Yamamoto, K., Sugiyama, S., 2008. Serum under-galactosylated IgA1 is increased in Japanese patients with IgA nephropathy. Nephrol Dial Transplant 23, 1931–1939.

Silva, F.G., Chander, P., Pirani, C.L., Hardy, M.A., 1982. Disappearance of glomerular mesangial IgA deposits after renal allograft transplantation. Transplantation 33, 241–6.

Sinniah, R., 1983. Occurrence of mesangial IgA and IgM deposits in a control necropsy population. J Clin Pathol 36, 276–279.

Smith, A.C., de Wolff, J.F., Molyneux, K., Feehally, J., Barratt, J., 2006a. O-glycosylation of serum IgD in IgA nephropathy. J Am Soc Nephrol 17, 1192–1199.

Smith, A.C., Molyneux, K., Feehally, J., Barratt, J., 2006b. O-glycosylation of serum IgA1 antibodies against mucosal and systemic antigens in IgA nephropathy. J Am Soc Nephrol 17, 3520–3528.

Stewart, J.H., McCredie, M.R.E., McDonald, S.P., 2004. Incidence of end-stage renal disease in overseas-born, compared with Australian-born, non-indigenous Australians. Nephrology 9, 247–252.

Stover, C.M., Lynch, N.J., Dahl, M.R., Hanson, S., Takahashi, M., Frankenberger, M., Ziegler-Heitbrock, L., Eperon, I., Thiel, S., Schwaeble, W.J., 2003. Murine serine proteases MASP-1 and MASP-3, components of the lectin pathway activation complex of complement, are encoded by a single structural gene. Genes Immun 4, 374–384.

Suzuki, H., Suzuki, Y., Aizawa, M., Yamanaka, T., Kihara, M., Pang, H., Horikoshi, S., Tomino, Y., 2007. Th1 polarization in murine IgA nephropathy directed by bone marrow-derived cells. Kidney Int 72, 319–27.

Suzuki, H., Moldoveanu, Z., Hall, S., Brown, R., Vu, H.L., Novak, L., Julian, B.A., Tomana, M., Wyatt, R.J., Edberg, J.C., Alarcón, G.S., Kimberly, R.P., Tomino, Y., Mestecky, J., Novak, J., 2008. IgA1-secreting cell lines from patients with IgA nephropathy produce aberrantly glycosylated IgA1. J Clin Invest 118, 629–39.

Suzuki, H., Fan, R., Zhang, Z., Brown, R., Hall, S., Julian, B.A., Chatham, W.W., Suzuki, Y., Wyatt, R.J., Moldoveanu, Z., Lee, J.Y., Robinson, J., Tomana, M., Tomino, Y., Mestecky, J., Novak, J., 2009. Aberrantly glycosylated IgA1 in IgA nephropathy patients is recognized by IgG antibodies with restricted heterogeneity. J Clin Invest 119, 1668–77.

Suzuki, H., Kiryluk, K., Novak, J., Moldoveanu, Z., Herr, A.B., Renfrow, M.B., Wyatt, R.J., Scolari, F., Mestecky, J., Gharavi, A.G., Julian, B.A., 2011. The pathophysiology of IgA nephropathy. J Am Soc Nephrol 22, 1795–803.

Suzuki, K., Honda, K., Tanabe, K., Toma, H., Nihei, H., Yamaguchi, Y., 2003. Incidence of latent mesangial IgA deposition in renal allograft donors in Japan.

Kidney Int 63, 2286–94.

Tachibana, K., Nakamura, S., Wang, H., Iwasaki, H., Tachibana, K., Maebara, K., Cheng, L., Hirabayashi, J., Narimatsu, H., 2006. Elucidation of binding specificity of Jacalin toward O-glycosylated peptides: quantitative analysis by frontal affinity chromatography. Glycobiology 16, 46–53.

Takahashi, K., Smith, A.D., Poulsen, K., Kilian, M., Julian, B.A., Mestecky, J., Novak, J., Renfrow, M.B., 2012. Naturally occurring structural isomers in serum IgA1 O -glycosylation. J Proteome Res 11, 692–702.

Tam, K.Y., Leung, J.C.K., Chan, L.Y.Y., Lam, M.F., Tang, S.C.W., Lai, K.N., 2009. Macromolecular IgA1 taken from patients with familial IgA nephropathy or their asymptomatic relatives have higher reactivity to mesangial cells in vitro. Kidney Int 75, 1330–9.

Tarelli, E., Smith, A.C., Hendry, B.M., Challacombe, S.J., Pouria, S., 2004. Human serum IgA1 is substituted with up to six O-glycans as shown by matrix assisted laser desorption ionisation time-of-flight mass spectrometry. Carbohydr Res 339, 2329–2335.

Thiel, S., 2007. Complement activating soluble pattern recognition molecules with collagen-like regions, mannan-binding lectin, ficolins and associated proteins. Mol Immunol 44, 3875–88.

Tomana, M., Matousovic, K., Julian, B.A., Radl, J., Konecny, K., Mestecky, J., 1997. Galactose-deficient IgA1 in sera of IgA nephropathy patients is present in complexes with IgG. Kidney Int 52, 509–16.

Tomana, M., Novak, J., Julian, B.A., Matousovic, K., Konecny, K., Mestecky, J., 1999. Circulating immune complexes in IgA nephropathy consist of IgA1 with galactose-deficient hinge region and antiglycan antibodies. J Clin Invest 104, 73–81.

Trachtman, H., Chan, J.C., Chan, W., Valderrama, E., Brandt, R., Wakely, P., Futterweit, S., Maesaka, J., Ma, C., 1996. Vitamin E ameliorates renal injury in an experimental model of immunoglobulin A nephropathy. Pediatr Res 40, 620–6.

Tumlin, J.A., Madaio, M.P., Hennigar, R., 2007. Idiopathic IgA nephropathy: pathogenesis, histopathology, and therapeutic options. Clin J Am Soc Nephrol 2, 1054–61.

Utsunomiya, Y., Koda, T., Kado, T., Okada, S., Hayashi, A., Kanzaki, S., Kasagi, T., Hayashibara, H., Okasora, T., 2003. Incidence of pediatric IgA nephropathy. Pediatr Nephrol 18, 511–515.

van der Boog, P.J.M., van Zandbergen, G., de Fijter, J.W., Klar-Mohamad, N., van Seggelen, A., Brandtzaeg, P., Daha, M.R., van Kooten, C., 2002. Fc alpha RI/CD89 circulates in human serum covalently linked to IgA in a polymeric state. J Immunol 168, 1252–8.

van der Boog, P.J.M., 2004. Injection of recombinant Fc RI/CD89 in mice does not induce mesangial IgA deposition. Nephrol Dial Transplant 19, 2729–2736.

van der Boog, P.J.M., van Kooten, C., de Fijter, J.W., Daha, M.R., 2005. Role of macromolecular IgA in IgA nephropathy. Kidney Int 67, 813–21.

van Zandbergen, G., Westerhuis, R., Mohamad, N.K., van De Winkel, J.G., Daha, M.R., van Kooten, C., 1999. Crosslinking of the human Fc receptor for IgA (FcalphaRI/CD89) triggers FcR gamma-chain-dependent shedding of soluble CD89. J Immunol 163, 5806–12.

Varis, J., Rantala, I., Pasternack, A., 1989. Immunofluorescence of immunoglobulins and complement in kidneys taken at necropsy. J Clin Pathol 42, 1211–1214.

Vuong, M.T., Hahn-Zoric, M., Lundberg, S., Gunnarsson, I., van Kooten, C., Wramner, L., Seddighzadeh, M., Fernström, A., Hanson, L.Å., Do, L.T., Jacobson, S.H., Padyukov, L., 2010. Association of soluble CD89 levels with disease progression but not susceptibility in IgA nephropathy. Kidney Int 78, 1281–7.

Wada, T., Nangaku, M., 2013. Novel roles of complement in renal diseases and their therapeutic consequences. Kidney Int 84, 441–50.

Wagner, M.C., Campos-Bilderback, S.B., Chowdhury, M., Flores, B., Lai, X., Myslinski, J., Pandit, S., Sandoval, R.M., Wean, S.E., Wei, Y., Satlin, L.M., Wiggins, R.C., Witzmann, F.A., Molitoris, B.A., 2016. Proximal Tubules Have the Capacity to Regulate Uptake of Albumin. J Am Soc Nephrol 27, 482–94.

Waldherr, R., Rambausek, M., Duncker, W.D., Ritz, E., 1989. Frequency of mesangial IgA deposits in a non-selected autopsy series. Nephrol Dial Transplant 4, 943–946.

Waldman, M., Crew, R.J., Valeri, A., Busch, J., Stokes, B., Markowitz, G., D'Agati, V., Appel, G., 2007. Adult minimal-change disease: clinical characteristics, treatment, and outcomes. Clin J Am Soc Nephrol 2, 445–53.

Waldo, F.B., 1988. Is Henoch-Schönlein purpura the systemic form of IgA nephropathy? Am J Kidney Dis 12, 373–377.

Walport, M.J., 2001. Complement. First of two parts. N Engl J Med 344, 1058–1066.

Wang, C., Ye, Z., Peng, H., Tang, H., Liu, X., Chen, Z., Yu, X., Lou, T., 2009. Effect of aggregated immunoglobulin A1 from immunoglobulin A nephropathy patients on nephrin expression in podocytes. Nephrology (Carlton) 14, 213–8.

Watanabe, H., Numata, K., Ito, T., Takagi, K., Matsukawa, A., 2004. Innate immune response in Th1- and Th2-dominant mouse strains. Shock 22, 460–6.

Weisbart, R.H., Kacena, A., Schuh, A., Golde, D.W., 1988. GM-CSF induces human neutrophil IgA-mediated phagocytosis by an IgA Fc receptor activation mechanism. Nature 332, 647–648.

Wharram, B.L., Goyal, M., Wiggins, J.E., Sanden, S.K., Hussain, S., Filipiak, W.E., Saunders, T.L., Dysko, R.C., Kohno, K., Holzman, L.B., Wiggins, R.C., 2005. Podocyte depletion causes glomerulosclerosis: diphtheria toxin-induced podocyte depletion in rats expressing human diphtheria toxin receptor transgene. J Am Soc Nephrol 16, 2941–52.

Woo, K.T., Lau, Y.K., Yap, H.K., Lee, G.S., Chiang, G.S., Lim, C.H., 1989. Protein selectivity: a prognostic index in IgA nephritis. Nephron 52, 300–306.

Woodrow, G., Innes, A., Boyd, S.M., Burden, R.P., 1993. A case of IgA nephropathy with coeliac disease responding to a gluten-free diet. Nephrol Dial Transplant 8, 1382–3.

Woof, J.M., Mestecky, J., 2005. Mucosal immunoglobulins. Immunol Rev 206, 64–82.

Woof, J.M., 2013. Immunoglobulin A: Molecular Mechanisms of Function and Role in Immune Defence, in: Nimmerjahn, F. (Ed.), Molecular and Cellular Mechanisms of Antibody Activity. Springer New York, New York, NY, NY, pp. 31–60.

Wyatt, R.J., Julian, B.A., Baehler, R.W., Stafford, C.C., McMorrow, R.G., Ferguson, T., Jackson, E., Woodford, S.Y., Miller, P.M., Kritchevsky, S., 1998. Epidemiology of IgA nephropathy in central and eastern Kentucky for the period 1975 through 1994. Central Kentucky Region of the Southeastern United States IgA Nephropathy DATABANK Project. J Am Soc Nephrol 9, 853–8.

Wyatt, R.J., Julian, B.A., 2013. IgA nephropathy. N Engl J Med 368, 2402–14.

Xiao, J., Leung, J.C.K., Chan, L.Y.Y., Guo, H., Lai, K.N., 2009. Protective effect of peroxisome proliferator-activated receptor-gamma agonists on activated renal proximal tubular epithelial cells in IgA nephropathy. Nephrol Dial Transplant 24, 2067–77.

Yamaji, K., Suzuki, Y., Suzuki, H., Satake, K., Horikoshi, S., Novak, J., Tomino, Y., 2014. The kinetics of glomerular deposition of nephritogenic IgA. PLoS One 9, e113005.

Yamanaka, T., Tamauchi, H., Suzuki, Y., Suzuki, H., Horikoshi, S., Terashima, M., Iwabuchi, K., Habu, S., Okumura, K., Tomino, Y., 2016. Release from Th1-type immune tolerance in spleen and enhanced production of IL-5 in Peyer's patch by cholera toxin B induce the glomerular deposition of IgA. Immunobiology 221, 577–85.

Yamashita, M., Chintalacharuvu, S.R., Kobayashi, N., Nedrud, J.G., Lamm, M.E., Tomino, Y., Emancipator, S.N., 2007. Analysis of innate immune responses in a model of IgA nephropathy induced by Sendai virus. Contrib Nephrol 157, 159–63.

Yasutake, J., Suzuki, Y., Suzuki, H., Hiura, N., Yanagawa, H., Makita, Y., Kaneko, E., Tomino, Y., 2015. Novel lectin-independent approach to detect galactose-deficient IgA1 in IgA nephropathy. Nephrol Dial Transplant 30, 1315–21.

Yi, Z.W., Rodriguez, G.E., Krieg, R.J., Tokieda, K., Chan, J.C., 1996. Rat macrophages in experimental IgA nephropathy. Biochem Mol Med 57, 152–5.

Yoshimura, M., Kida, H., Abe, T., Takeda, S., Katagiri, M., Hattori, N., 1987. Significance of IgA Deposits on the Glomerular Capillary Walls in IgA Nephropathy. Am J Kidney Dis 9, 404–409.

Yu, X.-Q., Li, M., Zhang, H., Low, H.-Q., Wei, X., Wang, J.-Q., Sun, L.-D., Sim, K.-S., Li, Y., Foo, J.-N., Wang, W., Li, Z.-J., Yin, X.-Y., Tang, X.-Q., Fan, L., Chen, J., Li, R.-S., Wan, J.-X., Liu, Z.-S., Lou, T.-Q., Zhu, L., Huang, X.-J., Zhang, X.-J., Liu, Z.-H., Liu, J.-J., 2012. A genome-wide association study in Han Chinese identifies multiple susceptibility loci for IgA nephropathy. Nat Genet 44, 178–82.

Zhao, N., Hou, P., Lv, J., Moldoveanu, Z., Li, Y., Kiryluk, K., Gharavi, A.G., Novak, J., Zhang, H., 2012. The level of galactose-deficient IgA1 in the sera of patients with IgA nephropathy is associated with disease progression. Kidney Int 82, 790–6.

Zikan, J., Mestecky, J., Kulhavy, R., Bennett, J.C., 1986. The stoichiometry of J chain in human secretory dimeric IgA. Mol Immunol 23, 541–544.

Zimmers, T.A., Jin, X., Hsiao, E.C., McGrath, S.A., Esquela, A.F., Koniaris, L.G., 2005. Growth differentiation factor-15/macrophage inhibitory cytokine-1 induction after kidney and lung injury. Shock 23, 543–8.

Zwirner, J., Burg, M., Schulze, M., Brunkhorst, R., Götze, O., Koch, K.M., Floege, J., 1997. Activated complement C3: a potentially novel predictor of progressive IgA nephropathy. Kidney Int 51, 1257–64.

Permissions

Figures 3 and 5 are reprinted from Feehally, J., Floege, J., 2010. IgA Nephropathy and Henoch-Schönlein Nephritis, in: Floege, J., Johnson, R.J., Feehally J. (Eds.), Comprehensive Clinical Nephrology. 4th Ed. St. Louis: Elsevier. pp. 270–281, with permission from Elsevier.

Figure 4 is reprinted from McQuarrie, E.P., MacKinnon, B., Young, B., Yeoman, L., Stewart, G., Fleming, S., Robertson, S., Simpson, K., Fox, J., Geddes, C.C., 2009. Centre variation in incidence, indication and diagnosis of adult native renal biopsy in Scotland. Nephrol Dial Transplant 24, 1524–1528, with permission from Oxford University Press.

Figure 6 is reprinted from Wyatt, R.J., Julian, B.A., 2013. IgA nephropathy. N Engl J Med 368, 2402–14, with permission from the Massachusetts Medical Society.

Figure 7 is reprinted from Boyd, J.K., Cheung, C.K., Molyneux, K., Feehally, J., Barratt, J., 2012. An update on the pathogenesis and treatment of IgA nephropathy. Kidney Int 81, 833–43, with permission from Elsevier.

Figure 10 is reprinted from Dunn, K.W., Sandoval, R.M., Kelly, K.J., Dagher, P.C., Tanner, G.A., Atkinson, S.J., Bacallao, R.L., Molitoris, B.A., 2002. Functional studies of the kidney of living animals using multicolor two-photon microscopy. Am J Physiol Cell Physiol 283, C905–16, with permission from the American Physiological Society.